



PHD

**A digital technique for temperature compensation of crystal oscillators.**

Warwick, G. A.

*Award date:*  
1980

*Awarding institution:*  
University of Bath

[Link to publication](#)

## Alternative formats

If you require this document in an alternative format, please contact:  
[openaccess@bath.ac.uk](mailto:openaccess@bath.ac.uk)

### General rights

Copyright and moral rights for the publications made accessible in the public portal are retained by the authors and/or other copyright owners and it is a condition of accessing publications that users recognise and abide by the legal requirements associated with these rights.

- Users may download and print one copy of any publication from the public portal for the purpose of private study or research.
- You may not further distribute the material or use it for any profit-making activity or commercial gain
- You may freely distribute the URL identifying the publication in the public portal ?

### Take down policy

If you believe that this document breaches copyright please contact us providing details, and we will remove access to the work immediately and investigate your claim.


A DIGITAL TECHNIQUE FOR TEMPERATURE  
COMPENSATION OF CRYSTAL OSCILLATORS

submitted by G A Warwick  
for the degree of Ph.D  
of the University of Bath  
1980

COPYRIGHT

Attention is drawn to the fact that copyright of this thesis rests with its author. This copy of the thesis has been supplied on condition that anyone who consults it is understood to recognise that its copyright rests with its author and that no quotation from the thesis and no information derived from it may be published without the prior written consent of the author.

This thesis may be made available for consultation within the University Library and may be photocopied or lent to other libraries for the purposes of consultation.

A handwritten signature in black ink, appearing to read 'G A Warwick', is written in a cursive style. The signature is located in the lower right quadrant of the page.



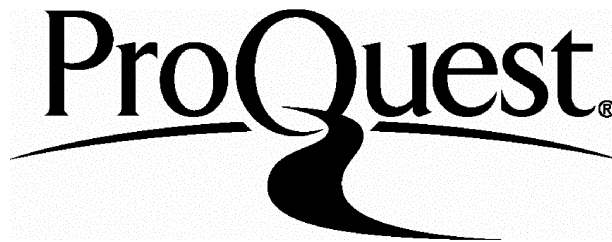
ProQuest Number: U317505

All rights reserved

INFORMATION TO ALL USERS

The quality of this reproduction is dependent upon the quality of the copy submitted.

In the unlikely event that the author did not send a complete manuscript and there are missing pages, these will be noted. Also, if material had to be removed, a note will indicate the deletion.



ProQuest U317505

Published by ProQuest LLC(2015). Copyright of the Dissertation is held by the Author.

All rights reserved.

This work is protected against unauthorized copying under Title 17, United States Code.  
Microform Edition © ProQuest LLC.

ProQuest LLC  
789 East Eisenhower Parkway  
P.O. Box 1346  
Ann Arbor, MI 48106-1346

UNIVERSITY OF BATH LIBRARY		
33	24 JUL 1980	
33		

SUMMARY

The likely growth in the importance of private land mobile radio in the future presents particular problems in achieving the necessary crystal oscillator reference frequency stability. The high power consumption and slow warm up time of oven controlled crystal oscillators is undesirable for mobile operation, so that frequency changes with temperature must be minimised by other means.

This thesis describes a technique for temperature compensation of crystal oscillators which is primarily digital in nature. The system is capable of high stability and offers advantages not present in conventional designs. The use of a digital memory as the compensation law governing element affords great versatility, the same hardware being appropriate in a variety of applications. Automatic calibration of the device is also possible, further improving its performance and reducing the likely cost of production.

Of particular importance in the realisation of the scheme is the method employed to adjust the output frequency. The requirement for a digitally controlled very high resolution frequency source of simple construction has led to the development of a new class of digital frequency synthesiser, a detailed discussion of which is included.

In order to improve upon conventional methods of thermometry and to maximise the use of digital circuitry a Y cut crystal is used as the temperature sensing element. This crystal is placed in close thermal contact with the primary crystal and its linearly temperature dependent frequency is counted digitally to afford temperature information.

The early chapters of the thesis discuss the underlying theory

(ii)

of precision frequency sources, quartz crystals and oscillators, and digital frequency synthesis, leading to a general discussion of the proposed system. Details of the design and performance of a prototype unit are then given, and some techniques of automatic programming of the device are considered. Some relevant mathematical derivations and experimental results are included among a series of appendices.

CONTENTS

SUMMARY	(i)
1. INTRODUCTION	1
2. PRECISION FREQUENCY SOURCES	6
2.1 Signal Characteristics	6
2.2 Active Atomic Frequency Sources	13
2.3 Passive Atomic Frequency Sources	17
2.4 Quartz Crystal Oscillators	28
2.5 A Comparison of the Performance of Precision Frequency Sources	29
3. QUARTZ CRYSTALS AND OSCILLATORS	36
3.1 Quartz Crystal Units	37
3.2 Crystal Oscillators	59
3.3 Oven Control	70
3.4 Temperature Compensation	71
4. FREQUENCY SYNTHESIS	84
4.1 Direct Coherent Synthesis	85
4.2 Indirect Coherent Synthesis	94
5. THE PROPOSED SYSTEM	109
5.1 Temperature Measurement	110
5.2 Frequency Counting	113
5.3 The Compensation Law Governing Element	114
5.4 Methods of Oscillator Correction	115
5.5 The Resulting System	126
6. THE SYSTEM PROTOTYPE	130
6.1 The Read-Only Memory	130
6.2 Temperature Measurement	132
6.3 Frequency Correction	142
6.4 The Construction and Operation of the Prototype	152

6.5 Performance of the Prototype	157
6.6 Further Developments	177
7. PROGRAMMING TECHNIQUES	184
7.1 Point-By-Point Automatic Programming	184
7.2 Programming by Mathematical Prediction	188
8. CONCLUSION	198
ACKNOWLEDGEMENTS	201
APPENDICES	
A Derivation of Crystal Equations	202
B Experiments with a Switched-Capacitor Programmable Crystal Oscillator	208
C "The Frequency Shifting Synthesizer"	213
D "A Digital Technique for Temperature Compensation of Crystal Oscillators"	219
E The 1702A Programmable Read-Only Memory	230
F The pROM Support Equipment	237
G A Study of some Thermal Effects within the Crystal Enclosures	243
H Partial Specification of the EFRATOM Rubidium Atomic Frequency Standard, Model FRK-H	247
I Results of the Short-Term Frequency Stability Tests	248
J Statement List of the Computer Programme used for the Evaluation of Algorithm Two	252

CHAPTER 1 - INTRODUCTION

Crystal oscillators have now been in use for well over fifty years. One of the first was described by W G Cady in October 1921 as "a new radio wavelength standard", thus coming at the beginning of the enormous growth in radiocommunication which is continuing up to the present day. Millions of crystal oscillators are now in service throughout the world covering frequencies from a few kilohertz to hundreds of megahertz, and stabilities from a few parts in  $10^9$  down to worse than 1%. Their importance in stabilising frequencies in transmitters and receivers is paramount, and without them the frequency spectrum would be in chaos and the world communications network at a near standstill.

The number of radio users to be accommodated in a limited and over congested frequency spectrum is continually increasing. Many technical innovations have been employed in attempts to utilise better the available channels, yet almost all of these require a tightening of the specifications of their associated oscillators. Whether narrower channels are employed or time-division or digital systems used, the importance of the crystal oscillator never diminishes. The quartz crystal plays its part in fields other than communications. Each of the enormous and continually growing number of microprocessors in use throughout the world employs a crystal oscillator as its clock rate generator. The majority of modern measurement and test instruments, including timers, oscilloscopes, counters and precision balances employ crystal frequency sources, and the total sales of quartz controlled watches and domestic clocks extend to tens of millions.

The stability of quartz crystal oscillators in their simplest form is not sufficient for all applications and steps must be taken

to improve their performance. The primary cause of their instability is the change which occurs in resonant frequency due to change in temperature, and this is commonly reduced in one of two ways.

Firstly, the crystal and its oscillator may be placed in a small oven and their temperature maintained constant, stabilising the output against changes in the temperature of the surroundings.

Secondly, the prevailing temperature of the crystal may be measured continually and the result used to compensate the output frequency of the oscillator.

Oven controlled oscillators achieve extremely high stability, but suffer from the disadvantages of large volume and weight, high power consumption and a long warm-up period. Temperature compensated crystal oscillators (TCXOs) largely overcome these difficulties but have certain drawbacks of their own. The stability possible by temperature compensation is considerably less than by oven control, and their noise performance is often rather poor. Moreover, the spread in the characteristics of crystals and other components used in manufacture necessitates individual calibration of each unit to achieve good performance, rendering them quite expensive to produce.

Despite these drawbacks, TCXOs find particular application in areas where their stability is adequate with careful design, but where the extra power consumption and other drawbacks of oven controlled sources are unacceptable. One such application is in private land mobile radio. Conservative estimates of the growth in this field put the number of mobile and portable radio equipments in service in the UK at 750,000 by 1990 and 2,000,000 by the year 2000. Although present land mobile vehicular equipments use crystals with tolerances as large as 5-10ppm, considerable system advantages would result if this tolerance could be reduced by an order of magnitude,



and for quasisynchronous working a tolerance of one or two parts in  $10^7$  would be needed. Taking into account the normal working environment of a mobile radio, particularly a portable unit, it is clear that the high power consumption of an oven controlled source is undesirable and accordingly the TCXO is of great importance in this application.

The projected growth in the land mobile radio market and its concomitant requirement for more stable frequency sources has led to the work described in this thesis. The existing techniques used for temperature compensation of crystal oscillators are considered and various alternative methods of reducing their shortcomings are put forward. The result is a proposal for a completely new compensation scheme which takes advantage of modern technology in its use of digital circuitry throughout. The technique is suited to both large-scale integration of the circuitry and automatic calibration, promising considerable economies in production costs over current types.

Before discussing the proposed system, several background topics are considered. Chapter 2 describes the action of various types of precision frequency source and illustrates the important role of quartz crystals in all of them. The parameters used to describe the quality of performance of frequency sources are also defined. Chapter 3 is a discussion of the principles of operation of quartz crystals and their use in oscillators. The principles of oven control are discussed briefly and existing techniques of temperature compensation are detailed. Chapter 4 is a general discussion of frequency synthesis, which proves to be of great importance to the proposed system. Particular emphasis is placed upon digital phase locked loop synthesis in its various forms.

Chapter 5 is a detailed discussion of the elements of the prototype system. The problems of temperature measurement, frequency counting, compensation law governing and oscillator correction are considered individually, and the objectives to be met by the overall system are itemised. Chapter 6 is a detailed description of the design, construction and performance of the system prototype, including various suggestions for improvements and further developments. Finally, several approaches to the automatic calibration of such a system are discussed and analysed in Chapter 7.

As an aid to the clarity of the work, those discussions which are relevant but not immediately essential to the topic under consideration have been removed to a series of appendices.

GENERAL REFERENCES

GERBER, E.A., and SYKES, R.A.: "A quarter century of progress in the theory and development of crystals for frequency control and selection", Proc. 25th Annual Frequency Control Symp., Atlantic City, July 1971.

CADY, W.G.: "Piezoelectricity", New York: Dover Publications, 1946.  
2nd ed. 1964.

HEISING, R.A.: "Quartz crystals for electrical circuits", New York: Van Nostrand, 1946.

GERBER, E.A., and SYKES, R.A.: "Quartz frequency standards", Proc. IEEE, Vol.55, No.6, June 1967.

MCCOUBREY, A.O.: "A survey of atomic frequency standards", Proc. IEEE, Vol.54, No.2, February 1966.

BARNES, J.A. et al.: "Characterisation of frequency stability", IEEE Trans. Inst. Meas., Vol.IM-20, No.2, May 1971.

PYE TELECOMMUNICATIONS LTD.: "A study of the future frequency spectrum requirements for private mobile radio in the United Kingdom", Cambridge: Pye Telecomms., 1976.

CHAPTER 2 - PRECISION FREQUENCY SOURCES

In the following sections the various types of precision frequency sources available are discussed. Brief descriptions of each type are given including their principles of operation and a qualitative discussion of their performance. A quantitative comparison is then made and the relative advantages and disadvantages of the sources are discussed. Firstly, however, it is necessary to consider those parameters which describe the quality of performance of any frequency source.

2.1 Signal Characteristics

The output of a frequency source may be represented by the equation:

$$v(t) = A \cdot \sin[2\pi f_0 t + \theta(t)] \quad (2.1)$$

where A is the amplitude (assumed constant) and  $f_0$  is the average frequency.  $\beta = 2\pi f_0 t + \theta(t)$  is defined as the instantaneous total phase of the signal and  $\theta(t)$  represents the phase variations about the linearly progressing phase  $2\pi f_0 t$ . The instantaneous total frequency is then defined as:

$$f'(t) = \frac{1}{2\pi} \frac{d\beta}{dt} = f_0 + \frac{1}{2\pi} \frac{d\theta(t)}{dt} \quad (2.2)$$

and the instantaneous frequency fluctuation as:

$$f(t) = \frac{1}{2\pi} \frac{d\theta(t)}{dt} = \frac{\dot{\theta}}{2\pi} \quad (2.3)$$

The nature of  $\theta(t)$  may be divided into two broad categories; deterministic and non-deterministic, which are now considered further.

### 2.1.1 Deterministic Variations

Deterministic variations are those which can be predicted from past history, or are dependent on environmental changes. These include frequency drift due to aging of the resonator, temperature coefficient effects, gravity or acceleration, magnetic field and atmospheric pressure. The method employed to quantify such effects is dependent on the effect itself, and is usually very simply stated.

The most common deterministic variations are the change in average output frequency with temperature variation, expressed in hertz per degree or normalised and expressed in parts in  $10^n$  per degree; and the change in average output frequency with elapsed time, expressed in hertz per day, hertz per month, parts in  $10^n$  per day etc. Such terms need no further explanation.

Consideration of the items above reveals that deterministic variations are all those which, in a practical situation, occur over a relatively long period of time. For this reason these effects are contributory only to what is known as the "long-term stability" of the source, where long-term would normally refer to periods in excess of a day.

### 2.1.2 Non-Deterministic Fluctuations

Non-deterministic fluctuations are random in nature and consequently their effects on the frequency at any instant cannot be predicted from past history. They may be assumed to be Gaussian random variables, and hence may be uniquely characterised by their autocorrelation function in the time domain, or by some spectral density function in the frequency domain. Non-deterministic

fluctuations occur continuously, but in the long-term their effects are swamped by deterministic variations. For this reason it is conventional to consider non-deterministic effects only in the short-term, assuming the absence of long-term changes. These effects therefore describe the "short-term stability" of a source. The various techniques for the characterisation of short-term stability are now discussed.

The autocorrelation function for the real variable  $x(t)$  is defined as<sup>(1)</sup>:

$$R_x(\tau) = \overline{x(t) \cdot x(t+\tau)} \quad (2.4)$$

where the bar indicates the statistical average.  $R_x(\tau)$  is an even function of  $\tau$ . The spectral density of  $x$  may then be defined:

$$S_x(f) = 4 \int_0^{\infty} R_x(\tau) \cos 2\pi f \tau \cdot d\tau \quad (2.5)$$

$S_x(f)$  is an even function of  $f$ , so only positive frequencies need be considered. The autocorrelation function and the spectral density form a Fourier transform pair so that they may be related by

$$R_x(\tau) = \int_0^{\infty} S_x(f) \cos 2\pi f \tau \cdot df \quad (2.6)$$

considering one-sided spectral densities with the Fourier frequency variable  $f$ . The unit of  $f$  is hertz. The variance of  $x$  is:

$$\sigma^2(x) = R_x(0) - m^2 = \int_0^{\infty} S_x(f) \cdot df - m^2 \quad (2.7)$$

where  $m = \overline{x(t)}$  is the mean value of  $x$ . In most cases it may be arranged that  $m = 0$ .

The parameters employed to evaluate short-term frequency stability are the spectral densities of phase, frequency and fractional frequency; fractional frequency fluctuations in the time domain; and the so-called phase noise. Firstly, putting  $\theta(t) = x(t)$

in equation (2.5) we define the phase spectral density,

$$S_{\theta}(f) = 4 \int_0^{\infty} R_{\theta}(\tau) \cos 2\pi f \tau \cdot d\tau \quad (2.8)$$

By putting  $\dot{\theta}(t) = x(t)$ , the frequency spectral density is obtained:

$$S'_{\theta}(f) = 4 \int_0^{\infty} R'_{\theta}(\tau) \cos 2\pi f \tau \cdot d\tau \quad (2.9)$$

And if  $y(t) = x(t)$  where

$$y(t) = \frac{f(t)}{f_0} = \frac{\dot{\theta}}{2\pi f_0} \quad (2.10)$$

then the fractional frequency spectral density results:

$$S_y(f) = 4 \int_0^{\infty} R_y(\tau) \cos 2\pi f \tau \cdot d\tau \quad (2.11)$$

The relationship between these spectral densities may be shown to be (2):

$$S_y(f) = \left(\frac{1}{2\pi f_0}\right)^2 \cdot S'_{\theta}(f) = \left(\frac{1}{f_0}\right)^2 \cdot f^2 S_{\theta}(f) \quad (2.12)$$

The phase noise of a frequency source is a partly empirical parameter proposed by the US National Bureau of Standards<sup>(3)</sup>, and is defined as follows. The frequency spectrum of a signal in the absence of amplitude modulation may be considered as consisting of a large number of strips of width  $\Delta B$  (the measured passband) located a distance  $f$  away from the signal. The energy in  $\Delta B$  may now be viewed as being caused by a sinusoidal frequency modulating signal centred in  $\Delta B$  with a deviation proportional to the amplitude of the spectrum at  $f$ . It is assumed that  $\Delta B$  is much smaller than  $f$  so that the envelope of the noise spectrum may be considered flat within  $\Delta B$ . This amounts to treating a continuous noise spectrum as if it consisted of a very large number of sinusoidal sideband components symmetrically distributed about the signal so that, when all the

equivalent sinusoids are added on a power basis, the same total mean power as the actual noise spectrum is produced. It should be noted that this treatment assumes that all the noise is due to phase and frequency modulation and that amplitude modulation is absent.

Using this model, and taking  $\Delta B = 1\text{Hz}$ , the phase noise may be defined as a function of the Fourier (modulating) frequency as:

$$\alpha(f) = \frac{\text{Power Density (one sideband)}}{\text{Total Signal Power}}, \text{ in 1Hz bandwidth (2.13)}$$

This equation, in isolation, has no particular mathematical significance, but specifies well a measure of performance of a source. A comparison of  $S_y(f)$  with  $\alpha(f)$  indicates that the two quantities are directly proportional if the total signal power is assumed constant. It is known from frequency modulation theory that the ratio of a single sideband to the carrier is half the corresponding peak phase deviation, that is:

$$\alpha(f) = \frac{\theta_d}{2} \quad (2.14)$$

or, in decibels per hertz bandwidth,

$$\alpha(f) = 20 \log \frac{\theta_d}{2} \quad (2.15)$$

so that the phase noise,  $\alpha(f)$ , may be directly related to the peak phase jitter. Further, since

$$\theta_d = \frac{\Delta f_{\text{peak}}}{f} \quad (2.16)$$

where  $\Delta f_{\text{peak}}$  is the peak frequency deviation,  $\alpha(f)$  may be expressed as:

$$\alpha(f) = 20 \log \left( \frac{\Delta f_{\text{peak}}}{2f} \right) \text{ dB/Hz} \quad (2.17)$$

or

$$\alpha(f) = 20 \log \left( \frac{\Delta f_{\text{rms}}}{\sqrt{2}f} \right) \text{ dB/Hz} \quad (2.18)$$



Having measured  $\alpha(f)$  for various values of  $f$ , an equivalent peak phase or rms frequency may, therefore, be estimated. If the equivalent single-sideband to signal ratio is measured in some bandwidth other than 1Hz, then the conversion may be expressed:

$$\alpha(f) = \frac{\text{Sideband Noise Power}}{\text{Total Signal Power}} \Bigg|_{\Delta B_x} - 10 \log(\Delta B_x) \text{ dB/Hz} \quad (2.19)$$

where  $\Delta B_x$  is the measurement bandwidth. Equation (2.19) applies only to the noise-like content of the spectrum, the power in a discrete FM sideband being independent of the bandwidth of measurement.

The assumption made above that  $\Delta B \ll f$  is acceptable in most cases. In some applications of frequency sources, however, data describing the spectral purity is required for Fourier frequencies below 10Hz. This would require measurements to be made in a bandwidth less than 0.1Hz, which is beyond the capability of even the best wave analyser. Techniques of evaluating spectral purity close to the average frequency have been developed to meet such requirements, defining frequency stability in the time domain (2), (4).

The average fractional frequency offset obtained during the  $k$ th measurement interval of a series of measurements is defined as  $\overline{y_k}$ , where

$$\overline{y_k} = \frac{1}{\tau} \int_{t_k}^{t_k + \tau} y(t) dt = \frac{\theta(t_k + \tau) - \theta(t_k)}{2\pi f_0 \tau} \quad (2.20)$$

where  $y(t)$  is as defined in equation (2.10),  $t_k$  is the time at the start of the measurement and  $\tau$  is the measurement period.

Conventional frequency counters measure the number of cycles (or zero-crossings) in a period  $\tau$ , or  $f_0 \tau (1 + \overline{y_k})$ . The time domain definition of frequency stability is based on the sample variance of the fractional frequency fluctuations and is expressed in terms of

$\overline{y_k}$  as

$$\sigma_y^2(N,T,\tau) = \left\langle \frac{1}{N-1} \sum_{n=1}^N (\overline{y_n} - \frac{1}{N} \sum_{k=1}^N \overline{y_k})^2 \right\rangle \quad (2.21)$$

where  $\langle X \rangle$  is the infinite time average of  $X$ ,  $N$  is the number of data points considered in obtaining the sample variance, and  $T$  is the repetition interval of the measurements of duration  $\tau$ . If there is no dead time between measurements then  $T = \tau$ .

In practice  $N$  is a finite number, and in order to rationalise the measurements it is necessary to specify the particular  $N$  and  $T$  used in determining  $\sigma_y^2(N,T,\tau)$ . It is conventional to choose  $N = 2$  and  $T = \tau$  (ie no dead time), so that a new variable  $\sigma_y^2(\tau)$  may be defined:

$$\sigma_y^2(\tau) = \left\langle \sigma_y^2(N=2, T=\tau, \tau) \right\rangle \quad (2.22)$$

$\sigma_y^2(\tau)$  is known as the Allan variance<sup>(5)</sup>. If  $\overline{y_{k+1}}$  is the fractional frequency offset obtained during the  $(k+1)$ th measurement, then

$$\sigma_y^2(\tau) = \left\langle \frac{(\overline{y_{k+1}} - \overline{y_k})^2}{2} \right\rangle \quad (2.23)$$

is the required measure of frequency stability. The definition represents an estimate of the Allan variance of the fractional frequency fluctuations for  $N = 2$  made from two samples ( $\overline{y_k}$  and  $\overline{y_{k+1}}$ ) of the frequency averaged over the sample time  $\tau$ . A rigorous statement of spectral purity by this method must stipulate  $N$ ,  $\tau(=T)$ , and the bandwidth of the measuring instruments.

It is possible to relate the time domain and frequency domain expressions of spectral purity by<sup>(2)</sup>:

$$\sigma_y^2(\tau) = 2 \int_0^{\infty} S_y(f) \cdot \frac{\sin^2(\pi f \tau)}{(\pi f \tau)^2} \left[ 1 - \frac{\sin^2(2\pi f \tau)}{4\sin^2(\pi f \tau)} \right] \cdot df$$

which reduces to:

$$\sigma_y^2(\tau) = 2 \int_0^{\infty} S_y(f) \cdot \frac{\sin^4(\pi f \tau)}{(\pi f \tau)^2} \cdot df \quad (2.24)$$

Equation (2.24) is particularly useful when the performance of a source is to be compared with a written specification expressed by the alternative parameter. It is not recommended for use when it is possible to measure both sources by the same technique.

## 2.2 Active Atomic Frequency Sources

An active atomic frequency source consists of a resonator of high Q in which exist atoms (or molecules) in a state of energy higher than their ground state. If the cavity is made resonant at an allowed radiative transition frequency for the atoms, and its Q is sufficiently high, then provided that there are enough atoms present to overcome the losses, a self-excited oscillation will build up at the transition frequency. This oscillation forms the useful output signal from the device. Since the output power of such sources is low ( $10^{-10}$  -  $10^{-13}$  Watts), and the frequency is generally some non-cardinal value, a crystal oscillator with a multiplier and frequency synthesiser is usually phase locked to the primary signal.

Figure 2.1 shows the general block diagram of such an active atomic frequency source. The atomic oscillator is isolated from the following circuitry to prevent load changes from detuning the maser cavity and a voltage controlled crystal oscillator is phase locked to the maser frequency such that its output frequency  $f_1$  is related to  $f_M$  by:

$$f_1 = \frac{f_M}{M+N} \quad (2.25)$$

where M and N are chosen to give a convenient value of  $f_1$ , usually some cardinal value.

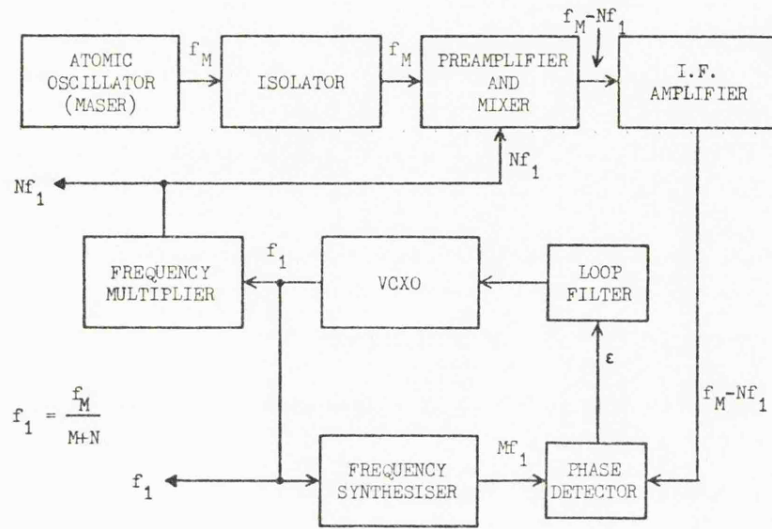


Figure 2.1 General arrangement of an Active Atomic Frequency Source

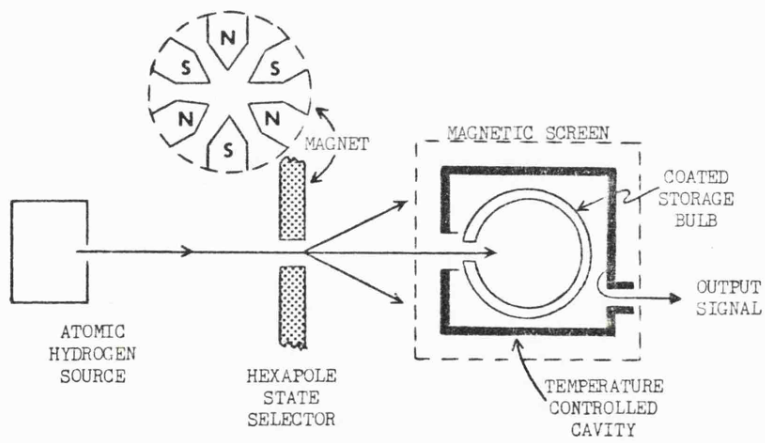


Figure 2.2 The Hydrogen Maser

The loop bandwidth is generally chosen to minimise overall noise, the characteristics of the particular atomic oscillator and VCXO being the determining factors.

### 2.2.1 The Ammonia Beam Maser (6),(7)

The ammonia beam maser utilises the inversion transition of ammonia at about 24GHz, molecules in the upper energy state being focused into a resonant cavity in which they radiate. The ammonia molecule has low mass, and hence a high thermal velocity which, together with the short cavity dictated by the high microwave frequency, leads to a short interaction time with the microwave field and a relatively low atomic Q of about  $5 \times 10^6$ . This makes the ammonia maser very susceptible to cavity detuning, travelling wave and Doppler effects, and for these reasons is not a very precise frequency source compared to other, more recent, atomic devices.

One important feature of the ammonia maser is its relatively high power level and high frequency. These give it a good fractional frequency spectral density at higher Fourier frequencies where additive noise dominates<sup>(1)</sup>.

### 2.2.2 The Optically Pumped Rubidium Vapour Maser

The optically pumped Rubidium 87 maser is very similar in construction to the passive rubidium vapour source described in section 2.3.3, the photo detector being omitted since it is not needed.

Though the rubidium maser is relatively simple and compact compared to the other masers, frequency drifts due to light intensity changes and cavity pulling are severe and lead to

considerable drift. For this reason it is seldom used.

### 2.2.3 The Hydrogen Maser

Figure 2.2 shows the elements of the atomic hydrogen oscillator. Molecular hydrogen is dissociated in a discharge bulb and a collimated beam is directed through the deflection magnet into the aperture of the storage bulb. The deflection magnet has a hexapole field which is weak on axis and increases in magnitude away from the axis. Some molecular hydrogen may also effuse from the collimator, but is not focused into the bulb. The storage bulb is made of fused quartz for low loss and is coated with a thin layer of teflon. The hydrogen atoms bounce off the walls of the bulb before relaxing (making a transition) or leaving through the entrance aperture. Interaction with the teflon surface is very small so that the atoms have a very long coherent lifetime (of the order of a second) yielding a very narrow spectral line and the highest atomic line Q of any of the atomic resonators (about  $2 \times 10^9$ ). To complete the maser there is a high Q fused quartz resonant cavity lined with a silver on copper conductive coating. The transition frequency is 1420.405751...MHz. The whole apparatus is enclosed in a temperature controlled vacuum bell jar and a set of magnetic shields.

Despite the high atomic line Q it is necessary to control the cavity temperature fairly closely to avoid relatively large frequency shifts (about  $5 \times 10^{-11}$ ) due to cavity detuning. The teflon lined wall of the bulb causes a small perturbation of the atoms during collision, and this also produces a frequency shift of the order of a part in  $10^{11}$  for a bulb of average size. This shift varies somewhat from bulb to bulb, so the absolute frequency of a particular maser may be in error by as much as several parts in  $10^{12}$ .

The long-term stability of the hydrogen maser is excellent provided the cavity remains tuned, and automatic control and other techniques have been developed for this purpose<sup>(8),(9)</sup>.

The low Fourier frequency part of the phase spectral density of the hydrogen maser is extremely good. The high Fourier frequency part, however, is poor, since the output power is low at about  $10^{-12}$  Watts and its frequency is rather lower than other masers. By phase locking a second oscillator to the maser as shown in Figure 2.1, however, the phase spectral density may be arranged to exhibit the characteristics of the maser within the loop filter cutoff frequency, and the characteristics of the phase locked oscillator elsewhere, yielding good overall spectral purity. In practical hydrogen maser frequency standards this technique is a necessity.

### 2.3 Passive Atomic Frequency Sources<sup>(10),(11),(12)</sup>

A passive atomic frequency source contains an atomic resonance device such as a cesium beam tube, thallium beam tube, or rubidium vapour gas cell, with an output signal that indicates the offset of an applied signal frequency from the atomic resonance. Also included is a frequency source, such as a voltage controlled crystal oscillator with a frequency multiplier and synthesiser, to produce the signal applied to the atomic resonator, and the necessary circuitry for locking this frequency to the centre of the atomic resonance.

The general block diagram for a passive atomic frequency source is shown in Figure 2.3. All useful atomic resonators have a response that is an even function of frequency departure from the resonance frequency. This means that the resonator output is either a maximum or a minimum at resonance, and that frequency modulation with

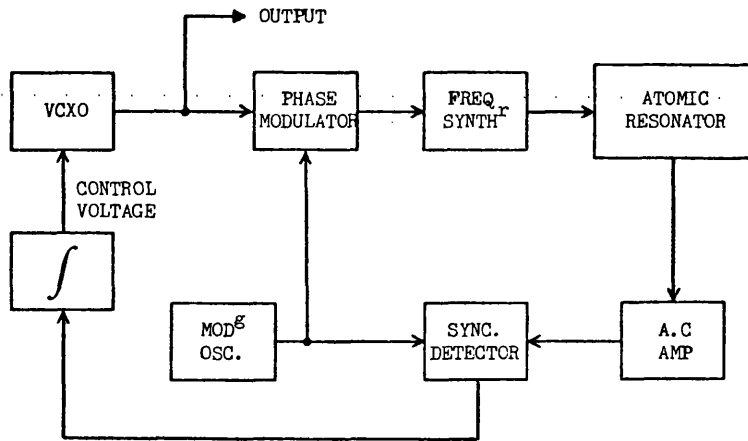


Figure 2.3 A Passive Atomic Frequency Source using a phase modulation technique

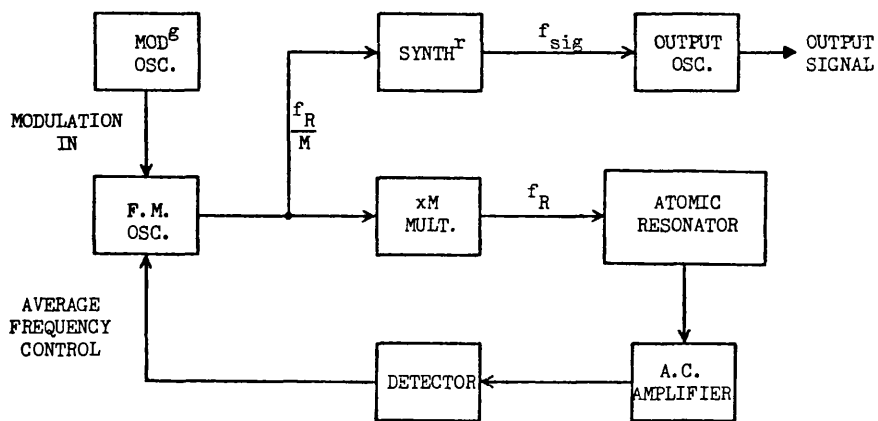


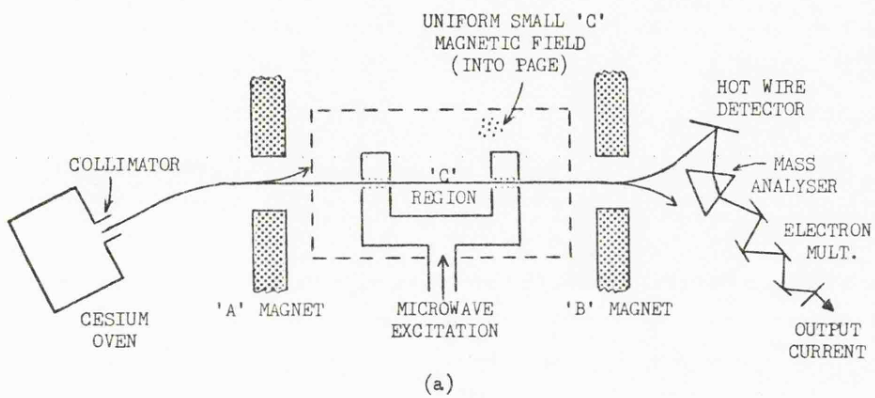
Figure 2.4 A Passive Atomic Frequency Source using frequency modulation



synchronous detection must be used to locate the centre of the resonance line accurately. Since a modulated output signal from the frequency source is undesirable, the necessary frequency modulation of the atomic resonator excitation signal is achieved without contamination of the output signal in one of several ways. Phase modulation is one method, and is illustrated in Figure 2.3. An alternative is the use of a frequency modulated oscillator to supply the excitation (as shown in Figure 2.4), being controlled in average frequency by the atomic resonator. A second oscillator, which supplies the useful output signal, is phase locked to the frequency modulated oscillator with a phase locked loop bandwidth chosen so as to effectively filter out the modulating frequency. In such a system the modulated oscillator may have a non-cardinal average frequency which is a submultiple of the atomic resonance, the output being made a cardinal frequency by means of the frequency synthesiser.

### 2.3.1 The Cesium Beam Atomic Resonator <sup>(13)</sup>

A schematic arrangement of a cesium beam atomic resonator is shown in Figure 2.5. Cesium 133 has a single valence electron. The electron spin has two possible orientations and two energy levels associated with these orientations. The corresponding energy states are designated by the quantum numbers  $F=3$  and  $F=4$ . Within an oven located in the cesium beam tube liquid cesium is vaporised. A collimator forms the cesium atoms into a narrow beam and directs the beam towards an input selector magnet ('A') which deflects  $F=4$  atoms into the microwave cavity. When the atoms enter the field in the 'C' region the  $F=4$  energy level splits into a number of discrete levels, designated by the quantum numbers  $m_F$ , which correspond to allowed orientations of the cesium atom with respect to the 'C' field. The



N.B. 'C' Region shown rotated 90° about beam axis for clarity

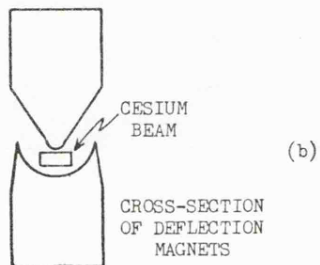


Figure 2.5 A Cesium Beam Atomic Resonator

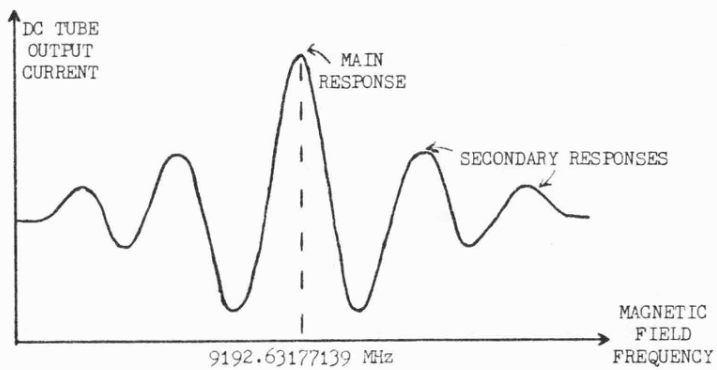


Figure 2.6 Transfer Response of the Resonator of Figure 2.5

transition used in the frequency standard is that separating  $F=4$ ,  $m_F=0$  and  $F=3$ ,  $m_F=0$  states, designated as the  $(4,0)-(3,0)$  transition. This particular transition is selected because the atomic frequency associated with it is nearly independent of any external magnetic field, whereas other allowable transitions are linearly dependent on the field. With the exception of magnetic field effects, the frequency associated with the  $(4,0)-(3,0)$  transition is completely independent of all environmental conditions.

On the application of a linearly polarised alternating magnetic field parallel to the 'C' field at the appropriate frequency, transitions  $(4,0)-(3,0)$  take place in the microwave cavity. The maximum number of transitions is induced when the frequency of the magnetic field exactly matches the atomic frequency of cesium 133. An output state selector magnet ('B') deflects all the atoms that underwent  $(4,0)-(3,0)$  transitions to a hot-wire ioniser, where the cesium atoms are ionised with almost 100% efficiency. The ions are accelerated and passed through a mass filter to remove impurities and then further accelerated into the first stage of an electron multiplier where they bombard the surface and eject secondary electrons which are further multiplied in the remaining stages. The output signal current is taken from the collector electrode and is typically about  $10^{-7}$ A.

Figure 2.6 shows the dc response characteristic of a cesium beam tube, known as a Ramsey curve<sup>(14)</sup>. The main response of the curve is utilised in the frequency discrimination action of the tube, the secondary responses being employed only in the calibration procedure. The width of the main response and the distance between successive peaks are functions of the length of the microwave cavity and the average velocity of the cesium atoms. For a tube of overall

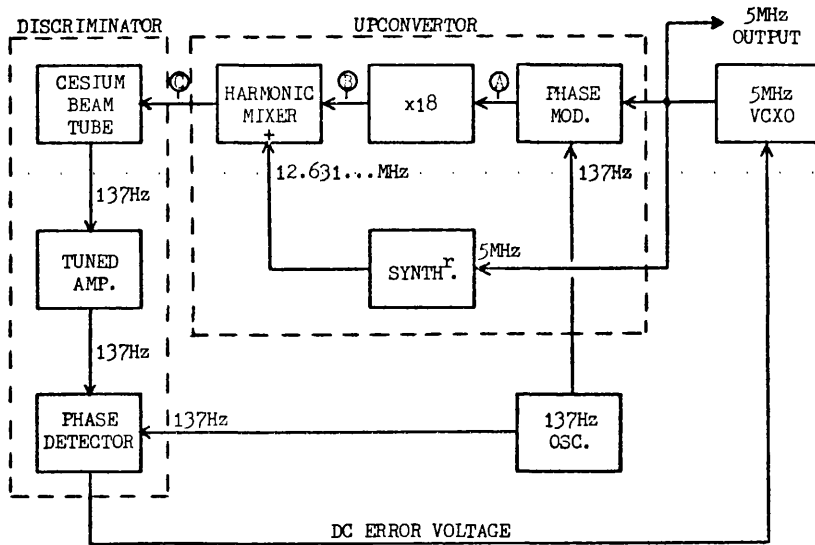
length 40cms the width of the main response is about 550Hz, representing a line Q of about  $1.7 \times 10^7$ .

A functional block diagram of a typical cesium beam frequency standard is shown in Figure 2.7. Figure 2.8 is an expanded view of the peak portion of the main response of the tube. By modulating the alternating magnetic field an ac component of the tube output current is generated. The amplitude of this component is a measure of the frequency offset of the tube input from the resonant frequency, equal frequency offsets above and below the resonant frequency being distinguishable by their  $180^\circ$  phase difference. When the tube input is equal to the resonance frequency, however, the alternating component of the output current is at 274Hz and, due to the action of its tuned amplifier, the discriminator output is held steady.

The long-term frequency stability of the cesium beam frequency standard is excellent, rivalling that of the hydrogen maser, though its shorter term stability is rather less than other passive sources. Since the early 1960s the cesium beam frequency source has been the basis for the definition of the unit of time, the second being defined as that time interval during which the free cesium atom transition in zero magnetic field occurs 9192631770 times.

### 2.3.2 The Thallium Beam Atomic Resonator (15)

A thallium 205 beam tube has very similar construction to a cesium beam tube, the transition frequency being about 21.3GHz. One desirable advantage of the thallium beam tube is its reduced sensitivity to stray and fluctuating magnetic fields. This, however, in turn poses considerable problems in that the power required for its magnets to produce the required deflections is correspondingly



Signals at : (A) 5MHz phase modulated at 137Hz  
 (B) 90MHz phase modulated at 137Hz  
 (C) 9192.631...MHz phase modulated at 137Hz  
 ( $102 \times 90 + 12.631... = 9192.631...$ )

Figure 2.7 A Cesium Beam Frequency Standard

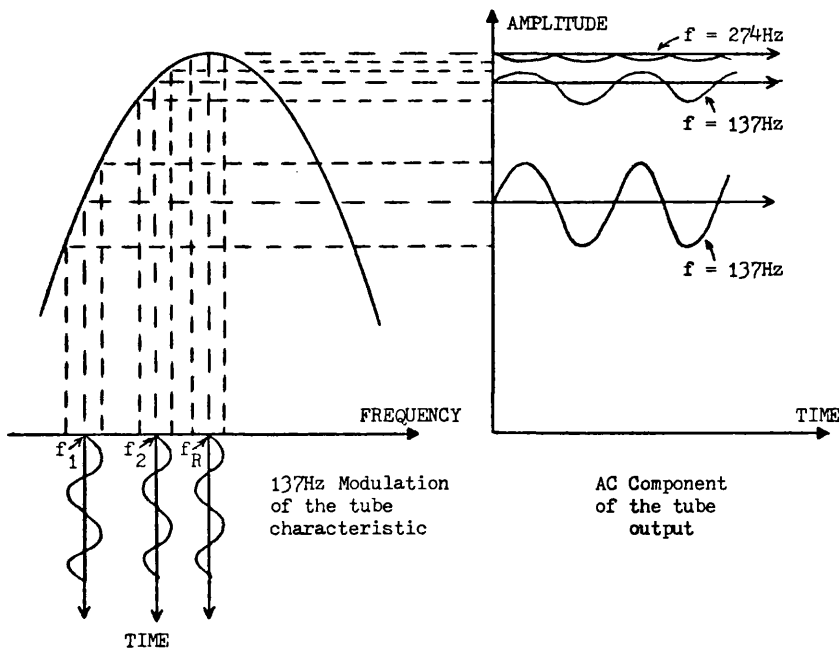
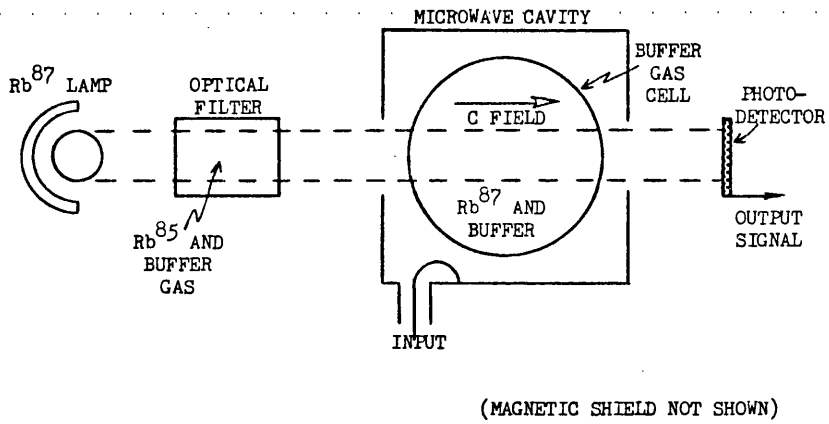
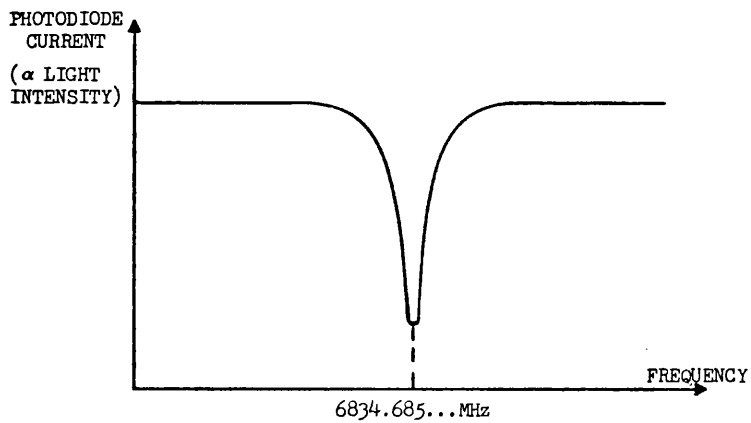


Figure 2.8 Frequency Discrimination by modulation of the Cesium Beam Resonator microwave excitation



**Figure 2.9** An Optically Pumped Rubidium Vapour Cell



**Figure 2.10** Transfer Response of the Cell of Figure 2.9

increased, though novel techniques have been developed to minimise this problem.

Due to their high ionisation energy, thallium atoms are very difficult to detect by the hot-wire method, oxidised tungsten being the only useful target, requiring a long servomechanism time constant. There are no commercially available thallium tubes and it is believed that they will never emerge as a useful alternative to established standards.

### 2.3.3 The Passive Rubidium Vapour Cell Frequency Source<sup>(16)</sup>

The discriminator operation in a rubidium frequency standard is based on the energy absorption characteristic of rubidium 87. The reference element is an optically pumped rubidium 87 vapour cell located in a microwave cavity. Optical pumping is used because absorption of optical radiation is easier to detect than absorption of electromagnetic radiation. The energy absorption phenomenon is used to control the frequency of a voltage controlled crystal oscillator, usually at 5MHz or 10MHz, in the following manner.

A functional block diagram of a typical rubidium vapour cell standard is shown in Figure 2.11. It may be seen that it bears a strong resemblance to a cesium beam standard in its external circuitry, the modulating frequency being only slightly different.

A light beam from a rubidium lamp is applied to a filter cell which absorbs the energy at the undesired wavelength of  $7947 \text{ \AA}$  and passes the energy at the  $7800 \text{ \AA}$  wavelength to the rubidium absorption cell almost unattenuated. The rubidium vapour cell absorbs some of the light energy, and the unabsorbed light leaving the cavity is monitored by a photo detector (usually a photodiode). An electromagnetic field is generated in the cavity which consists

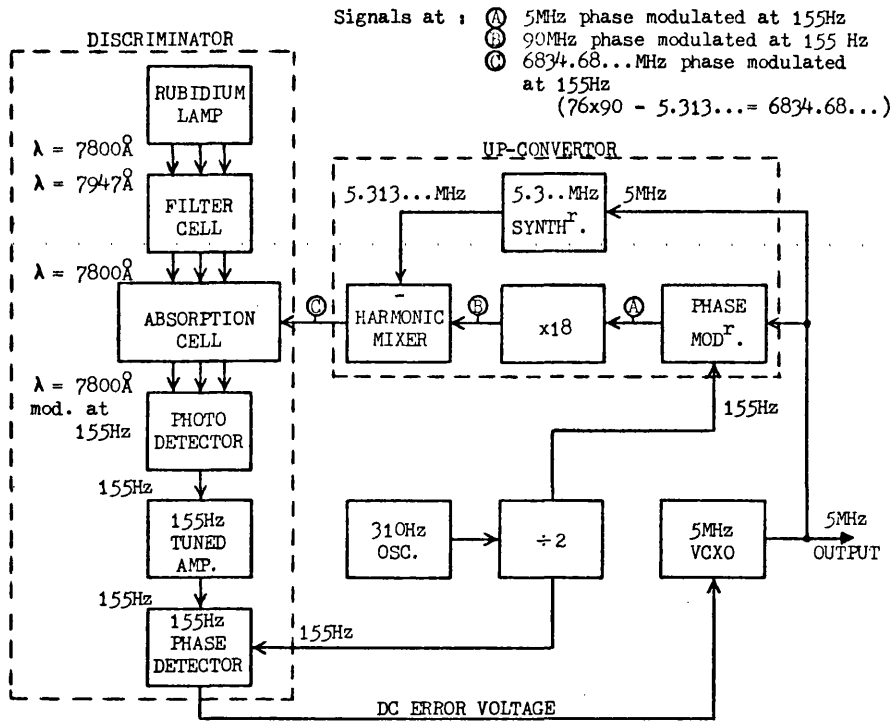


Figure 2.11 A Typical Rubidium Vapour Cell Frequency Standard

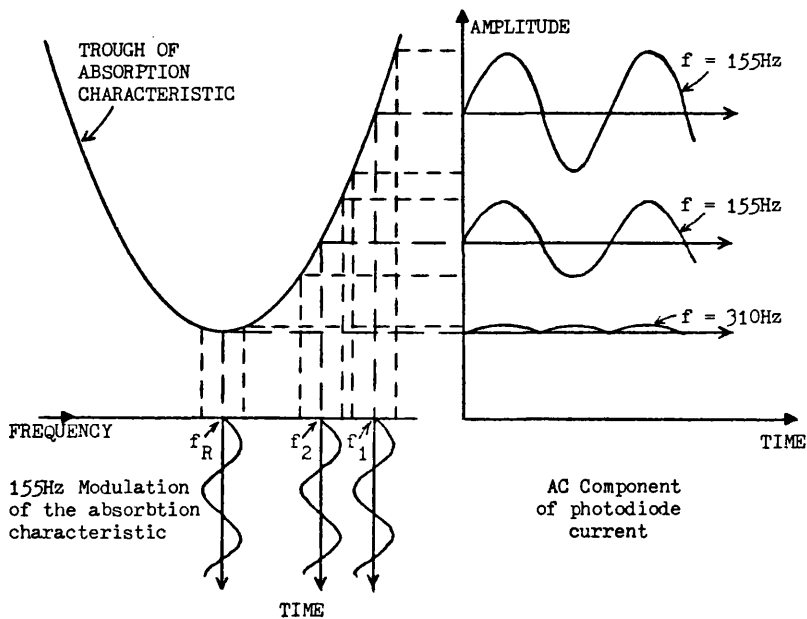


Figure 2.12 Frequency Discrimination by modulation of the Magnetic Field Frequency of a Rubidium Vapour Cell



of a small static 'C' field and an additive alternating field. When the frequency of the field approaches the resonant frequency of the rubidium vapour (6834.685...MHz), the number of energy level transitions in the Rb<sup>87</sup> gas is increased, more of the light is hence absorbed by the cell and the photodiode current decreases as shown in Figure 2.10.

Figure 2.12 illustrates how, by modulating the alternating component of the magnetic field, the VCXO may be locked onto the atomic resonance frequency in exactly the same way as in a cesium beam source.

The transition utilised in the rubidium vapour cell is the (2,0)-(1,0) transition, again because of its relative insensitivity to changes in external magnetic fields. The maximum frequency error due to magnetic field changes is less than a part in  $10^{11}$ . The absorption cell, as well as the filter cell, contains a buffer gas which serves to confine the rubidium atoms by making essentially elastic collisions with them, keeping the atoms available for a relatively long period of time to interact with the field. This produces a narrow resonance line which, though dependent on the buffer gas, may have a Q of about  $10^7$ . The collision rate is very high so that, in spite of the small interaction, there is substantial frequency shift caused by the buffer gas, though this may be minimised by using mixtures of nitrogen and the noble gases. Another mechanism causing frequency shift is the interaction of the optical and microwave radiations with the rubidium 87 atoms in the absorption cell. If the optical radiation spectrum is assymmetric about the absorption line of the atoms there will be a frequency shift in the cavity resonant frequency.

Since the temperature and pressure of the buffer gas and the

spectrum of the lamp may change with time and environment, the rubidium vapour cell frequency source is sensitive to these effects. The shifts caused by the presence of the buffer gas are as large as a part in  $10^7$ , and light intensity shifts can be as large as 1 part in  $10^9$ . The rubidium cell cannot, therefore, be considered a primary standard as it must be calibrated to frequency periodically. It exhibits excellent short-term frequency stability, however, and has considerable advantages over the cesium beam standard and hydrogen maser in its lack of deflection magnets which require high voltage drive and increase the total weight considerably. Rubidium sources are commercially available at about 50% of the cost of a cesium beam source.

#### 2.4 Quartz Crystal Oscillators

A detailed study of quartz crystal oscillators is contained in Chapter 3. It is sufficient here to say that the only type of crystal controlled sources which would qualify as 'precision' are those incorporating very precise temperature control apparatus. The most precise quartz crystal units available are fifth-overtone types operating in the 2.5MHz to 5MHz region. In order to obtain acceptable levels of long-term drift from such devices it is necessary to operate them at very low power levels, leading to rather poor phase spectral density of noise.

A typical commercially available crystal controlled frequency standard uses a double oven to control the temperature of the crystal and oscillator. The noise performance is improved by incorporating a high-order crystal filter at the output, which must also be enclosed in the oven. The stabilisation time of the double oven is long, but once the warm-up period has passed the

oscillator's stability is better than 5 parts in  $10^{10}$  per day, improving to 1 part in  $10^{10}$  per day after two months continuous operation.

Though these stability figures are poor in comparison with atomic standards, the performance of crystal controlled sources is more than adequate for most laboratory applications provided that periodic recalibration is ensured.

## 2.5 A Comparison of the Performance of Precision Frequency Sources

It is now possible to draw comparisons between the various types of precision frequency source, primarily considering their long-term and short-term stability but also taking into account size, weight, cost and other factors. For clarity, the data is restricted to the four most important sources, namely the hydrogen maser, the cesium beam resonator, the rubidium vapour cell and the oven controlled crystal oscillator.

Table 2.1 shows the physical data relating to the sources, and a summary of their stability performance data.

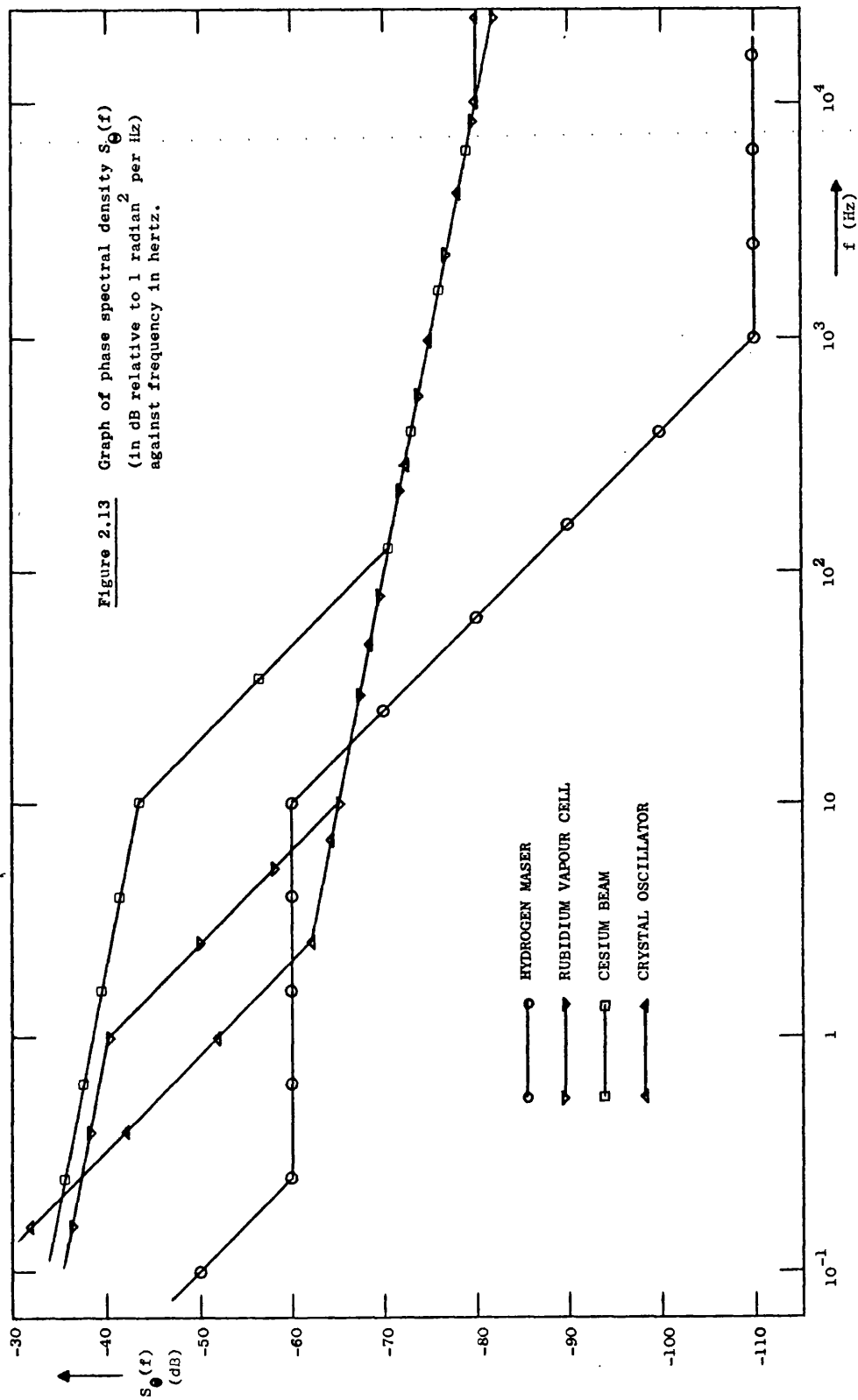
It is the high intrinsic reproducibility of hydrogen and cesium standards which allow them to be termed 'primary frequency standards', relegating the rubidium standard to 'secondary' and the crystal oscillator to 'local' or 'tertiary'.

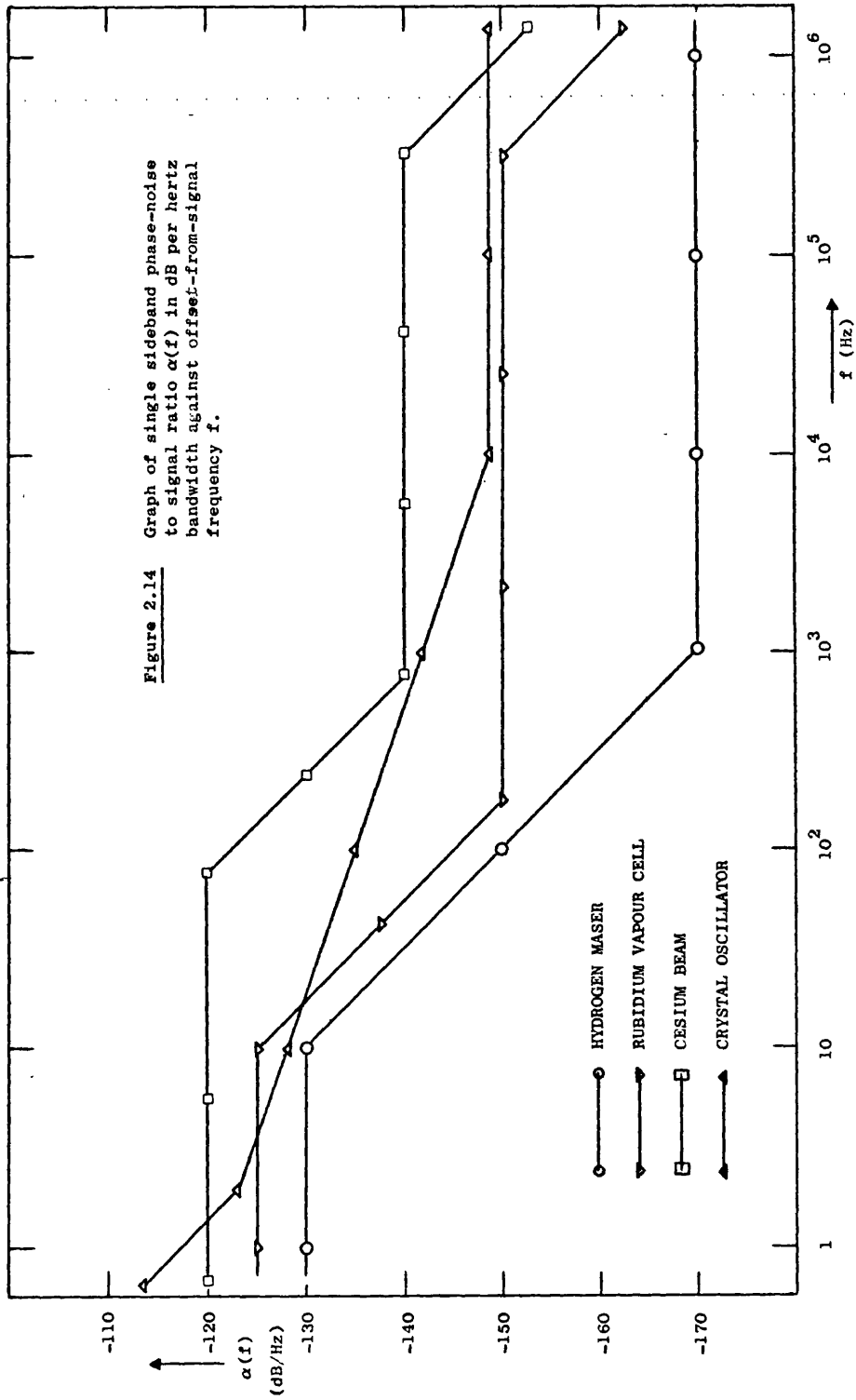
Typical asymptotic spectral density curves for the four sources are shown in Figure 2.13. Similar curves for frequency spectral density and fractional frequency spectral density may be obtained from this by consideration of equation (2.12). Figure 2.14 shows the single-sideband phase-noise-to-signal ratio plotted against Fourier frequency as measured in a 1Hz bandwidth, while Figure 2.15 shows the time domain stability parameter, the Allan variance  $\sigma_y^2(\tau)$ ,

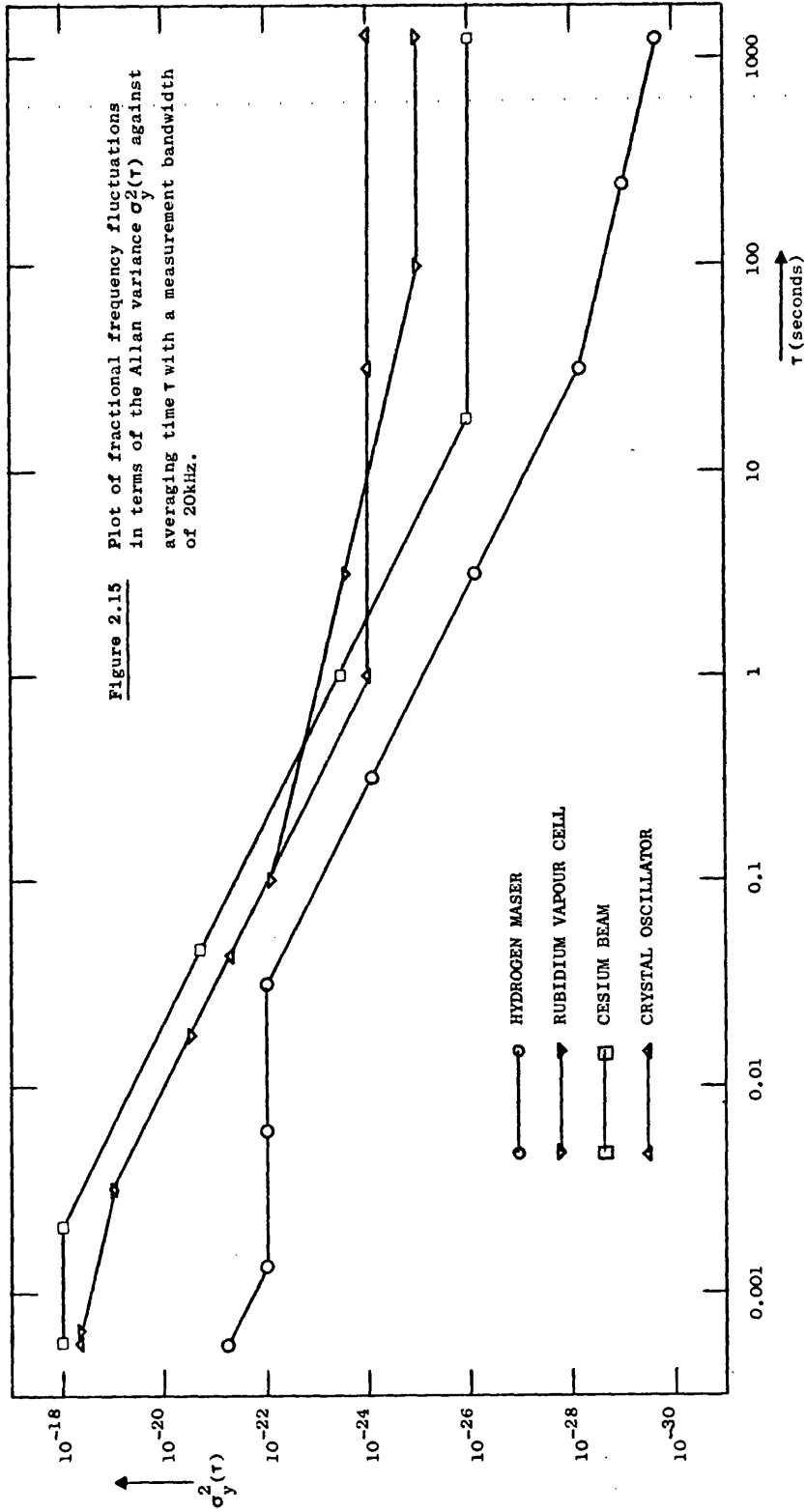
Characteristic	Hydrogen Maser	Cesium Beam Resonator	Rubidium Vapour Cell	Double Oven Crystal Osc.
Resonance Frequency	1420.405751MHz	9192.631770MHz	6834.682608MHz	5MHz
Resonance Width	1Hz	250Hz	200Hz	-
Atomic Interaction Time	0.5sec	$2.5 \times 10^{-3}$ sec	$2 \times 10^{-3}$ sec	-
Resonance Events	$10^{12}$ /sec	$10^6$ /sec	$10^{12}$ /sec	-
Frequency Offset due to: Magnetic Vibration* Collisions	$5 \times 10^{-13}$ typ. $4 \times 10^{-11}$ $2 \times 10^{-11}$	$1 \times 10^{-10}$ typ. $3 \times 10^{-13}$ none	$1 \times 10^{-9}$ typ. $8 \times 10^{-13}$ $3 \times 10^{-7}$	- $1 \times 10^{-8}$ -
State Selection	Hexapole Magnets	Multipole Magnets	Optical Pumping	-
Resonance Detection	(Active Maser)	Surface Ionisation	Optical Absorption	-
Temperature of Atoms	300°K	360°K	330°K	-
Intrinsic Reproducibility	$\pm 5 \times 10^{-13}$	$\pm 3 \times 10^{-12}$	does not apply	does not apply
Stability: (rms deviation) one second one minute one hour one day	$5 \times 10^{-13}$ $6 \times 10^{-14}$ $3 \times 10^{-14}$ $2 \times 10^{-14}$	$5 \times 10^{-11}$ $6 \times 10^{-12}$ $8 \times 10^{-13}$ $2 \times 10^{-13}$	$1 \times 10^{-11}$ $2 \times 10^{-12}$ $5 \times 10^{-12}$ $5 \times 10^{-12}$	$5 \times 10^{-12}$ $5 \times 10^{-12}$ $5 \times 10^{-12}$ $5 \times 10^{-12}$
Systematic Drift	None detectable ( $< 1 \times 10^{-12}$ /yr)	None detectable ( $< 3 \times 10^{-12}$ /yr)	Less than $3 \times 10^{-11}$ /mo.	About $1 \times 10^{-10}$ /day after 2 mo.
Power Consumption	200W	60W	40W	20W
Cost Factor	11.0	3.0	2.0	1.0

\* for  $\frac{dA}{dt} = 1.4 \times 10^{-13}/^{\circ}\text{K}$

Table 2.1







plotted against the averaging time  $\tau$ . The fluctuations shown in Figure 2.15 are the results of random processes only, any deterministic or environmental changes having been removed, where the data refers to a measurement bandwidth of 20kHz. It must be noted that only time domain data is presented for Fourier frequencies less than 0.1Hz, and that frequency domain data for Fourier frequencies less than 10Hz is highly subject to errors.



REFERENCES - Chapter 2

- (1) CUTLER, L.S., and SEARLE, C.L.: "Some aspects of the theory and measurement of frequency fluctuations in frequency standards", Proc. IEEE, Vol.54, No.2, February 1966, pp.136-54.
- (2) BARNES, J.A., CHI, A.R., CUTLER, L.S., HEALEY, D.J., LEESON, D.B., MCGUNIGAL, T.E., MULLEN, J.A., SMITH, W.L., SYDNOR, R.L., VESSOT, R.F.C., and WINKLER, G.: "Characterisation of frequency stability", IEEE Trans. Inst. Meas., Vol.IM-20, No.2, May 1971, pp.105-20.
- (3) HALFORD, D.: "Frequency and time stability", Proc. National Bureau of Standards Seminar, 1969.
- (4) BAGHDADY, E.J., LINCOLN, R.M., and NELIN, B.D.: "Short-term frequency stability: characterisation, theory, and measurement", Proc. IEEE, July 1965, pp.704-22.
- (5) ALLAN, D.W.: "Statistics of atomic frequency standards", Proc. IEEE, Vol.54, February 1966, pp.136-54.
- (6) GORDON, J., ZEIGER, H., and TOWNES, C.: "The maser - a new type of microwave amplifier, frequency standard, and spectrometer", Phys. Rev., Vol.99, August 1955, p.1264.
- (7) GORDON, J., ZEIGER, H., and TOWNES, C.: "Molecular microwave oscillator and new hyperfine structure in the microwave spectrum of  $\text{NH}_3$ ", Phys. Rev., Vol.95, July 1954, pp.282-4.
- (8) VESSOT, R., LEVINE, M., MUELLER, L., and BAKER, M.: "The design of an atomic hydrogen maser system for satellite experiments", Proc. 21st Annual Frequency Control Symp., Atlantic City, 1967, pp.512-42.

CHAPTER 3 - QUARTZ CRYSTALS AND OSCILLATORS

The piezoelectric effect, and particularly its predictable occurrence in quartz, has been employed in the control of resonators for nearly sixty years. The first record of the effect was by the Curies in 1880, though it was not until the first world war that the effect was put into practice as an underwater transducer and later in telephone microphones and ear pieces. In 1921 W G Cady<sup>(1)</sup> first described the use of a quartz plate to govern the resonant frequency of an oscillator feedback network. Cady's crystals were X cut and operated in the longitudinal mode at about 70kHz in almost exactly the manner in which modern low frequency crystals are used.

Today, millions of crystal controlled oscillators are employed throughout the world in applications which require frequency stabilities ranging from a few parts in  $10^9$  to less than 1%. If it were not for the action of quartz crystals the world communications network would be in chaos. The increasing congestion of the frequency spectrum leads to more elaborate communications systems utilising narrower channels and hence requiring correspondingly more stable frequency sources. Where time division multiplexing of existing channels is employed the crystal oscillator is still essential in accurately defining the time slots. Even the rapidly increasing use of the microprocessor, both in communications and an enormous range of other applications, depends on the action of a crystal controlled clock oscillator in every unit.

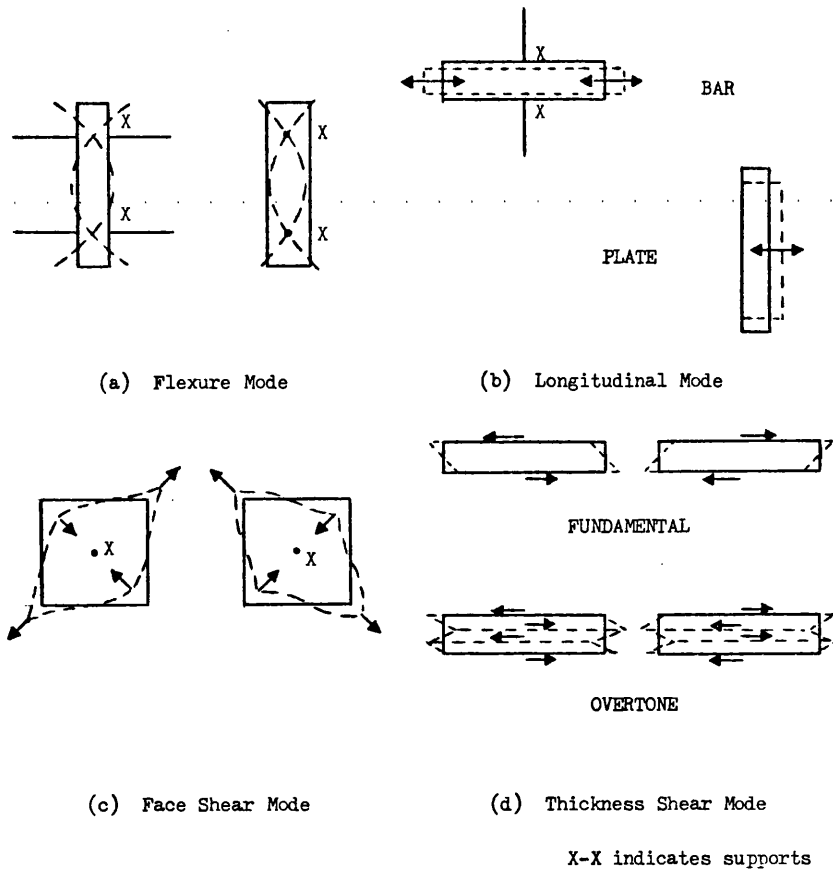
This chapter describes the general principles of quartz crystals, their use in controlling electronic oscillators and means by which the frequency stability of these oscillators may be optimised.

### 3.1 Quartz Crystal Units<sup>(2)</sup>

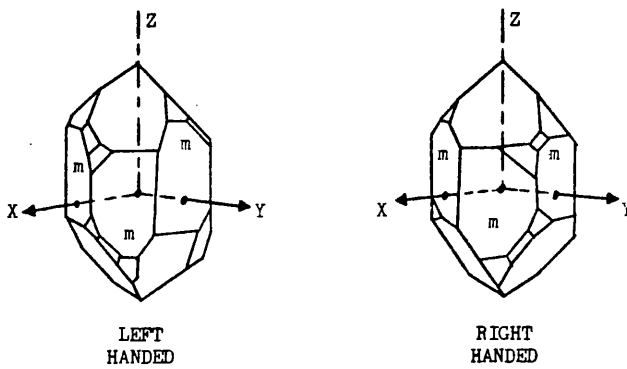
A piece of quartz may be constrained by the application of an electric field to vibrate in one or more of four modes of vibration. These are the torsional, flexure, longitudinal and shear modes. The torsional mode is not used due to the considerable difficulties encountered in its mounting, but all the other modes find uses in various applications.

Figure 3.1 illustrates the useful modes of vibration. The flexure mode is applicable to audio frequency oscillations, its commercial importance having increased rapidly in the last few years as a common control element for electronic clocks and wristwatches. The longitudinal (or extensional) mode is used at frequencies from the upper audio band to about 500kHz by utilising odd overtones of the fundamental resonance. The fundamental face shear mode is used from about 500kHz to 1MHz, though its use is uncommon as the same band is more easily covered by the fundamental thickness shear mode. The face shear mode may, however, be vibrated at its even overtones, leading to some special applications. The fundamental thickness shear mode operates from 500kHz to 20MHz, the third overtone thickness shear mode from 10MHz to about 50MHz and the fifth overtone thickness shear mode up to at least 130MHz.

The vibration mode employed in any given crystal application is dictated by the crystal cut, which is in turn governed by the required temperature coefficient and various other considerations. By far the most commonly used crystal type is the so-called AT cut plate operating in either the fundamental or overtone thickness shear mode and usually above 1MHz. The reasons for the popularity of this type are discussed in the following sections.



**Figure 3.1** The four useful modes of vibration of crystalline quartz



**Figure 3.2** Left Handed and Right Handed quartz

### 3.1.1 Crystal Cuts <sup>(3)</sup>

Natural quartz occurs in a left-handed and right-handed form as shown in Figure 3.2. Due consideration must be given to the 'hand' of the crystal in defining the customary crystallographic axes, but thereafter the cut of the crystal refers only to these axes. A section of the crystal taken perpendicular to all of the main faces (marked *m*) would appear as in Figure 3.3. The axes may now be defined as follows: firstly the Z axis or optic axis is that direction parallel to all of the main faces *m*, that is into the page of Figure 3.3. Secondly the Y axis or mechanical axis is that direction normal to the main faces of the crystal, *m*. Three such directions exist, therefore, and the conventional ordering of these axes uniquely defines the 'hand' of the crystal. Thirdly the X axis or electrical axis is that direction perpendicular to both the Z axis and the Y axis, three such axes existing, therefore.

The geometry of such a crystal section is worthy of note in that since there are three pairs of parallel sides, all the angles included by the faces are  $120^\circ$ . Since the Y axes are normal to the faces, the angle between adjacent Y axes is  $60^\circ$ , and since the X axes are perpendicular to the Y axes, each X axis bisects the angle formed by the other two Y axes. The X and Y axes therefore form a regular pattern in the plane of the Z axis as shown.

It is now possible to define the various cuts by reference to these axes. Three categories of cut are possible. On-axis cuts are those made such that the three dimensions of the plate lie directly along the X, Y and Z axes and are defined as follows: an X cut plate has its smallest dimension in the X axis, a Y cut plate has its smallest dimension in the Y axis and a Z cut plate has its smallest dimension in the Z axis. Singly inclined cuts are those which have

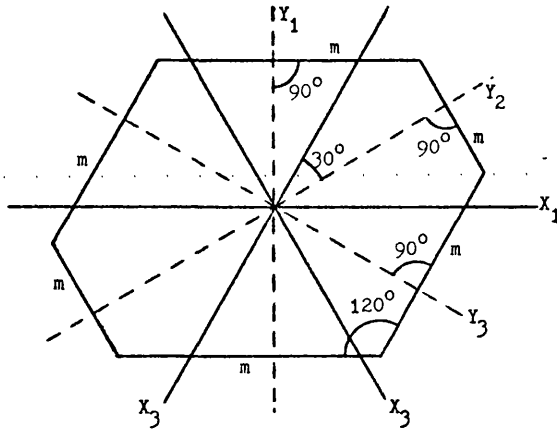


**Figure 3.3** Section through a quartz crystal perpendicular to all of the main faces m

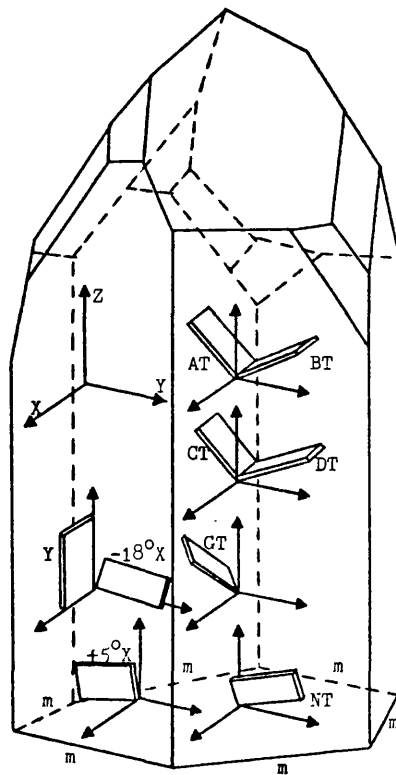


**Figure 3.4** Orientation of the various crystal cuts

their smallest dimension along a line in the X plane inclined to the Z axis by some angle. Doubly inclined cuts are those whose smallest dimension lies along none of the axes. The orientation of the various cuts is illustrated in Figure 3.4.

Though all the early crystal plates were on-axis cuts, these are no longer in common use. Early X cut crystals yielded temperature coefficients of more than ten parts per million per  $^{\circ}\text{C}$ , yet were still considered a great step forward in realisable stability. Y cut crystals display an even greater temperature coefficient of about 85 parts per million per  $^{\circ}\text{C}$ , though great use may be made of this fact as may be seen later. Z cut crystals are non-piezoelectric in normal modes of vibration.

By far the most common of modern crystals are the singly inclined cuts. These all resemble a Y cut plate rotated in the X plane to some defined angle from the Z axis, as illustrated in Figure 3.4. Within a given frequency range, it is found that as the angle of rotation changes the temperature coefficient of resonant frequency of the plate also changes. The nature of this change for high frequency crystals is shown in the graph of Figure 3.5, which shows that at rotations of  $-49^{\circ}$  and  $+35^{\circ}$  the temperature coefficient becomes zero. Similarly, Figure 3.6 shows that at low frequencies the temperature coefficient becomes zero at rotations of  $-52^{\circ}$  and  $+38^{\circ}$ . These four points of zero temperature coefficient specify the four optimal singly inclined crystal cuts, AT and BT for high frequencies and CT and DT for low frequencies. The operational differences between CT and DT cut plates are, in fact, minimal and most modern manufacturers produce only CT cuts. The choice between AT and BT cut plates for use at high frequencies must be made by consideration of their differing temperature coefficient

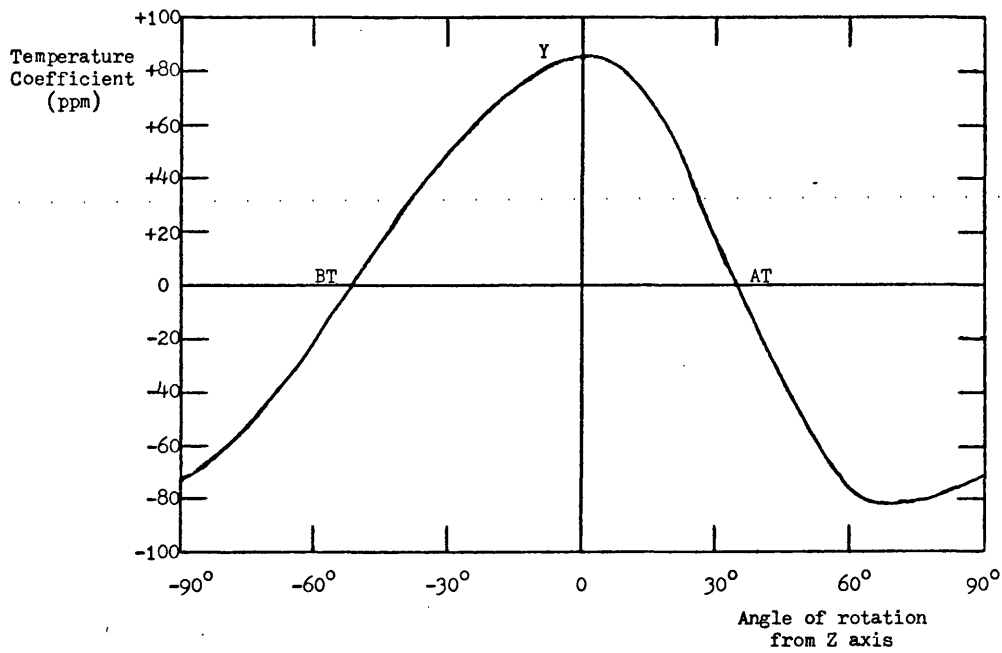


**Figure 3.5** Temperature coefficient of infinitely thin high frequency plates against angle of rotation

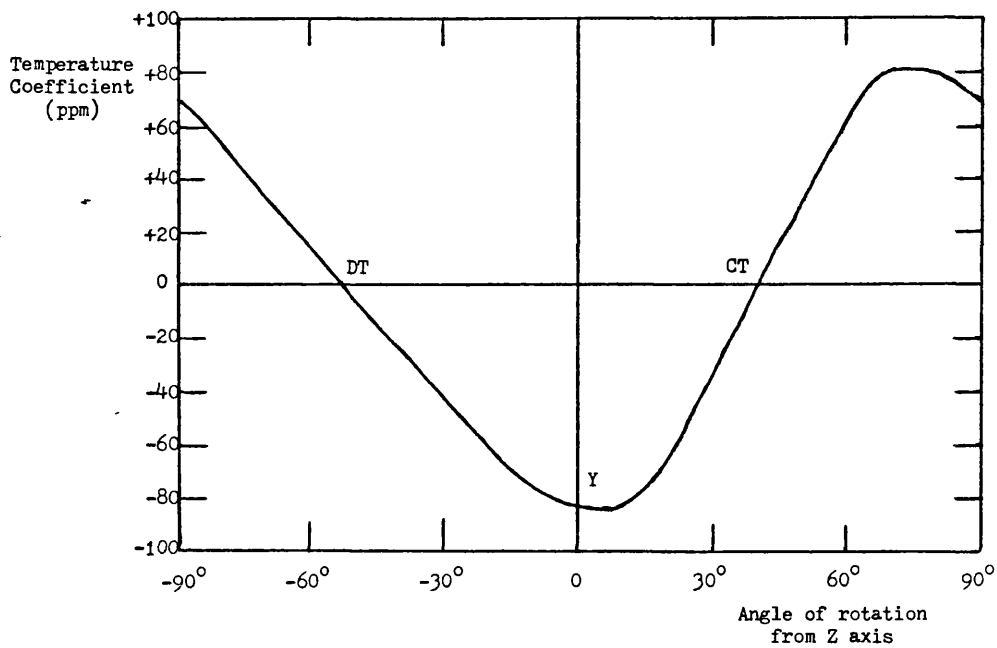


**Figure 3.6** Temperature coefficient of infinitely thin low frequency plates against angle of rotation



characteristics over a broad range, a question dealt with in section 3.1.3. Figure 3.7 summarises the on-axis and singly inclined cuts by reference to a section of the crystal in the X plane.

The doubly inclined crystal cuts GT and NT are shown in Figure 3.4. The NT cut is often used due to its high stability when operating at low frequencies in the flexural mode. By varying both the rotational angles and the dimensional aspect ratio such a plate may be assigned a variety of operating characteristics to meet special requirements. The GT cut is very similar to the CT cut crystal, the differences being that the GT is cut at  $+51^\circ$  to the Z axis and the orientation of the plate is further rotated  $45^\circ$  about the Y axis. By careful control of the plate dimensions, the mode of vibration is modified from the face shear mode of the CT cut, yielding a very stable unit of low to medium resonant frequency. The drawback with doubly inclined cuts is their increased difficulty of manufacture due to the extra rotational operation. In the past such units have found use only in very exacting applications and are currently very seldom employed, the use of high frequency plates now being possible in such cases by means of modern frequency division techniques. It must be noted at this point, however, that the various new strains of quartz crystal being developed to meet the far more stringent stability and environmental requirements of the future all rely upon doubly inclined cuts. Once the manufacturing difficulties are overcome there could well be an enormous increase in the importance of such cuts.

### 3.1.2 The Frequency Thickness Constant<sup>(4)</sup>

As the angle of rotation of a plate is changed it is found that not only does the temperature coefficient vary as in Figures 3.5 and

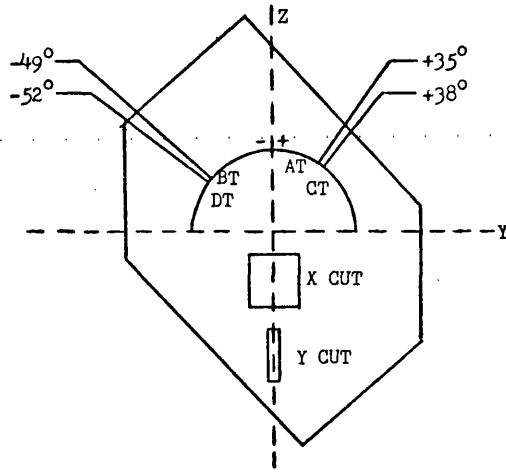


Figure 3.7 Summary of common on-axis and singly inclined crystal cuts

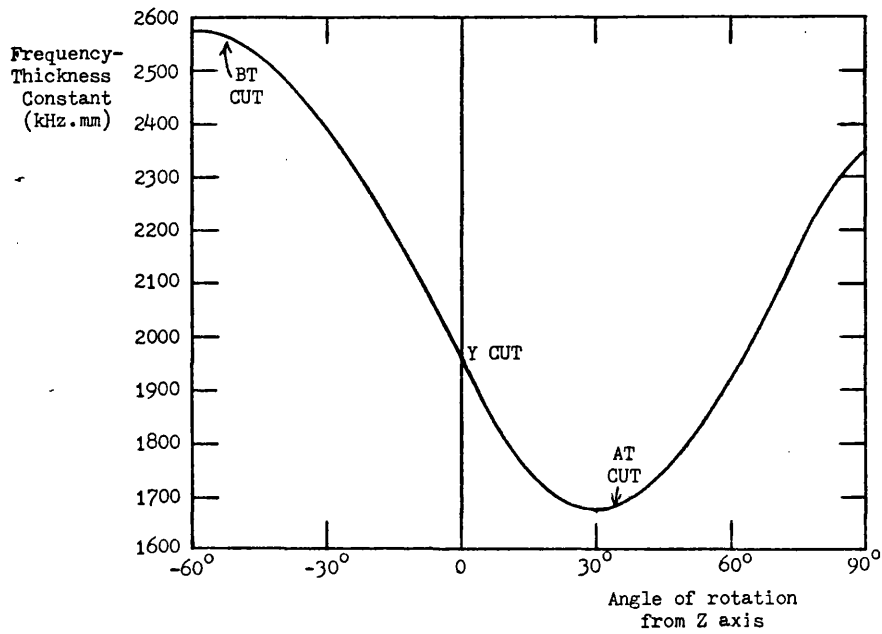


Figure 3.8 Graph of Frequency-Thickness Constant against angle of rotation for high-frequency plates

3.6, but also the relationship between the physical dimensions and the resonant frequency changes. The frequency thickness constant of any plate is defined as the resonant frequency in kilohertz of a similar plate of thickness 1mm. It is more practical, however, simply to write:

$$f_0 = \frac{K}{d} \text{ kHz} \quad (3.1)$$

where  $f_0$  is the resonant frequency in kHz,  $d$  is the thickness of the plate in millimetres and  $K$  is the frequency thickness constant.  $K$  has the dimensions of metres per second, which leads to the very confusing term "crystal velocity" which has been used in some texts.

The relationship between  $K$  and the angle of rotation of the plate is given in Figure 3.8. From this graph it may be seen that the value of  $K$  for the AT cut plate is 1670 (kHz.mm), for the BT cut plate is 2550 and for the Y cut plate is 1950.

### 3.1.3 Temperature Coefficient

In defining the singly inclined crystal cuts, the angles of rotation required to give zero temperature coefficient were considered. These angles apply, however, only to an infinitely thin plate. The finite value of frequency thickness constant discussed above indicates that unless the length and width of the plate are made very large, which is not practical from the point of view of production or use, the thickness cannot be negligible compared with its other dimensions. Practical crystals, therefore, have finite temperature coefficients over a range of temperatures, though points of zero temperature coefficient may still exist in their overall characteristic.

The frequency of any crystal plate may be expressed as a

function of temperature as follows:

$$f(T) = f_0 \left( 1 + a_1(T-T_0) + a_2(T-T_0)^2 + a_3(T-T_0)^3 \dots \right) \quad (3.2)$$

where  $T_0$  is some reference temperature at which the frequency is  $f_0$ , and  $a_1$ ,  $a_2$ ,  $a_3$ , etc are constants for any given sample. The different crystal cuts all exhibit different values for the constants, though three distinct types of temperature characteristic emerge.

It is found that in the on-axis X cut and Y cut plates the magnitude of  $a_1$  is quite large and the values of  $a_2$ ,  $a_3$ , etc extremely small, yielding the linear relationship:

$$f(T) = f_0 \left( 1 + a_1(T-T_0) \right) \quad (3.3)$$

In BT and CT cut plates the value of  $a_1$  and  $a_3$  is found to be negligible compared with  $a_2$ , yielding the parabolic relationship:

$$f(T) = f_0 \left( 1 + a_2(T-T_0)^2 \right) \quad (3.4)$$

The temperature coefficient may then be evaluated as a function of temperature:

$$\frac{df(T)}{dT} = 2a_2f_0(T-T_0) \quad (3.5)$$

so that only one point of zero temperature coefficient exists, at  $T = T_0$ . For this reason in BT and CT types  $T_0$  is known as the inflexion temperature or turnover point. The value of  $a_2$  is largely independent of the angle of cut, so that the shape of the temperature characteristic is fixed. As the angle of cut changes, however, the turnover point shifts as shown in Figure 3.9 so that the user may specify his operating temperature and obtain optimal stability at that point.

In AT cut plates  $a_2$  is negligible, giving the linear-plus-cubic relationship:

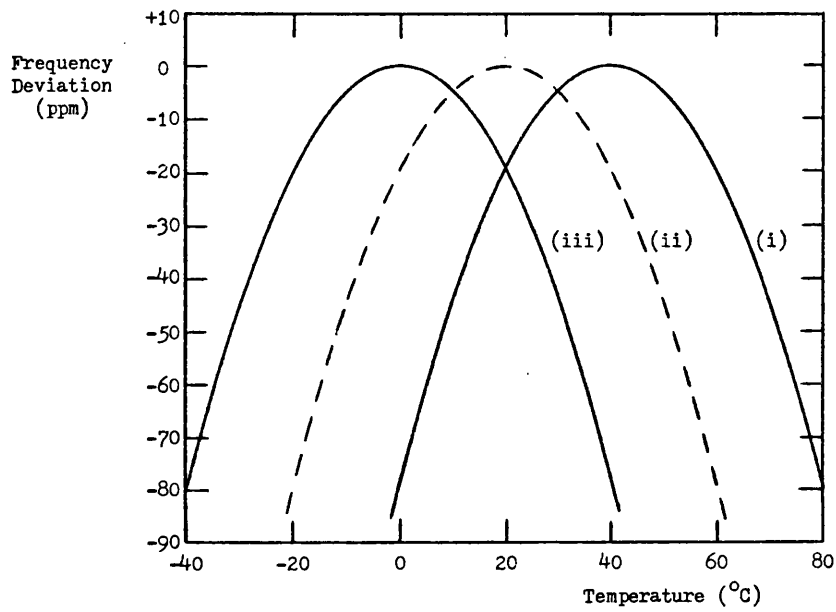


**Figure 3.9** Typical graph of frequency against temperature for BT and CT cut plates:

- (i) with high inflexion temperature
- (ii) with room temperature inflexion
- (iii) with low inflexion temperature

(axis data pertains to high frequency BT cut plates)

$$f(T) = f_0 \left( 1 + a_1(T-T_0) + a_3(T-T_0)^3 \right) \quad (3.6)$$

The temperature coefficient is then given by:

$$\frac{df(T)}{dT} = a_1 f_0 + 3a_3 f_0 (T-T_0)^2 \quad (3.7)$$

It is found that  $a_1$  is dependent on the angle of cut and may take both positive and negative values.  $a_3$ , however, is always positive and is independent of the cutting angle.

A study of equation (3.7) reveals that, since  $a_3$  is positive, points of zero temperature coefficient can only exist when  $a_1$  is negative, in which case they occur at temperatures:

$$T_{ZTC} = T_0 \pm \sqrt{\frac{|a_1|}{3a_3}} \quad (3.8)$$

Equations (3.6) to (3.8) then lead to the familiar family of curves characterising the temperature stability of AT cut plates shown in Figure 3.10. If  $a_1$  is negative and large, then a sigmoidal curve results as shown by curve (1). As  $a_1$  becomes less negative the points of zero temperature coefficient move inwards towards  $T_0$  as shown by curves (2), (3) and (4). At  $a_1 = 0$ , the two points of zero temperature coefficient converge on  $T_0$ , the overall curve becoming a cubic symmetrically distributed about  $T_0$  and  $f_0$ . As  $a_1$  becomes positive, no points of zero temperature coefficient exist and the curve tends to the linear case. For most applications angles of cut yielding curves in the region of (3) and (4) are preferred as these give the smallest total frequency excursion over a broad temperature range. If an operating temperature can be specified, however, then it is possible to select a crystal such that the temperature coefficient is zero at that temperature. Due consideration must also be given to the total required temperature range.

Figures 3.9 and 3.10 show typical values for the frequency

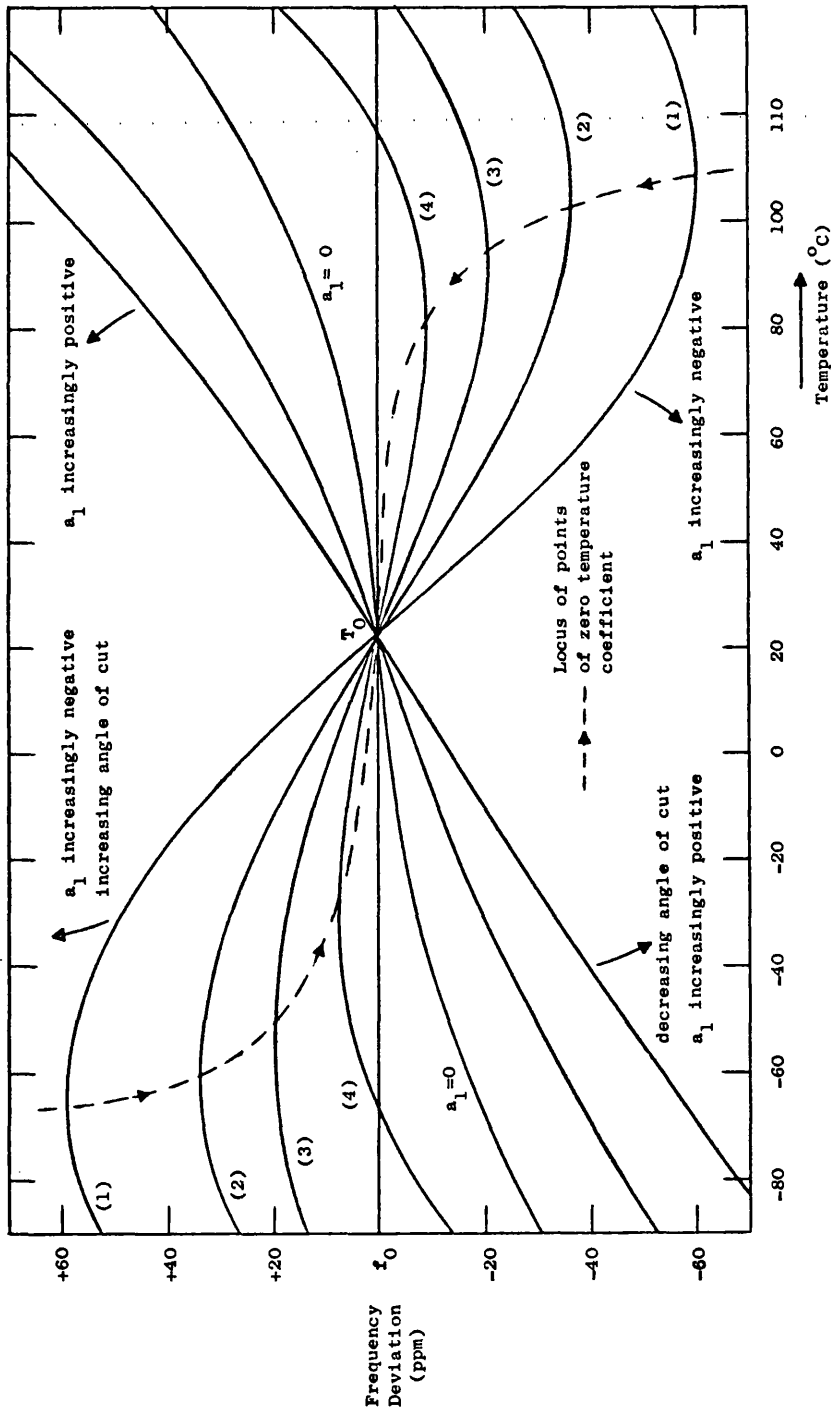


Figure 3.10 Typical graphs of frequency against temperature for AT cut crystals of various angles of cut.

deviation of high frequency plates operating in the fundamental thickness shear mode for BT and AT cut types respectively. Y cut plates operating in the same mode exhibit a linear temperature coefficient of 86 parts per million per degree Celcius.

#### 3.1.4 Crystal Aging

Ideally, if changes in the crystal resonant frequency due to temperature variations are eliminated by holding its temperature steady, a crystal controlled oscillator should maintain its calibrated frequency for all time. This, sadly, is not the case. Crystals fabricated in large quantities display a unidirectional frequency drift, generally known as aging, for the early period of their use. This aging drift tends to occur in two distinct phases. Firstly, during the initial three or four weeks of operation there is a rapid frequency change, often in the order of 1 part in  $10^8$  per day. Experimental data taken from crystals during this period shows that this early drift, usually known as stabilisation, follows an exponential relationship of the form<sup>(17)</sup>:

$$\Delta f/f = a + b \cdot \ln(1 + t/t_0) \quad (3.9)$$

where  $a$ ,  $b$  and  $t_0$  are independent constants. Secondly, when this initial stabilisation is over there is a continuing, approximately linear, frequency drift which, provided the exponential change of equation (3.9) nears completion, may produce changes of about 5 parts in  $10^{10}$  per month.

Attempts to explain these aging phenomena have progressed along various conflicting arguments for the last thirty years. By accepting that aging exists in modern crystals, it is possible to gather the accumulated findings of the published work and, though



not explain the aging, list the various techniques which may be employed to minimise its extent.

As a result of the enormous demand for crystals during wartime, continuing development had brought about the early plated units described by Sykes<sup>(6)</sup> in 1948. These units were fundamental thickness shear mode types having flat gold plated surfaces as electrodes. Overtone modes were avoided wherever possible as such units displayed adverse electrical properties. In 1952 in the first of a series of classical papers, Warner<sup>(7)</sup> described a technique of lapping the crystal plates to a planoconvex or biconvex shape which allowed the use of overtone modes without the adverse electrical properties found previously. High Q factors were obtained since the activity was constrained to the centre of the plate, leaving the edges of the crystal quiescent and eliminating the damping effect of the mounting posts. Because overtone mode plates are thicker than the equivalent fundamental mode type, any changes in the surface finish of the plate or electrodes has a smaller proportional effect upon the frequency determining dimension (in this case the thickness), which Warner reasoned should improve the aging rate. His experimental findings bore this out.

Later<sup>(8)</sup>, he attributed the observed aging to the transfer of mass, in the form of impurity atoms, to and from the surface of the crystal and its electrode, the source of the impurities being the metal holder. By using a carefully cleaned glass enclosure, optical polishing of the plate, and employing a high temperature vacuum bake prior to sealing he reduced the negative aging of 2 parts in  $10^6$  over the first month for the metal enclosed units to a positive aging of less than 1 part in  $10^7$  over the same period for the new units.

In an attempt to fabricate an extremely precise unit, Warner then devised a new mounting technique<sup>(9)</sup> which permitted the use of a large (30mm dia.) planoconvex plate operating on its nickel ribbon suspension in a hermetically sealed glass enclosure. High temperature vacuum baking was employed leading to an aging of about 1 part in  $10^8$  over the first 5 months, falling to less than 2 parts in  $10^9$  per month thereafter. Strangely, such units were shown to follow an exponential law for several years.

The tendency for changes in crystal processing to bring about changes in the direction of aging suggested that effects other than mass adsorption were coming into play. In 1963<sup>(10)</sup>, Warner assigned the observed positive aging tendency to the relief of thermally induced stresses at the quartz-gold interface. In successful designs this effect balanced the negative aging due to mass transfer. This explained the results obtained by some manufacturers who had tried high temperature baking of good existing crystal designs in an attempt to reduce the aging still further, and had in fact made the aging rates rather worse, though in the opposite direction. To combat the stress effects, the use of parallel field excitation was proposed as outlined previously by Bechmann<sup>(11)</sup>, the advantage being that the centre of the plate in such a unit was not plated with an electrode so that the stress was alleviated in the region of maximum crystal activity. The recovery of such crystals from the effects of thermal transients was considerably improved, overtone mode conventional types being particularly poor in this respect, and it was shown that the best aging was displayed by crystals having the coolest thermal history, the lowest operational temperature and the lowest drive power.

Various other effects contributing to aging were described

concentrating on defects in the quartz itself<sup>(12),(13)</sup>, leading to a fundamental study of the effects of various impurities by the kinetic theory of rate processes, establishing the exponential nature of not only the mass transfer but also the thermal recovery effects.

By 1966, Belser and Hicklin<sup>(15)</sup> had experimented with plates having annular aluminium electrodes which were thermocompression bonded to the mount. This combination allowed very high temperature baking, there being no solder to melt and no electrode over the active portion of the plate to induce thermal stress. By varying the ratio of external to internal radii of the electrode annulus, optimum designs giving aging rates less than 1 part in  $10^9$  per week were achieved by techniques suitable for mass production. At about the same time Armstrong<sup>(16)</sup> had been experimenting with variations on the conditions of baking, concentrating on maintaining an oil-free environment and employing two high temperature bakes, the first in dry hydrogen and the second in high vacuum, to accelerate the mass transfer process. Using these techniques, together with thermocompression bonding and hermetic sealing of the enclosure, units were developed by 1968<sup>(17)</sup> displaying aging rates of less than 3 parts in  $10^{10}$  per month after only 10 days. These units also achieved vastly improved response to thermal transients and were readily mass produced.

To summarise, the resonant frequency of quartz crystal plates changes during their early life, tending to some steady-state drift rate according to an exponential law. The drift appears to be caused mainly by an adsorption or desorption of impurity elements at the quartz and electrode surface, to a lesser extent by the relief of thermal disturbances at the quartz-electrode interface, and possibly

to some small extent to irregularities of the crystal lattice. These effects are combatted firstly by rigorous cleaning and polishing of the crystal and its enclosure to reduce the impurities present and the effective surface area over which they may be adsorbed.

Secondly, the rate of mass transfer may be accelerated by high temperature vacuum or dry hydrogen baking (or both) prior to hermetic sealing, effectively accelerating the early aging process. Such techniques require special solder-free mounting processes, and often give rise to even greater drift due to relaxation of thermal stress. This thermal stress effect may be reduced by employing annular electrodes or alternative vibration modes to eliminate the presence of plated electrode at the active region of the plate.

Commercially available crystals never employ all of the above refinements in their construction or processing. Satisfactory aging performance is obtained from units produced by the million by rather more practical and less time consuming techniques. Thermocompression bonding is seldom used, sprung wire mounts and silver-loaded epoxy cement serving as a workable alternative. Careful cleaning techniques, very high vacua and hermetic sealing are employed to advantage. Baking in vacuo prior to sealing is a very expensive process in large numbers and is often replaced by a longer-term warm annealing after sealing. In this way the most extreme portion of the aging is passed prior to dispatch. Large scale users of crystals often store their units in hot cupboards for as long as possible before use. Most manufacturers agree that the lowest aging rates are obtained from fifth overtone AT cut plates operating at about 5MHz, probably because the various aging effects tend to cancel out. Higher stability glass encapsulated units are also available, though their use is limited to temperature controlled environments and they

are too delicate for most portable equipment. A typical manufacturer's specification for the type of crystal considered in this work is given in section 3.1.6.

### 3.1.5 Crystal Electrodes and Enclosures

It is clear from a consideration of the various modes of vibration employed in crystal plates that different mounts must be employed for each. Only those techniques applicable to high frequency thickness shear types will be discussed here, details and illustrations of other mounts being obtainable from references (3) and (5).

Before the second world war, high frequency quartz plates were excited by means of two flat steel electrodes between which the quartz was sandwiched in such a way that the electrodes were close to, but not in contact with, the quartz. Such a mount is illustrated in reference (6). If the electrodes had been placed in contact with the quartz, the  $Q$  of the resonator so formed would be very low due to the high electrode mass. During the war, due mainly to the massive demand, a means of crystal unit assembly which took less time, skill and materials was needed, and the result was the plated unit. Such units were first described by Sykes<sup>(6)</sup> in 1949 and the electrode pattern used then is still the most commonly used today. It consists simply of two "keyhole" shaped areas of vacuum deposited gold, arranged on either side of the plate such that the tails reach the edge of the plate diametrically opposite one another as shown in Figure 3.11. The plate is then mounted in a holder such as that of Figure 3.12 so that the two electrode tails are clipped into the sprung ends of the supports and cemented in place as shown in the photograph of Figure 3.13.

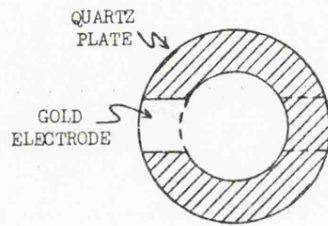


Figure 3.11 A plated quartz crystal unit

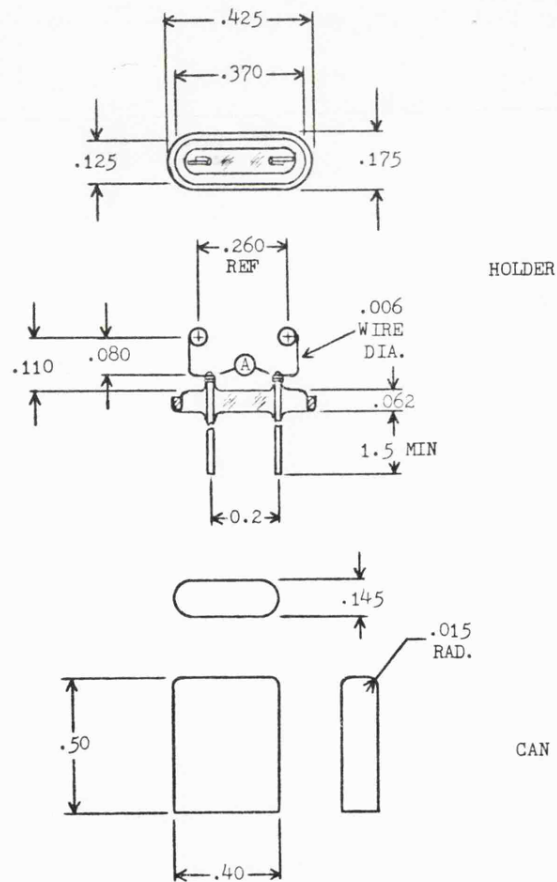


Figure 3.12 A typical crystal holder and can (HC 18/U)  
(dimensions in inches)

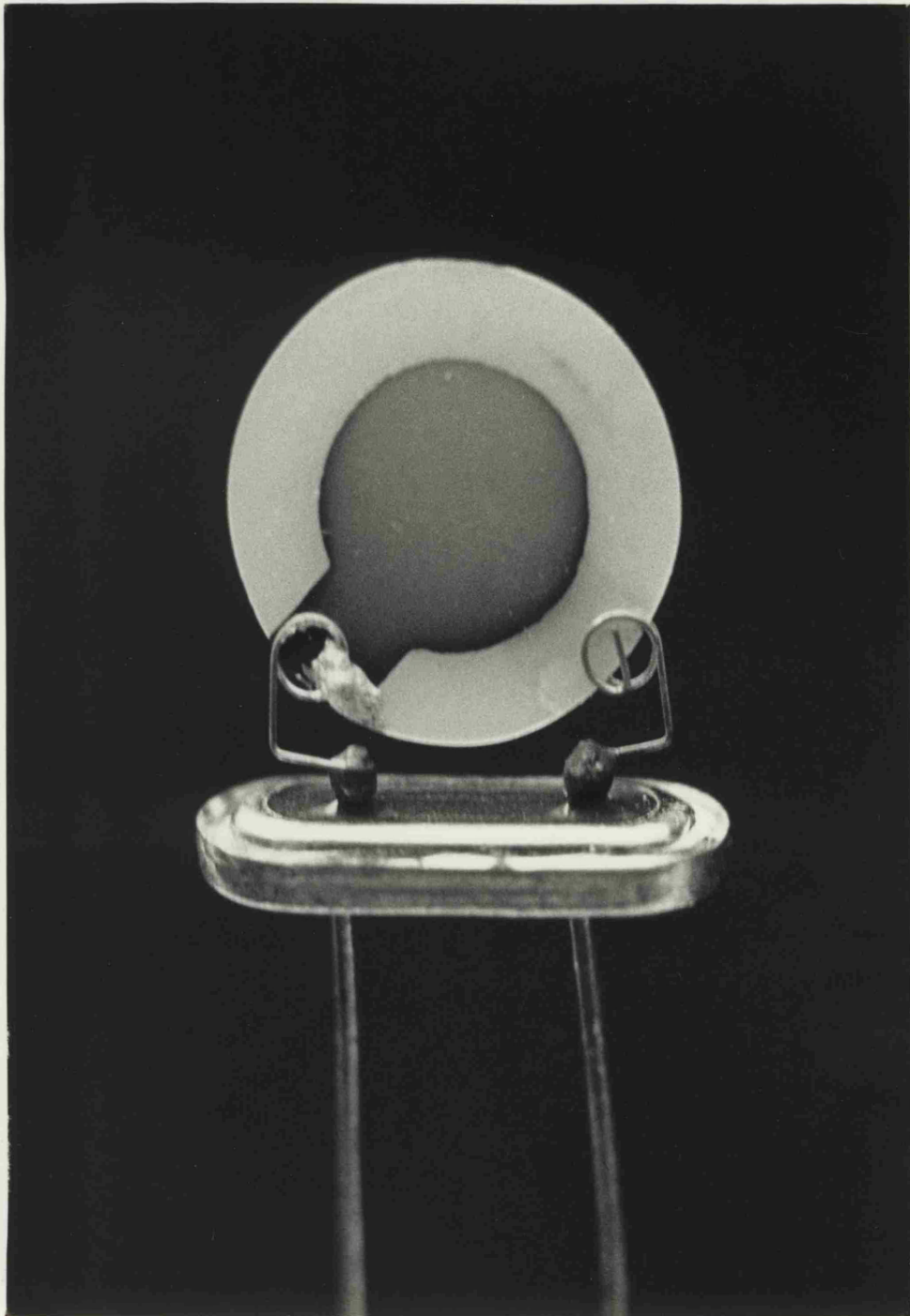


Figure 3.13 Photograph of a typical crystal plate mounted in a HC 18/U holder (enlarged to approximately eight times full size)

The mass of these plated electrodes, though not sufficient to reduce the resonator Q inordinately, does have the effect of reducing the resonant frequency below that of the quartz in isolation. This fact was turned to the advantage of the designers by employing a mass-loading technique for final frequency adjustment. The plates are lapped to a thickness which is known empirically to give a resonant frequency rather higher than that required when plated to a standard electrode thickness, all the units being plated thus in large batches. After mounting, but before sealing, each unit is individually tested in a vacuum and more gold is deposited onto the electrodes until the resonant frequency is adjusted to that required. The cover is then fixed, the unit evacuated (the air often being replaced by a Noble gas) and sealed by solder or cold welding.

In order to obtain the optimum aging rate for a given crystal, manufacturers often vary the procedure slightly (as defined in the previous section), but the basic mounting concept is the same for all mass produced crystals. The HC 18/U mounts shown in Figure 3.12 are mass produced by machine and are found in practice to be held to much closer tolerances than those indicated, the only significant variable being the amount of solder present at the points marked A.

### 3.1.6 Typical Manufacturer's Specification

- |                          |                                             |
|--------------------------|---------------------------------------------|
| (a) Operating frequency  | 10MHz $\pm$ 20ppm (or $\pm$ 10ppm to order) |
| (b) Mode of vibration    | fundamental thickness shear                 |
| (c) Load capacitance     | 30pF                                        |
| (d) Holder type          | HC 18/U (style J)                           |
| (e) Drive level          | 5mW maximum                                 |
| (f) Frequency shift with |                                             |

temperature

(continued overleaf...)



Temperature range	Frequency shift (ppm)	
	Normal tolerance	Close tolerance
-20 to +70°C	± 25	± 10
-40 to +70°C	± 30	± 20
-55 to +90°C	± 40	± 25
-55 to +105°C	± 40	± 25

### 3.2 Crystal Oscillators

In practice, any crystal resonator as described in the previous section may be employed as a circuit element without any knowledge of its operational mechanism or construction, provided that the manufacturer's specification is completely observed. This is accomplished by means of the electrical equivalent circuit, which is a valid model of the crystal in the region of its resonant operation and leads to straightforward design procedures for configurations of oscillator offering various advantages and disadvantages.

#### 3.2.1 The Equivalent Circuit

Though the transmission line equivalent of a quartz crystal finds applications in crystal-filter design<sup>(18)</sup>, the most useful equivalent circuit for oscillators is the Butterworth-Van Dyke equivalent of Figure 3.14<sup>(19)</sup>. The inductor  $L_1$  is a function of the mass of the quartz plate, the capacitor  $C_1$  is associated with its stiffness, and  $R_1$  represents the loss in the quartz and the mounting structure. This series trio is known as the motional arm of the equivalent circuit. The capacitor  $C_0$  represents the sum of the interelectrode capacitance and the capacitance between the lead-

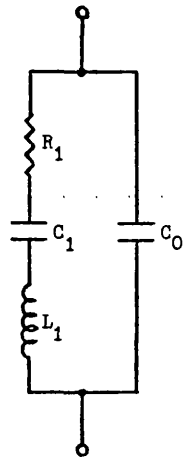


Figure 3.14 The Butterworth-Van Dyke equivalent of a quartz resonator

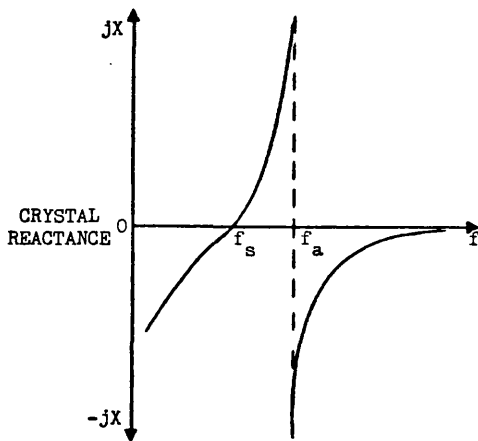


Figure 3.15 Plot of reactance against frequency for a crystal

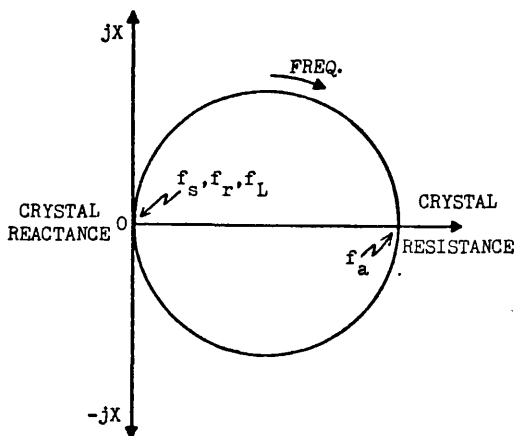


Figure 3.16 Plot of reactance against resistance for a crystal

wires of the mount. Plots of the reactance of the crystal against frequency and against resistance are shown in Figures 3.15 and 3.16. More detailed versions of these plots in the region of zero resistance are given in Figures 3.17 and 3.18.

A detailed analysis of the equivalent circuit, both in isolation and with a known load capacitance is included in Appendix A, the most important results of which are now given. In Figures 3.15 to 3.18 four important frequencies are marked, the first of these being  $f_s$ . This is the frequency at which the crystal is series resonant, and is given by

$$f_s = \frac{1}{2\pi} \left( \frac{1}{L_1 C_1} \right)^{\frac{1}{2}} \quad (3.10)$$

The second point,  $f_r$ , represents the frequency at which the crystal appears purely resistive and differs from  $f_s$  only due to the presence of  $C_0$ , and for practical crystals may be considered equal to  $f_s$ . The third point,  $f_L$ , is the frequency at which the crystal is antiresonant with an external load capacitance  $C_L$ , and if  $\Delta f$  is the frequency shift ( $f_L - f_s$ ) then

$$\frac{\Delta f}{f_s} = \frac{C_1}{2(C_0 + C_L)} \quad (3.11)$$

The point labelled  $f_a$  is the antiresonant frequency of the crystal with its own holder capacitance  $C_0$ , and may be obtained by putting  $C_L = 0$  in equation (3.11) and noting that  $f_L = (f_s + \Delta f)$ , so that

$$f_a = f_s \left[ 1 + \frac{C_1}{2C_0} \right] \quad (3.12)$$

It is also shown in Appendix A that the equivalent resistance of the crystal,  $R_e$ , in the region between  $f_s$  and  $f_a$  is given by

$$R_e = R_1 \left[ \frac{C_L + C_0}{C_L} \right]^2 \quad (3.13)$$

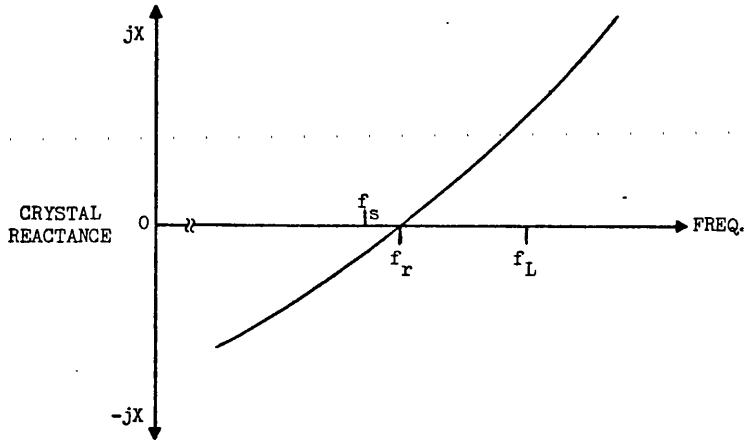


Figure 3.17 Enlarged portion of Figure 3.15 in the region of low crystal reactance

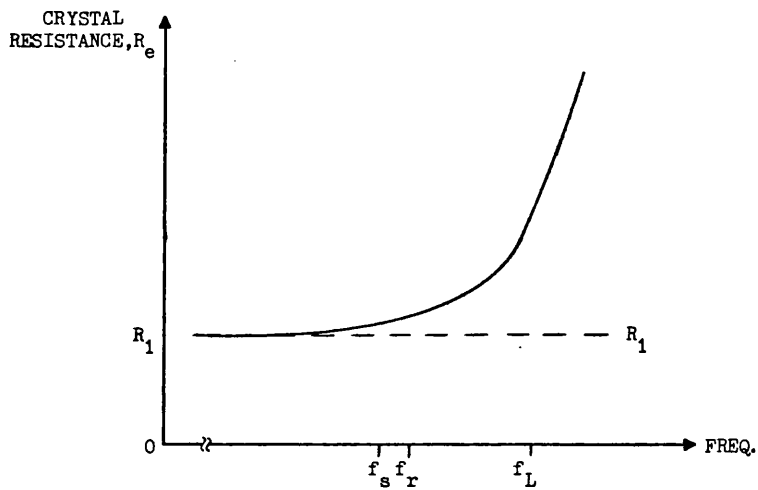


Figure 3.18 Graph of crystal resistance against frequency in the region of series resonance

In normal use, crystals are operated between their series resonant frequency and antiresonant frequency so that the crystal reactance is either zero or inductive. In the specification of a crystal for use at some particular frequency it is necessary, therefore, to specify the intended load capacitance.

Typical values for the elements of the equivalent circuit of a 10MHz fundamental mode AT cut crystal are given in Table 3.1.

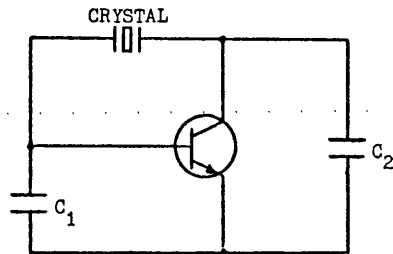
Parameter	Value
$R_1$	$30\Omega$
$L_1$	50mH
$C_1$	0.005pF
$C_0$	5pF
$C_L$	30pF
Q	$10^5$

Table 3.1

### 3.2.2 Oscillator Circuits

A detailed discussion of the various circuit configurations applicable to crystal oscillators will not be included here; rather their general types will be described and their relative merits itemised. For a detailed treatment the reader is referred to references (20) and (21).

The majority of crystal oscillators currently in use are of either the Pierce, Colpitts or Clapp (sometimes called Clapp-Gouriet) types. All three may be represented by the circuit of Figure 3.19. If the signal ground is placed at the emitter of the



**Figure 3.19** General configuration of the Pierce, Colpitts, and Clapp Oscillators

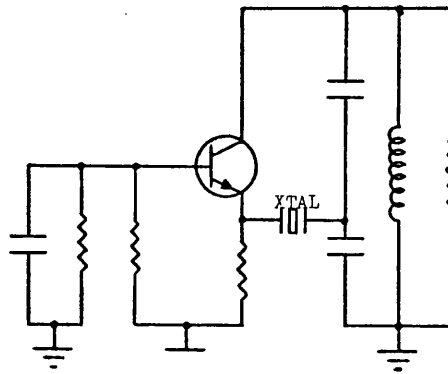


**Figure 3.20** Basic configuration of the Grounded-Base Oscillator

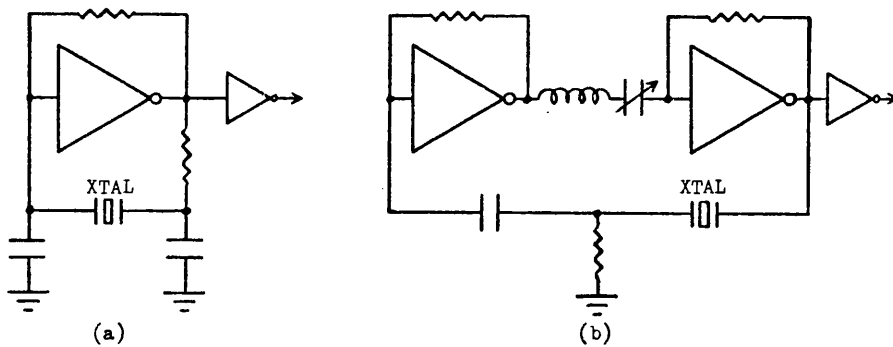


**Figure 3.21** Single-Gate and Dual-Gate Oscillators

transistor, the Pierce circuit results; if placed at the collector, the Colpitts circuit results; and the Clapp circuit has its signal ground at the base. Despite their apparent similarity, the three configurations perform quite differently, the Pierce circuit tending to be better than the others at lower frequencies and the Clapp offering advantages at higher frequencies. The fact that the crystal may not be grounded at either terminal often biases the choice of circuit against the Pierce, whilst the poor efficiency of the Clapp may also pose problems. Though it has definite weaknesses at its extremes of operation, the Colpitts circuit is by far the most popular with designers because of its simplicity of design and proven reliability.

It is possible to modify the Pierce circuit for the operation of crystals at their series resonant frequency by use of an inductor in series with the crystal. The so-called Impedance Inverting Pierce circuit has the advantage that the general level of circuit impedances is higher so that the available amplifier gain is greater, improving power output and efficiency. It is, however, prone to free-running.

The basic configuration of the Grounded-Base oscillator is shown in Figure 3.20. The circuit is used at high frequencies, where it exhibits relatively high efficiency and power output. It is impractical in applications where the circuit stray reactances are large or variable, and is quite difficult to design.

Gate oscillators such as those of Figure 3.21(a) and (b) have become very common in recent years, particularly for use as microprocessor clocks. They have the advantage of being immediately compatible with their logic system in terms of signal waveform and loading, and for this reason gates are often provided for use as

oscillators on specialised MSI logic circuits such as divider chains and phase locked loops. Their overall frequency stability is, in fact, rather low, though is usually adequate for logic systems and their power consumption, particularly when CMOS inverters are used, is very small indeed. Design of such oscillators is usually an empirical process using the information furnished by the gate manufacturers, such as that of reference (22).

Monolithic crystal oscillator maintaining circuits are available which utilise one of the above configurations with various modifications such as AGC, reactance compensation circuits and high current-drive buffer amplifiers. Details of one such circuit which is capable of excellent frequency stability at very low crystal drive power may be found in reference (23). In general, however, each design must be taken on its own merits as there are also poor types available. The integration of the oscillator components onto one chip finds particular use in the fabrication of hybrid crystal oscillators in which the oscillator and crystal are hermetically sealed together into a particularly compact package.

The salient points of this short description of the various types of crystal oscillators are condensed into Table 3.2 overleaf.

The amplifier stages in all of the oscillators may be realised using bipolar transistors, though the use of field-effect transistors (notably dual-gate MOSFETS) in applications up to about 30MHz are growing in popularity due to their high frequency stability, low noise and high efficiency<sup>(24)</sup>. In gate oscillators, wherever a choice is possible and the frequency will allow, CMOS gates offer considerable advantages, though above 7 or 8MHz TTL becomes necessary and above 50MHz ECL is probably best.

It will be shown later on in Chapter 5 that for application in



Oscillator Type	Frequency Range	Frequency Stability	Power Output	Waveform	Susceptibility To Stray Reactance	Bandwidth	Ease Of Design
Pierce	100kHz to 20MHz	High	Mod	Fair	Very Low	High	Simple
Colpitts	1MHz to 20MHz	Mod	Mod	Good	Low	High	Moderate
Clapp	2MHz to 20MHz	Mod	Mod	Good	Low	High	Moderate
Impedance-Inverting Pierce	20MHz to 75MHz	High	Low	Very Good	Fair	Low	Difficult
Grounded-Base	20MHz to 150MHz	Mod	High	Square	Low	High	Empirical

Table 3.2

the proposed system the oscillator configuration employed is not important provided that its frequency stability is good. For this reason it was decided to adopt the Colpitts type of Figure 3.22. This circuit has been used by the Racal group in high stability applications for a number of years and offers proven reliability, ease of construction and a good output without the need for any specialised components. It is quite easily buffered to comply with the requirements of various logic systems, and is suitable for use with high-precision crystals operating in parallel resonance with a series load capacitance of nominally 30pF.

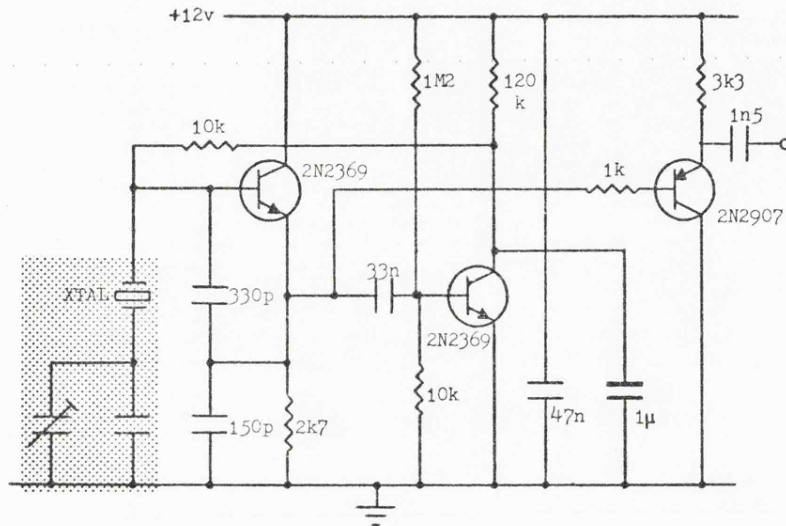


Figure 3.22 The Colpitts oscillator used in the prototype

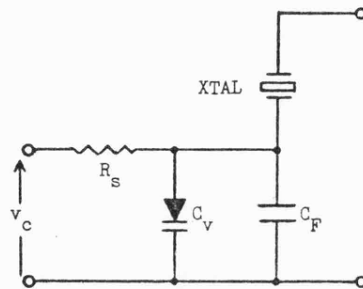


Figure 3.23 Voltage variable load capacitance for the VCXO version of the circuit of Figure 3.22

### 3.2.3 Voltage Control of Crystal Oscillators

It may be seen from Figure 3.15 that the total possible range of operation of a given crystal is that between the series resonant and antiresonant frequencies. Substituting  $\Delta f = f_L - f_s$  in equation (3.11) yields

$$f_L = f_s \left( 1 + \frac{C_1}{2(C_0 + C_L)} \right) \quad (3.14)$$

from which it may be seen that the resonant frequency of any crystal is a function of the load capacitance  $C_L$ . If  $C_L$  is infinite, then  $f_L = f_s$ ; if  $C_L$  is zero, then by reference to equation (3.12),  $f_L = f_a$ . This fact is made use of in most oscillators to afford a fine-trim facility, but further use may be found by making the load capacitance voltage variable by means of a varactor diode. In practice, the range of such a voltage controlled crystal oscillator (VCXO) is considerably less than  $(f_a - f_s)$  because the load capacitance may not vary excessively from the rated value without bringing about unacceptable changes in the crystal drive power and Q factor. At 10MHz, however, pulling ranges of up to 5kHz are possible without unduly affecting performance. Techniques have been described<sup>(25)</sup> for extending the frequency range of VCXOs beyond  $(f_a - f_s)$ , though such measures are found not to be required here. An excellent treatment of the design considerations of VCXOs is given in reference (26).

An added advantage of the use of the oscillator of Figure 3.22 in this work is that it may easily be voltage controlled by replacing the load capacitance pair shown in the shaded box by a voltage-variable version as shown in Figure 3.23. A dc block is provided by the crystal itself so that the varactor current has no

effect on the oscillator bias conditions. Choice of the values of  $C_F$  and  $C_V$  are discussed later, consideration being given to other possible performance defects of the VCXO as they arise.

### 3.3 Oven Control

The change in resonant frequency of a quartz crystal with temperature is the dominant source of frequency instability. The simplest means by which this may be reduced is to attempt to maintain the crystal at a constant temperature. This is difficult to achieve at room temperature, since a means of both warming and cooling the crystal is required. For this reason the crystal is usually held in an ovened enclosure at some constant elevated temperature, equal to (or a little above) the highest possible ambient temperature. The oscillator maintaining circuitry and reactance controller are usually included inside the oven to eliminate frequency changes with their temperature.

The early versions of crystal ovens operated by means of heater elements being switched in and out of circuit by temperature sensors such as bimetallic strip switches. Such ovens were unsatisfactory as they exhibited considerable hysteresis so that the temperature continually drifted up and down, causing a corresponding fluctuation in frequency. Modern ovens, however, utilise proportional feedback control of temperature using thermistors as sensors and power transistors to control the heater. In many cases the power transistor itself acts as the heating element. Proportionally controlled ovens are capable of governing the temperature of the crystal and oscillator to within  $\pm 0.1^\circ\text{C}$  over a temperature range of  $-55^\circ\text{C}$  to  $+75^\circ\text{C}$ , resulting in a frequency stability in the order of one part in  $10^8$ . The use of a second oven affords even more accurate

temperature control and such units are capable of frequency stabilities up to a part in  $10^{10}$ .

Crystal ovens have several disadvantages which make them inappropriate in many applications. Firstly, their power requirement is usually quite large, typically 10W at switch-on, making them undesirable for portable equipment. Their volume, too, is often greater than would be desired for such equipment. They exhibit a warm-up period extending to several minutes whilst the oven temperature stabilises. This dictates that the equipment may not be switched on and off for short periods without frequency errors occurring. It is often necessary for the oven to be kept on continually in a stand-by mode. The high temperature of operation of the crystal within an oven tends to accelerate its aging rate. As was described in section 3.1.4, crystals age fastest in the early part of their life so that it is usually necessary to allow this aging to proceed as far as possible before using the ovened oscillator. This entails long soak periods after manufacture before final calibration of the unit and dispatch, increasing production costs. Further, whilst the cost of most electronic components reduces due to economies of scale and the use of new processes, the cost of crystal ovens continues to rise with that of raw materials and manpower.

Despite these drawbacks, where the frequency stability requirements dictate there is currently no substitute for an oven controlled crystal oscillator at a comparable price.

### 3.4 Temperature Compensation

In applications where an oven controlled crystal oscillator may not be used, yet where the frequency stability of an isolated

crystal cannot meet the requirements it is necessary to perform some type of temperature compensation. All currently employed compensation schemes may be represented by the general schematic diagram of Figure 3.24. The temperature of the crystal is measured by one or more temperature transducers, the outputs of which are fed into a functional stage whose transfer function  $G(T)$  is such that its output, when fed forward to a frequency controlling input to the oscillator, produces an effect opposing that due to the temperature change.

In modern compensated oscillators the temperature sensing is performed by means of semiconductor thermistors bonded to the crystal. The frequency control of the oscillator is performed by voltage control of a varactor load. Various techniques are employed, however, to convert the thermistor output to the required varactor input and these are discussed briefly below. For a full treatment of methods of temperature compensation the reader is referred to reference (27).

#### 3.4.1 Analogue Temperature Compensation

Equation (3.6) shows the frequency of an AT cut crystal depends upon temperature according to a linear-plus-cubic relationship. In practical oscillators, however, other temperature effects on the oscillator usually introduce a significant degree of square-law dependence so that the frequency-temperature relationship becomes

$$f(T) = f_0 \left( 1 + a_1(T-T_0) + a_2(T-T_0)^2 + a_3(T-T_0)^3 \right) \quad (3.15)$$

where  $f_0$  is the frequency at temperature  $T_0$  and  $a_1, a_2, a_3$  are constants for any given crystal sample. Clearly, the required compensating voltage to be applied to the frequency control input of

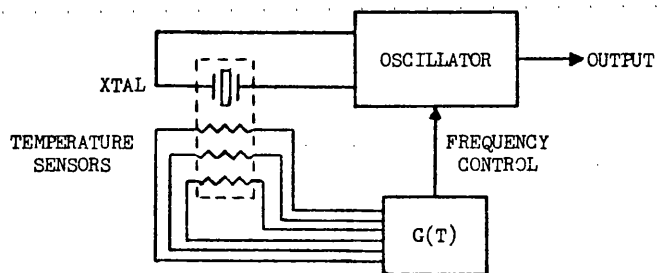


**Figure 3.24** General configuration of a temperature compensation scheme

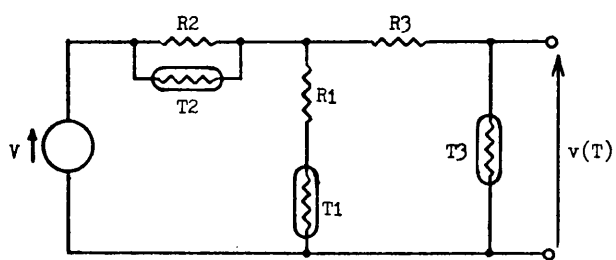


**Figure 3.25** A three-stage thermistor network

the oscillator must also be cubic in nature, being represented generally by

$$v(T) = v_0 \left( 1 + b_1(T-T_0) + b_2(T-T_0)^2 + b_3(T-T_0)^3 \right) \quad (3.16)$$

where  $v_0$  is the voltage required to give the correct output frequency at temperature  $T_0$  and  $b_1$ ,  $b_2$ ,  $b_3$  are constants for the given crystal.

One network which may be used to generate such a voltage is shown in Figure 3.25. By careful choice of the thermistor exponents and resistor values it is possible to arrange the temperature characteristic of the network to resemble closely that of the given crystal over a broad temperature range. Each crystal sample, however, will need different component values and the process of adjustment and calibration must be undertaken for each unit individually, a laborious and time consuming process often involving more than one temperature test cycle. In order to reduce production costs, manufacturers often adopt batch selection of crystals, mating these with one of a limited range of compensation networks without further calibration<sup>(28)</sup>, sacrificing overall frequency stability as a consequence.

Most analogue temperature compensated crystal oscillators have a frequency stability in the range  $\pm 5$  parts in  $10^7$  to  $\pm 10$  parts in  $10^6$ , the cost of the best of these approaching that of an ovened type offering a stability two orders of magnitude better.

#### 3.4.2 Hybrid Temperature Compensation

In the late 1960s the emergence of digital memories which could be programmed by the user (pROMs) offered new scope for the designer of temperature compensation schemes. It became feasible to store the



data describing the required temperature compensation in digital form so that the hardware was the same for all units, only the data itself varying from sample to sample. The memories of this period, however, were limited in capacity and still quite expensive, causing designers to opt for a hybrid analogue/digital approach<sup>(29)</sup> such as that shown in Figure 3.26.

A conventional thermistor voltage divider was used, without individual adjustment, to afford coarse temperature compensation. The finer corrections were supplied by the digital chain comprising a linear temperature sensitive RC oscillator, digital counter, memory and digital to analogue convertor. The required memory data was determined by stabilising the unit at a number of fixed temperatures, recording the counter output word and determining the required memory data by simulation with manual switches at each temperature. The data required for intermediary points was then predicted by mathematical interpolation and the memory programmed.

The performance of such units differs notably from that of an all-analogue scheme in that, where a small temperature change is encountered, the output of the counter may change by one bit, accessing a new data word from the memory which causes a sudden step in the analogue output of the D/A convertor and hence a sudden small step in frequency. The overall frequency-temperature relationship is, therefore, segmented in nature resembling the graph of Figure 3.27. Hybrid compensation schemes achieved a frequency stability of more than a part in  $10^7$  over a broad temperature range, though they remained expensive and quite laborious to programme.

### 3.4.3 Digital Temperature Compensation

In the hybrid compensation scheme described above the

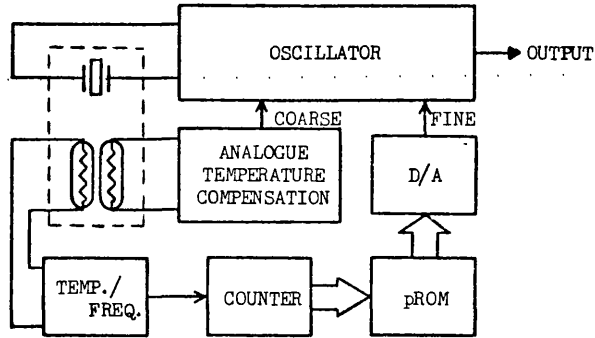


Figure 3.26 Hybrid temperature compensation scheme

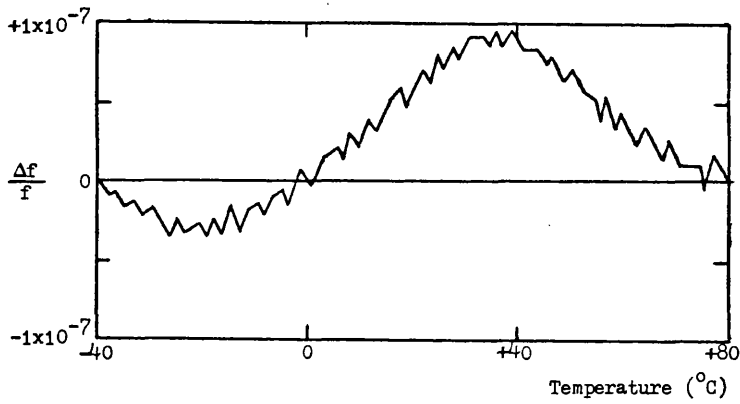


Figure 3.27 Typical plot of hybrid TCXO performance

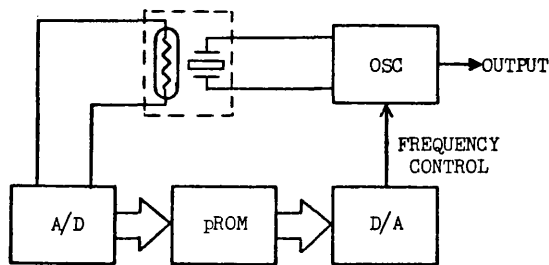


Figure 3.28 A digital temperature compensation scheme

temperature sensitive RC oscillator and counter were used simply in order to eliminate the need for an analogue to digital convertor, an expensive item at the time. The analogue coarse-compensation was employed only because the memory size required for an all digital scheme was not readily available. The advent of larger pROMs and cheaper integrated A/D convertors in the early and mid 1970s made the extension of the digital techniques to handle all of the compensation a possibility<sup>(30)</sup>.

Figure 3.28 shows a digital temperature compensation scheme. Its operation is merely an extension of that of Figure 3.26, the range being extended to accommodate the full frequency excursion of the crystal. Temperature sensing is performed by a simple single-stage thermistor sensor whose non-linearity is also compensated for in calibration. Programming and calibration are again accomplished by simulation of data by hand switches at various temperatures and interpolation of the intermediary data. Automatic programming is also possible, in which case each data word in the memory may be evaluated individually. Because crystal temperatures change slowly in most applications it is possible to operate much of the digital circuitry at a low duty cycle by applying frequency corrections only once every second or so, thereby conserving power.

It is shown later that the performance of such a system depends largely upon the size of memory employed. In an attempt to minimise this requirement schemes have been proposed using small memories to store the measured data points and a microprocessor to predict the intermediate data in situ as required<sup>(31),(32)</sup>. Unfortunately, the amount of memory capacity required to store the processor's prediction programme is greater than that which is saved. Where a processor is already present in an equipment with unused memory

available, the approach proves practical. At the time of writing, the best frequency stability achieved using microprocessor control has been about 5 parts in  $10^7$ .

#### 3.4.4 Drawbacks of Existing Temperature Compensation Schemes

The performance of each of the preceding methods of temperature compensation is severely dependent upon power supply regulation, since they all employ a voltage-referred temperature sensing and oscillator controlling technique. The stability of the voltage supply available in an equipment is seldom sufficient to meet the requirements of a compensated oscillator so that additional regulation must be employed, adding to the cost, and inevitably dissipating power uselessly.

The exponents of the thermistors involved in temperature sensing vary from sample to sample, resulting in non-linearities which tend to reduce the measurement sensitivity at one or other end of its range. Even where sensor linearity may be assured, errors occur due to differences in temperature between the sensors and the crystal plate. These differential temperature effects are particularly likely after severe thermal shocks, or during the period immediately after switch-on.

It is usually necessary to ensure good linearity of the frequency with changes in varactor voltage. Although theoretically the calibration or programming procedure should compensate for non-linearities in the overall system, extreme non-linearities have the effect of restricting the operating range of the scheme, thereby reducing the frequency stability obtainable. Linearisation of the oscillator control usually involves the use of two varactors, back-to-back, fed from the same dc source and requiring isolation from

the signal circuit path.

Analogue to digital and digital to analogue conversion as employed in the hybrid and digital compensation schemes is another source of power supply dependence and non-linearity. Their cost, though continually reducing, still represents as much as 25% of the total material cost of a digitally compensated oscillator.

Furthermore, extension of the process to higher orders of control entails a disproportionate increase in the cost of these units.

Despite these drawbacks, temperature compensated oscillators fulfil an important role. Their combination of good frequency stability, low power consumption and small volume meets the requirement of a great deal of portable, battery-operated communications and instrumentation equipment. Current trends in these and other areas suggest an even larger sphere of application for compensated oscillators in the near future.

REFERENCES - Chapter 3

- (1) CADY, W.G.: "The piezo-electric resonator", Proc. IRE, 1921, pp.83-114.
- (2) GERBER, E.A., and SYKES, R.A.: "State of the art - quartz crystal units and oscillators", Proc. IEEE, Vol.54, No.2, February 1966, pp.103-16.
- (3) MARCONI'S WIRELESS TELEGRAPH CO. LTD.: "Quartz crystal units and their use in oscillators", Ref. SP. 51, Chelmsford, England, September 1955.
- (4) BECHMANN, R.: "Elastic and piezoelectric constants of  $\alpha$  - quartz", Phys. Rev., Vol.110, 1958, pp.1060-1.
- (5) MCDERMOTT, J.: "Focus on crystals for frequency control", Electronic Design 14, July 5th 1976, pp.40-5.
- (6) SYKES, R.A.: "High frequency plated quartz crystal units", Proc. IRE, January 1948, pp.4-7.
- (7) WARNER, A.W.: "High frequency crystal units for primary frequency standards", Proc. IRE, September 1952, pp.1030-3.
- (8) WARNER, A.W.: "Frequency aging of high frequency plated crystal units", Proc. IRE, July 1955, pp.790-2.
- (9) WARNER, A.W.: "Design and performance of ultraprecise 2.5-mc quartz crystal units", BSTJ, Vol.39, September 1960, pp.1193-1217.
- (10) WARNER, A.W.: "Use of parallel-field excitation in the design of quartz crystal units", Proc. 17th Annual Frequency Control

Symp., Atlantic City, 1963, pp.248-66.

- (11) BECHMANN, R.: "Improved high-precision quartz oscillators using parallel-field excitation", Proc. IRE, Vol.48, March 1960, pp.367-8.
- (12) SYKES, R.A., SMITH, W.L., and SPENCER, W.J.: "Studies on high precision resonators", Proc. 17th Annual Frequency Control Symp., Atlantic City, 1963, pp.4-19.
- (13) GROIS, O.Sh.: "One possible mechanism of quartz aging", Radiotekhnika i Elektronika (USSR), Vol.7, April 1962, pp.702-5. English translation in Radio Engineering, Electronic Phys., Vol.7, April 1963, pp.659-61.
- (14) WARNER, A.W., FRASER, D.B., and STOCKBRIDGE, C.D.: "Fundamental studies of aging in quartz resonators", IEEE Trans. Sonics and Ultrasonics, Vol.SU-12, June 1965, pp.52-9.
- (15) BELSER, R.B., and HICKLIN, W.H.: "Aging of aluminum plated 3MC semi-precision resonators", Proc. 20th Annual Frequency Control Symp., Atlantic City, 1966, pp.180-91.
- (16) ARMSTRONG, J.H., BLOMSTER, P.R., and HOKANSON, J.L.: "Aging characteristics of quartz crystal resonators", Proc. 20th Annual Frequency Control Symp., Atlantic City, 1966, pp.192-207.
- (17) BYRNE, R.J., and HOKANSON, J.L.: "Effect of high-temperature processing on the aging behaviour of precision 5 MHz quartz crystal units", IEEE Trans. Inst. Meas., Vol.IM-17, No.1, March 1968, pp.76-9.
- (18) STEVENSON, J.K., and REDWOOD, M.: "The motional reactance of a

piezoelectric resonator - a more accurate and simple representation for use in filter design", IEEE Trans. on Circuit Theory, Vol.C-16, pp.568-72.

- (19) VANDYKE, K.S.: "The piezo-electric resonator and its equivalent network", Proc. IRE, Vol.16, June 1928, p.742.
- (20) FRERKING, M.E.: "Crystal oscillator design and temperature compensation", New York: Van Nostrand Reinhold, 1978, Chapter 7, pp.56-129.
- (21) MARKER, T.F.: "Crystal oscillator design notes", Frequency, April 1968, pp.12-6.
- (22) EATON, S.S.: "Micropower crystal-controlled oscillator design using RCA COS/MOS inverters", RCA Appn. Note ICAN-6539, January 1971.
- (23) PLESSEY SEMICONDUCTORS: "Linear integrated circuits databook", Swindon, England, August 1977, pp.107-9.
- (24) TEXAS INSTRUMENTS: "Economical crystal-controlled clock generator", Electronic Engineering, August 1978, p.19.
- (25) GARNER, P.J.: "Voltage controlled crystal oscillators", Proc. IERE Conference on Radio Receivers and Associated Systems, No.40, Southampton, July 1978, pp.227-35.
- (26) MANASSEWITSCH, V.: "Frequency synthesisers - theory and design", New York: John Wiley and Sons, 1976, Chapter 6.
- (27) FRERKING, M.E.: "Crystal oscillator design and temperature compensation", New York: Van Nostrand Reinhold, 1978, Chapter 10, p.130.



- (28) BANGERT, R.H., HINNAH, H.D., and NEWELL, D.E.: "Recent developments in crystal oscillator temperature compensation", Proc. 19th Annual Frequency Control Symp., Atlantic City, 1965, pp.617-41.
- (29) BUROKER, G.E., and FRERKING, M.E.: "A digitally compensated TCXO", Proc. 27th Annual Frequency Control Symp., Atlantic City, 1973, pp.431-48.
- (30) PRAK, J.W.L., and PEDUTO, R.J.: "Digital ICs set temperature compensation for oscillators", Electronics, August 14th 1972, pp.124-6.
- (31) ONOE, M., YAMAGISHI, I., and NARIAI, H.: "Temperature compensation of crystal oscillator by microprocessor", Proc. 32nd Annual Frequency Control Symp., Atlantic City, 1978, pp.398-402.
- (32) FRERKING, M.E.: "Crystal oscillator design and temperature compensation", New York: Van Nostrand Reinhold, 1978, Section 10.4, p.157.

CHAPTER 4 - FREQUENCY SYNTHESIS

Frequency synthesis is a general term to describe processes by which one or many frequencies may be generated by derivation from a reference source. The advantages of synthesis over direct generation are that by using a synthesis technique it is possible to generate very many frequencies using only one reference source; and that the long-term stability of the generated frequencies is governed by the reference. The first advantage enables the replacement of a set of many generators by one synthesiser; the second allows generation of system-defined frequencies from an optimally designed standard frequency operating in a different frequency range, the former retaining the long-term stability of the latter.

The available techniques of frequency synthesis fall into two broad categories; incoherent synthesis and coherent synthesis. As the names imply, incoherent synthesis utilises a number of sources from which its output frequencies are generated; coherent synthesis derives all its outputs from the same reference. Incoherent types fail to realise much of the potential of synthesis, the instabilities in their various source frequencies often adding together to produce a much less stable output. This fact, together with their considerable complexity, makes incoherent synthesisers seldom used, coherent types of better performance being readily available.

Coherent frequency synthesis may be further subdivided into two types; direct and indirect. Direct synthesis involves the mixing together of harmonics and subharmonics of the reference frequency to obtain the required output. Indirect synthesis is achieved by phase locking a second oscillator to the reference. In laboratory frequency synthesisers it is common for both types of coherent

synthesis to be combined to afford high frequency resolution over a broad range. In dedicated applications, however, particularly in communications, indirect synthesis tends to dominate in importance.

The different forms of coherent synthesis will now be discussed; briefly in the cases of direct synthesis, and in a little more detail for indirect types. For a full treatment of all available techniques of frequency synthesis the reader is referred to references (1) and (5).

#### 4.1 Direct Coherent Synthesis (6), (10)

Six approaches to direct synthesis from one source are available offering varying performances at varying cost. The first approach is of importance only where several frequencies are to be generated at once. The other approaches all produce one output only whose frequency may be varied in uniform steps.

##### 4.1.1 The 'Brute-Force' Approach

By using a configuration of frequency multipliers, dividers and mixers with associated amplifiers and filters it is very simple to produce a limited number of output frequencies by the so-called 'brute-force' approach. One such configuration is shown in Figure 4.1, which may be implemented in either analogue or digital circuitry, or a combination.

There are two basic drawbacks with the brute-force approach: firstly, the spurious outputs generated in the mixing, multiplying and dividing circuits are often difficult to suppress; and secondly, the level of phase noise tends to increase with successive mixing processes. Applications of such an approach are very limited, though

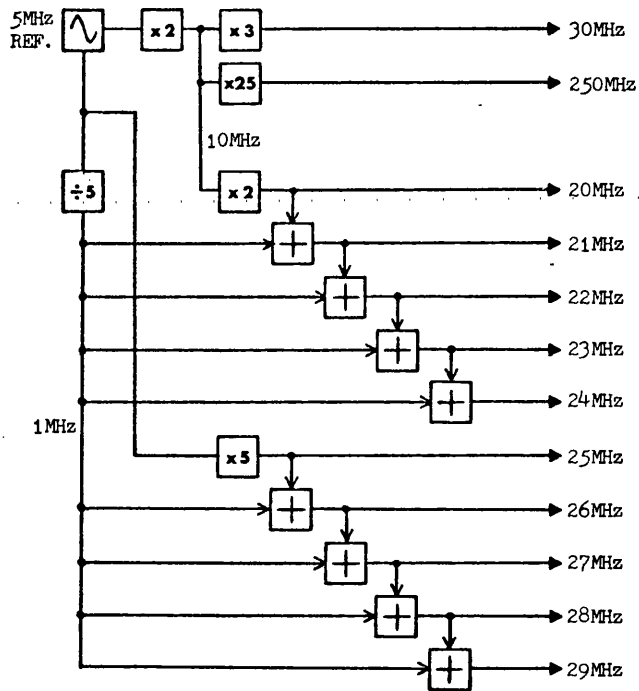


Figure 4.1 The 'brute force' approach to direct coherent frequency synthesis

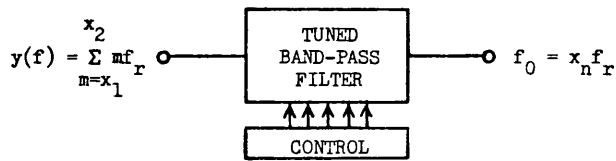


Figure 4.2 The passive filter technique of direct coherent frequency synthesis

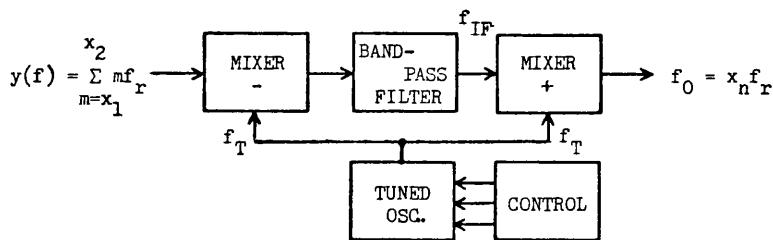


Figure 4.3 Double-mix direct coherent frequency synthesis

it is commonly used as an adjunct to the double-mix-divide synthesiser described in section 4.1.6.

#### 4.1.2 Harmonic Approach Using a Passive Filter

Wherever one frequency only need be generated at one time, and where the steps between available frequencies is uniform, a harmonic approach may usually be employed. The simplest such approach uses only a tuned, passive band-pass filter and is shown in Figure 4.2. The input signal is in the form of a pulse train whose fundamental frequency is the required step size and whose harmonic content is large, so that many frequencies are present simultaneously at the input and may be represented by:

$$y(f) = \sum_{m=x_1}^{x_2} mf_r \quad (4.1)$$

where  $y(f)$  is the input pulse train,  $f_r$  is the frequency step size and  $m$  is an integer in the range  $x_1 \leq m \leq x_2$ . The tunable filter then simply selects the required harmonic.

Narrow-band tunable filters of high selectivity are costly and difficult to implement so that this approach is only practical where the frequency difference between adjacent harmonics is large in relation to the output frequency.

#### 4.1.3 Double-Mix Approach

Where the frequency step size is small, the double-mix approach as shown in Figure 4.3 may be used. The input is again a pulse train as defined by equation (4.1) which is mixed with the output of an oscillator tuned to a frequency,  $f_T$ , below the required output by an amount  $f_{IF}$ . A fixed band-pass filter then selects the difference

component  $f_{IF}$  and adds it in the second mixer to  $f_T$  to yield the required output frequency.

The advantages of this approach as compared to passive filtering are numerous. The band-pass filter operates at a fixed frequency and may therefore be of as high an order as necessary to resolve the required frequency steps, even to the extent of employing a crystal filter. The downconversion of the input increases the relative spacing of the harmonics so that the filtering requirements are eased. The effects of frequency instabilities in the tuned oscillator are effectively cancelled out by the double-mix process since:

$$f_{IF} = x_n f_r - f_T \quad (4.2)$$

and 
$$f_0 = f_{IF} + f_T = x_n f_r - f_T + f_t$$

so that 
$$f_0 = x_n f_r \quad (4.3)$$

as required,  $f_T$  being absent from the equation.

Phase noise degradation will occur, but only where the input noise level is very low and where the circuitry is mismatched. As with any heterodyned technique, spurious outputs will inevitably occur and their level may only be minimised by careful design.

#### 4.1.4 Harmonically Phase Locked Loop

Where the spacing between required frequencies is too small for either of the above techniques the phase locked loop approach, as shown in Figure 4.4, may be employed. A voltage controlled oscillator (VCO) with coarse range control is phase locked to one only of the harmonics contained in the input signal. The spurious outputs generated are extremely small due to the absence of any mixers, though phase-detector output ripple may modulate the VCO in

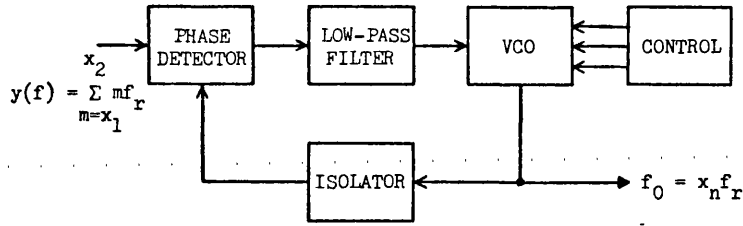


Figure 4.4 Harmonically phase-locked loop

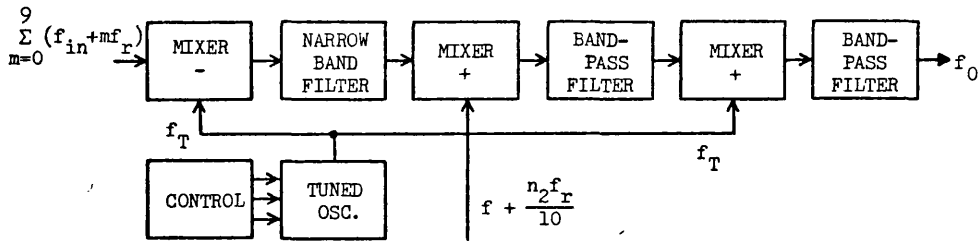


Figure 4.5 A decade module of a triple-mix direct coherent synthesiser

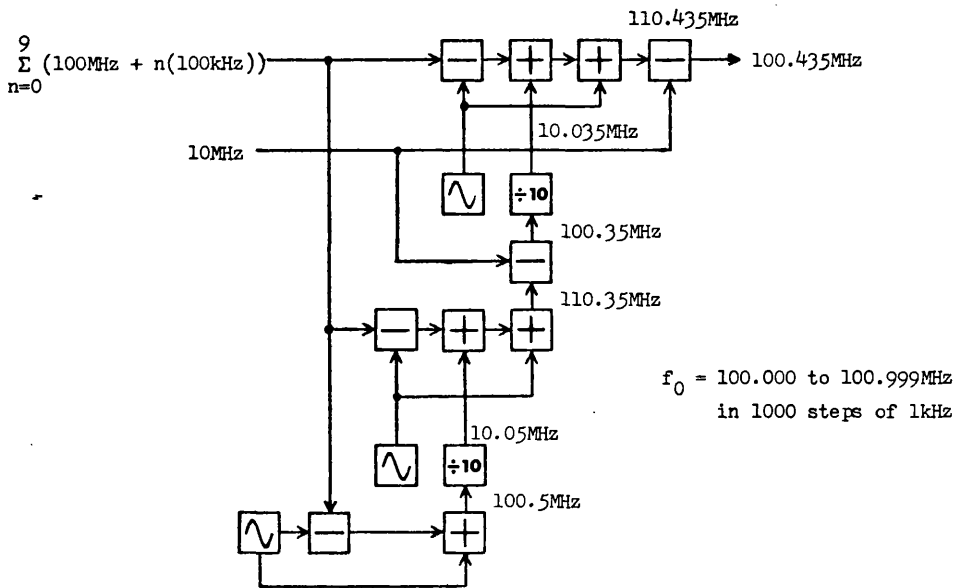


Figure 4.6 Example of triple-mix frequency synthesis

a poorly designed loop. It will be shown later that although the long-term frequency stability of the output of a phase locked loop is equal to that at the input, the phase noise spectrum is essentially that of the output oscillator. For this reason a high-quality VCO is required to afford good phase noise performance.

The only serious limitation on the performance of the phase locked loop approach is the presence of leakage components at unwanted harmonics which influence the VCO either by direct modulation of the control line or by injection back through the isolator stage. It should be further noted that such a synthesiser could be said to be an indirect type due to the phase locking action, though its overall action is an extension of the harmonic selection principle.

#### 4.1.5 Triple-Mix Approach

Triple-mix synthesis was developed to meet the requirement for modular construction of various synthesisers from standard circuit blocks in order to reduce costs, simplify design and improve reliability. A block diagram of such a module is given in Figure 4.5, and may be seen to be a modification of the double-mix approach utilising the principle of drift cancellation. An additional mixer, however, is interspersed between the double-mix pair to inject the next lower order frequency increments.

The input signal is again a set of harmonics, this time translated up in frequency by an amount  $f_{in}$  so that the input signal may be written:

$$y(f) = \sum_{m=0}^9 (f_{in} + mf_r) \quad (4.4)$$

where  $f_r$  is normally a submultiple of the reference frequency. After



mixing and filtering, the first intermediate frequency is given by:

$$f_{IF1} = f_{in} + n_1 f_r - f_T \quad (4.5)$$

The output of the second band-pass filter is then:

$$f_{IF2} = f_{in} + n_1 f_r - f_T + f + \frac{n_2 f_r}{10} \quad (4.6)$$

so that the overall output is:

$$f_0 = f_{in} + f + n_1 f_r + \frac{n_2 f_r}{10} \quad (4.7)$$

which is independent of  $f_T$  as required. The offset frequency,  $f$ , is not a problem when other similar stages are to be cascaded, but if necessary it may be removed by simple subtractive mixing and filtering.

The use of these modules to form a synthesiser is illustrated in the example of Figure 4.6 in which two such modules are combined with a double-mix stage to give an output frequency variable in steps of 1kHz from 100.000 to 100.999MHz. The offset frequency,  $f$ , is 10MHz in this case and is removed by subtraction after each stage. The harmonics selected in the example are the fourth for the primary stage, third for the second stage and fifth for the final double-mix stage, giving an output of 100.435MHz. It is clear that more such stages may be readily added.

#### 4.1.6 Double-Mix-Divide Approach

The requirement for repeatable modules which may be combined to meet the needs of a particular application is best met by the double-mix-divide approach as shown in Figure 4.7. The module shown is a single decade block suitable for continued cascading. Its inputs are separately derived frequencies, which must be present simultaneously. A set of harmonics is not required.

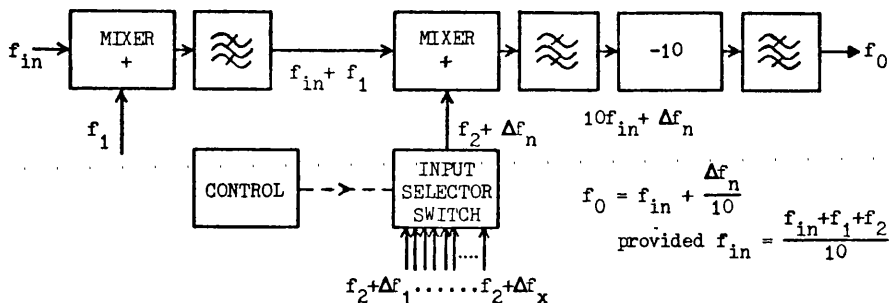


Figure 4.7 Decade module of a double-mix-divide direct coherent frequency synthesiser

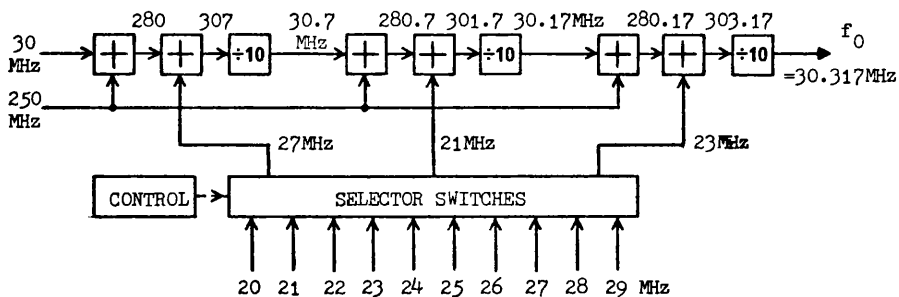


Figure 4.8 Example of double-mix-divide synthesis

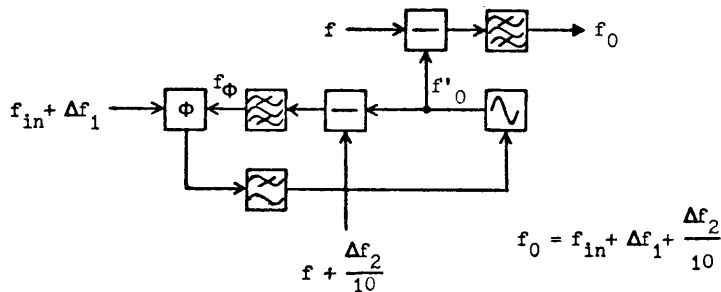


Figure 4.9 Analogue phase-locked loop synthesis

The input signal is mixed first with the fixed frequency  $f_1$ , and then with one of a set of frequencies  $(f_2 + \Delta f_1), (f_2 + \Delta f_2), (f_2 + \Delta f_3) \dots (f_2 + \Delta f_x)$  as selected by the control panel and switching arrangement. The output of the second band-pass filter is, therefore, equal to  $f_{in} + f_1 + f_2 + \Delta f_n$  where  $(f_2 + \Delta f_n)$  is the particular input selected. Now if  $f_1$  and  $f_2$  are chosen such that they relate to  $f_{in}$  according to the relation:

$$f_{in} = \frac{f_{in} + f_1 + f_2}{10} \quad (4.8)$$

then the output of the second band-pass filter may be rewritten as  $10f_{in} + \Delta f_n$ , so that after division by ten, the output is given by:

$$f_0 = f_{in} + \frac{\Delta f_n}{10} \quad (4.9)$$

The example of Figure 4.8 demonstrates how three identical decade modules may be combined to give an output frequency variable from 30.000 to 30.999MHz in steps of 1kHz. The twelve input frequencies must also be derived by synthesis, the brute-force method being appropriate in this case. The circuit given in Figure 4.1 fits the bill ideally. A comparison of the triple-mix and double-mix-divide approaches must always take into consideration the complexity of the circuitry required to generate the input frequencies to each module. Although laboratory equipment manufacturers tend to adopt double-mix-divide, their decision is based on large scale production economies as well as the technical aspects. In dedicated synthesisers, the choice between the various approaches must be made on consideration of the particular requirements and may not necessarily favour this approach.

## 4.2 Indirect Coherent Synthesis

Indirect synthesis relies upon the properties of feedback control systems in generating frequencies. By phase locking a modified version of the output of an auxiliary oscillator to the reference input, frequencies may be generated which are a function of the process of modification.

Two subdivisions of this class of synthesis emerge; analogue phase locked loop synthesis and digital phase locked loop synthesis. These terms lead, however, to certain ambiguities. Analogue phase locked loops certainly exist and may be employed in the synthesis of a small number of well-spaced frequencies. For higher frequency resolution and broader range, however, fixed frequency dividers are required which, in practical systems, would consist of digital hardware. True digital phase locked loops, on the other hand, are very rare, though the term is used to describe a very common class of synthesisers which consist primarily of digital circuitry but also include some analogue sections. The majority of indirect coherent synthesisers are, therefore, a hybrid of analogue and digital circuitry. In this discussion the following terminology is adopted: techniques of frequency synthesis employing digital circuitry only are termed "true digital synthesisers" and are dealt with separately in section 4.2.3; of the remaining hybrid approaches those whose frequency selection process is achieved by adjustment of its analogue components are termed "analogue phase locked loop synthesisers", and those whose frequency is changed by adjustment of the digital circuitry are termed "digital phase locked loop synthesisers".

On this basis the three categories are now discussed by consideration of their frequency selection, range and resolution

capabilities only. A full system analysis depends upon the consideration of the dynamic performance of phase locked loops; their acquisition, hold-in, phase-noise and switching performance, etc. These factors will be discussed later as they arise in the specific system description. For a full treatment of phase lock techniques the reader is referred to references (2), (3), (9) and (11). In their more advanced forms phase locked loop synthesisers are capable of high performance combined with low volume and power consumption.

#### 4.2.1 Analogue Phase Locked Loop Synthesisers

Figure 4.9 is a functional block diagram of an analogue phase locked loop decade synthesiser. The output frequency of the auxiliary voltage controlled oscillator (VCO) is downconverted and phase-compared to the reference frequency of  $(f_{in} + \Delta f_1)$  where  $\Delta f_1$  is one of a number of separately generated interpolation frequencies,  $\Delta f_2$  being another. When the loop is phase locked,

$$f = f'_0 - f - \frac{\Delta f_2}{10} = f_{in} + \Delta f_1$$

so that:

$$f'_0 = f_{in} + f + \Delta f_1 + \frac{\Delta f_2}{10} \quad (4.10)$$

The offset frequency,  $f$ , may then be mixed out to give:

$$f_0 = f_{in} + \Delta f_1 + \frac{\Delta f_2}{10} \quad (4.11)$$

In practice,  $\Delta f_1$  represents the offset from  $f_{in}$  resulting from previous similar stages, and for the first stage  $\Delta f_1$  may be zero.

Figure 4.10 shows an equivalent block diagram of a phase locked loop, with noise injected at the input and at the VCO, and serves to

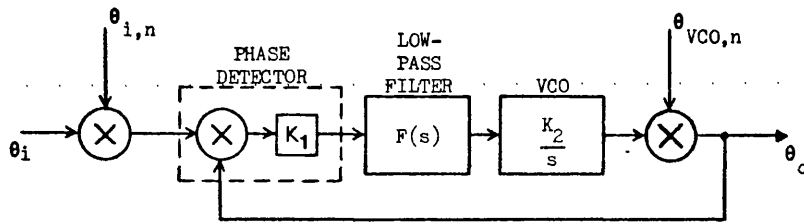


Figure 4.10 Equivalent block diagram of an analogue phase-locked loop

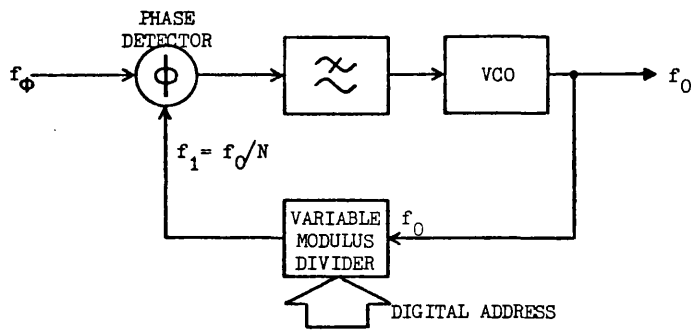


Figure 4.11 Digital phase-locked loop frequency synthesis

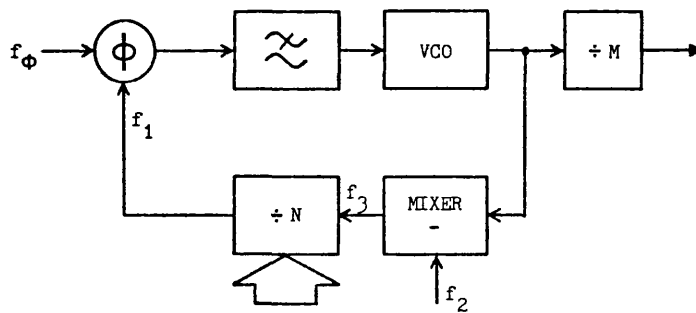


Figure 4.11 Digital phase-locked loop synthesis incorporating a mixer

illustrate one of the most important characteristics of such loops. If  $K_1$  is the phase-detector gain constant,  $K_2$  is the VCO transfer gain and  $F(s)$  is taken as unity for simplicity, then the transfer function of the loop with respect to the input noise may be written:

$$\frac{\bar{\theta}_0}{\bar{\theta}_{i,n}} = \frac{1}{1 + (1/K_1 K_3)s} \quad (4.12)$$

The loop, therefore, acts as a low-pass filter of time constant  $(1/K_1 K_3)$  to any noise appearing at the input. Similarly, the transfer function with respect to VCO noise is:

$$\frac{\bar{\theta}_0}{\bar{\theta}_{VCO,n}} = \frac{1}{1 + (K_1 K_3/s)} \quad (4.13)$$

so that the loop acts as a high-pass filter to output oscillator noise.

Because of these filtering effects it is a characteristic of phase locked loops that the output noise spectrum resembles that of the input for frequencies offset from the signal by an amount less than the loop bandwidth, whilst for frequencies offset by an amount greater than the loop bandwidth the output spectrum resembles that of the VCO. Put into the parlance of frequency sources, this means that with a judicious choice of loop bandwidth the output of a phase locked system may exhibit the long-term frequency stability of the input signal and the short-term stability of the VCO. This effect is made particularly useful in atomic frequency standards as described in Chapter 2.

Analogue phase locked loop synthesis suffers from the drawback that a large number of interpolation frequencies must be externally generated. This may be achieved by direct harmonic selection, separate analogue synthesis or by digital synthesis but in all cases leads to a complex system in practice. Analogue indirect synthesis

is very rarely used as direct or digital synthesis prove simpler and more effective.

#### 4.2.2 Digital Phase Locked Loop Synthesis <sup>(7),(12)</sup>

The basic block diagram of a digital phase locked loop synthesiser is given in Figure 4.11 and consists of a VCO, phase comparator, low-pass filter and a programmable divider whose modulus of division may be adjusted by means of a digital address. When the loop is phase locked,  $f_1 = f_\phi$  and therefore:

$$f_0 = N \cdot f_\phi \quad (4.14)$$

$f_\phi$  is termed the phase comparator frequency and may be a divided version of a frequency standard. It is clear that as  $N$  varies,  $f_0$  changes accordingly. The frequency resolution is defined as the smallest change in frequency which may be produced by a change in  $N$  and is given by:

$$R = \frac{\delta f_0}{\delta N} \quad (4.15)$$

In the system of Figure 4.11 the resolution is  $f_\phi$ , the phase comparator frequency, so that by choice of  $f_\phi$  the output channel spacing may be easily specified.

The simplicity of the above system would suggest that high resolution may be realised by choosing a low value of  $f_\phi$  and a correspondingly high  $N$ . This is not the case in practice. Any alternating component of voltage which occurs on the VCO control line will phase modulate the output. In order to minimise this effect it is necessary for the loop filter to reject frequency components at  $f_\phi$  and  $2f_\phi$  to a high degree. This may be achieved readily for high  $f_\phi$  (above 100Hz, say), but as  $f_\phi$  is reduced the loop bandwidth must become so narrow that the locking time,



transient response and noise rejection characteristics become very poor.

A simple method of achieving higher resolution is to perform the whole synthesis at a frequency  $M$  times higher and then to divide the output by  $M$ . This technique is useful in many applications but is strictly limited by the maximum possible clock frequency of programmable dividers which dictates the maximum VCO frequency. Figure 4.12 is the block diagram of a variation on the basic approach which allows the use of higher VCO frequencies. The output of the VCO is downconverted by mixing with an externally generated frequency  $f_2$  before entering the divider. By inspection, it may be seen that:

$$f_1 = (f'_0 - f_2)/N$$

so that when the loop is phase locked and  $f_1 = f_\phi$ :

$$f'_0 = Nf_\phi + f_2 \quad (4.16)$$

and:

$$f_0 = \frac{Nf_\phi + f_2}{M} \quad (4.17)$$

so that the resolution at outputs  $f'_0$  and  $f_0$  may be written:

$$R_{f'_0} = f_\phi \quad (4.18)$$

and:

$$R_{f_0} = \frac{f_\phi}{M} \quad (4.19)$$

This approach may, therefore, be viewed in two lights. Firstly, by taking the output at  $f'_0$  the same resolution is maintained at a frequency higher by an amount  $f_2$ ; secondly, by taking the output at  $f_0$ , the resolution has been improved by a factor  $M$ . In practice  $f_2$  may itself be variable in discrete steps thereby increasing the

range and resolution of the system<sup>(4)</sup>.

Using those blocks included in Figure 4.12, several novel arrangements have been proposed to meet the requirement for high resolution without compromising performance<sup>(13)</sup>. Sidestep programming is a technique which seeks to vary the modulus of a programmable divider in increments less than unity. The conventional divider is replaced by the network of Figure 4.13 in which the input clock must be enabled by the output of a feedback divider which is normally high, but which goes low once every ten cycles of the output. The division modulus is therefore  $N$  for nine cycles and  $(N + 1)$  for one cycle, making the average division modulus  $(N + 0.1)$  over ten cycles. By varying the modulus of the feedback divider the average forward division modulus may be varied in small increments. The disadvantage of the scheme is that the output of the composite divider stage is not a symmetric waveform so that jitter is generated at the output of the phase comparator. In order to remove this jitter it is usually necessary to reduce the bandwidth of the loop filter thereby defeating the object of the exercise to some extent.

An example of the Vernier System is shown in Figure 4.14. It makes use of the fact that if the outputs of two synthesizers having resolutions of, in this case, 10kHz and 9.9kHz are mixed together, then frequency steps of 0.1kHz may be produced. The short-term stability of the system is in accordance with that of a wider band, 10kHz resolution loop. The action of the system is analagous to that of a vernier scale only when  $N$  and  $M$  are each changed by one simultaneously. In a practical system, therefore, binary adders are needed to sum the digital addresses, and a further code conversion is usually necessary.

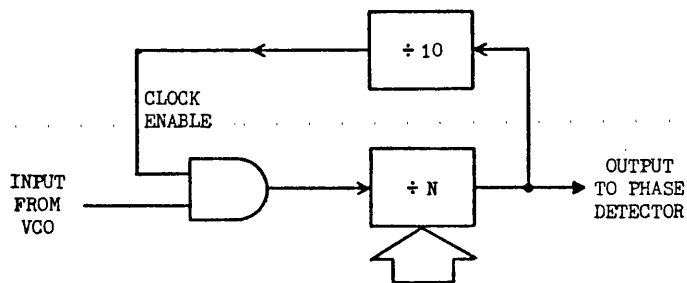


Figure 4.13 Sidestep programming

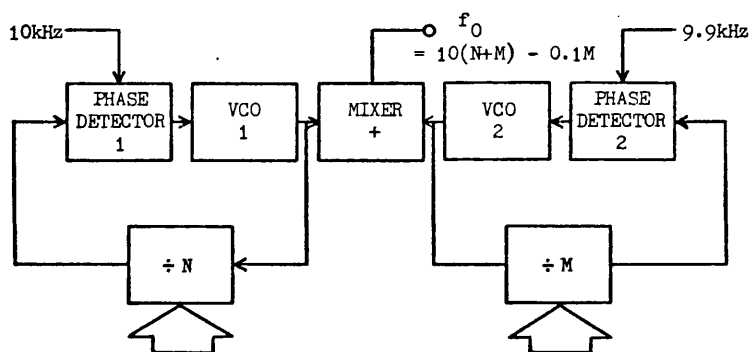


Figure 4.14 The Vernier System

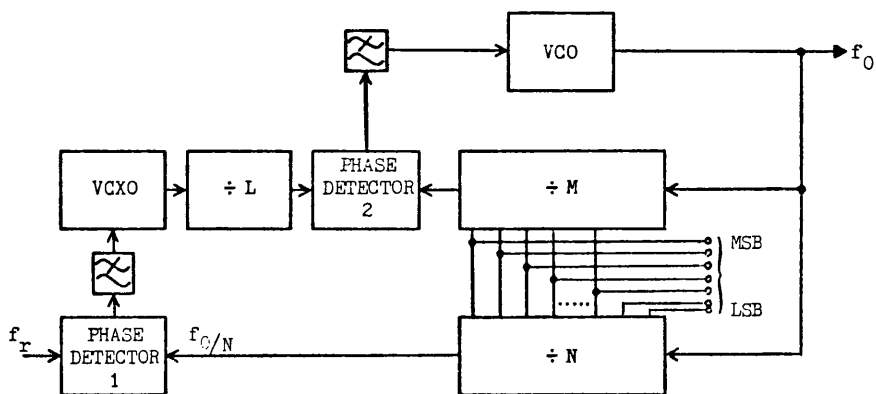


Figure 4.15 The Tandem System

A more obvious approach to the design of a high resolution synthesiser is to vary the input reference frequency in small steps. This may be accomplished by simply using a low frequency, high resolution synthesiser as a pre-synthesis stage, the Tandem System<sup>(14)</sup> of Figure 4.15 being an example. The main (upper) loop is a straightforward fairly wide band synthesiser. The tandem (lower) loop is a narrow band loop which generates a varying phase comparator frequency by pulling a voltage controlled crystal oscillator until the loops both phase lock. In the locked condition,  $f_0 = Nf_r$  so that increments of the small reference frequency may be achieved. A VCXO may be used because only a narrow range is required. The wide band output loop exhibits a stability which is that of the reference frequency  $f_r$  in the long-term and of the VCXO in the short-term leading to excellent overall performance. In order to ensure that both loops are within their lock range for all control commands it is necessary to gang the two programmable dividers as shown so that their moduli change simultaneously.

Equation (4.16) describes the summing effect typical of synthesisers incorporating mixers, such as that of Figure 4.12. The Gemini System makes use of this summing effect by adding small interpolation frequencies to the reference. Its block diagram is shown in Figure 4.16. A study of the system shows that when the loop is phase locked:

$$f_0 = Nf_r + f_i \quad (4.20)$$

provided that the moduli of the programmable dividers are equal, which is easily assured. The bandwidth of the loop may be quite high, in keeping with a fairly high phase comparator frequency, so that the output stability is excellent. The interpolation frequency may be generated simply by an external narrow band loop, its

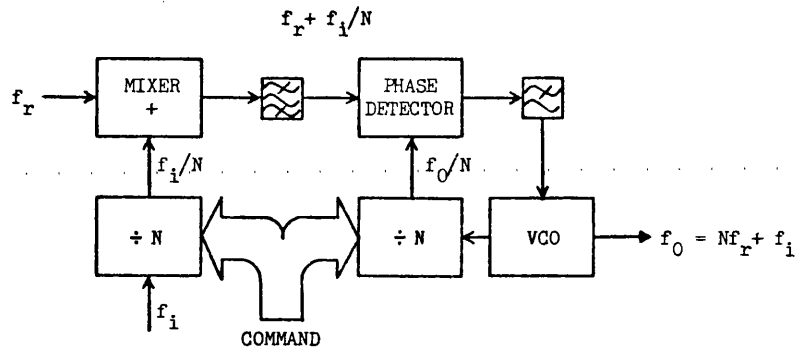


Figure 4.16 The Gemini System

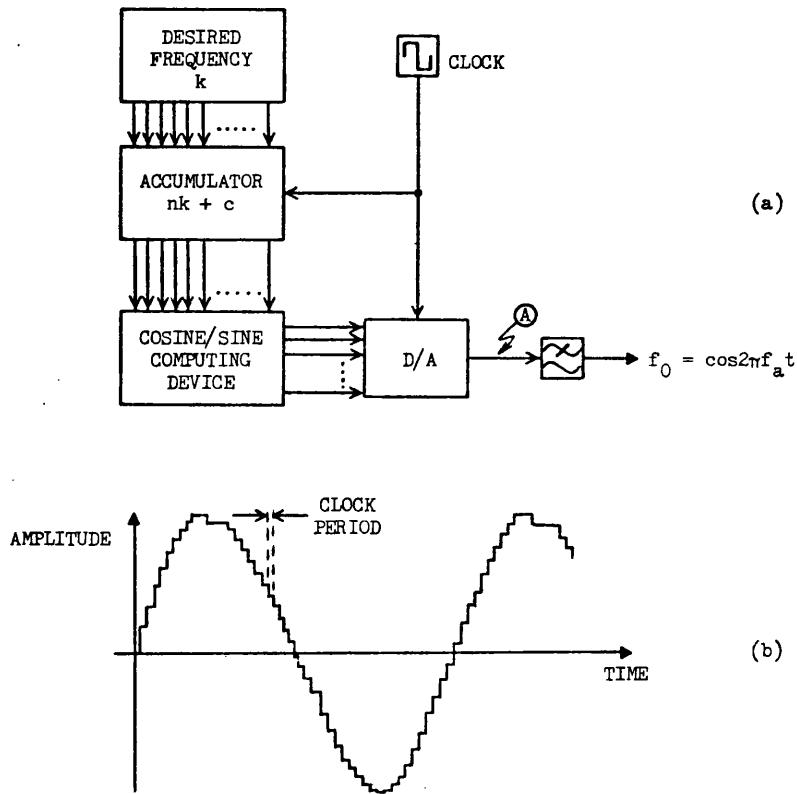


Figure 4.17 A 'true' digital frequency synthesiser  
 (a) block diagram  
 (b) waveform at A

instability contributing only slightly to the output signal. As the resolution is increased, however,  $f_i$  becomes smaller and the problem of selecting the mixer output component at  $(f_r + f_i/M)$  from that at  $(f_r - f_i/M)$  becomes difficult unless a ceramic filter is employed.

The above techniques are those currently employed in obtaining high resolution synthesis. It will be shown in Chapter 5 that the synthesiser required in this application is unusual in many respects, and a new technique is described which meets these requirements very simply.

#### 4.2.3 "True" Digital Synthesis<sup>(8)</sup>

During the development of the science of frequency synthesis, many digital components have been employed in synthesisers, largely out of the context of their intended use. For example, a digital exclusive-OR gate may be used as an excellent phase comparator<sup>(15)</sup> provided it is followed by an analogue low-pass filter, strictly rendering the whole an analogue operation. Both D-type and R-S flip-flops may be employed as mixers or phase comparators with digital inputs and outputs<sup>(16)</sup>. Digital counters and magnitude comparators have been used to provide both frequency and phase comparison<sup>(17)</sup>. All of these instances, however, include the logic blocks in an overall system which is, at least in some part, analogue in its operation.

The difficulty which prohibits the use of true digital systems is usually that of arriving at a "digital VCO"; that is, a device whose output frequency may be controlled solely by digital means. Three techniques have been developed, however, and are now briefly described in turn.

Binary-rate-multipliers (or decimal-rate-multipliers) are devices whose average output pulse rate is a multiple of a constant rate related to its input clock frequency. The exact multiple is defined by a parallel digital address, and a rate multiplier with a fixed clock may therefore be employed as a digitally controlled frequency source<sup>(18),(19)</sup>. In conjunction with other digital blocks a true digital synthesiser may be realised. The disadvantage of rate multipliers is that their output pulse train is irregular in the short-term, averaging out at the correct number of pulses-per-second only over a period of  $2^n$  clock pulses, where  $n$  is the number of address bits. This irregularity is akin to that found in sidestep synthesiser programming as described in section 4.2.2, and may be eradicated only by analogue filtering or integration. Its effects may be minimised, however, by carrying out the rate-scaling at a high frequency and digitally dividing down, the resultant performance being sufficient for non-exacting applications<sup>(20)</sup>.

In contrast with the rate-multiplier, an all digital oscillator has been described<sup>(21)</sup> whose output is a regular pulse train of rate given by:

$$f_0 = \frac{f_c}{K+N} \quad (4.21)$$

where  $f_c$  is the clock frequency,  $K$  is a system-defined constant and  $N$  is a number defined by a parallel digital address. The oscillator may be considered in isolation as a direct synthesiser, or used with other digital blocks in an all-digital indirect synthesiser. In isolation, its frequency resolution is:

$$\frac{\delta f_0}{\delta N} = \frac{-f_c}{(K+N)^2} \quad (4.22)$$

which may be made small by choosing a large  $K$  and/or  $N$ , but will in

turn entail the output frequency being very much lower than  $f_c$ . Equation (4.21) shows the relationship between  $N$  and  $f_0$  to be non-linear. When the oscillator is incorporated into a digital phase locked loop, this non-linearity causes a high level of quantization noise at one extreme of its range.

The most fundamental digital synthesisers are those of the class known as successive computation synthesisers<sup>(22)</sup>, such as that shown in Figure 4.17(a). They operate by computing the amplitude of the required output waveform, as defined by a digital command, at each successive clock period. The computed amplitude takes the form of a parallel digital word which is then converted to an analogue waveform such as that of Figure 4.17(b) and filtered to give a smooth sinusoid. The computational operation may be accomplished by microprocessor or, in straightforward applications, simply by direct memory look-up. The output frequency of such systems is limited mainly by the maximum possible computational speed or memory acquisition time, though frequencies up to 1MHz have been generated with extremely high resolution<sup>(11)</sup>. Successive computation synthesisers, though classed as true indirect digital synthesisers, still require analogue processing of the output signal and, under certain terms of reference, may be included among the classes of direct synthesisers.



REFERENCES - Chapter 4

- (1) MANASSEWITSCH, V.: "Frequency synthesizers - theory and design", New York: Wiley Interscience, 1976.
- (2) op. cit.: Chapter 4, pp.226-82.
- (3) op. cit.: Chapter 5, pp.283-310.
- (4) op. cit.: Chapter 7, pp.428-84.
- (5) GORSKI-POPIEL, J. ed.: "Frequency synthesis: techniques and applications", New York: IEEE Press, 1975.
- (6) op. cit.: Chapter 3, pp.47-68.
- (7) op. cit.: Chapter 4, pp.69-120.
- (8) op. cit.: Chapter 5, pp.121-50.
- (9) GARDNER, F.M.: "Phase lock techniques", New York: John Wiley and Sons, 1979. 2nd ed.
- (10) NOORDANUS, J.: "Frequency synthesizers - a survey of techniques", IEEE Trans. on Comm. Tech., Vol.COM-17, No.2, April 1969, pp.257-71.
- (11) BLANCHARD, A.: "Phase-locked loops: application to coherent receiver design", New York: John Wiley and Sons, 1976.
- (12) STOKES, V.O.: "Techniques of frequency synthesis", Proc. IEE, Vol.120, No.10R, IEE Reviews, October 1973, pp.1057-77.
- (13) EVERS, A.F., and MARTIN, D.J.: "Improved forms of digital frequency synthesizers" in 'Digital Frequency Synthesis in Communication Systems', IEE Colloquium Digest 72/11, May 1972,

pp.9/1-5.

- (14) FADRHONS, J.: "Blending a wideband PLL with a narrowband PLL", Electronic Design 14, July 5th 1976, pp.46-51.
- (15) SIGNETICS CORPORATION: "Linear integrated circuits applications manual", Section 9 - 'Phase Locked Loop Applications', 1972, pp.235-304.
- (16) NEMAC, J.: "Build a high-frequency synthesizer with a digital mixer", Electronic Design 4, February 15th 1977, pp.120-2.
- (17) GILLETTE, G.C.: "The digiphase synthesizer", Frequency Technology, August 1969, pp.25-9.
- (18) MARTIN, J.D.: "Signal processing and computation using pulse-rate techniques", The Radio and Electronic Engineer, Vol.38, No.6, December 1969, pp.329-44.
- (19) DEN DULK, R.C., and VAN WILLIGEN, D.: "Application of the loose-locked oscillator in a professional short-wave receiver", The Radio and Electronic Engineer, Vol.49, No.5, May 1979, pp.241-9.
- (20) STRAUSS, G.M.: "An AF synthesiser", Electronic Design 17, August 16th 1971, pp.62-5.
- (21) SZYMANSKI, J.W.: "An improved DCO scheme for digital phase locked loops", Electronic Engineering, March 1977, pp.24-5.
- (22) TIERNEY, J., RADER, C.M., and GOLD, B.: "A digital frequency synthesizer", IEEE Trans. on Audio and Electroacoustics, Vol.AU-19, No.1, March 1971, pp.48-57.

CHAPTER 5 - THE PROPOSED SYSTEM

At the outset of the work described here certain basic objectives for any proposed temperature compensation scheme were laid down. These are listed below, including in the list any immediate consequences of each objective and any points of conflicting requirements. It was resolved that as many of these objectives as possible should apply.

- (i) The compensation scheme should make use as far as possible of digital circuitry. This affords repeatability and reliability and, if LSI is employed, cheapness. A digital system readily allows the use of a read-only memory or microprocessor as the compensation law governing element. Consideration of the choice of logic family, however, depends largely upon other factors.
- (ii) The scheme should make use only of readily obtainable components. This may not apply, of course, to any custom LSI circuit but is applicable to all others, including crystals, and is greatly advantageous for prototyping purposes.
- (iii) The output frequency of the system should be a recognised standard. 5MHz is the most common at present, but many equipment designers would prefer 10MHz or 100MHz, though 100MHz leads to some difficulty in logic design with some families.
- (iv) The scheme should ideally exhibit no dependence upon temperature varying components, with the exception of the crystal itself. This, of course, can never be fully

realised but makes an admirable objective.

(v) The scheme should exhibit no dependence upon small changes in power supply voltage. This may be achieved by including voltage regulation in the system, but an inherent voltage independence would be preferable. The use of digital circuitry is promising in this respect.

(vi) The system should allow easy calibration. If a memory is employed, then a software-based technique would afford both simplicity and the possibility of automatic calibration.

On the basis of these objectives a temperature compensation technique was proposed. The processes involved in arriving at this proposal were very complex, all the elements being interdependent so that many of the decisions are difficult to define in isolation. The following sections describe as accurately as possible the rationale behind the choice of each of the system elements.

### 5.1 Temperature Measurement

In any temperature compensation scheme it is necessary to derive information describing the prevailing temperature of the controlling crystal. In the systems of Chapter 3 this is accomplished by measurement of the changes in resistance of temperature sensitive semiconductors, either thermistors or diodes. These techniques, however, conflict with objectives (iv), (v) and (vi). Although any temperature sensor must, of necessity, be temperature dependent, the real point of interest is whether its change is predictable and repeatable (and preferably fairly linear)

or whether it is susceptible to errors due to temperature-borne changes in auxiliary circuits. Resistance-bridge temperature sensors are all influenced to some extent by such external factors, notably power supply voltage variation. This influence may be reduced to the point where it is negligible in comparison with the resolution of the control scheme, but this involves complex and laborious calibration procedures such as those described in section 3.4.

If objective (i) is to be met, then conversion of the temperature information into digital form must also be accomplished. One method was discussed, namely the use of a temperature sensing element as the frequency controlling component of a low frequency oscillator. The frequency may then be counted digitally against the compensated output frequency to derive a digital description of temperature. The LF oscillator is, however, somewhat sensitive to temperature changes in its other components and to power supply variations, leading to errors.

In Chapter 3, it was explained that the axially orientated Y cut quartz crystal plate exhibits a large temperature coefficient which is substantially linear. Such crystal plates are manufactured by the same procedure as conventional AT cut plates, the crystal cutting, lapping, plating and mounting being identical. When such a crystal is used to control an oscillator, therefore, the output frequency is linearly dependent upon the crystal temperature with a high coefficient in the order of  $10^2$  to  $10^3$  Hz per  $^{\circ}\text{C}$  for HF units. This temperature coefficient, in conjunction with the inherently high Q of a quartz resonator render the oscillator extremely insensitive to temperature-borne changes other than those of the crystal. Y cut quartz crystal oscillators have been used for some time as accurate thermometers<sup>(1),(2)</sup>, leading to the derivation of

particular doubly-rotated cuts to afford exact temperature coefficients at desired frequencies<sup>(3),(4)</sup>. The resolution of such thermometers is in all cases a direct function of the resolution of the frequency measurement.

The advantages of using quartz transducers in digital systems have been described for the measurement of both temperature and mass<sup>(5)</sup>, and fall into two main categories. Firstly, the application of the precision manufacturing techniques of the crystal industry yields transducers of exceptionally high stability and reproducibility. In thermometry of resolution up to about  $0.01^{\circ}\text{C}$ , Y cut crystals may be employed, exactly as supplied by the manufacturer, in standard oscillator circuits without any dependence upon secondary temperature effects in the oscillator circuitry. For higher resolution applications it is necessary to isolate the oscillator components from extremes of temperature, in which case temperature resolutions up to about  $10^{-4}\text{C}$  may be readily achieved. In most applications the linearity of Y cut crystals is adequate for direct measurements, but if calibration is necessary, that calibration will apply to other like crystal units to a high degree of accuracy. The second advantage is that already mentioned of the simplicity with which frequency may be converted into parallel logic information. Section 5.2 considers various counting techniques, any of which are easily realised in current logic families. All frequency counting schemes require a stable reference frequency, but since the object of the system is to derive such a reference that would appear to present no problem.

In any temperature measurement, the accuracy is only as good as the temperature coincidence between the sensor and the subject. Coincidence should be maintained both in the steady state and

transient temperature conditions. In conventional compensation schemes the sensors are bonded onto the crystal enclosure with thermally conductive adhesive and then insulated from the external environment. In the steady state, the sensor and crystal should then be at exactly the same temperature, whilst the insulation prevents fast transients of temperature from occurring. The insulation has the disadvantage, however, that in its presence changes in ambient temperature take a long time to affect the crystal, and rather less time to influence the sensor since it is outside the crystal enclosure. Furthermore, as the crystal plate and the sensor differ in mass and shape their responses to incident heat occur at different rates. A second crystal, on the other hand, when used as a temperature sensor will tend to respond to temperature transients similarly to the prime crystal, and if both are mounted in the same enclosure the temperature coincidence may be improved still further. This factor is discussed in detail in Chapter 6.

## 5.2 Frequency Counting

The various methods of digital frequency measurement have been described, analysed and compared previously by Martin<sup>(6)</sup> and will not be repeated here. The final choice of counter will be influenced not only by its absolute performance but also, inevitably, by the choice of logic family to be employed and so, at this stage, general points only will be discussed.

Three parameters must be considered in specifying a frequency counter, namely its static uncertainty, its small-signal tracking rate and its large-signal response time. These parameters are compared by Martin for various counters and show that the simple gated counter displays optimum large-signal response time under all

conditions. Provided that its input frequency is high compared with its gating period, it also displays the lowest static measurement uncertainty. Though its small-signal tracking rate is quite low, it is adequate for this application as it is expected that the frequency to be counted will be high, whilst the rate of change of temperature, and hence the rate of change of frequency, will be relatively low. Accordingly, it appears that simple gated counting will suffice for this task, though this will be verified quantitatively in Chapter 6.

### 5.3 The Compensation Law Governing Element

In keeping with objective (i), the aim of a predominantly digital system leads naturally to the use of either a read-only memory or microprocessor as the system element which defines the compensation law. It was shown in section 3.4.3 that where a microprocessor is already present in an equipment, this may be employed to generate the required compensation data provided that spare memory space is available. With currently available processors, however, the total memory requirements for the compensation programme are greater than would be required for straightforward ROM look-up, and hence their dedicated use serves little purpose.

For this reason it was decided to employ a ROM look-up technique to define the required compensation law. Objectives (ii) and (vi) both preclude the use of mask-programmed ROMs since it is assumed that the data required for each unit will be unique. Field-programmable ROMs, however, are ideal in this application and it was decided that, if possible, an ultra-violet erasable type would be used at the prototype stage for convenience. The choice of exact



device is dependent upon the other system parameters and is discussed in Chapter 6.

#### 5.4 Methods of Oscillator Correction

The memory described above will supply a parallel digital data word whose value may be made to represent the required frequency correction at any temperature. Some means is now required to use that data to vary the output frequency of the system.

The means used in all digital compensation schemes to date has been to convert the data to an analogue voltage and use this to pull the oscillator back onto the required frequency. Such schemes are discussed in section 3.4.3. The use of a D/A convertor conflicts with objective (v) in that a stable voltage reference is a necessity. Fluctuations in reference voltage or supply voltage will be translated directly into frequency modulation of the output signal. The use of a simple varactor diode frequency control for the oscillator also may cause problems. It exhibits considerable temperature dependence of the frequency/control voltage characteristic and may be susceptible to long-term drift in varactor capacitance. Non-linearities in the voltage controlled crystal oscillator may reduce the operating range of the system under some conditions and measures such as the use of a two-varactor bridge are often needed to reduce this effect.

The combination of these factors led to various attempts to arrive at an alternative method of digitally controlling the system's output frequency, falling into two distinct categories as follows.

#### 5.4.1 Digital Selection of Oscillator Load Capacitance

The availability of low power solid-stage analogue switches<sup>(7)</sup> led to the investigation of a very simple approach to digital oscillator control. Figure 5.1 illustrates a conventional crystal oscillator circuit and crystal whose series load capacitance is variable by selection of one or more of a bank of capacitors. The selection switches may consist of solid-state analogue gates such that the capacitors may be selected by a digital command, hence forming a digitally programmable oscillator. At this stage it was noted that the idea conflicts with objective (iv) in that variations in the temperature will alter the selected load capacitance and hence produce frequency drift. If the capacitors were thermally bonded to the crystal, however, it was thought possible that this effect would be reproducible, and hence accounted for in the programming.

Appendix B contains details of experiments carried out on such an oscillator. It was found that in order to ensure reproducibility of frequency it was necessary to employ a revised capacitor configuration as described which led to a frequency resolution of at best 8 parts per million. Its frequency steps were irregular and as its tuning relied largely upon the existence of stray capacitance it proved unlikely that temperature effects could be allowed for. For these reasons the approach was abandoned in favour of digital frequency synthesis.

#### 5.4.2 Digital Frequency Synthesis

With the failure of the above approach it was decided that, in order to meet the objectives of the system, some form of digital

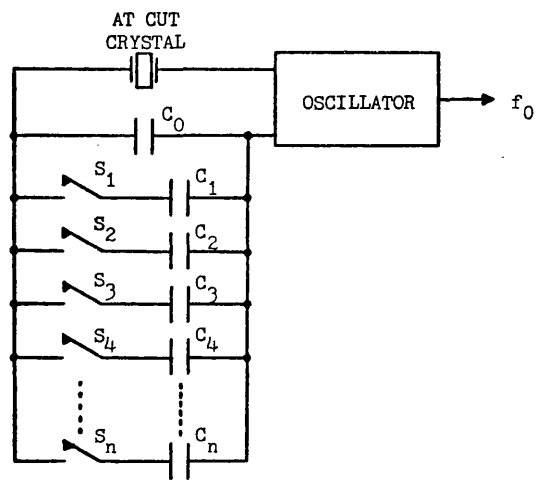


Figure 5.1 Switched-capacitor variable crystal oscillator

synthesis of a corrected frequency from the temperature varying frequency was necessary. Synthesis would give good repeatability and reliability using readily obtainable components, and also be suitable for large-scale integration. The operating frequency may be almost any value depending upon preference and the logic family employed. Due to the phase locked nature of digital synthesis, temperature dependence is that of the input frequency only, and within specified limits frequency synthesisers display no power supply voltage dependence. Furthermore, phase locked synthesisers display absolute repeatability of their frequency/command characteristic.

Certain particular requirements for the synthesiser were noted. Firstly, in contrast to the usual use of a frequency synthesiser, the output frequency is to be held constant while the input frequency varies. The relevant measure of its resolution is given, therefore, by:

$$R = \left. \frac{\delta f_1}{\delta N} \right|_{f_0 \text{ constant}} \quad (5.1)$$

where  $f_1$  and  $f_0$  are the input and output frequencies respectively and  $N$  is the magnitude of the digital command. All other aspects of its performance are conventional. Secondly, for accurate frequency compensation it is necessary for the synthesiser to display very high resolution. For example, to correct an oscillator to one part in  $10^7$ , the synthesiser must be able to resolve 1Hz in 10MHz. This requirement appears less stringent, however, when it is remembered that the total frequency range over which the device must operate is relatively narrow, perhaps a few hundred hertz. Thirdly, the input frequency must be in the HF region in order to take advantage of the good aging performance of crystals operating in the 2-10MHz band.

The output frequency, in order to be a recognised standard as required, must not differ greatly from the input and hence the overall frequency transfer factor must be close to unity.

This third requirement immediately led to the consideration of synthesis techniques using a mixer because of the summing nature of their characteristic, exemplified by that of equation (4.16) in Chapter 4. Using a mixer, a small adjustment frequency may be added to that of the primary source and varied to keep the sum constant as the temperature changes. The general form of such a synthesiser is shown in Figure 5.2, its output frequency being:

$$f_0 = f_1 - f_3 \quad (5.2)$$

for  $f_1 > f_0$ .

Two alternatives are now possible. Either the frequency  $f_2$  may be operated upon so that at phase lock it is equal to  $f_3$ , which may then be fixed; or  $f_3$  may be varied by some means. The obvious operation to perform on  $f_2$  is simple variable-modulus division, comparing the divider's output with a fixed  $f_3$  directly derived from  $f_0$ . Such a system is shown in Figure 5.3. Again taking  $f_1 > f_0$ ,

$$f_1 = f_0 + Nf_3 \quad (5.3)$$

giving a frequency resolution of:

$$R = \frac{\delta f_1}{\delta N} = f_3 = \frac{f_0}{M} \quad (5.4)$$

For high resolution, therefore,  $f_3$  must be small, and hence  $M$  large. In Chapter 4, the considerable disadvantages of a low phase comparator frequency were described, and for these reasons this system was not thought appropriate. By inspection of equation (5.2) it may be seen that if  $f_3$  is varied in small steps about some higher nominal frequency, then small steps in  $f_1$  may be compensated for. This may be stated mathematically by taking any digital address  $N$

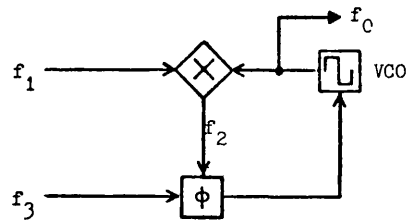


**Figure 5.2** The general form of additive frequency synthesis

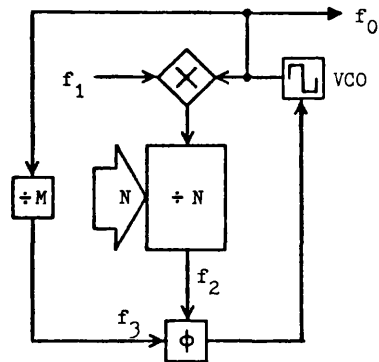


**Figure 5.3** Additive synthesis with variation of  $f_2$

which varies  $f_3$  and noting that, from equation (5.2):

$$R = \frac{\delta f_1}{\delta N} = \frac{\delta f_3}{\delta N} \quad (5.5)$$

Three methods of varying  $f_3$  in small steps about some higher frequency presented themselves.

Firstly, an auxiliary, lower frequency synthesiser may be employed as shown in Figure 5.4. Since

$$f_3 = Nf_4 = \frac{Nf_0}{M} \quad (5.6)$$

then

$$R = \frac{\delta f_3}{\delta N} = \frac{f_0}{M} \quad (5.7)$$

Thus high frequency resolution may be obtained, but only by choosing  $M$  large and hence again leading to a low phase comparator frequency, this time in the auxiliary loop. This is far less of a problem than if it occurred in the main loop for the reasons already discussed, but is nonetheless better avoided if possible. In any case the use of a double loop synthesiser conflicts somewhat with the objective of simplicity of calibration and adjustment.

Secondly, a rate-multiplier may be employed as in Figure 5.5<sup>(8)</sup>. If the rate-multiplier is commanded by an  $n$ -bit word  $N$ , then its output  $f_4$  is given by:

$$\langle f_4 \rangle = N \cdot \frac{f_0}{2^n}, \quad 1 \leq N \leq 2^n \quad (5.8)$$

where  $\langle f_4 \rangle$  denotes the average frequency taken over many periods.

The irregularity of the output pulse train is reduced by the fixed divider  $M$ . Neglecting this for the time being and considering average frequencies only, when the loop is phase locked,

$$f_1 = f_0 \left( \frac{2^n M + N}{2^n M} \right) \quad (5.9)$$

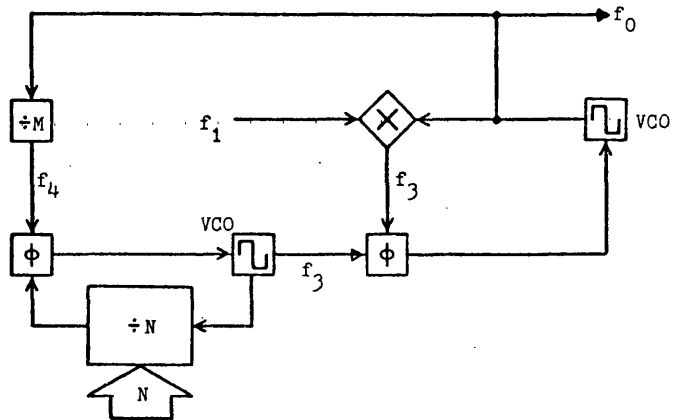


Figure 5.4 Double loop additive synthesis

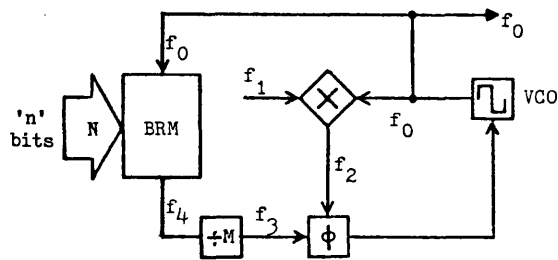


Figure 5.5 Additive synthesis incorporating a binary rate multiplier

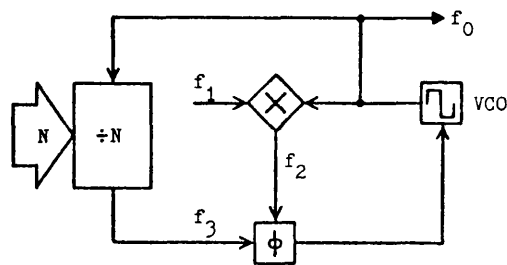


Figure 5.6 The Frequency Shifting Synthesiser



and the resolution may be written:

$$R = \frac{\delta f_1}{\delta N} = \frac{f_0}{2^{nM}} \quad (5.10)$$

showing that high resolution may be obtained by choosing a large value for the product  $2^{nM}$ . If  $M$  is made large, which is desirable in reducing the effect of fluctuations in  $f_4$ , then  $f_4$  is small and the attendant disadvantages of a low comparison frequency result. If  $n$  is made large, on the other hand, high resolution will be obtained but the corresponding increase in the total range of  $N$  (since  $1 \leq N \leq 2^n$ ) causes the frequency transfer factor to vary over a greater range. For example, if  $n = 12$ ,  $M = 1$  then  $f_1/f_0$  varies from 1.0002 to 2.0. The transfer factor may be brought closer to unity by an increase in  $M$  only. Though the binary rate-multiplier approach shows some advantages over the other systems discussed, these must be set against the detrimental effects of its irregular output pulse train upon the overall noise performance of the system.

The third approach to variation of  $f_3$  is direct programmable division of  $f_0$ , as shown in Figure 5.6. When the loop is phase locked:

$$f_1 - f_0 = f_0/N$$

from which

$$f_1 = f_0 \left( \frac{N+1}{N} \right) \quad (5.11)$$

The resolution is then given by:

$$R = \frac{\delta f_1}{\delta N} = \frac{-f_0}{N^2} \quad (5.12)$$

so that very high resolution may be obtained with a value of  $N$  which is not particularly large, due to the inverse-square nature of equation (5.12). Moreover, the frequency transfer factor is close to

unity for  $N$  greater than about 50. The most important factor here, however, is that since  $N$  need not be very large,  $f_3$  may remain higher than in the alternative approaches, improving the loop dynamics.

The parameter  $N$  is present in the expression for frequency resolution of this technique, in contrast with the others. This indicates that the frequency step size varies with  $N$  and therefore that the approach is non-linear in this sense. Despite this irregularity the frequency steps are entirely predictable and repeatable. This non-linearity is illustrated in Figure 5.7 from which it may be seen that for values of  $N$  greater than about 500 the relationship is very nearly linear and very close to unity. In any case, in this application such non-linearities may readily be accounted for by the programmed data. It was decided to adopt this approach to frequency correction.

The frequency synthesiser of Figure 5.6 is one of a class dubbed Frequency Shifting Synthesisers by the author to indicate their ability to produce very small frequency increments over a narrow range. Several applications other than that discussed here have arisen and are detailed, with a full theoretical discussion, in the published paper "The Frequency Shifting Synthesizer" included as Appendix C. It must be pointed out that the equations derived in the paper apply to the more usual case of synthesis of a varying output frequency from a fixed input frequency.

Having decided to employ a Frequency Shifting Synthesiser, it was desirable to decide upon its operating frequency. Preliminary tests were undertaken, and it appeared that no problems would present themselves at 5MHz or 10MHz. Difficulties in the construction of logic prototypes for use at 100MHz were experienced,

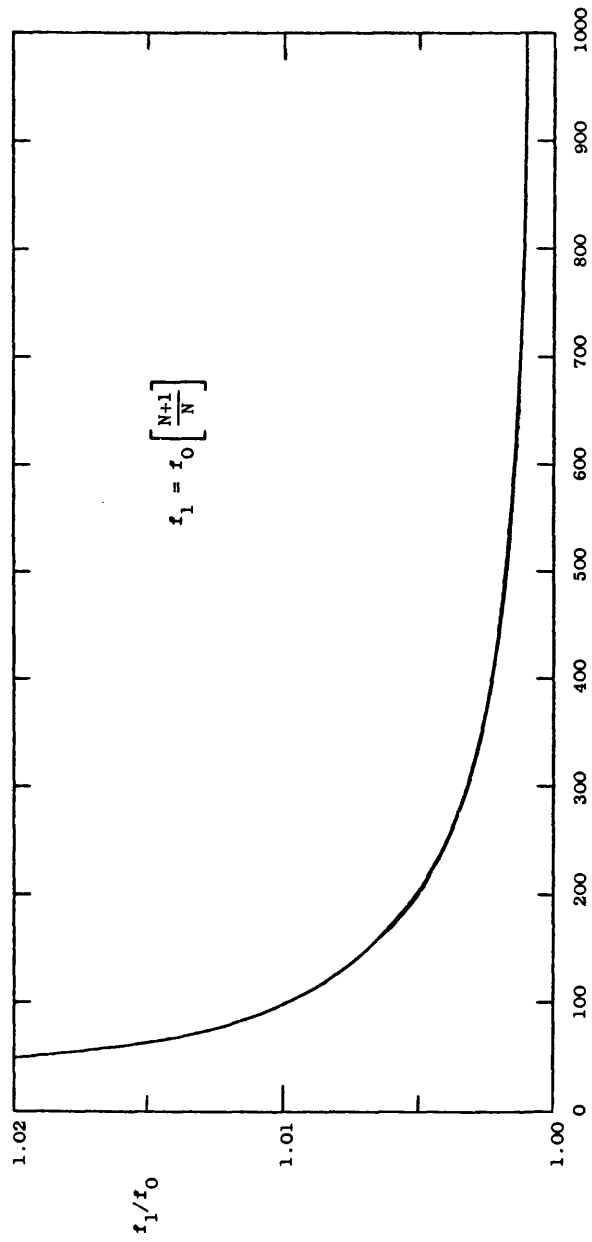


Figure 5.7 The frequency transfer characteristic of the frequency shifting synthesiser

however, and it was thought best to employ one of the lower frequencies. Accordingly it was decided to design the compensated oscillator for operation at 10MHz. Arguably the aging performance of 5MHz crystals is superior to that at 10MHz, but since this effect is, in the short term, secondary to its temperature instability 10MHz was preferred. It will be seen in Chapter 6 that this decision proved fortunate in one respect.

### 5.5 The Resulting System<sup>(9)</sup>

Having decided upon the nature of each element of the proposed temperature compensation scheme a block diagram may be drawn in summary, as in Figure 5.8. The fixed divider M derives the gating pulse for the counter and offers the added facility that subharmonics of  $f_0$  may be obtained by tapping the divider chain at various points. In the next chapter, details of a prototype of the system are given, the various parameters of design discussed as they arise, and measurements of its performance detailed. Certain general points concerning the system parameters may, however, be raised beforehand.

The output of the counter must, of course, be latched in order that the pROM address remains constant between gate pulses. The frequency of these pulses, the gating rate, defines the frequency resolution of the counter and hence the temperature resolution of the Y cut crystal thermometer. If the gating rate is made very low, then the temperature resolution is large and for any given temperature range the number of possible states of the counter increases. In order to discern all of these states the number of bits in the output data word of the counter must be large, as must the number of data words stored in the pROM. Further, it must be

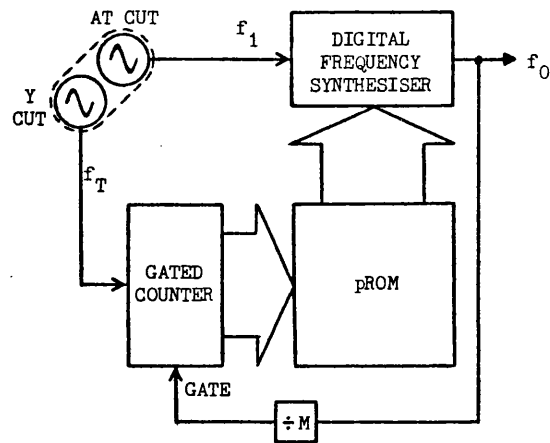


**Figure 5.8** Block diagram of the proposed temperature compensation scheme

remembered that no frequency compensation is made except at the instants of gating. If the gating rate is too low, therefore, considerable frequency change may occur during the count cycle between gate pulses. If the gating rate is too high, on the other hand, then the temperature resolution falls and the smallest frequency changes in  $f_1$  which may be corrected become larger, decreasing the overall frequency stability.

Once the operating temperature range is defined, the expected total frequency excursion of the AT cut crystal is predictable within reasonable limits. The total range of operation of the synthesiser, therefore, is also defined. The required frequency stability of the output directly dictates the resolution of the synthesiser and hence the total number of required frequency steps is defined. This in turn defines the word length of the command and therefore the size of each data word contained in the pROM.

These points illustrate the fact, (which will be demonstrated in Chapter 6), that the quality of operation of the system, whether in terms of frequency stability or total operating range, is inextricably bound up in the choice of digital memory capacity.

REFERENCES - Chapter 5

- (1) WADE, W.H., and SLUTSKY, L.J.: "Quartz crystal thermometer", Review of Scientific Instruments, Vol.33, No.2, February 1962.
- (2) GORINI, I., and SARTORI, S.: "Quartz thermometer", Review of Scientific Instruments, Vol.33, No.8, August 1962.
- (3) SMITH, W.L., and SPENCER, W.J.: "Quartz crystal thermometer for measuring temperature deviations in the  $10^{-3}$  to  $10^{-6}$ °C range", Review of Scientific Instruments, Vol.34, No.3, March 1963.
- (4) HAMMOND, D.L., ADAMS, C.A., and SCHMIDT, P.: "A linear, quartz-crystal, temperature-sensing element", ISA Transactions, Vol.4, October 1965, pp.349-54.
- (5) HAMMOND, D.L., and BENJAMINSON, A.: "The crystal resonator - a digital transducer", IEEE Spectrum, April 1969, pp.53-8.
- (6) MARTIN, J.D.: "Digital methods of frequency measurement: a comparison", The Radio and Electronic Engineer, Vol.42, No.6, June 1972, pp.285-94.
- (7) LITUS, J., NIEMIEC, S., and PARADISE, J.: "Transmission and multiplexing of analog or digital signals utilizing the CD4016A quad bilateral switch", RCA Appn. Note ICAN-6601.
- (8) MARTIN, J.D.: "Frequency scaling, by digital means", Proc. IEE Conference on Digital Instrumentation, No.106, November 1973, pp.67-73.
- (9) UK Provisional Patent no.39657/77: "Corrected oscillator", (W. Gosling, assigned to Racal Instruments Ltd., Maidenhead, Berkshire), November 1978.

## CHAPTER 6 - THE SYSTEM PROTOTYPE

In Chapter 5, each element of the proposed temperature compensation scheme was defined in principle. This chapter describes the design, construction and performance of a prototype unit which was produced in order to verify the operation of the system.

In the design of the prototype various features were included which have no direct bearing upon its operation but which served as an aid to measurement and calibration. The construction of the unit was arranged to afford easy modification and adjustment and was, therefore, not representative of a production model in size or power consumption. The performance of the unit was intended to be as nearly as possible that required of a production model. As will be seen, this proved impossible to achieve with the facilities available and a prototype design was adopted which allowed the simulation of practical operating conditions for each of the system elements in isolation, and the operation of the system as a whole under less stringent conditions. Each of these features will be detailed as they arise.

The proposed system and its prototype have been described in the published paper "A Digital Technique for Temperature Compensation of Crystal Oscillators" which is included as Appendix D. It must be pointed out, however, that various differences exist between the prototype described in the paper and the more general model described here.

### 6.1 The Read-Only Memory<sup>(1)</sup>

It was evident that the data to be stored in the read-only memory would need continual alteration and editing during both



calibration and measurement of the unit. To allow this facility it was necessary to substitute a read-write memory, of the same configuration, for the read-only memory. At the time of the prototype's design this was best achieved by the use of commercial pROM simulation and programming equipment which had recently become available in an appropriate form. For this reason it was decided to adopt the 2048-bit ultra-violet erasable pROM 1702A, details of which are included in Appendix E. The device is available from several manufacturers with differing performance only in respect of its access time, which is not critical here. It is compatible with TTL logic circuits throughout, features tri-state outputs to facilitate expansion, is cheap, reliable and usable over a wide temperature range. Its most important advantage in this application, however, was the fact that simulation and programming equipment was readily available. Using this equipment it was possible to observe the action of the device while in use, to edit the data either in part using a keyboard loader or in bulk or part using a teletype interface. With the aid of a teletype it was possible to record the data on punched tape, obtain paper print-out of the memory data and to transfer the data to another device for copying. Details of the memory support equipment employed may be found in Appendix F.

The 2048 storage elements of the 1702A are arranged as 256 8-bit words, so that the address is also an 8-bit word. The limitation of counter output and synthesiser input to 8 bits each represents the primary constraint upon the prototype. Using a 1702A it was only possible to vary the frequency synthesiser among 256 discrete steps, and to define 256 increments of measured temperature. More than one memory circuit could have been employed to expand the total memory capacity, but such an arrangement could not have been

simulated with the available equipment and therefore was impractical. In the period between the design of the prototype and the writing of this thesis the availability and use of much larger memories has increased considerably and the difference in cost between large and small memories and their support equipment has narrowed accordingly. If this work were to be repeated now a much larger memory system could be employed at no extra cost. Nevertheless, the use of the 1702A in no way invalidates the findings of the following sections as, wherever necessary, the consequences of the use of a larger memory were considered and accounted for.

## 6.2 Temperature Measurement

In Chapter 3 the resonant frequency of Y cut quartz was shown to vary linearly with temperature at the rate of 86 parts per million per degree Celcius over its total operating range. By choosing a Y cut crystal of nominal resonant frequency 11.6MHz for the temperature sensing element, therefore, a temperature coefficient of  $1\text{kHz}/^{\circ}\text{C}$  was obtained. This was convenient as the temperature resolution of the overall measurement could then be related to the frequency resolution, and hence to the gating period, of the counter by a numerically simple expression. Figure 6.1 is a graph of the measured frequency/temperature relationship of the first of a batch of six 11.6MHz Y cut crystals obtained specifically for this work, and shows excellent agreement between the theoretical and measured performance.

It was decided to employ 74LS series low power Schottky TTL logic circuits in the prototype unit for all the digital functions. This family was capable of direct interface with the 1702A pROM, capable of operation up to about 15MHz, readily obtainable from the

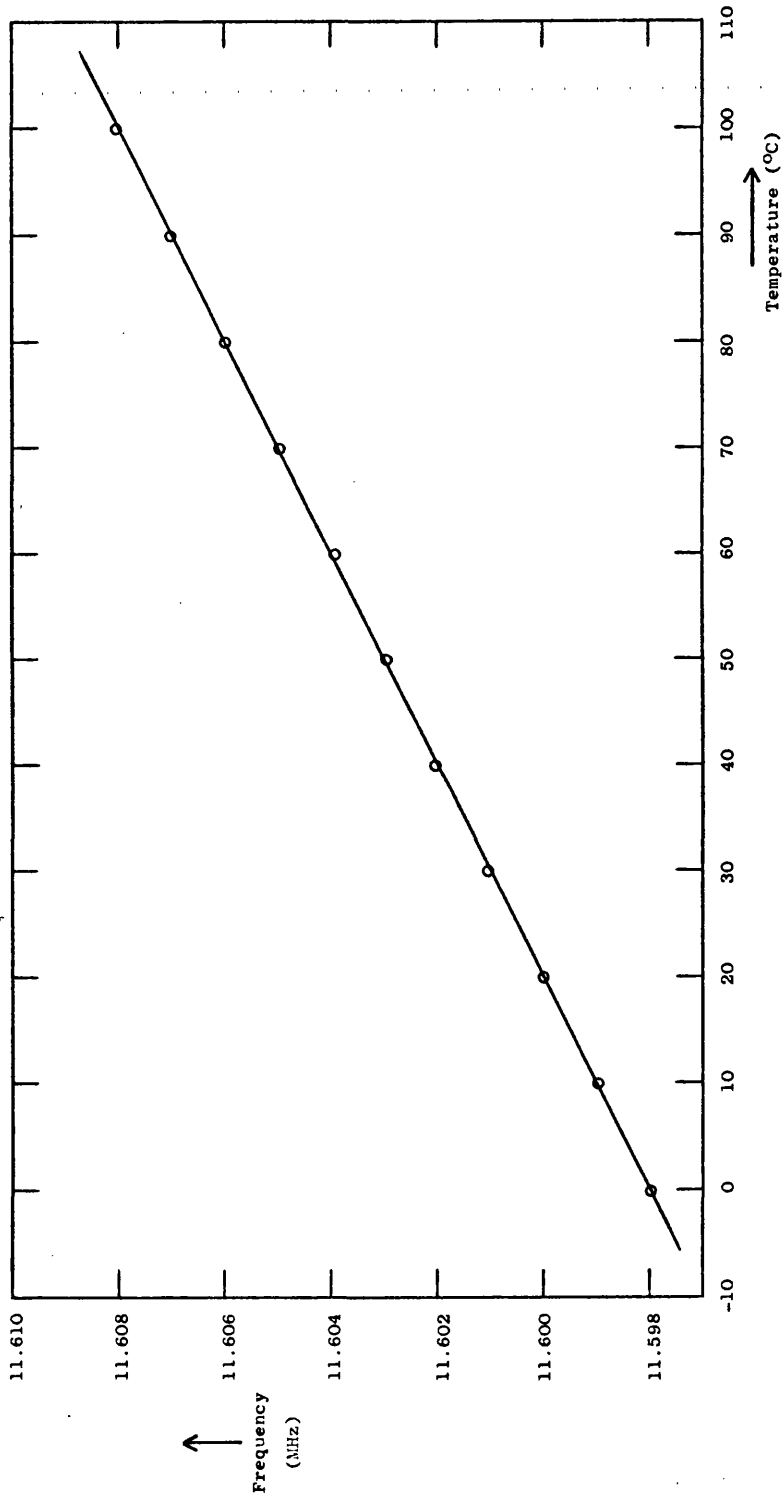


Figure 6.1 Measured performance of the Y cut crystal temperature sensor

departmental stores yet was reasonably economical in its cost and power consumption. MSI and SSI circuits of this family were used to construct a conventional gated counter to resolve frequency increments of 100Hz in the 11.6MHz Y cut crystal frequency, corresponding to a temperature resolution of  $0.1^{\circ}\text{C}$ . It was necessary to latch the output word of the counter after each gate cycle so that only valid addresses appeared at the input to the pROM. The gating waveform was arranged as a 10 millisecond pulse occurring once every second as shown in Figure 6.2. In this way it was possible to obtain the required frequency resolution yet obtain an update of temperature data only at the fairly infrequent rate of one per second. This was considered adequate to follow the fastest temperature changes likely to occur at the crystal pair, whilst preventing unnecessary hunting between adjacent temperature counts.

Two 74LS163 synchronous binary counters together with two 74LS95A shift registers were employed in the counter/latch arrangement as shown in the schematic of Figure 6.3. The required gating waveform was derived from the final 10MHz output signal by means of two 74LS390 dual decade counters, one 74LS90 decade counter and two 74LS192 decade counters as shown in the figure, the  $\div 2$  prescaler stage being common to other parts of the system. This chain of digital dividers served the additional purpose of supplying signals at various frequencies subharmonically related to 10MHz whilst retaining the frequency stability and spectral purity of the main output. Despite the fact that within the gate period of 10 milliseconds approximately 116000 cycles of the Y cut crystal oscillator output occur, it was not necessary to resolve all of these since to do so would require a 17-bit counter. As the pROM can contain only 256 words, only 8 bits were required at its address,

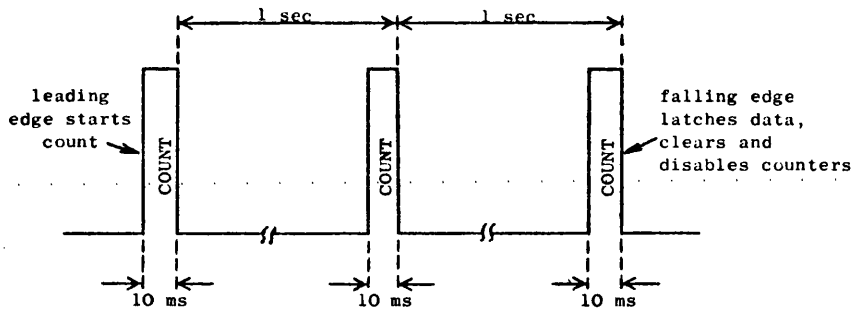


Figure 6.2 The frequency counter gating waveform

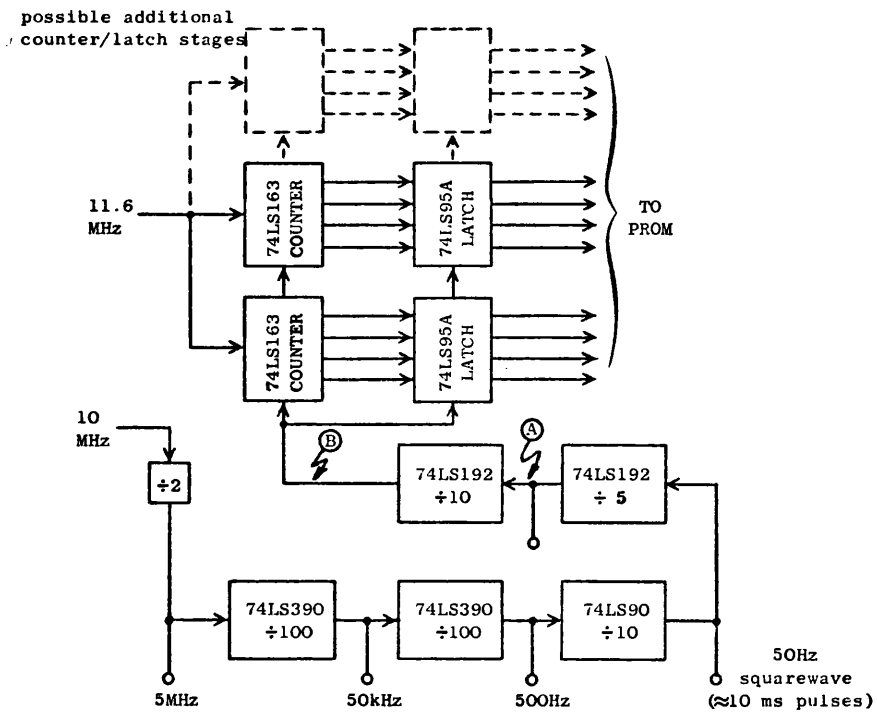


Figure 6.3 Schematic of the counter, latch and gating circuitry

- waveform (A) : 10 ms pulses every 100 ms
- waveform (B) : 10 ms pulses every 1 sec, as shown in Figure 6.2

and hence only the least significant 8 bits of the total count need be registered. During each gate period, therefore, the 8-bit counter cycles from zero to its maximum count of 255 about 453 times before the output is latched during the 454th cycle. The counter resolves 256 frequencies 100Hz apart giving it a total range of 25.5kHz. At frequencies at the extremes and towards the centre of its range the following counts result:

At 11.5875MHz the count will be  $115875 - (452 \times 256) = 163$

At 11.6000MHz the count will be  $116000 - (453 \times 256) = 32$

At 11.6130MHz the count will be  $116130 - (453 \times 256) = 162$

These counts show that as the temperature increases through the effective range the counter output changes not from zero to 255 but from 163 up to 255 and then from zero to 162. This 'folding over' of the counter output posed no problem as each count merely addresses a unique store in the pROM into which any required data may be programmed. In practice, this folding over also dispensed with the need to adjust the Y cut crystal frequency, hence allowing a fixed capacitor to be used in place of the usual trimmer in its oscillator circuit.

As discussed in section 5.2 of Chapter 5, the gated counter as used in the prototype displays the optimum large-signal response time. Since the counter is effectively one of total range  $2^{17}$  and nominal count 116000, then its normalised input as defined by Martin<sup>(2)</sup> is:

$$\frac{116000}{2^{17}} = 0.885$$

in which case its static measurement uncertainty is also the optimum which may be achieved. The small-signal tracking performance of a counter is considered acceptable when it may be assured that the

input frequency will not change by more than the counter's resolution during any one gating period. For this counter to fail, therefore, the input frequency would have to change by 100Hz in 10 milliseconds, which corresponds to a rate of change of temperature of  $10^{\circ}\text{C}$  per second at the Y cut crystal. Such a rapid change in temperature would be most unlikely to occur under normal conditions in a standard crystal unit. As will be seen later, the crystals used in the prototype were, in any case, enclosed in a block of sufficient thermal mass to ensure that the tracking rate of the counter could never be exceeded whilst in normal use or under calibration or test.

Since the temperature measurement system could resolve only 256 increments of  $0.1^{\circ}\text{C}$  each, then the total operating range was limited to  $25.6^{\circ}\text{C}$ . This was a definite limitation in the performance of the overall compensation scheme but, as will be seen later, was commensurate with the available frequency compensation range and resolution of the frequency synthesiser. The constraints placed upon both these devices were the direct results of the limited storage capacity of the pROM. Despite the limitation of the prototype, the principles exhibited are completely valid for both wider range and higher resolution temperature measurement. For example, if the gating pulses were narrowed to 1 millisecond, then the temperature resolution would fall to  $1^{\circ}\text{C}$ , but the range using an 8-bit counter would be  $256^{\circ}\text{C}$ . Conversely, if a larger pROM were to be employed, the total range could be extended accordingly with no loss in temperature resolution simply by the use of additional counter/latch stages as shown in Figure 6.3. It must be remembered, however, that any improvement in range or resolution is fruitless unless a corresponding improvement in the frequency correction process is

achieved.

As mentioned in Chapter 5, any temperature measurement can only be as accurate as the temperature coincidence between the sensor and the subject. In this application both sensor and subject are quartz crystals mounted in identical holders, so that for use in the prototype it was necessary to ensure that the heat conducted to and from each of the crystals was equal. To do so required some general investigation of the thermal paths within the crystal unit<sup>(3)</sup>.

When the crystal plate is mounted in its holder and sealed in the conventional way, two thermal paths to the plate are significant. Firstly, heat may flow from the main body of the can across the inert gas (which is used to flush out the air during manufacture and remains at low pressure within the enclosure) to the plate. Secondly, heat may flow from the circuit board conductors up the mounting leads to the plate. It is shown in Appendix G that the effects of each of these paths must be considered in ensuring thermal equalisation of the two crystals and were accounted for in the prototype in the following manner.

The AT cut and Y cut crystal units were mounted close together in a small aluminium block of outer dimensions 25 x 20 x 20mm into which were milled two slots to accommodate the HC 18/U crystal holders such that their normal mounting plane was flush with the bottom face of the block. The units were bonded into position with silver-loaded epoxy resin which afforded a low thermal resistance between the crystals and the block. The photograph of Figure 6.4 shows the underside of a block with the crystals in place. Two threaded holes are included so that the block may be firmly mounted onto a circuit board in good thermal contact with the ground-plane.

Both oscillators comprised the circuit shown in Figure 3.22 of



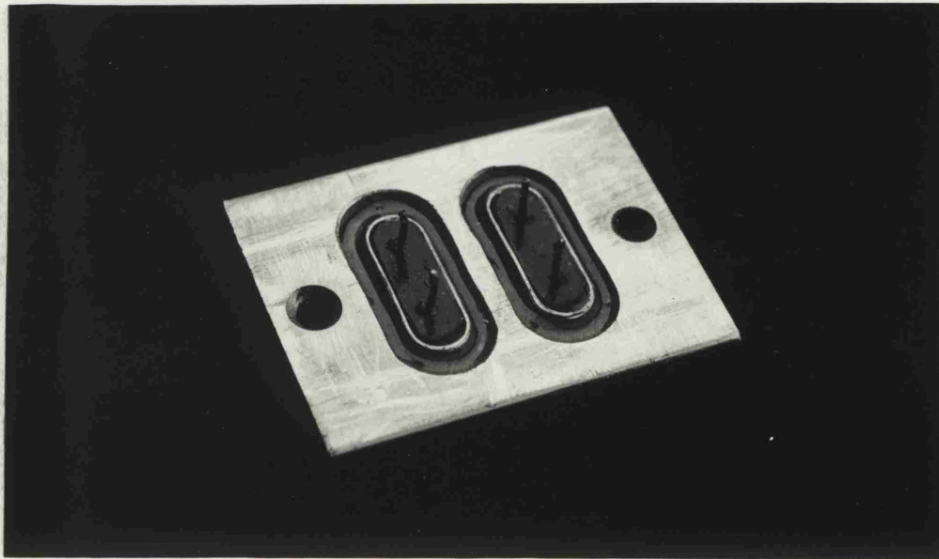


Figure 6.4 Photograph of the underside of a crystal block as used in the prototype

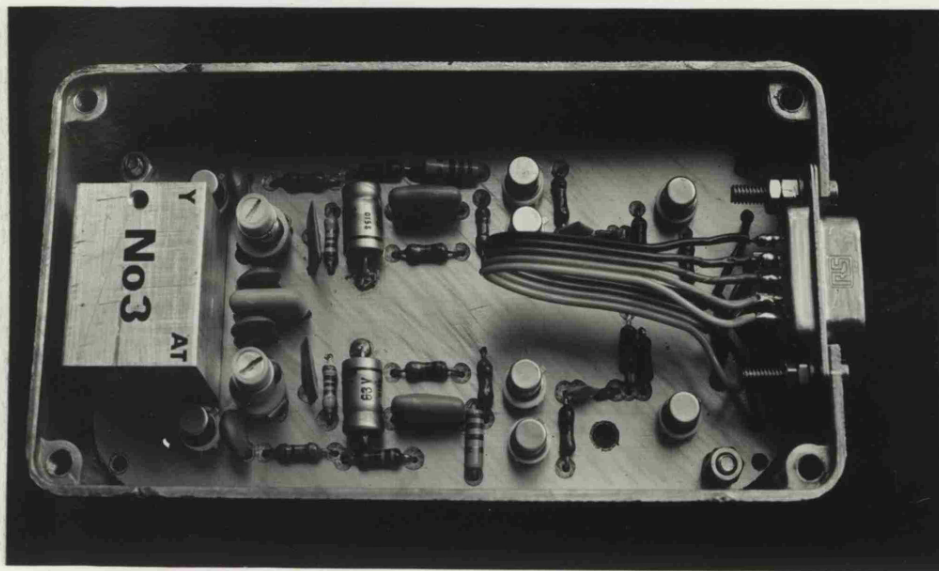


Figure 6.5 The prototype twin oscillator unit showing the crystal block on the left and the symmetrical arrangement of the components

Chapter 3 and were assembled with the crystal block on a single printed circuit board. The conductor layout of the board was arranged such that each oscillator component was positioned as the mirror image of its counterpart in the other oscillator, about an axis of symmetry passing between the two crystals. In this way the conductor paths leading to the crystals were made the same length and shape for each, and hence the thermal paths were equalised. For reasons described later in section 6.4, the oscillator pair was enclosed in a separate die-cast box from the remainder of the circuitry and the space between the circuit board conductors and the box was insulated by a thin layer of polystyrene. The crystal block and symmetrically arranged oscillator components are clearly visible in the photograph of Figure 6.5.

It is not in the steady state but the transient condition that temperature measurement is most likely to be in error. Even if the resistances of the thermal paths to the crystals could be perfectly equalised, the rate of change of temperature of the crystals would differ unless their thermal capacities were equal. The thermal capacity (or thermal mass) of a body is defined as the product of its mass and its specific heat, so that since both crystals are made of quartz of the same specific heat, the thermal capacities of the crystals will be equal if their masses are equal. Both of the crystals used in the prototype were in the form of a 9mm diameter disc plate the thickness of which is related to its resonant frequency by equation (3.1) of Chapter 3,

$$f_0 = \frac{K}{d} \text{ kHz}$$

where  $d$  is the plate thickness in millimetres and  $K$  is the frequency thickness constant. As was shown in Chapter 3, the value of  $K$  for an AT cut plate is 1670kHz.mm, and for a Y cut plate is 1950kHz.mm. The

thickness of each plate is, therefore:

$$d_{AT} = 0.167\text{mm}$$

$$d_Y = 0.168\text{mm}$$

which leads to the very fortuitous result that in the prototype, the masses, and hence the thermal capacities, of the two crystals differ by less than one percent, promising accurate temperature measurement under both steady-state and transient conditions.

In order to test the temperature equalisation of the twin crystal arrangement, a special block was prepared containing two 11.6MHz Y cut crystals. This was used in a twin oscillator as described above, but without the aid of a box as insulation. A counter, similar to that of Figure 6.3, was used to count the frequency of one of the crystals against the other as shown in Figure 6.6, and the result shown on a hexadecimal alphanumeric display. The two oscillators were adjusted at room temperature to give a count of zero, allowed to stabilise for about two hours, readjusted and then subjected to a series of abrupt temperature changes. The resolution of the counter was about 2.3Hz, so that by noting the maximum deviation of the count from zero during each test operation the corresponding maximum temperature difference between the crystals could be estimated.

It was found that at no temperature between about 0°C and 60°C did the count deviate by more than three, indicating a steady-state equalisation of temperature closer than 7m°C. The greatest change in the count was noted when the unit, having been heated rapidly to 60°C, was sprayed with freezing agent on one side of the crystal block only. During this test the count changed by a maximum of 26, corresponding to a temperature difference of about 60m°C between the crystals. Even during this last, unrealistically extreme, test, the

temperature equalisation fell within that required for the prototype of temperature resolution  $0.1^{\circ}\text{C}$ . With the added insulation afforded by its box, it could reasonably be assumed that the temperature equalisation of the twin oscillator board would be adequate for use in the prototype.

### 6.3 Frequency Correction

As outlined in Chapter 5, it was decided to employ a Frequency Shifting Synthesiser of output frequency 10MHz as the frequency correcting element of the prototype. A frequency resolution of approximately 0.3Hz was chosen, as the resulting total range of the synthesiser would then be about 75Hz, corresponding well with the expected frequency excursion of a good AT cut crystal over the  $25^{\circ}\text{C}$  temperature range under consideration.

The decision to use a good crystal (in the sense that it exhibited a small total frequency excursion) in the prototype was a carefully considered one. On the one hand, such a choice conflicts with the primary intention that components for the compensated oscillator should not require any careful selection procedure. If a crystal of more usual specification had been used, on the other hand, the range of the synthesiser would have needed to be larger and, given the limitation of only 256 address steps, the resolution lower, leading to a less stable output frequency. There was no doubt that a larger pROM storage capacity would increase the number of synthesiser frequency steps, but it had yet to be proved that such a high frequency resolution could be achieved with a simple synthesiser, and accordingly a good crystal and a resolution of 0.3Hz were decided upon.

The maximum slope of the frequency/temperature characteristic

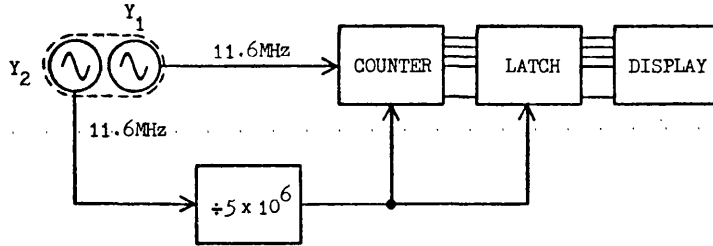


Figure 6.6 Test arrangement for temperature equalisation of crystals

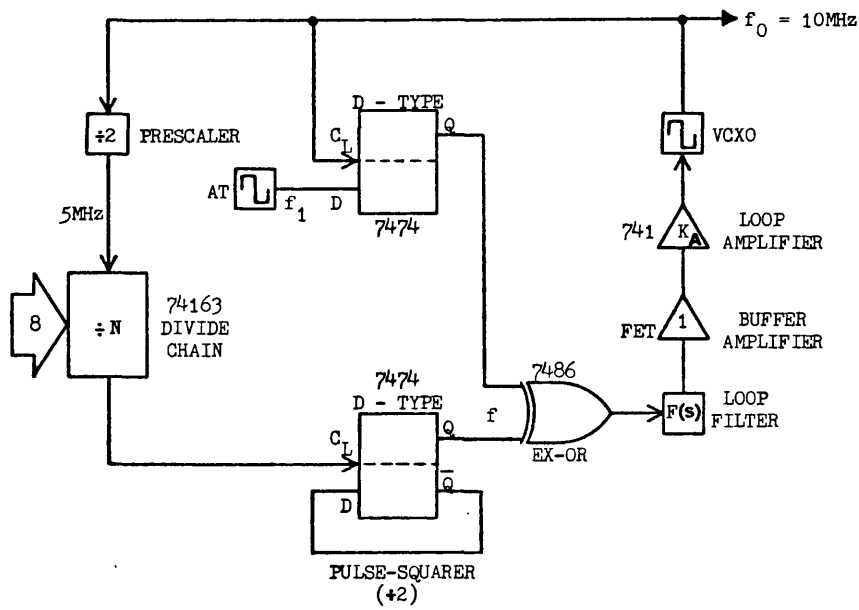


Figure 6.7 The Frequency Shifting Synthesiser of the prototype

of an AT cut crystal occurs at the inflexion temperature, and for a crystal such as that of the prototype was expected to be at the most 5Hz/°C. The maximum possible frequency shift within a detectable temperature change of 0.1°C was, therefore, 0.5Hz. This figure defined the expected frequency stability of the overall system as 5 parts in  $10^8$  which, if it could be achieved, represented a worthwhile improvement in the performance of corrected oscillators.

It was decided to employ digital circuitry to realise the functions of the mixer and phase comparator of the synthesiser as described in Appendix C. A 74LS74 dual D-type flip-flop<sup>(4)</sup> was used as a frequency downconverter, and a 74LS86 quadruple exclusive-OR as the phase comparator<sup>(5)</sup>. The programmable divider arrangement consisted of successive stages of 74LS163 synchronous binary counters whose input was taken from the 5MHz prescaled output shown in Figure 6.3. The output of such a counter chain consists of narrow pulses whose width vary with division modulus. Such a signal was unsuitable as input to an exclusive-OR phase comparator and it was necessary to square the waveform by means of the second flip-flop of the 74LS74 pack. It was necessary to include an analogue loop amplifier to supply the required gain, and this consisted of a 72741 operational amplifier used in a conventional configuration between ground and a 12 volt supply rail so that its output was always a positive voltage. A unity-gain buffer amplifier with a FET input was also employed to enable measurements of loop parameters to be made without disturbance. Figure 6.7 shows the Frequency Shifting Synthesiser of the prototype in its digital form. Details of the VCO and loop filter are discussed later in the section.

The divide-by-2 action of the prescaler and pulse squarer modify the transfer equation of the prototype synthesiser to:

$$f_0 = f_1 \left( \frac{4N}{4N + 1} \right) \quad (6.1)$$

so that the resolution of increments of  $f_1$  for constant  $f_0$  is:

$$\frac{\delta f_1}{\delta N} = f_0 \left[ \frac{-1}{4N^2} \right] \quad (6.2)$$

For the required resolution of 0.3Hz at  $f_0 = 10^7$ Hz,  $N$  may be found to be 2887, to the nearest whole number. A division ratio of 2887 requires a 12-bit divider so that in the prototype three 4-bit 74LS163 counters were required. The binary equivalent of 2887 is:

$$2887 = 1011 \ 0100 \ 0111$$

Since only eight bits were available from the pROM to address the synthesiser, only the least significant eight bits of the above binary number were adjustable, the four most significant being fixed, so that the range of available division moduli was:

$$1011 \ 0000 \ 0000 = 2816$$

$$\text{to } 1011 \ 1111 \ 1111 = 3071$$

and the mid-range modulus was:

$$1011 \ 1000 \ 0000 = 2944$$

The nominal frequency resolution is obtained by putting  $N = 2944$  in equation (6.2) to give:

$$R_{\text{nom}} = 0.288\text{Hz}$$

The worst-case resolution is obtained for  $N = 2816$ , giving:

$$R_{\text{max}} = 0.315\text{Hz}$$

The value of  $f_1$  required to give an output of 10MHz at  $N = 2944$ , assuming  $f_1 > f_0$ , was:

$$f_1 = 10000849\text{Hz}$$

The nominal resolution resulting from the prototype synthesiser was rather lower than had been intended but was allowed to remain in this form as a later adjustment could readily be performed by

changing the hard-wired address to the ninth counter stage. The required value for the AT cut crystal oscillator frequency  $f_1$  was close enough to 10MHz for it to be possible to pull the frequency of a 10MHz crystal to the required value by reduction of its load capacitance. Had a correctly lapped 10.000849MHz crystal been employed the equalisation of thermal transients as described in the previous section would not have been significantly affected, the masses of the two crystals still differing by less than one percent.

In the steady-state, the phase locked loop of the frequency synthesiser will correct the frequency of the AT cut crystal as required. A transient condition can occur in the loop only once every second at the most as this is the rate at which temperature data is updated by the counter/latch arrangement. These transients will consist of very small frequency hops in normal operation, and of a large frequency error only at switch-on when the conventional acquisition process occurs. At switch-on, it is not necessary for the loop to acquire lock particularly quickly as the correct data will only arrive at the synthesiser after two clock periods due to the delay through the latch. The required dynamic performance of the loop, therefore, was unexacting and it was possible to design the loop to perform advantageously in other respects.

In section 4.2 of Chapter 4 it was shown how a phase locked loop may be used to modify the noise spectrum of a frequency source. By judicious choice of the loop bandwidth it is possible to arrange for the output to exhibit the long-term stability of the input and the short-term stability of the VCO. For the aging rate of quartz crystals to be as low as possible it is necessary to operate them at a correspondingly low drive level. Unfortunately the signal-to-noise ratio of a crystal oscillator falls as its drive level is reduced



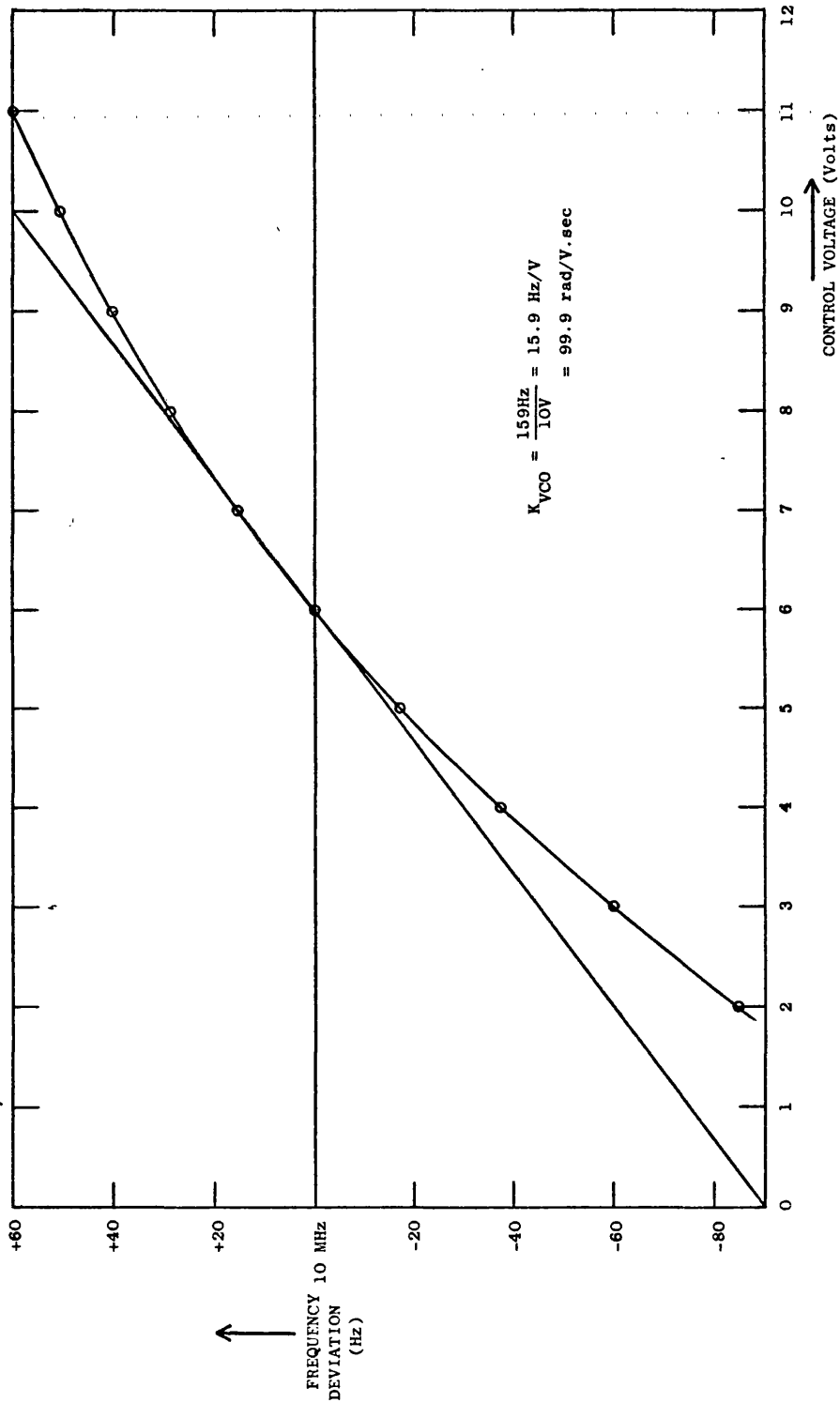


Figure 6.8 The Prototype VCXO characteristic

and the goals of good aging rate and low noise conflict in free-running oscillators. Using a phase locked loop, however, it is possible to clean up the noise spectrum of a low-power oscillator by utilising a VCO of high spectral purity and choosing a narrow loop noise-bandwidth. This was accomplished in the prototype by employing a low-gain, high drive level voltage controlled crystal oscillator (VCXO) as the output of the loop. The circuit was similar to that of Figures 3.22 and 3.23 of Chapter 3 with a reduced value of R1 and operating on a higher voltage supply of 30-50 volts. A graph of the frequency against control voltage of the VCXO is given in Figure 6.8. The crystal used in the VCXO need not be of high quality or close calibration tolerance as the phase locked loop compensates for any free-running frequency offset.

The characteristic of an exclusive-OR phase comparator is shown in Figure 6.9<sup>(5)</sup>, from which it may be seen that for a TTL exclusive-OR gate operating on a 5 volt supply, the phase-detector gain constant,  $K_d$ , is 0.796 volts per radian. From Figure 6.8 the gain constant of the VCXO,  $K_{VCO}$ , may be determined as 99.9 radians per second per volt. It was decided to employ a loop filter of the conventional passive lag-lead configuration as shown in Figure 6.10, its transfer function being:

$$F(s) = \frac{1 + s\tau_2}{1 + s\tau_1} \quad (6.3)$$

where  $\tau_1 = (R_1 + R_2)C$  (6.4)

and  $\tau_2 = R_2C$  (6.5)

Figures 6.11(a) and 6.11(b) show how a simple equivalent phase locked loop may be derived for a Frequency Shifting Synthesiser, eliminating the mixer and programmable divider. If the gains of the loop amplifier, VCO and mixer are combined to form an element of

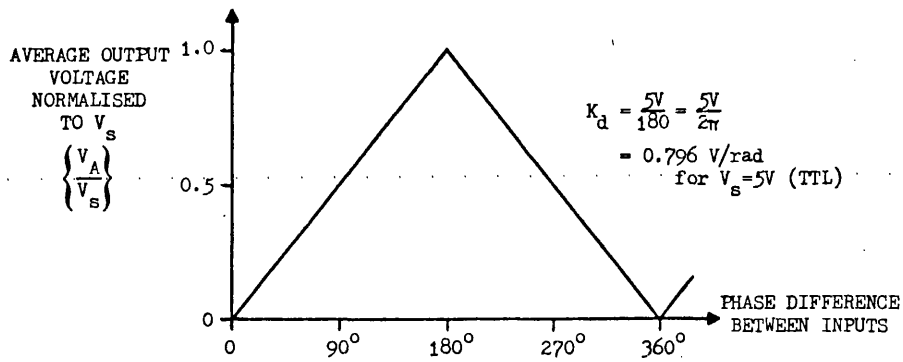


Figure 6.9 Exclusive-OR phase comparator characteristic

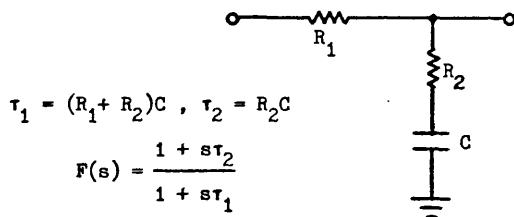


Figure 6.10 The passive lag-lead loop filter of the prototype

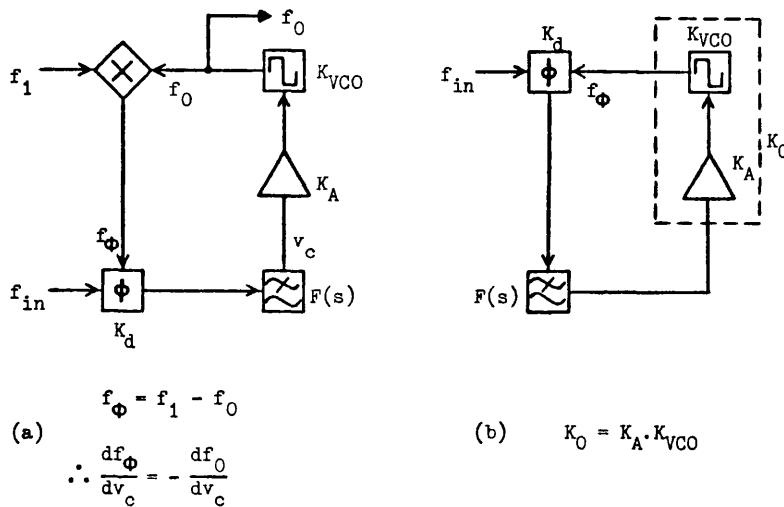


Figure 6.11 The Frequency Shifting Synthesiser  
 (a) basic arrangement  
 (b) simple phase-locked loop equivalent

gain  $K_0$  radians per second per volt, then the loop takes the canonical form of a second-order phase locked loop with a passive filter. Using the usual servomechanism notation, the closed-loop transfer function may be written<sup>(6)</sup>:

$$H(s) = \frac{s(2\zeta\omega_n - \omega_n^2/K_0K_d) + \omega_n^2}{s^2 + 2\zeta\omega_n s + \omega_n^2} \quad (6.6)$$

where

$$\omega_n = \left( \frac{K_0K_d}{\tau_1} \right)^{\frac{1}{2}} \quad (6.7)$$

is the natural frequency of the loop, and

$$\zeta = \frac{1}{2}\omega_n \left( \tau_2 + \frac{1}{K_0K_d} \right) \quad (6.8)$$

is the damping factor. Other loop parameters of interest are the dc gain of the loop,  $K_v$ , given by

$$K_v = K_0K_d \quad \text{sec}^{-1} \quad (6.9)$$

and the loop gain,  $K$ , given by

$$K = K_0K_d \frac{\tau_2}{\tau_1} \quad \text{sec}^{-1} \quad (6.10)$$

The noise bandwidth of the loop is defined by the relation<sup>(7)</sup>

$$B_L = \int_0^{\infty} |H(j2\pi f)|^2 \cdot df \quad \text{Hz} \quad (6.11)$$

which for the loop in question may be simplified to

$$B_L = \frac{K}{4} \left( \frac{K + 1/\tau_2}{K + 1/\tau_1} \right) \quad \text{Hz} \quad (6.12)$$

Furthermore, it may be shown that the minimum noise bandwidth occurs when  $\zeta = 0.5$ , though this minimum is not exceeded by more than 1dB for any value of damping between 0.25 and 1.0.

It was therefore decided to design the loop with a damping factor close to 0.5. The following component values were arrived at:

$$R_1 = 220\text{k}\Omega, R_2 = 4.7\text{k}\Omega, C = 0.68\mu\text{F}$$

which, together with a loop amplifier gain of about 200, yield the following values:

$$\omega_n = 320 \text{ rad}\cdot\text{sec}^{-1}$$

$$\zeta = 0.52$$

$$K_V = 15750 \text{ sec}^{-1}$$

$$K = 329 \text{ sec}^{-1}$$

$$B_L = 157 \text{ Hz}$$

Furthermore, these values allow estimates to be made of the loop's capture range,  $f_c$ , and acquisition time,  $t_a$ <sup>(8)</sup>. These yield

$$f_c = 104\text{Hz}$$

and, assuming an initial frequency error at the extreme of the capture range,

$$t_a = 3.96 \text{ milliseconds}$$

The prototype synthesiser was constructed and tested and found to perform in close agreement with the theory. The observed capture range was rather larger than that calculated at about 120Hz, and the acquisition time somewhat slower, approaching 10 milliseconds in the worst case. No adjustment was made for these discrepancies as they may be accounted for by the expected spread of values of commercial components, and because the operation of the compensated oscillator was not jeopardized in any respect.

Some details of the construction and operation of the prototype system are given in the following section and its performance is analysed in section 6.5.

#### 6.4 The Construction and Operation of the Prototype

For convenience, the prototype was constructed in three parts, each of which could be modified or changed without affecting the operation of the others. Firstly, the twin oscillator board and block containing the crystal pair were housed in a die-cast box measuring about 110 x 60 x 27mm, with a nine-way D-type connector used to interface this with the remainder of the system. The ability to separate the oscillators from the remainder of the system was advantageous in that it allowed effective temperature cycling of the system for programming or test by heating or cooling the oscillator unit alone, reconnecting it to the system, and then allowing it to cool or warm to room temperature. By using this technique the need to temperature cycle the digital circuitry was eliminated, which was of particular importance when the pROM simulation equipment was used as its operating temperature range was limited.

The VCXO was assembled alone on a small circuit board. This allowed variation of its power supply voltage, and hence its drive power level, during testing. It had also been intended to facilitate the testing of conventional VCO configurations for comparison with the VCXO, though these tests were not performed. For the purposes of normal running, programming and long-term frequency stability tests it was unnecessary to use a high voltage power supply for the VCXO, and under these conditions it was operated at 12 volts, in common with the other oscillators. A short length of low-loss screened wire was used for connection of the VCXO control voltage, whilst all other oscillator interconnections were made by multi-way ribbon cable. The outputs of all three oscillators were available as both a sinusoid of about 1 volt peak-to-peak and a TTL compatible squarewave. Buffer switches were employed at the logic outputs in

order to drive the signals into the higher load presented by the interface leads.

The remainder of the prototype hardware - memory, counter/latch, synthesiser, loop filter components and analogue amplifier - were assembled onto a printed circuit board of about 90 x 150mm. Signals at subharmonics of the output frequency were made available by tapping the divide chain as shown in Figure 6.3. Trimming potentiometers were included in the analogue amplifier circuit to allow minor adjustment of the loop gain. Conventional decoupling of all power supply rails was employed throughout, including a -9 volts rail required only to power the pROM output buffers.

The logic board, VCXO and twin oscillator unit were all assembled into a die-cast box of about 170 x 120 x 50mm. The photograph of Figure 6.12 shows the completed prototype with the twin oscillator unit removed. The VCXO board was mounted on its side as shown at the bottom of the picture, the pROM being clearly visible towards the centre of the logic board. The twin oscillator unit, whose interface connector may be seen at the left of the picture, was fixed to the lid of the box so that when closed it fitted above the logic board.

The method employed to programme the prototype corrected oscillator manually was, in essence, as follows. The twin oscillator unit was slowly temperature cycled. Using the pROM simulator keyboard loader, the synthesiser command required to give an output frequency as close as possible to 10MHz was determined by trial and error. This command was then stored in the pROM simulator at a location corresponding to the prevailing temperature word. The operator then waited for the temperature word to change before repeating the search process and storing the data. This process was

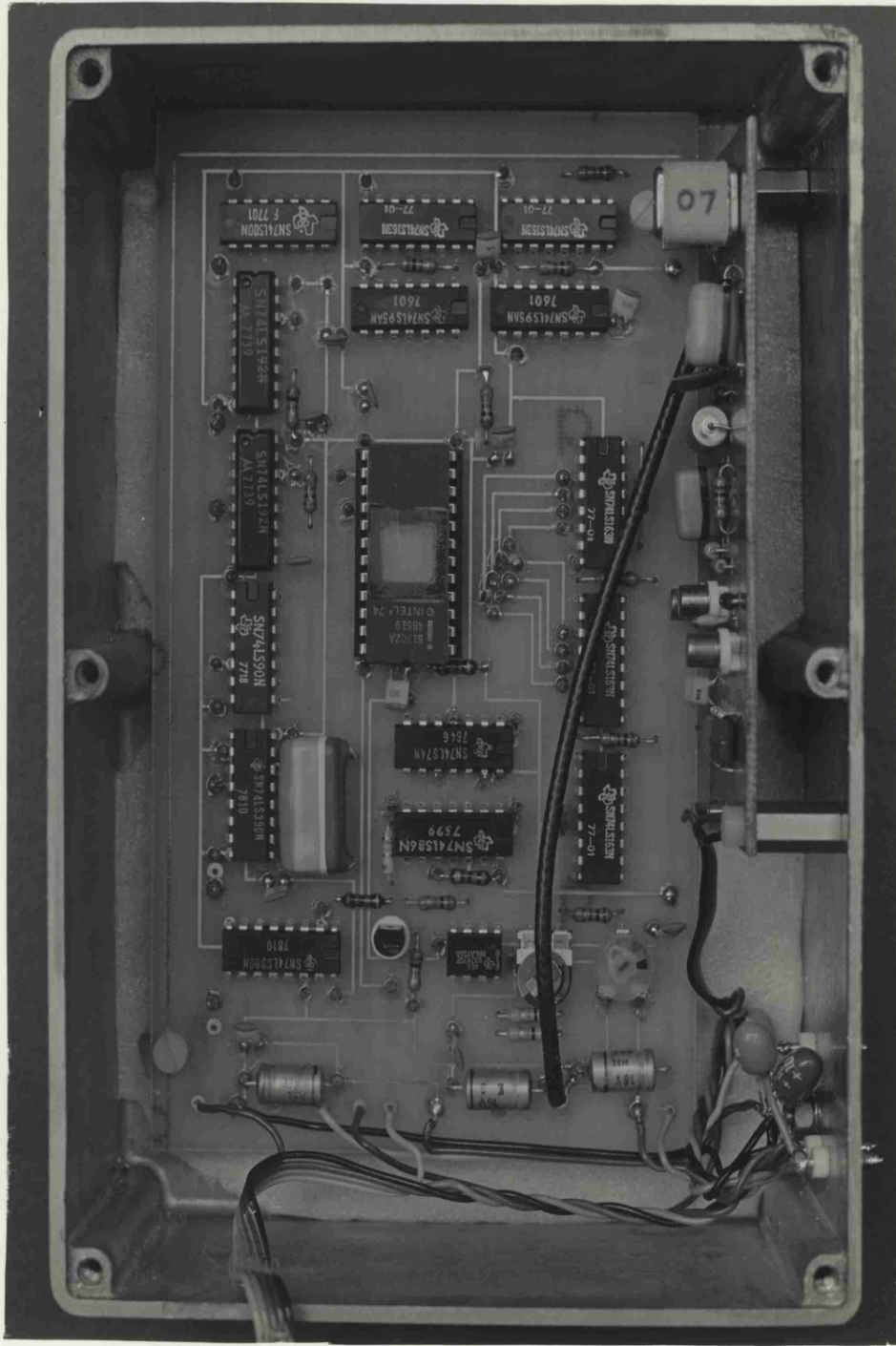


Figure 6.12 The completed prototype with the twin oscillator unit removed



continued until all the required data was determined, requiring 256 complete operations.

Several drawbacks of this method became apparent. Firstly, in order to realise the full potential of the system it was necessary to measure its output frequency to a resolution of 0.1Hz. With a conventional digital frequency meter this requires a gate time of 10 seconds, and hence each measurement must take at least that long, and typically rather longer. The search for the correct data usually required three or four measurements (with the exception of the very first search, which necessarily took more), so that the total programming time was two to three hours. Secondly, a steady temperature change of the unit lasting the full duration of the programming would have proved impossible to achieve. Thirdly, the vigilance required of the operator during such a tedious process proved to be a severely limiting factor, a high incidence of errors being inevitable.

The first of these drawbacks was overcome by the use of a frequency error multiplier. This is an instrument which multiplies the error between its input frequency and some reference frequency standard by a preselected factor. For example, if the error between the input and the standard is  $\Delta f$ , then the output frequency of a typical frequency error multiplier would be:

$$f_M = 10\text{MHz} + N \cdot \Delta f \quad (6.13)$$

where  $N = 10^0, 10^1, 10^2$  or  $10^3$  as selected by a front-panel control. If  $\Delta f = 0.1\text{Hz}$ , therefore, a selected value of  $N = 10^3$  will give an output of 10000100Hz so that the input frequency may be resolved to 0.1Hz in a gate time of only 10 milliseconds. Early programming was achieved using a purpose built frequency error multiplier as described in Appendix C, section 3.3. Later, a commercially built

frequency difference meter was employed which had the additional facility of an analogue display of frequency difference with resolution up to a maximum of  $\pm 1$  part in  $10^{11}$  full-scale deflection. Using the commercial meter, the measurement time during programming was reduced considerably so that the total search time was defined only by the time required to execute the programming keystrokes.

Having reduced the required programming time, the problem of assuring a slow enough temperature change was considerably relaxed. It was found to be convenient to heat the twin oscillator unit alone in an oven, as described previously, and allow it to cool naturally whilst the programming operation was carried out for temperatures above the ambient. Temperatures below the ambient were accounted for by cooling the unit in a refrigerator and programming during its warm up. The rate of increase of temperature during this latter process, however, was found to be rather faster than was convenient for reliable programming. Accordingly, an insulating jacket was fashioned into which the cold unit was placed so that the resulting rate of increase of its temperature was more suitable for manual programming.

Despite taking these measures to alleviate the initial difficulties encountered during manual programming, the problem of human error remained. One of the primary objectives of this oscillator correction technique was the removal of the requirement for such human action during the calibration process. An examination of the repetitive search-and-store action of the programming procedure reveals that its function is one readily achieved using an automatic process. Chapter 7 contains a discussion of such processes, and an analysis of various methods of adapting the programming

technique to different requirements.

## 6.5 Performance of the Prototype

In spite of the difficulties encountered, data was determined for the temperature compensation of a crystal pair (housed in block number three) over the approximate range 15°C to 40°C. This data was programmed into a 1702A pROM designated ROM 1. Using ROM 1, the performance of the prototype was evaluated for its temperature stability, short-term frequency stability and long-term frequency aging. The results of the tests are now described.

### 6.5,1 Temperature Stability

The temperature stability of the prototype was tested by means of the arrangement of Figure 6.13. Any accurate frequency measurement depends upon the availability of a stable reference frequency standard. The reference must necessarily be at least two orders of magnitude more stable than the test signal under all circumstances for the measurements to be reliable. To ensure this, in all tests performed on the prototype unit a rubidium vapour cell passive atomic frequency standard was used, a partial specification of which is given in Appendix H. The test signal was applied to the commercial frequency difference meter, the error-multiplied output of which was fed to a conventional digital frequency meter. A second output consisting of a dc error voltage proportional to  $\Delta f$  was fed to a strip chart recorder having selectable paper feed rates between 8 inches per minute and 1 inch per hour. The use of an X-Y plotter to record the frequency measurements was not convenient since no signal directly representing temperature was available. A steady

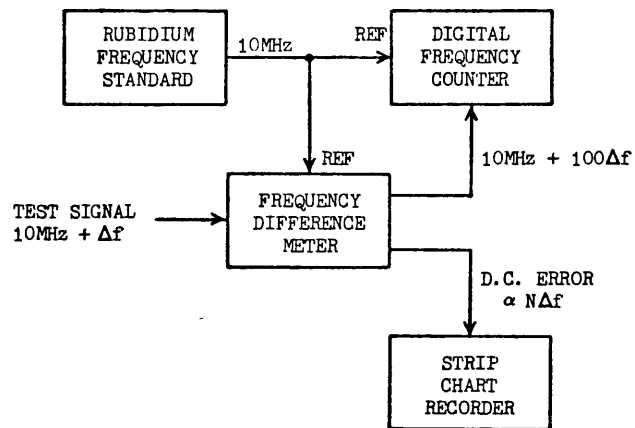


Figure 6.13 Test arrangement for measurement of the temperature stability of the prototype

time coordinate, however, was adequate for the purpose of expanding the variations in frequency-error voltage and so a chart recorder was ideal. An event marker was used to record occasional stages in the temperature change of the unit manually.

The procedure adopted for temperature stability tests was to first cool the twin oscillator unit to about  $10^{\circ}\text{C}$ , reconnect it to the system and allow it to warm naturally in its insulating jacket. Outside its programmed temperature range the output frequency of the prototype was clearly in error by a large amount. As soon as it warmed into range, however, the output frequency was properly compensated to a value close to 10MHz. When this was apparent the frequency difference meter was engaged and the strip chart recorder switched on at a feed rate of two inches per minute. The unit warmed naturally towards room temperature, but was thereafter gently heated with a hot air blower up to the top of its range. Throughout this temperature change, which took approximately twenty minutes, the event marker was used to label the chart at every sixteenth temperature increment encountered (in hexadecimal notation, at temperatures 00, 10, 20....F0).

A typical chart is shown in Figures 6.14(a), (b), (c) and (d). The approximate temperature coordinates are shown in hexadecimal notation along the top of the chart and may be seen to progress irregularly with time. Much of the erratic behaviour of the trace may be attributed to noise produced by the measuring arrangement, though some features are due to irregularities in the programmed data. Nevertheless, a study of the trace reveals much about the performance of the prototype.

The maximum frequency error may be seen to be about 0.5 parts in  $10^7$ . This is in accordance with the prediction of worst-case

HEWLETT-PACKARD 2270-1012

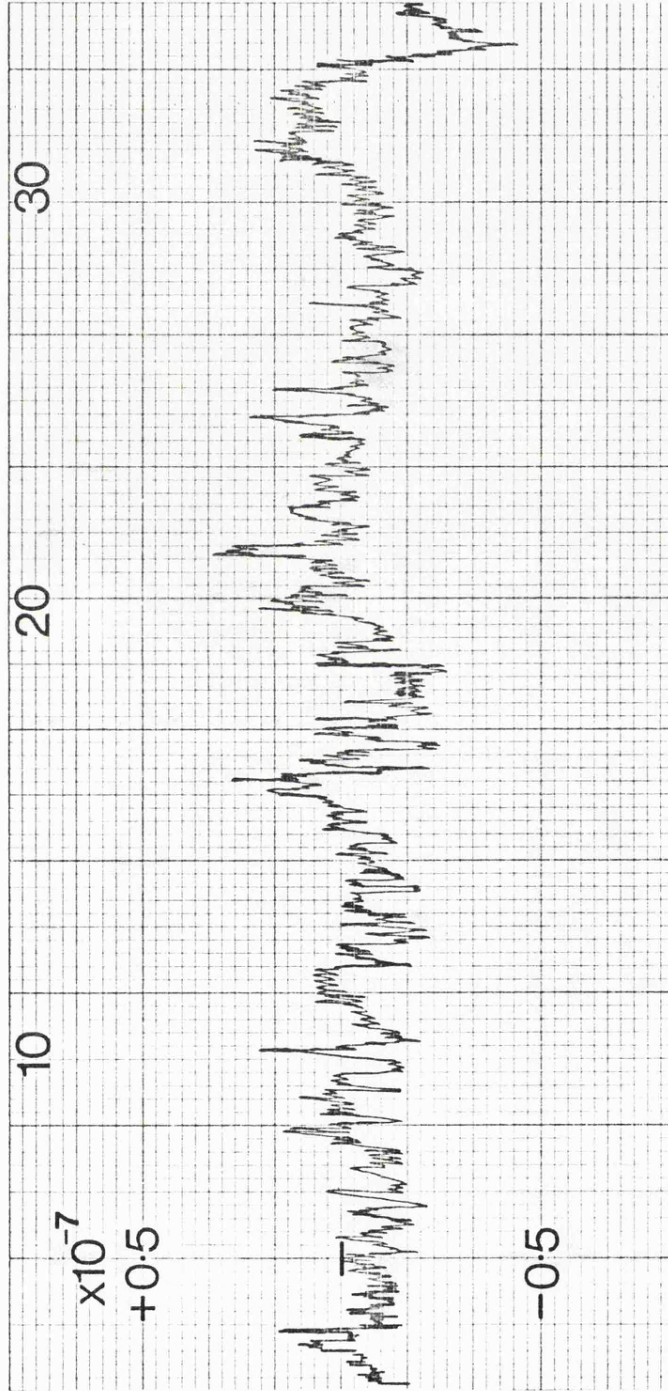


Figure 6 14(a) A typical recording of frequency against temperature obtained from the test arrangement of Figure 6.13

HEWLETT-PACKARD 9270-1012

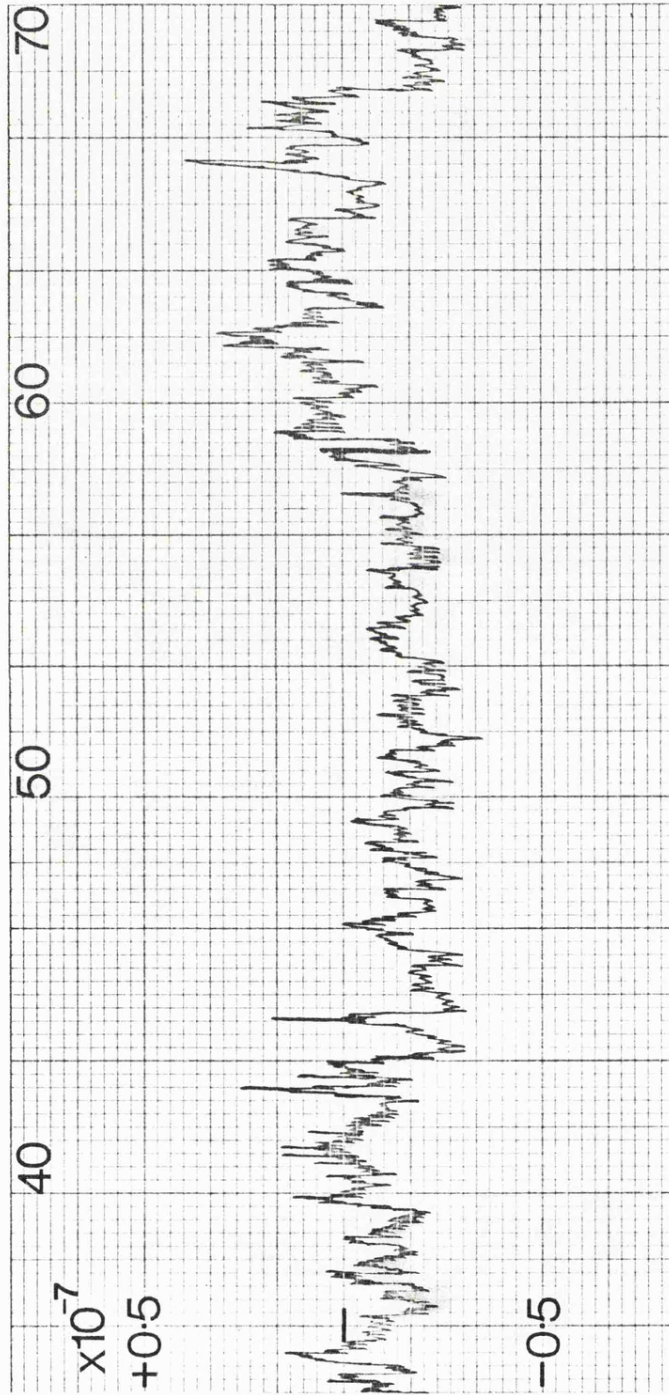


Figure 6.14(b) A typical recording of frequency against temperature obtained from the test arrangement of Figure 6.13 (continued)



HEWLETT PACKARD 9270-1012

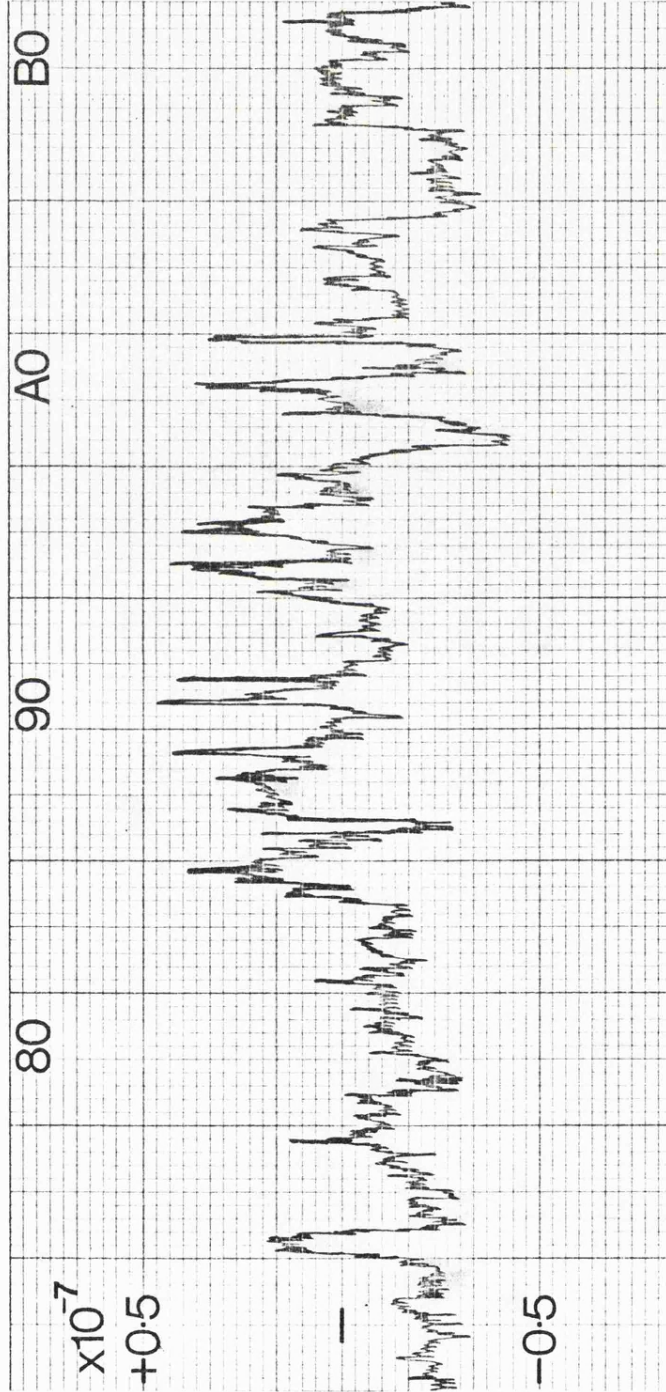


Figure 6.14(c) A typical recording of frequency against temperature obtained from the test arrangement of Figure 6.13 (continued)



HEWLETT-PACKARD 820-1012

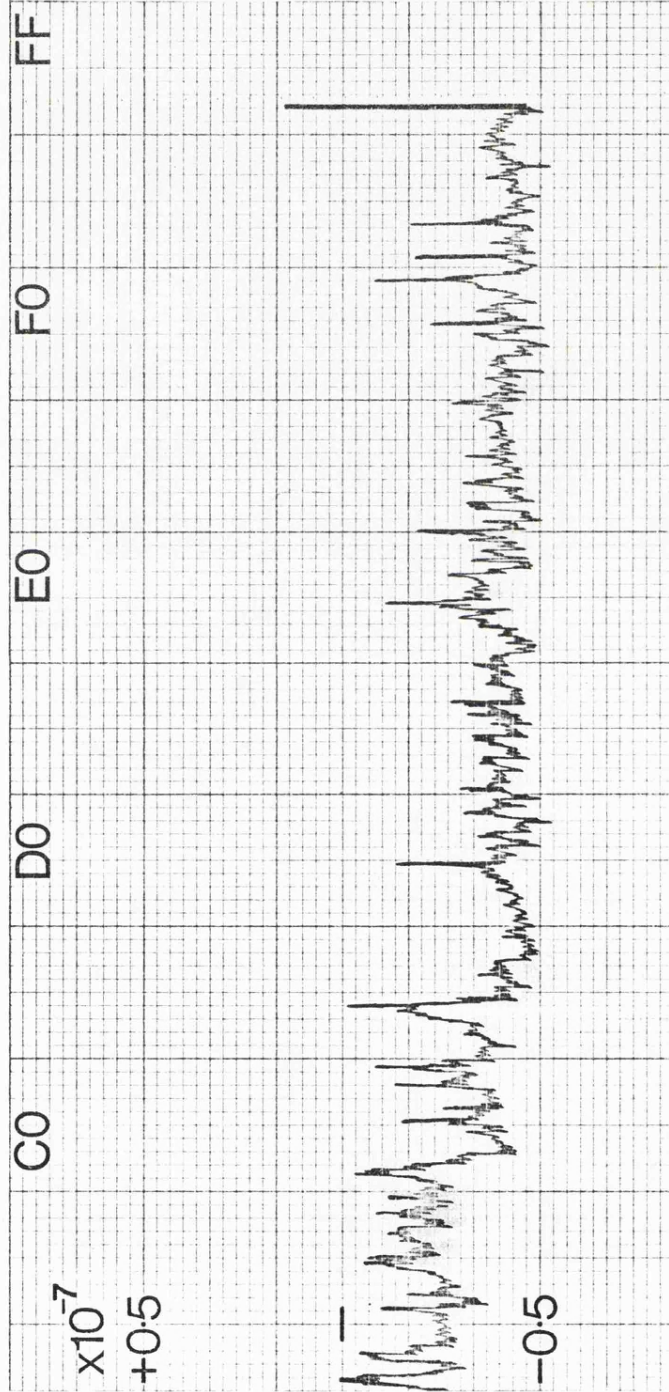


Figure 6.14(d) A typical recording of frequency against temperature obtained from the test arrangement of Figure 6.13 (continued)

frequency error of the prototype made in section 6.3 and may be attributed to that particular AT cut crystal used. The general step-correction action of the compensation scheme is clearly visible throughout the chart, though the apparent trend towards a constant frequency error at the higher temperature end of the scale is believed to be attributable to a steady drift in the chart recorder reference voltage rather than to an actual drift in frequency. This suspicion may not be verified, however.

The twin oscillator unit was warmed in its insulating jacket until the temperature coordinate 80 had been reached, when the jacket was removed. The more immediate response of the uninsulated unit to variations in the hot air supply probably accounts for the increased activity immediately afterwards. It was possible to produce a much more regular chart during such tests by insertion of a low-pass filter in the signal path between the frequency difference meter and the strip chart recorder. Such charts, however, although showing the extent of the frequency excursions, tended to obscure the detailed action of the system and were found to be of less use overall than those similar to Figure 6.14.

Much of the activity evident in the charts is unnecessary. The system in the form of the prototype has a clear tendency to hunt between adjacent temperature counts causing the frequency to hop accordingly. This hunting may be eliminated by allowing a change in temperature count to be applied to the pROM address only when it has become established for more than one gate period, a process readily achieved by simple digital processing. The modifications required are detailed in section 6.6, though in order to evaluate its worst-case performance they were not carried out on the prototype.

### 6.5.2 Short-Term Frequency Stability

The various parameters by which short-term frequency stability may be defined were listed in section 2.1.2 of Chapter 2, and measurement techniques for the evaluation of each of these parameters are described in reference (9). Interpretation of the results of such measurements is difficult. Unless information is available on the performance of alternative oscillators under identical test conditions, the results are meaningless. The closest approach to a standard definition is that of phase noise as given in equation (2.13), which requires a very low bandwidth measurement arrangement. Difficulty in accurately specifying the bandwidth of measurement leads to the common practice of testing by comparison, in which other types of frequency source are subjected to the same tests as the source under evaluation and the results compared. In this way the effects of measurement sensitivity, instability of the reference oscillator, and measurement bandwidth are effectively cancelled.

Two comparative short-term frequency stability tests were performed. Firstly, the phase noise of the prototype as measured on a laboratory spectrum analyser was compared with that of the rubidium frequency standard, an oven controlled free-running crystal oscillator, and an analogue temperature compensated crystal oscillator. Secondly, a comparison of the frequency variance of the prototype and the oven controlled oscillator was made by taking measurements in the time domain using the rubidium frequency standard as a reference. The test procedures and results are now described.

A Hewlett-Packard HP 141T series spectrum analyser was used to compare the phase noise of the various sources. The minimum

measurement bandwidth of the instrument is 10Hz so that, from equation (2.19), a correction factor of  $10\log(10) = 10\text{dB}$  must be taken into account in comparing the measured values with the formal definition of phase noise. An X-Y plotter was connected to the spectrum analyser to allow recording of the measured spectrum.

Spectral analysis of the prototype required that the temperature compensation process was disabled by removing the pROM and replacing it with the Pseudo Prom module operating in its keyboard mode. In this way the frequency synthesiser was prevented from hopping in frequency during the spectrum analyser scan, which lasted two minutes. Had the synthesiser been allowed to hop, the resulting trace on the spectrum analyser would have been overwritten by a comb of spikes representing the instantaneous bursts of noise which occur at each hop set against the timebase of the scan. Hence the trace intended to represent the performance of the prototype in the frequency domain would have been modified by instantaneous changes in that performance occurring in the time domain. By using the Pseudo Prom and keyboard the address to the synthesiser could be held constant for the duration of the measurement and hence prevent frequency hopping.

Figures 6.15(a), (b), (c) and (d) show the resulting traces for the four oscillators under comparison. Apart from differences in the peak signal power and slight frequency offsets, there is no visible difference between the four traces. Furthermore, the measured phase noise at an offset-from-signal frequency of 50Hz is only -77dB which is at least 40dB worse than the specified performance of the rubidium standard. These results are not surprising, however, when it is remembered that the short-term frequency stability of the frequency sources within the spectrum analyser is almost certainly

**Figure 6.15(a)** Measured frequency spectrum of a Racal Instruments oven-controlled crystal oscillator

$f_0 = 5\text{MHz}$   
RF bandwidth = 10Hz  
IF bandwidth = 10Hz  
scan width = 10Hz/div.  
scan time = 5sec/div.  
amplitude = 10dB/div.

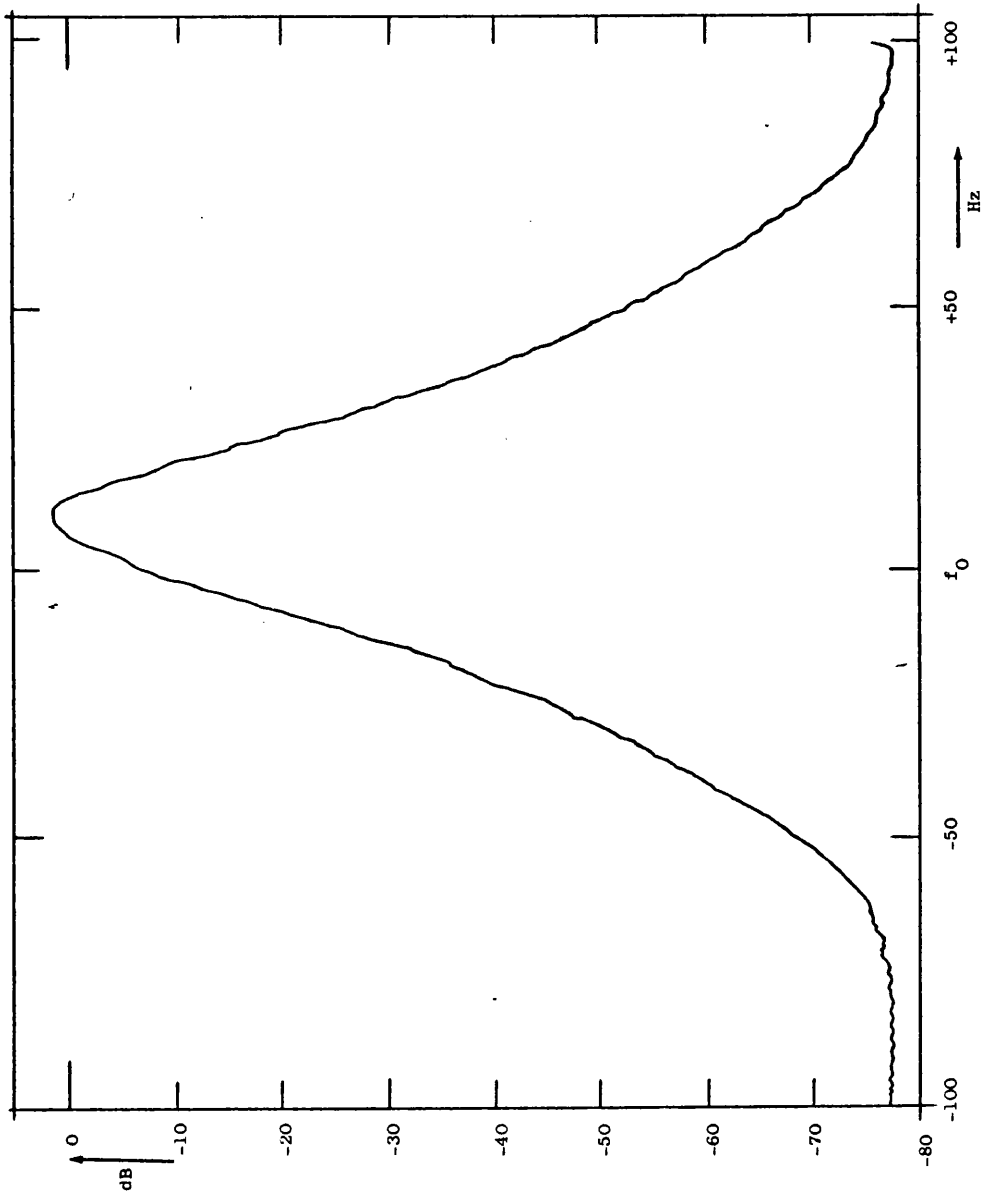


**Figure 6.15(b)** Measured frequency spectrum of Efratom rubidium frequency standard

$f_0 = 10\text{MHz}$

RF bandwidth = 10Hz

IF bandwidth = 10Hz

scan width = 10Hz/div.

scan time = 5sec/div.

amplitude = 10dB/div.

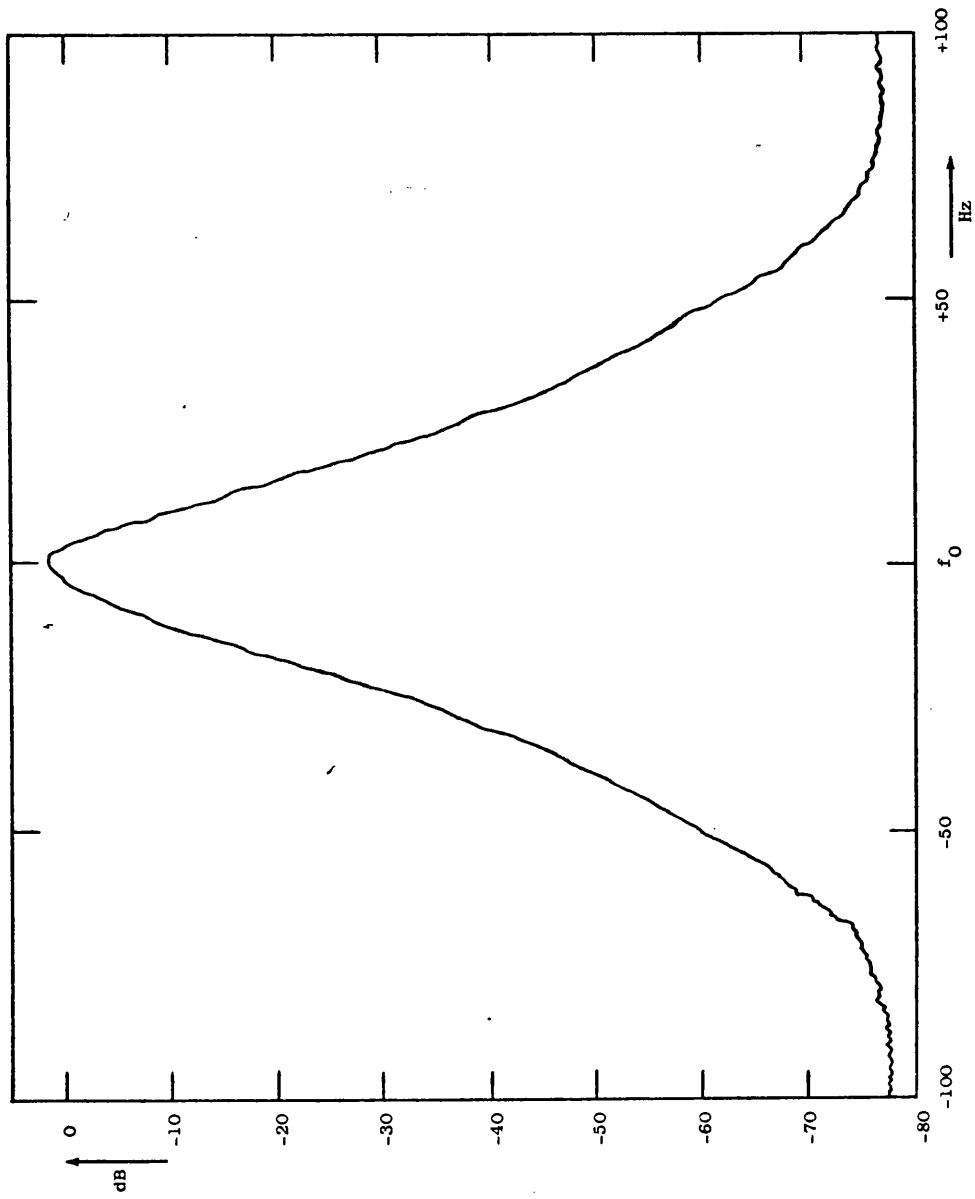


**Figure 6.15(c)** Measured frequency spectrum of an analogue temperature compensated crystal oscillator

$f_0 = 5\text{MHz}$   
RF bandwidth = 10Hz  
IF bandwidth = 10Hz  
scan width = 10Hz/div.  
scan time = 5sec/div.  
amplitude = 5dB/div.

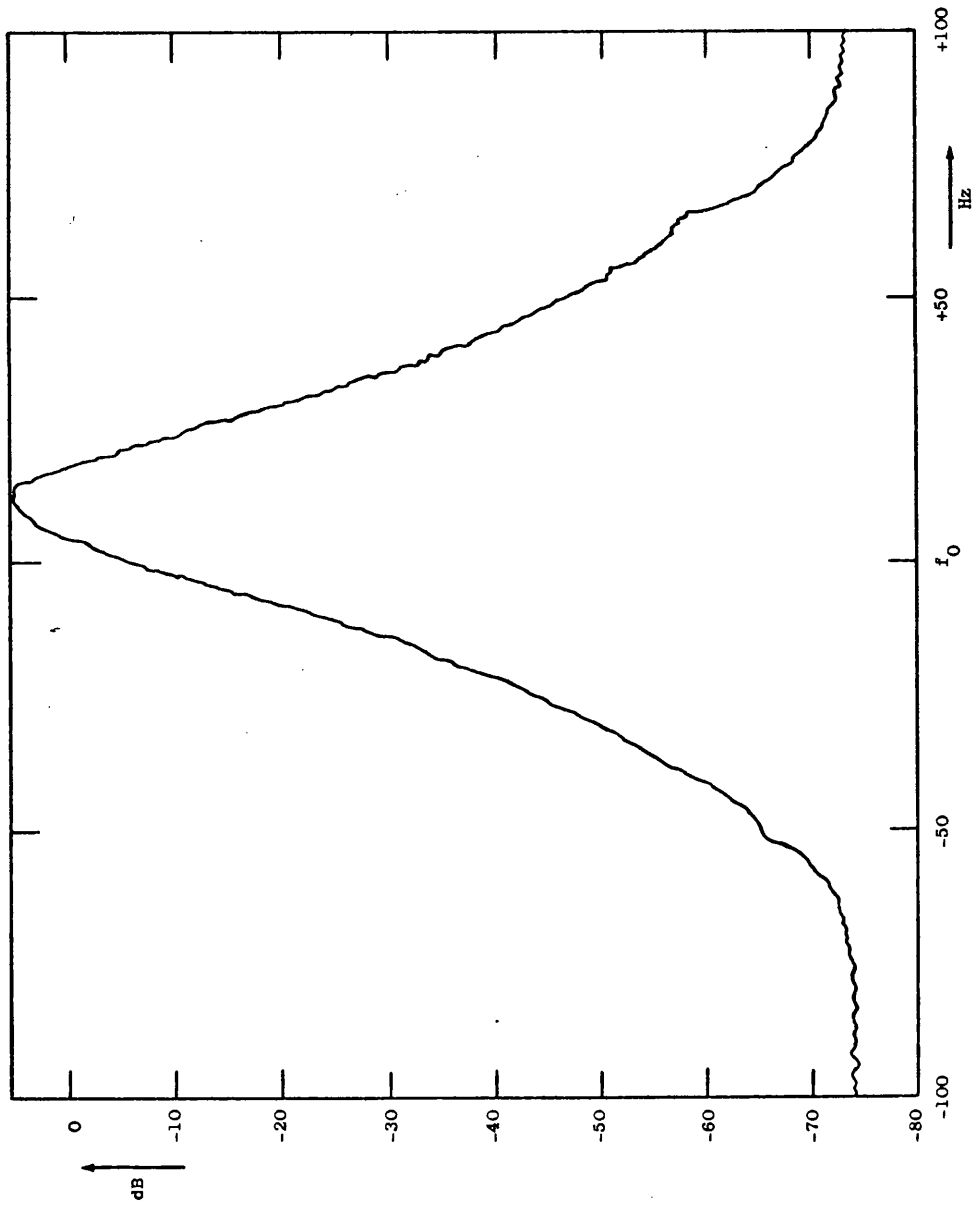


**Figure 6.15(d)** Measured frequency spectrum of the prototype digitally temperature-compensated oscillator

$f_0 = 10\text{MHz}$

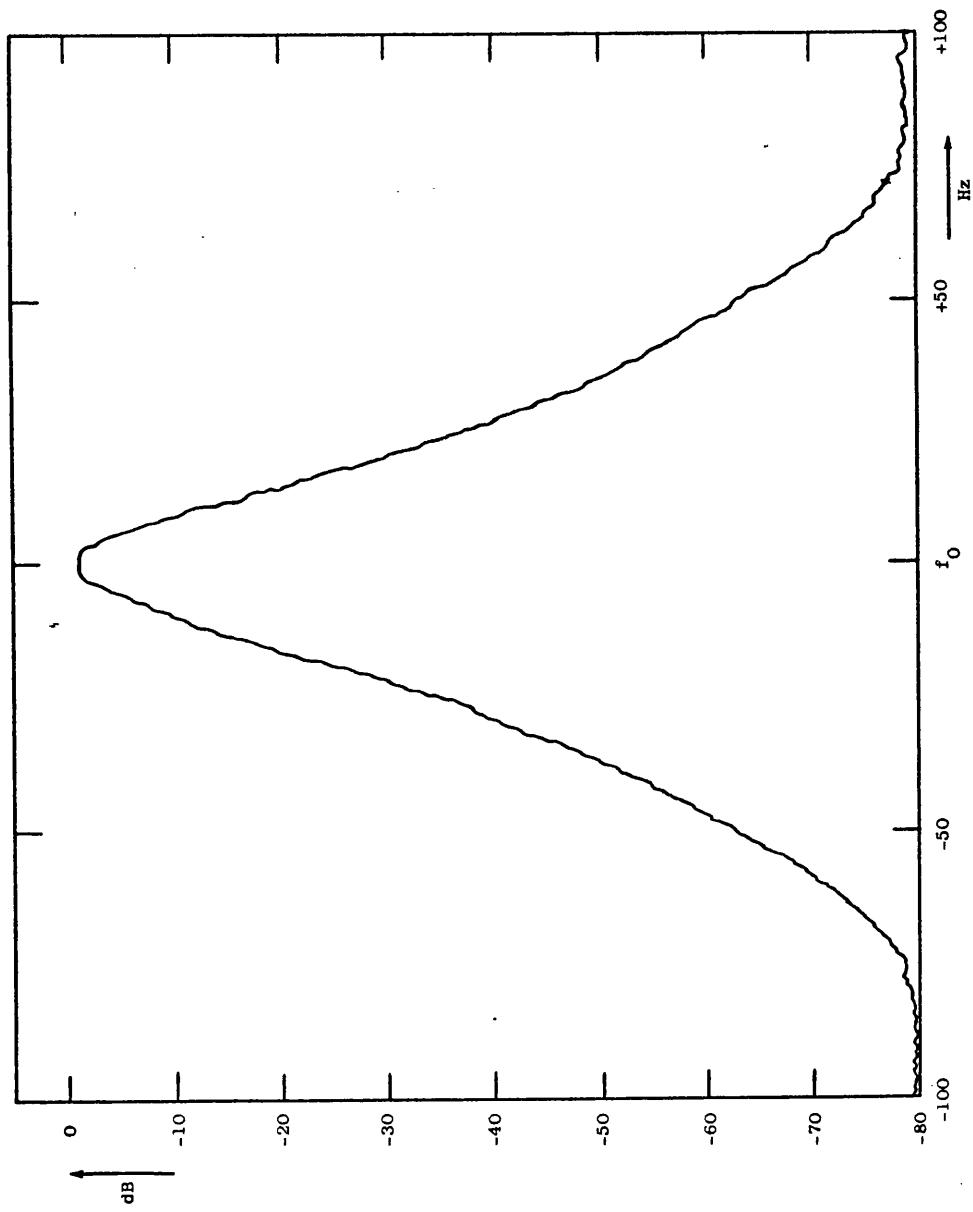
RF bandwidth = 10Hz

IF bandwidth = 10Hz

scan width = 10Hz/div.

scan time = 5sec/div.

amplitude = 10dB/div.





lower than that of the sources under test. In addition, the dynamic range of the analyser is limited by the residual noise level of its own circuitry and is incapable of measuring power levels in the order of magnitude expected of stable frequency sources. The results of these frequency domain tests, therefore, are inconclusive and serve only to prove that all four sources perform at least as well as the spectral traces suggest. More accurate measurements of short-term frequency stability made in the frequency domain require a very narrow bandwidth wave analyser. Because such an instrument was not available, it was decided to carry out comparative tests in the time domain.

The measurement of short-term stability in the time domain is best achieved by evaluation of the Allan variance of frequency as defined by equation (2.23). If  $M$  samples of frequency are taken, each over a period of  $\tau$  seconds, then the variance of  $(M - 1)$  pairs of samples may be evaluated so that (2.23) may be rewritten

$$\sigma_y^2(\tau) = \frac{1}{M-1} \sum_{k=1}^{M-1} \frac{(\overline{y_{k+1}} - \overline{y_k})^2}{2} \quad (6.14)$$

where  $\overline{y_k}$  is the average fractional frequency offset during the  $k$ th measurement period. Figure 6.16 shows the arrangement employed to evaluate the Allan variance. The output of the source under test was fed to the input of a frequency difference meter whose reference frequency was derived from the rubidium standard. The error multiplied output of this was then measured by means of a digital frequency meter, also governed by the atomic standard. If the long-term average output frequency of the source was  $f_0$ , then its frequency as averaged over the  $k$ th measurement interval may be written

$$f'_k = f_0 + f_0 \overline{y_k} = f_0 (1 + \overline{y_k}) \quad (6.15)$$

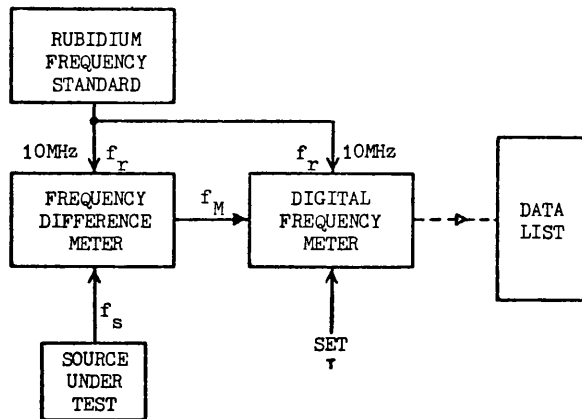


Figure 6.16 Arrangement for the measurement of short-term frequency stability

If the frequency difference meter multiplied the error by 100, then the frequency applied to the digital frequency meter during the  $k$ th measurement interval would be

$$f_k = 10\text{MHz} + 100f_0 \overline{y_k} \quad (6.16)$$

Substitution of (6.16) in (6.14) yields a useable form of the expression for Allan variance

$$\sigma_y^2(\tau) = \frac{1}{(100f_0)^2} \cdot \frac{1}{M-1} \sum_{k=1}^{M-1} \frac{(f_{k+1} - f_k)^2}{2} \quad (6.17)$$

Hence by listing  $M$  consecutive values of  $f_k$ , the Allan variance may be evaluated for various values of averaging time  $\tau$ .

In all the tests performed, the value of  $M$  taken was 101 so that 100 pairs of readings were considered. The Allan variance was measured for averaging times of 100msec, 1sec and 10sec for both sources, and at various VCXO power supply voltages in the case of the prototype. Averaging times of 100 seconds and longer are quite possible by this technique, but the total time required for the measurement (2 hours 50 minutes for  $\tau = 100\text{sec}$ ) makes them inappropriate unless automatic logging of the data may be achieved. In each test the gate repetition frequency was 10 seconds, allowing ample time for the manual recording of the data, so that each measurement took about 30 minutes. Details and examples of the data as recorded are given in Appendix I, and the results are repeated in Table 6.1 and condensed in the graph of Figure 6.17.

The graph shows that at low VCXO drive power the short-term stability of the prototype falls short of that of a free-running oscillator by a factor of about five. As the drive power to the VCXO is increased, however, the difference narrows, and at a VCXO supply voltage of 50V the prototype shows an improvement in short-term

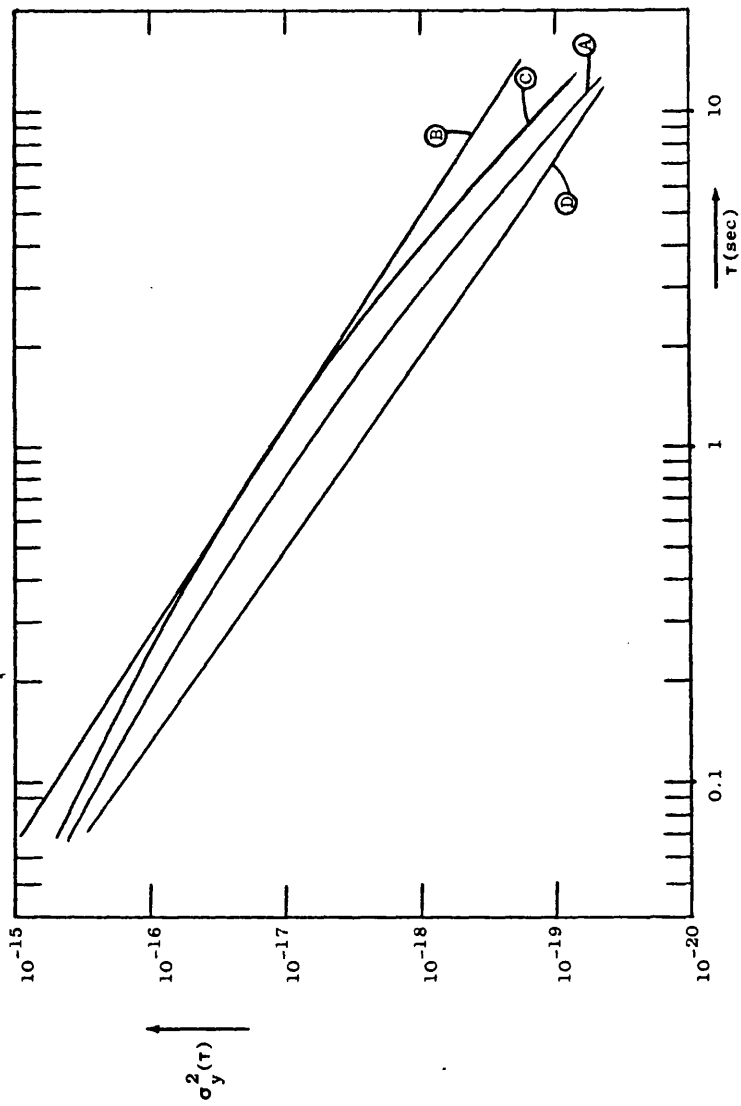


Figure 6.17 Graph of measured Allan variance  $\sigma_y^2(\tau)$  against averaging time

- Curve (A) - for an oven-controlled crystal oscillator
- Curve (B) - for the prototype unit with VCXO supply voltage of 10V
- Curve (C) - for the prototype unit with VCXO supply voltage of 30V
- Curve (D) - for the prototype unit with VCXO supply voltage of 50V

stability over the free-running oscillator.

Test No.	Source	$\tau$ (sec)	$\sigma_y^2(\tau)$
1	Oven controlled crystal oscillator	0.1	$2.42 \times 10^{-16}$
2		1	$7.08 \times 10^{-18}$
3		10	$7.94 \times 10^{-20}$
4	Prototype with $V_s = 10V$	0.1	$5.02 \times 10^{-16}$
5		1	$1.39 \times 10^{-17}$
6		10	$3.15 \times 10^{-19}$
7	Prototype with $V_s = 30V$	0.1	$3.98 \times 10^{-16}$
8		1	$1.28 \times 10^{-17}$
9		10	$1.26 \times 10^{-19}$
10	Prototype with $V_s = 50V$	0.1	$1.69 \times 10^{-16}$
11		1	$2.99 \times 10^{-18}$
12		10	$5.84 \times 10^{-20}$

Table 6.1 - Comparative values of measured Allan variance for the oven controlled oscillator and prototype

### 6.5.3 Aging Performance

Due to the time involved for such tests, measurement of the aging rate of the prototype was not possible. Numerous deductions may be made, however, about the probable performance of the unit in this respect.

Firstly, it is clear that the temperature compensation scheme as described can never automatically compensate for frequency aging, and in that respect does not differ from any other compensation scheme. Where it does differ, however, is in its use of a high drive power output oscillator phase locked to the primary crystal. It has

been shown that the noise performance of the unit depends upon the output oscillator and not the primary source, so that it is possible to operate the primary source at as low a drive level as desired without adversely affecting overall noise performance. By choosing a low drive level for the primary crystal the aging rate of the unit may be reduced, therefore, to a lower level than is usual in free-running sources.

Secondly, a study of the equation describing the transfer characteristic of the frequency synthesiser used in the prototype reveals that the sensitivity of the output frequency to changes in primary crystal frequency,

$$\frac{\delta f_0}{\delta f_1} = \frac{4N}{4N + 1} \quad (6.18)$$

is very close to unity for the large values of N employed. Accordingly, it is possible to adjust the frequency of the primary crystal oscillator to compensate for aging without jeopardizing the programmed temperature compensation action. Evidence presented during the discussion of frequency aging of crystals in Chapter 3 indicates that the shape of the graph of frequency against temperature is unchanged during aging, but is simply translated vertically with respect to the temperature axis. The required temperature correction data, therefore, is also unchanged during aging and a simple trimming of the primary crystal oscillator is all that is required for the readjustment of the unit.

For the above reasons, the aging performance of the digitally temperature compensated oscillator may be specified generally as being equal to that of its primary AT cut crystal at the particular drive power employed. The trim range of the unit may then be specified as required to allow readjustment of the expected

frequency drift.

The results of the tests for temperature stability and short-term stability, together with the consideration of frequency aging of the prototype show it to perform creditably in comparison with alternative systems. When this performance is considered in the light of its other advantages the system appears very promising. Its potential cheapness of manufacture and calibration, potentially low power consumption and its ability to supply subharmonics of the main output frequency all represent advantages over existing systems. Further improvements and modifications may, however, be envisaged, and these are now discussed.

## 6.6 Further Developments

As discussed in section 6.5.1, the system in the form of the prototype has a tendency to hunt between adjacent temperature counts in the manner of any gated counter. This produces a great deal of unproductive activity within the pROM decoder, increasing the power supply consumption, and causes the frequency to hop between adjacent increments of the frequency synthesiser at the clock rate of 1Hz, causing unnecessary noise disturbances at the output. Fortunately, this hunting may be simply eliminated by means of the arrangement of Figure 6.18 which compares each count with the previous one and only allows it to address the memory if the two counts are of the same magnitude. In this way any change in the temperature count must establish itself for two consecutive clock periods before it is allowed to reach the pROM. This technique not only eliminates hunting, but also detects any completely spurious count which may occur due to injected noise or other interference. The schematic as

shown is unlikely to operate satisfactorily in practice, however, due to the propagation delay through the auxiliary latch and comparator which would prevent the shift signal to the main comparator from being gated out in time. This may be overcome by the inclusion of a third latch (as shown dotted) which delays each count by an extra clock period to allow the selective shift signal to become established. One disadvantage of the scheme is that, when the unit is switched on, three or possibly four one-second clock periods must elapse before accurate temperature data reaches the pROM and compensation is achieved.

It has been stressed throughout this and the previous chapter that the overall performance of the system depends upon the size of the memory employed. The replacement of the AT cut crystal of the prototype with a 10MHz BT cut plate would not affect the operation of the system, but would cause a symmetrical distribution of the required frequency correction about the inflexion temperature of the crystal, due to its parabolic temperature coefficient (as shown in Figure 3.9 of Chapter 3). The synthesiser address required for frequency correction at temperatures equally spaced above and below the inversion temperature of the crystal will, therefore, also be the same. By incrementing the temperature count up to the inversion temperature and decrementing it thereafter, it appears possible to halve the memory capacity required for any given performance.

If a 10MHz BT cut crystal was used, then its thickness would be, from equation (3.1),

$$d_{BT} = \frac{2550}{10000} = 0.255\text{mm}$$

In order to ensure good thermal equalisation between this and the Y cut plate during transient conditions, the thickness of the Y cut



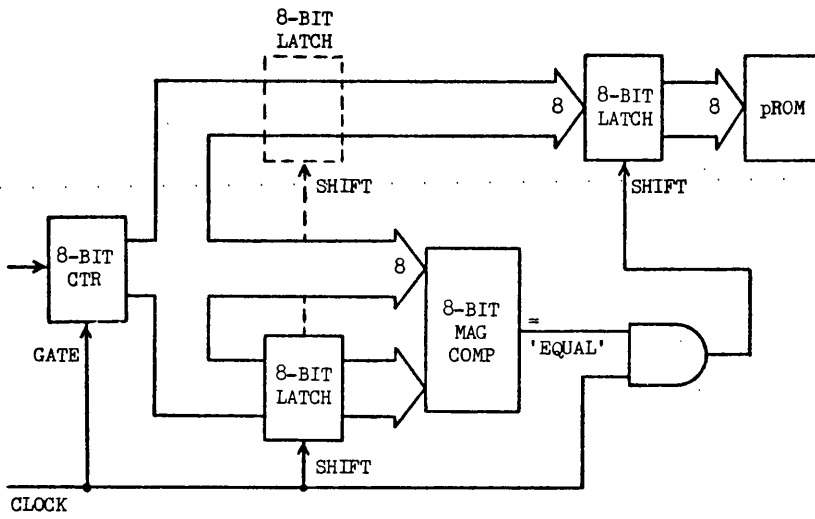


Figure 6.18 Schematic of the proposed anti-hunt gating

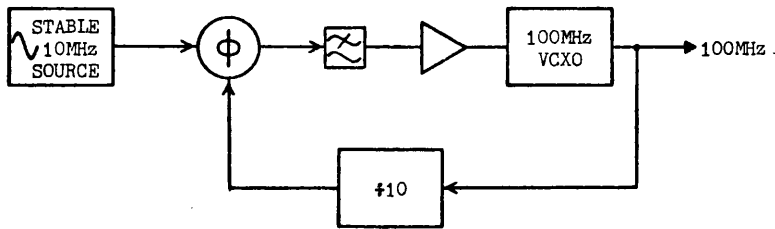


Figure 6.19(a) Production of stable 100MHz signal by x10 multiplier

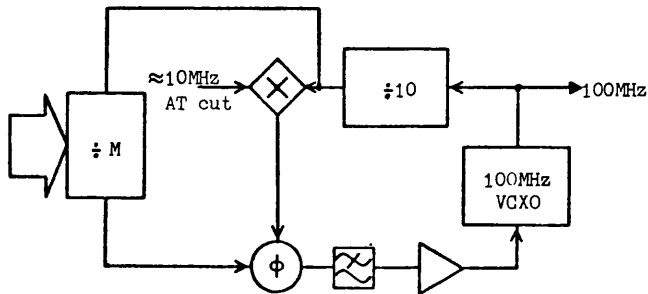


Figure 6.19(b) Direct production of 100MHz signal from the digitally compensated oscillator

crystal should be the same for the reasons discussed in section 6.2. This would require a Y cut crystal frequency of

$$f_Y = \frac{1950}{0.255} \approx 7.65\text{MHz}$$

which would in turn afford a measurement temperature coefficient of about  $658\text{Hz}/^\circ\text{C}$ . This figure is not particularly convenient for the design of the system, but would present no real problem to its operation.

The drawback to the use of a BT cut crystal as a means of minimising memory requirement is that the approach requires a knowledge of the exact inflexion temperature of the crystal used. Such information could only be programmed into the system by careful manual adjustment, hence negating many of the advantages of automatic calibration procedures. The saving in cost by halving the memory size in this manner is thought unlikely to compensate for the added human effort.

Section 6.2 discussed the requirement for temperature equalisation between the AT and Y cut crystals and described the measures taken to ensure this. An obvious improvement upon the milled block arrangement used in the prototype would be the mounting of both crystals in the same enclosure. In this way the thermal effects in the two crystals could be even more closely controlled by ensuring exactly the same manufacturing and sealing process for each. It must be noted, however, that even using such a co-mounted crystal pair, the thermal conduction path along the lead wires from the oscillator circuitry is still of great importance and must always be taken into account.

The frequency of operation of the prototype was chosen as 10MHz for convenience. There is considerable evidence, however, that the

majority of temperature compensated oscillators in service are used as a reference for the derivation of higher frequencies, suggesting that a 100MHz compensated oscillator, for example, would be of more general use to equipment designers. A feature of the compensation scheme described here is its adaptability to higher output frequencies with little increase in complexity. Furthermore, when compared with the corresponding HF source and multiplier arrangement, a reduction in complexity is evident. Figures 6.19(a) and 6.19(b) show the conventional approach and proposed alternative approach to the production of a stable 100MHz source, and clearly indicate the advantages of the latter. The resulting frequency stability and noise performance is likely to be very similar in both cases. The technique is applicable to any frequency rationally related to 10MHz, if a 10MHz AT cut crystal is used, and to almost any other frequency if an AT cut crystal is chosen accordingly.

From a production point of view, the most far reaching development would be the incorporation of the system into a Large Scale Integrated package. The increasing use of computer-based design procedures continue to reduce the primary development costs of LSI circuitry, and the Advanced Development Division of Racal Group Services Ltd are currently developing a thick film hybrid version of the prototype<sup>(10)</sup>. The hybrid will contain the oscillator circuits, the pROM, a thermally co-mounted crystal pair and a CMOS digital chip containing the remainder of the system, all encapsulated in a hermetically sealed metal can of dimensions about 25 x 25 x 40mm, only slightly larger than the crystal pair of the prototype.

The possible approaches to programming digitally compensated oscillators in a production environment are discussed in the next

chapter together with various other aspects of programming. It is important to stress under the current heading, however, that the memory employed in the prototype was chosen for convenience only. To make the most of this system a larger memory capacity is clearly needed, but the nature of that memory may depend upon future developments. The importance of electrically alterable read-only memories (EAROMs) and other non-volatile read-write stores is already apparent, and these and others may well have a considerable effect upon the worth of this system in the future.

REFERENCES - Chapter 6

- (1) LEE, E.: "How to use 1702A MOS PROMs reliably". In: 'The PROM User's Guide, Monterey, California: Pro-Log Corporation, May 1977, pp.3-8. Rev. ed.
- (2) MARTIN, J.D.: "Digital methods of frequency measurement: a comparison", The Radio and Electronic Engineer, Vol.42, No.6, June 1972, pp.285-94.
- (3) KAYE, G.W.C., and LABY, T.H.: "Tables of physical and chemical constants", London: Longman, 1973, pp.56-62. 14th ed.
- (4) NEMEC, J.: "A high-frequency synthesiser with a digital mixer", Electronic Design 4, February 15th 1977, pp.120-2.
- (5) MORGAN, D.K., and STEUDEL, G.: "The COS/MOS phase-locked loop", RCA Appn. Note ICAN-6101, p.2.
- (6) GARDNER, F.M.: "Phase lock techniques", New York: John Wiley and Sons, 1979. 2nd ed.
- (7) op. cit.: Chapter 3, pp.25-42.
- (8) MANASSEWITCH, V.: "Frequency synthesisers - theory and design", New York: Wiley Interscience, 1976, Chapter 4, pp.226-82.
- (9) op. cit.: Chapter 2, pp.117-36.
- (10) RACAL GROUP SERVICES LTD.: "Digital techniques for temperature compensation of quartz crystal oscillators", Advanced Development Division Publication No.A2002-1, September 1979.

CHAPTER 7 - PROGRAMMING TECHNIQUES

The satisfactory operation of the digitally compensated oscillator depends primarily upon the correct compensation law data being determined and stored in the memory of each individual sample. The programming procedure must be carried out on each unit, therefore, and would clearly be too time consuming and expensive for large volume production unless some means of automatic calibration were devised.

Two possible approaches are considered here: firstly, a full point-by-point determination of the data by means of an equipment which searches for and stores each data point in turn during a temperature cycle; secondly, a mathematical prediction of the remaining data from a knowledge of a few data points only.

7.1 Point-By-Point Automatic Programming

In the production environment it would be necessary to programme a large number of units. In order to accomplish this, a programming technique must be adopted which represents a compromise between the two extremes of programming each unit singly in a very short time or programming many units together in a longer time. In view of the practical difficulties of temperature cycling any object quickly, it is felt that the slower, larger volume approach would inevitably be preferred. By slowly temperature cycling the units, the effects of any thermal transients will be minimised and prevented from influencing the programming procedure unduly.

One possible automatic calibration arrangement is represented by Figure 7.1. The units under calibration are placed in an enclosure which is slowly cycled in temperature. By means of data

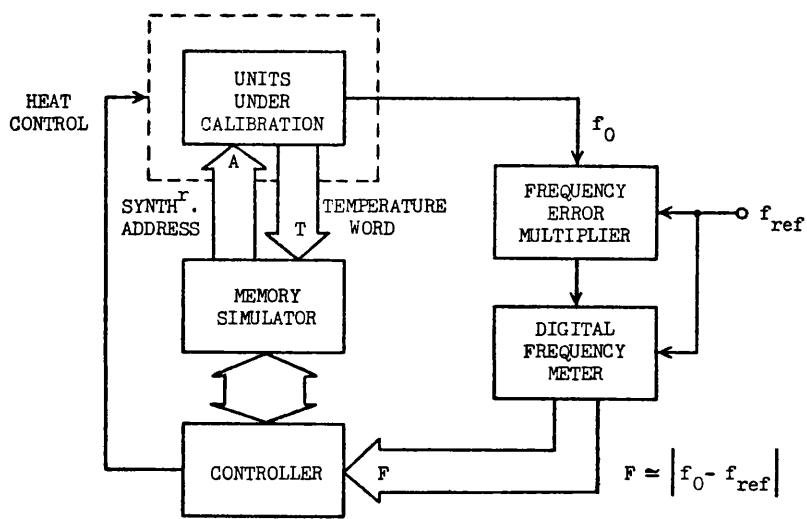


Figure 7.1 Arrangement for automatic point-by-point calibration

selection and multiplexing, each unit in turn is accessed via its memory ports and its output frequency is examined. Under the direction of a digital controller, the data stored in a memory simulator is adjusted until the output frequency is as close as possible to that required. The controller then repeats the process for the next unit and so on.

One important feature of this procedure is that no absolute measure of the temperature of each unit is required since it is the increments as registered by the temperature counter which are the governing parameter. It is only necessary to ensure that the initial and final temperatures of the environmental enclosure encompass the required range of operation of the units. The search procedure need only be carried out when the temperature address data of any unit has changed since its last examination.

A frequency error multiplier is employed so that measurement of the output of each unit, to the required resolution, may be accomplished quickly. The output of the digital frequency meter is constrained to represent the modulus of the frequency error so that only positive values of  $F$  are encountered, simplifying the search procedure somewhat.

The action of the controller may be represented by the flow-chart of Table 7.1. This shows, as an example, the procedure carried out upon unit number 1, so that  $T_1$  and  $A_1$  are the temperature and synthesiser address words used during the search,  $TP_1$ ,  $FP_1$  and  $N$  are running variables and  $MA_1(T_1)$  is the array of temperature correction data as compiled and stored in the memory simulator. When the sequence is initiated it is convenient to set  $A_1$  and  $TP_1$  to half their maximum value (128 in the case of 8-bit words), and to set  $FP_1$  to zero. When a data point has been determined, the controller



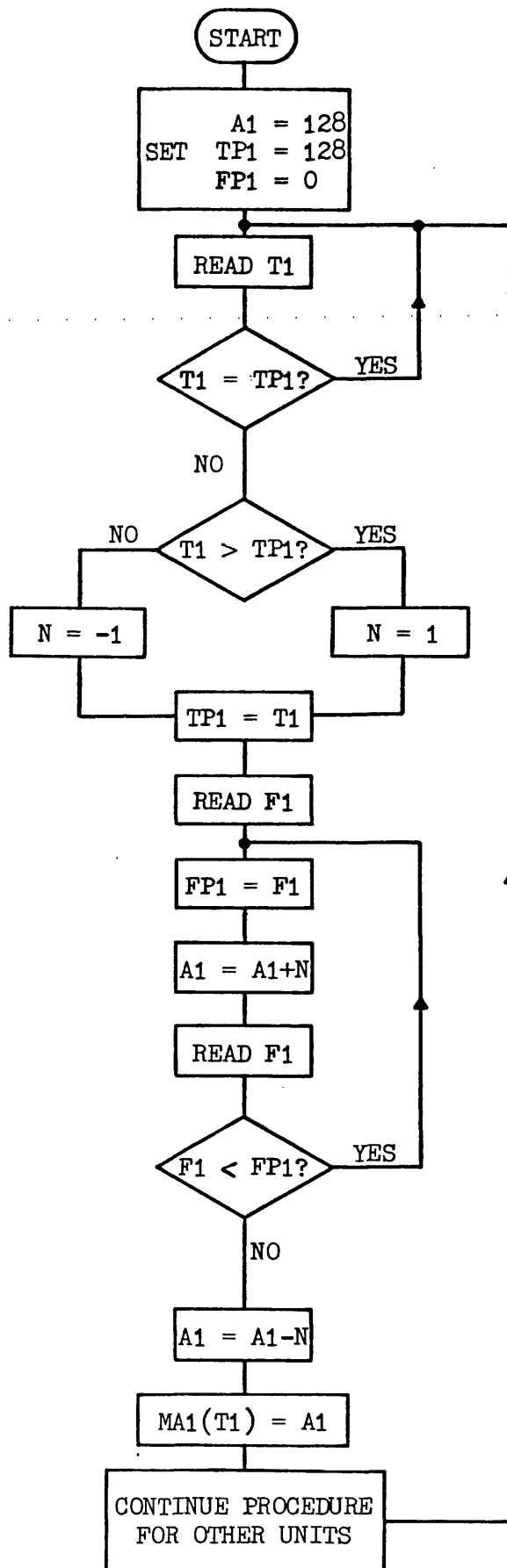


Table 7.1 - Flow chart representing the action of the programmer controller

continues with the next unit using  $T_2$ ,  $A_2$  etc as variables and storing its findings in  $MA_2(T_2)$ , finally arriving back at unit number 1 for its next examination and so on.

Depending upon the number of units to be programmed, the total memory capacity required for the controller and memory simulator could be very large. For this reason the use of a minicomputer with disc storage has been proposed to act as a combined controller and bulk store. One major advantage of such an approach is the security with which the data may be held once determined, preventing a power supply failure from causing a complete erasure of the memory. It may also be possible to carry out the programming procedure unattended overnight, taking advantage of the use of existing equipment when it would otherwise be idle.

Once the data has been arrived at, the controller may be used to carry out further tasks. Each data array could be checked to ensure that the data points conform to a general pattern, hence detecting and correcting any obvious errors. The controller could be used to supervise the programming of the individual memories of each unit. This could be carried out either with the memories already in circuit, or externally for insertion manually. Alternatively, for less exacting applications it would be possible to use the controller to compare each data array with a selection of standard memories available from stock and select the most appropriate.

## 7.2 Programming by Mathematical Prediction

In Chapter 3 it was shown how the relationship between frequency  $f_1$  and temperature  $T$  of an AT cut crystal may be characterised by an expression of the form:

$$f_1 = a_0 + a_1T + a_3T^3 \quad (7.1)$$

where  $a_0$ ,  $a_1$  and  $a_3$  are constants describing the particular crystal plate sample. The equivalent relationship for a BT cut plate is:

$$f_b = b_0 + b_2T^2$$

Provided that one of these types of crystal, or any other whose frequency/temperature relationship is easily defined, is used as the primary source for a digitally compensated oscillator, the required compensation law data is theoretically predictable.

The transfer characteristic of the prototype synthesiser in terms of programmable divider modulus  $M$  is given by equation (6.1) as

$$f_0 = \left( \frac{4M}{4M + 1} \right) f_1$$

Combining this with equation (7.1), as the prototype employs an AT cut crystal, gives

$$\frac{1}{M} = k_0 + k_1T + k_3T^3 = A \quad (7.2)$$

where

$$k_0 = \frac{4(a_0 - f_0)}{f_0},$$

$$k_1 = 4a_1/f_0,$$

$$k_3 = 4a_3/f_0,$$

and

$$A = 1/M$$

In order to predict the compensation data it is necessary to determine the coefficients  $k_0$ ,  $k_1$  and  $k_3$ . If three corresponding values of  $A$  and  $T$  may be accurately determined by calibration at three temperatures, then these coefficients may be written

$$k_0 = \left( T_1T_2A_3(T_2^2 - T_1^2) + T_2T_3A_1(T_3^2 - T_2^2) + T_1T_3A_2(T_1^2 - T_3^2) \right) / D \quad (7.3)$$

$$k_1 = \left( A_1(T_2^3 - T_3^3) + A_2(T_3^3 - T_1^3) + A_3(T_1^3 - T_2^3) \right) / D \quad (7.4)$$

$$k_3 = (A_1(T_3 - T_2) + A_2(T_1 - T_3) + A_3(T_2 - T_1))/D \quad (7.5)$$

$$\text{where } D = T_1 T_2 (T_2^2 - T_1^2) + T_2 T_3 (T_3^2 - T_2^2) + T_1 T_3 (T_1^2 - T_3^2) \quad (7.6)$$

and from  $k_0$ ,  $k_1$  and  $k_3$  the whole compensation data array may be calculated. Clearly, equations (7.3) to (7.6) are rather unwieldy for hand calculations and are best handled with the aid of a digital computer.

Preliminary calculations revealed that over a large range of  $T$  the practical contribution of  $k_0$  to the resulting value of  $A$  in equation (7.2) was negligible, suggesting that a simpler equation of the form

$$A = a_1 T + a_3 T^3 \quad (7.7)$$

may suffice in this application. The potential advantage of such an approximation would be that only two accurate data points need be determined, from which

$$a_1 = \frac{A_1 T_2^3 - A_2 T_1^3}{T_1 T_2^3 - T_2 T_1^3} \quad (7.8)$$

$$\text{and } a_3 = \frac{T_1 A_2 - T_2 A_1}{T_1 T_2^3 - T_2 T_1^3} \quad (7.9)$$

may be calculated. The prediction algorithm of equation (7.7) was assessed by comparison with equation (7.2) in the calculation of the data points of a known cubic relationship. A computer programme was written to determine the results using Algorithm 1 (equation (7.7)) with two data pairs, using Algorithm 2 (equation (7.2)) with three data pairs and for completeness using Algorithm 1 and averaging its results between the three possible combinations of data pairs available. The results showed errors of as much as eight units in the prediction by the simple version of Algorithm 1 and as much as

five units in the averaged version of Algorithm 1, whilst the errors occurring by the use of Algorithm 2 were only as large as the rounding error of the computation. Accordingly, Algorithm 1 was abandoned and further investigations into the use of Algorithm 2 were undertaken.

Appendix J contains the statement list of a computer programme written in the FORTRAN language<sup>(1)</sup>, for the investigation of Algorithm 2. The input and output of data is undertaken using Z format fields in order that hexadecimal notation may be used. This is advantageous as the pROM support equipment used during calibration and test also uses this number system. Any number of groups of three established data pairs may be read in and the values of  $k_0$ ,  $k_1$  and  $k_3$  evaluated for each. The averaged values of  $k_0$ ,  $k_1$  and  $k_3$  may then be used in one of two ways as flagged by the input value of L. In either case the predicted data array is calculated, rounded to the nearest integer (since the memory can store integer numbers only), and printed out in the same format as the memory maps generated by the pROM support equipment together with the input data and averaged coefficients. If L is initially set to three, the programme ends there. If L is set to zero, however, the predicted data is compared with a known array of data defined by coefficients late in the statement list. A third array is then generated representing the errors between the predicted and required data, and this array is also printed. An example of a typical printout is given in Table 7.2, for which one set of three data pairs were used. In the data error map, a negative value of the error is denoted by the prefix B.

The programme was used to investigate three separate aspects of the use of Algorithm 2. Firstly, if one or more sets of data points

40 5C  
DATA C0 D4  
80 98

E0 = 32.0260  
E1 = 0.9375  
E3 = 0.806E-06

PREDICTED DATA  
-----

	0	1	2	3	4	5	6	7	8	9	A	B	C	D	E	F
0	<del>02F</del> 021	022	023	024	025	026	027	028	028	029	02A	02B	02C	02D	02E	
1	02F	030	031	032	033	034	035	036	037	037	038	039	03A	03B	03C	03D
2	03E	03F	040	041	042	043	044	045	046	046	047	048	049	04A	04B	04C
3	04D	04E	04F	050	051	052	053	054	055	055	056	057	058	059	05A	05B
4	05C	05D	05E	05F	060	061	062	063	064	064	065	066	067	068	069	06A
5	06B	06C	06D	06E	06F	070	071	072	073	073	074	075	076	077	078	079
6	07A	07B	07C	07D	07E	07F	080	081	082	082	083	084	085	086	087	088
7	089	08A	08B	08C	08D	08E	08F	090	091	091	092	093	094	095	096	097
8	098	099	09A	09B	09C	09D	09E	09F	0A0	0A0	0A1	0A2	0A3	0A4	0A5	0A6
9	0A7	0A8	0A9	0AA	0AB	0AC	0AD	0AE	0AF	0AF	0B0	0B1	0B2	0B3	0B4	0B5
A	0B6	0B7	0B8	0B9	0BA	0BB	0BC	0BD	0BE	0BE	0BF	0C0	0C1	0C2	0C3	0C4
B	0C5	0C6	0C7	0C8	0C9	0CA	0CB	0CC	0CD	0CD	0CE	0CF	0D0	0D1	0D2	0D3
C	0D4	0D5	0D6	0D7	0D8	0D9	0DA	0DB	0DC	0DC	0DD	0DE	0DF	0E0	0E1	0E2
D	0E3	0E4	0E5	0E6	0E7	0E8	0E9	0EA	0EB	0EB	0EC	0ED	0EE	0EF	0F0	0F1
E	0F2	0F3	0F4	0F5	0F6	0F7	0F8	0F9	0FA	0FA	0FB	0FC	0FD	0FE	0FF	100
F	101	102	103	104	105	106	107	108	109	109	10A	10B	10C	10D	10E	10F

DATA ERROR MAP 'B' DENOTES 'MINUS'  
-----

	0	1	2	3	4	5	6	7	8	9	A	B	C	D	E	F
0	<del>000</del> 001	001	001	001	001	001	001	001	001	000	000	000	000	000	000	000
1	000	000	001	001	001	001	001	001	001	000	000	000	000	000	000	000
2	000	000	000	001	001	001	001	001	001	000	000	000	000	000	000	000
3	000	000	000	000	000	001	001	001	001	000	000	000	000	000	000	000
4	000	000	000	000	000	000	001	001	001	000	000	000	000	000	000	000
5	000	000	000	000	000	000	000	001	001	000	000	000	000	000	000	000
6	000	000	000	000	000	000	000	000	000	000	000	000	000	000	000	000
7	000	000	000	000	000	000	000	000	000	B01	000	000	000	000	000	000
8	000	000	000	000	000	000	000	000	000	B01	B01	000	000	000	000	000
9	000	000	000	000	000	000	000	000	000	B01	B01	B01	000	000	000	000
A	000	000	000	000	000	000	000	000	000	B01	B01	B01	B01	000	000	000
B	000	000	000	000	000	000	000	000	000	B01	B01	B01	B01	B01	000	000
C	000	000	000	000	000	000	000	000	000	B01	B01	B01	B01	B01	B01	000
D	000	000	000	000	000	000	000	000	000	B01	B01	B01	B01	B01	B01	B01
E	000	000	000	000	000	000	000	000	000	B01	B01	B01	B01	B01	B01	B01
F	000	000	000	000	000	000	000	000	000	B01	B01	B01	B01	B01	B01	B01

Table 7.2 - Example of the output format of the data prediction programme

are to be used as the basis of the prediction, where in the data array are these best situated? Secondly, what improvement in accuracy may be expected by increasing the number of input data points? Thirdly, what is the effect upon the predicted data of errors in the input values? The range of investigation was restricted to the memory capacity of the prototype, 00 to FF, but the findings will probably apply to prediction over a larger range equally as well.

By using one set of three input data pairs at various positions in the array, it was found that the least errors were introduced by choosing data at the  $\frac{1}{4}$ ,  $\frac{1}{2}$  and  $\frac{3}{4}$  positions; that is at temperature values 40, 80 and C0. Under these conditions the predicted data was in error by a maximum of one unit as shown in the example of Table 7.2. Changing the position of the input data by a small amount usually produced no increase in the errors incurred, but as their deviation from the optimum position was increased, the maximum error rose rapidly.

By using more than three input data pairs, the performance of the algorithm was found to improve dramatically. By considering the input data three pairs at a time, a number of combinations could be employed to calculate the coefficients. If  $n$  input data pairs were used, then  $N_k$  combinations of three pairs were available, where<sup>(2)</sup>

$$N_k = \frac{n!}{3!(n-3)!} \quad (7.10)$$

The values of  $k_0$ ,  $k_1$  and  $k_3$  so produced could then be averaged for use in compilation of the predicted data. If  $n = 4$ , then  $N_k = 4$ , and it was found that by choosing four data points equally distributed throughout the array (at 33, 66, 99 and CC) and averaging the four values of coefficients so obtained, no errors were incurred in the predicted data.

All of this analysis, of course, assumes that the input data is correct. In practice, experimentally determined data will always be subject to error, and the influence of such errors upon the predicted data was investigated accordingly. Initially, the case involving three input data pairs was considered. It was found that, not surprisingly, if all three pairs erred equally and in the same sense, then an equal error was introduced across the whole predicted array. A more practical case of data points at 40 and 60 being in error by +1 unit and the point at 80 in error by -1 unit was next considered. The resulting array was found to exhibit a maximum error of two units. If the data at 40 and 80 were in error by +1 and the data at 60 by -1, however, the maximum error was found to reach seven units.

When the number of input data pairs was increased, the algorithm was found to be much more tolerant of errors. The more input pairs used, the less effect was observed in the error map. Table 7.3 shows the results of a data prediction carried out using six data pairs ( $n = 6$ ), so that  $N_k = 20$  combinations of input data were used to calculate the average coefficients. An error of -1 unit was introduced into one data pair and an error of +2 in another as shown, yet the predicted data after rounding to the closest integer shows no errors.

Six data pairs spaced at approximately regular intervals in temperature were determined experimentally for the prototype unit using crystal pair number four. The programme was used to compile a predicted data array which was entered into a 1702A pROM designated ROM 2, the memory map of which is given as the example of Table F2 in Appendix F. The temperature stability of the prototype using crystal pair number four and ROM 2 was measured by the technique



```

      25 42
DATA  4A 64 *
      6F 88
      93 AC *
      B7 CC
      DC EF
    
```

```

EO = 31.5117
E1 = 0.9425
E3 = -0.160E-07
    
```

PREDICTED DATA

	0	1	2	3	4	5	6	7	8	9	A	B	C	D	E	F
0	***	020	021	022	023	024	025	026	027	028	029	02A	02B	02C	02D	02E
1	02F	030	030	031	032	033	034	035	036	037	038	039	03A	03B	03C	03D
2	03E	03F	040	040	041	042	043	044	045	046	047	048	049	04A	04B	04C
3	04D	04E	04F	050	051	051	052	053	054	055	056	057	058	059	05A	05B
4	05C	05D	05E	05F	060	061	061	062	063	064	065	066	067	068	069	06A
5	06B	06C	06D	06E	06F	070	071	071	072	073	074	075	076	077	078	079
6	07A	07B	07C	07D	07E	07F	080	081	082	082	083	084	085	086	087	088
7	089	08A	08B	08C	08D	08E	08F	090	091	092	092	093	094	095	096	097
8	098	099	09A	09B	09C	09D	09E	09F	0A0	0A1	0A2	0A2	0A3	0A4	0A5	0A6
9	0A7	0A8	0A9	0AA	0AB	0AC	0AD	0AE	0AF	0B0	0B1	0B2	0B2	0B3	0B4	0B5
A	0B6	0B7	0B8	0B9	0BA	0BB	0BC	0BD	0BE	0BF	0C0	0C1	0C2	0C2	0C3	0C4
B	0C5	0C6	0C7	0C8	0C9	0CA	0CB	0CC	0CD	0CE	0CF	0D0	0D1	0D2	0D2	0D3
C	0D4	0D5	0D6	0D7	0D8	0D9	0DA	0DB	0DC	0DD	0DE	0DF	0E0	0E1	0E2	0E2
D	0E3	0E4	0E5	0E6	0E7	0E8	0E9	0EA	0EB	0EC	0ED	0EE	0EF	0F0	0F1	0F2
E	0F2	0F3	0F4	0F5	0F6	0F7	0F8	0F9	0FA	0FB	0FC	0FD	0FE	0FF	100	101
F	101	102	103	104	105	106	107	108	109	10A	10B	10C	10D	10E	10F	110

DATA ERROR MAP 'B' DENOTES 'MINUS'

	0	1	2	3	4	5	6	7	8	9	A	B	C	D	E	F
0	***	000	000	000	000	000	000	000	000	000	000	000	000	000	000	000
1	000	000	000	000	000	000	000	000	000	000	000	000	000	000	000	000
2	000	000	000	000	000	000	000	000	000	000	000	000	000	000	000	000
3	000	000	000	000	000	000	000	000	000	000	000	000	000	000	000	000
4	000	000	000	000	000	000	000	000	000	000	000	000	000	000	000	000
5	000	000	000	000	000	000	000	000	000	000	000	000	000	000	000	000
6	000	000	000	000	000	000	000	000	000	000	000	000	000	000	000	000
7	000	000	000	000	000	000	000	000	000	000	000	000	000	000	000	000
8	000	000	000	000	000	000	000	000	000	000	000	000	000	000	000	000
9	000	000	000	000	000	000	000	000	000	000	000	000	000	000	000	000
A	000	000	000	000	000	000	000	000	000	000	000	000	000	000	000	000
B	000	000	000	000	000	000	000	000	000	000	000	000	000	000	000	000
C	000	000	000	000	000	000	000	000	000	000	000	000	000	000	000	000
D	000	000	000	000	000	000	000	000	000	000	000	000	000	000	000	000
E	000	000	000	000	000	000	000	000	000	000	000	000	000	000	000	000
F	000	000	000	000	000	000	000	000	000	000	000	000	000	000	000	000

Table 7.3 - Example of data prediction using Algorithm 2 with six input data pairs, errors having been deliberately introduced into those marked \*

described in section 6.5.1, and the maximum frequency error found to be very nearly 1Hz, or 1 part in  $10^7$ . This was somewhat disappointing in the light of the theoretical results, but nevertheless represents excellent performance as compared with conventional temperature compensated crystal oscillators.

Practical implementation of predictive programming may be achieved by various means. One possibility is to place a large number of units into a fixed temperature environment and allow them to stabilise. The required correction at that temperature is then determined for each unit and recorded. The process is then repeated at a number of other temperatures and the combined data used to predict the required memory contents. The technique is perhaps better suited to the option of selection of memory from stock rather than its individual preparation, though this would depend upon the total number of units.

The advantages of predictive programming are firstly, that far less search procedures need be executed to arrive at the compensation data, and secondly that the units need not be fully temperature cycled and may be allowed to stabilise at each stage. The advantage of needing no absolute measurement of temperature during calibration also accrues as with point-by-point programming. There are drawbacks, however. Some means of data selection and storage are still needed, and these together with the considerable computational requirements represent a total of equipment as great as that required for programming by the alternative method. It is felt that the advantages of mathematical prediction do not merit the consequent loss in overall performance and that automatic point-by-point calibration is preferable.

REFERENCES - Chapter 7

- (1) INTERNATIONAL COMPUTERS LTD.: "H level Fortran", Technical Publication 4950, October 1971.
- (2) KREYSIG, E.: "Advanced engineering mathematics", New York: John Wiley and Sons, 1962, Chapter 19, pp.699-788.

CHAPTER 8 - CONCLUSION

The difficulties in design and manufacture and the shortcomings in performance of conventional temperature compensated quartz crystal oscillators has led to the re-evaluation of each aspect of their operation. Consideration has been given in three broad areas: firstly, the means employed to sense the prevailing temperature of the governing crystal; secondly, the method used to adjust the final output frequency; and thirdly, the means by which the temperature compensation is governed.

The use of a Y cut crystal as a temperature sensing element has been discussed in some depth and shown to offer considerable advantages over current methods. Since its operation is one of conversion of temperature to frequency, its temperature resolution may be adjusted simply by changing the resolution to which its frequency is measured. This frequency measurement is in turn ideally suited to incorporation into a digital system.

Though modern techniques of digital frequency synthesis appear attractive at first for use in adjustment of the output frequency, it has been shown that none of the commonly used methods is appropriate. Accordingly, the technique of Frequency Shifting Synthesis has been developed to afford the high frequency resolution required whilst using only very simple circuitry. The technique is not restricted to applications in frequency generation, and various other uses have been suggested.

Many of the difficulties in manufacturing TCXOs result from the need to calibrate each unit to account for the spread in crystal and other characteristics. If the only difference from unit to unit is programmed software, however, many drawbacks are overcome and automatic calibration becomes possible. The use of a read-only

memory as the compensation governing element allows this software based calibration to be performed on otherwise identical units. In the case of the technique proposed, the ability to adjust for long-term aging of the unit is not sacrificed, and by using erasable pROMs, complete recalibration is still possible if desired.

The system which results from these basic building blocks is very versatile. The quality of its performance is primarily a function of the memory capacity employed. Having decided upon a particular memory size, various options are still open to the designer. A high frequency stability may be achieved over a narrow range of temperatures, or a more modest stability over a broader range. Since the hardware involved differs only slightly, an extremely wide variety of developmental options is available.

In large volume production, the effects of Large-Scale Integrated Circuitry in the reduction of prime costs and ease of manufacture are well known. The aggregate use of digital techniques in the proposed scheme has made the use of an LSI version of the circuitry worthwhile. If due consideration is given to some of the more subtle aspects of the action of such a device, an extremely versatile tool could result, not only of use in TCXOs but also in more general high resolution frequency synthesis.

Alternatively, it is possible to envisage systems which employ only a portion of the proposed scheme, the advantages of which may still accrue in certain applications. For example, a wide range corrected oscillator of medium stability may be constructed taking advantage of a ROM as compensation governing element and a FSS for frequency adjustment whilst saving the extra cost of a Y cut crystal by using a thermistor controlled oscillator as temperature sensor. Many other combinations of the system elements are possible and much

useful work may still be undertaken in their relative evaluation.

In conclusion, then, it is still not possible to define an absolute optimum configuration of digital TCXO for use in all applications. It is felt, however, that the use of a combination of some or all of the techniques described here can make a significant contribution in meeting the requirements for frequency sources in the future.

ACKNOWLEDGEMENTS

The author gratefully acknowledges the support of the UK Science Research Council and the Advanced Development Division of the Racal Group who collaborated to provide the CASE studentship which funded this research.

Particular thanks are due to the following:

Professor W Gosling and Mr A J Prescott of the School of Electrical Engineering, University of Bath, who supervised the project and provided invaluable help and encouragement to both research and researcher;

Mr K Thrower of A D D Racal for helpful guidance throughout;

Mr T McKnight of the McKnight Crystal Company, Hythe, Hampshire, for the construction of special Y cut crystals;

the staff and postgraduate students of the School of Electrical Engineering, particularly Dr R F Ormondroyd, Mr M S Shipton, Mr G A Alatsatianos and Mr A Lymer, who sowed the seeds of many an idea in the course of healthy argument;

and to my wife who did far more towards the completion of the work than merely type the draft and final copies.

APPENDIX A - DERIVATION OF CRYSTAL EQUATIONS

The Butterworth-Van Dyke equivalent circuit as used in section 3.2.1 is shown in Figure A1. The definitions of the components are as follows:

- $C_0$  = the static arm capacitance,
- $L_1$  = the motional arm inductance,
- $C_1$  = the motional arm capacitance, and
- $R_1$  = the motional arm resistance.

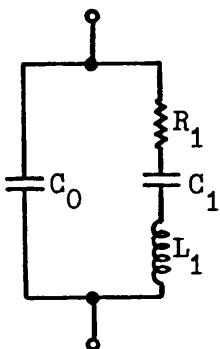


Figure A1 - The Butterworth-Van Dyke Equivalent Circuit

If  $Z_0$  and  $Z_1$  are the impedances of the static and motional arms respectively, then:

$$Z_0 = \frac{-j}{2\pi f C_0} \quad (\text{A1.1})$$

and

$$Z_1 = R_1 + j \left( 2\pi f L_1 - \frac{1}{2\pi f C_1} \right) \quad (\text{A1.2})$$

The complex impedance of the crystal at any frequency is then given by:

$$\frac{Z_0 \cdot Z_1}{Z_0 + Z_1} = \frac{\frac{-j}{2\pi f C_0} \cdot \left[ R_1 + j \left( 2\pi f L_1 - \frac{1}{2\pi f C_1} \right) \right]}{R_1 + j \left( 2\pi f L_1 - \frac{1}{2\pi f C_1} - \frac{1}{2\pi f C_0} \right)} = Z_p \quad (\text{A1.3})$$

which may be rewritten:



$$Z_p = \frac{\left[ \frac{2\pi f L_1 - (1/2\pi f C_1)}{2\pi f C_0} \right] - j \left[ \frac{R_1}{2\pi f C_0} \right]}{R_1 + j \left( 2\pi f L_1 - \frac{1}{2\pi f C_1} - \frac{1}{2\pi f C_0} \right)} \quad (\text{A1.4})$$

which is an expression of the form:

$$Z = \frac{a + jb}{c + jd}$$

so that at resonance,  $Z_p$  must be resistive and, therefore:

$$\frac{\frac{-R_1}{2\pi f C_0}}{\frac{2\pi f L_1 - (1/2\pi f C_1)}{2\pi f C_0}} = \frac{2\pi f L_1 - \frac{1}{2\pi f C_1} - \frac{1}{2\pi f C_0}}{R_1} \quad (\text{A1.5})$$

$$-R_1^2 = \left( 2\pi f L_1 - \frac{1}{2\pi f C_1} \right) \left( 2\pi f L_1 - \frac{1}{2\pi f C_1} - \frac{1}{2\pi f C_0} \right) \quad (\text{A1.6})$$

$$R_1^2 + (2\pi f L_1)^2 - \frac{2L_1}{C_1} - \frac{L_1}{C_0} + \frac{1}{(2\pi f)^2 C_1^2} + \frac{1}{(2\pi f)^2 C_1 C_0} = 0 \quad (\text{A1.7})$$

$$(2\pi f)^4 + (2\pi f)^2 \left( \frac{R_1^2}{L_1^2} - \frac{2}{L_1 C_1} - \frac{1}{L_1 C_0} \right) + \left( \frac{1}{L_1^2 C_1^2} + \frac{1}{L_1^2 C_1 C_0} \right) = 0 \quad (\text{A1.8})$$

Solving this quadratic for  $(2\pi f)^2$  gives:

$$(2\pi f)^2 = \frac{1}{2} \left\{ \left( \frac{2}{L_1 C_1} + \frac{1}{L_1 C_0} - \frac{R_1^2}{L_1^2} \right) \pm \left[ \left( \frac{2}{L_1 C_1} + \frac{1}{L_1 C_0} - \frac{R_1^2}{L_1^2} \right)^2 - 4 \left( \frac{1}{L_1^2 C_1^2} + \frac{1}{L_1^2 C_1 C_0} \right) \right]^{\frac{1}{2}} \right\} \quad (\text{A1.9})$$

from which:

$$f = \frac{1}{2\pi} \left\{ \left( \frac{1}{L_1 C_1} + \frac{1}{2L_1 C_0} - \frac{R_1^2}{2L_1^2} \right) + \left[ \left( \frac{1}{L_1 C_1} + \frac{1}{2L_1 C_0} - \frac{R_1^2}{2L_1^2} \right)^2 - \left( \frac{1}{L_1^2 C_1^2} + \frac{1}{L_1^2 C_1 C_0} \right) \right]^{\frac{1}{2}} \right\}^{\frac{1}{2}} \quad (\text{A1.10})$$

The quantity in the square brackets may be rewritten:

$$\left[ \left( \frac{1}{L_1 C_1} + \frac{1}{2L_1 C_0} - \frac{R_1^2}{2L_1^2} \right)^2 - \left( \frac{1}{L_1^2 C_1^2} + \frac{1}{L_1^2 C_1 C_0} \right) \right]^{\frac{1}{2}} = \left[ \left( \frac{1}{2L_1 C_0} - \frac{R_1^2}{2L_1^2} \right)^2 - \frac{R_1^2}{L_1^3 C_1} \right]^{\frac{1}{2}} \quad (\text{A1.11})$$

For practical crystals, however,

$$\left( \frac{1}{2L_1 C_0} - \frac{R_1^2}{2L_1^2} \right)^2 \gg \frac{R_1^2}{L_1^3 C_1}$$

then

$$\left[ \left( \frac{1}{2L_1 C_0} - \frac{R_1^2}{2L_1^2} \right)^2 - \frac{R_1^2}{L_1^3 C_1} \right]^{\frac{1}{2}} \approx \left[ \frac{1}{2L_1 C_0} - \frac{R_1^2}{2L_1^2} \right] \quad (\text{A1.12})$$

so that, by substitution into equation (A1.10):

$$f \approx \frac{1}{2\pi} \left[ \left\{ \frac{1}{L_1 C_1} + \frac{1}{2L_1 C_0} - \frac{R_1^2}{2L_1^2} \right\} + \left\{ \frac{1}{2L_1 C_0} - \frac{R_1^2}{2L_1^2} \right\} \right]^{\frac{1}{2}} \quad (\text{A1.13})$$

This equation defines the two resonant frequencies of the crystal.

By taking the minus sign the series resonant frequency is obtained:

$$f_s = \frac{1}{2\pi} \left[ \frac{1}{L_1 C_1} \right]^{\frac{1}{2}} \quad (\text{A1.14})$$

the plus sign yielding the parallel resonant or antiresonant frequency:

$$f_a = \frac{1}{2\pi} \left[ \frac{1}{L_1 C_1} + \frac{1}{L_1 C_0} - \frac{R_1^2}{L_1^2} \right]^{\frac{1}{2}} \quad (\text{A1.15})$$

But,

$$\frac{1}{L_1 C_0} \gg \frac{R_1^2}{L_1^2}$$

so that  $f_a$  may be written:

$$f_a \approx \frac{1}{2\pi} \left( \frac{1}{L_1 C_1} \right)^{\frac{1}{2}} \cdot \left( 1 + \frac{C_1}{C_0} \right)^{\frac{1}{2}} \quad (\text{A1.16})$$

Further, since  $C_1/C_0 \ll 1$ , the binomial approximation:

$$(1 + x)^n \approx 1 + nx$$

may be used, so that:

$$f_a \approx \frac{1}{2\pi} \left( \frac{1}{L_1 C_1} \right)^{\frac{1}{2}} \left( 1 + \frac{C_1}{2C_0} \right) = f_s \left( 1 + \frac{C_1}{2C_0} \right) \quad (\text{A1.17})$$

If  $\Delta f = f_a - f_s$ , then  $\Delta f = f_s (C_1/2C_0)$  and the pullability is given

by:

$$\frac{\Delta f}{f_s} = \frac{C_1}{2C_0}$$

The frequency at any load capacitance  $C_L$  may be determined by replacing  $C_0$  in the preceding expressions by the sum of the holder capacitance and  $C_L$ , so that:

$$\frac{\Delta f}{f_s} = \frac{C_1}{2(C_0 + C_L)} \quad (\text{A1.18})$$

Putting  $r = C_0/C_1$  gives:

$$\frac{\Delta f}{f_s} = \frac{C_0}{2r(C_0 + C_L)} \quad (\text{A1.19})$$

The resistance of the crystal at any load capacitance  $C_L$  may be found by writing the resultant reactance of  $L_1$  and  $C_1$  as  $X$ , then by inspection of Figure A1 the impedance of the circuit may be written:

$$Z = \frac{(R_1 + jX)(jX_{CO})}{R_1 + j(X + X_{CO})} \quad (\text{A1.20})$$

where  $X_{CO} = -1/\omega C_0$ . Separating into real and imaginary parts gives:

$$Z = \frac{R_1 X_{CO}^2}{R_1^2 + (X + X_{CO})^2} + j \frac{X_{CO} [R_1^2 + X(X + X_{CO})]}{R_1^2 + (X + X_{CO})^2} \quad (\text{A1.21})$$

The effective resistance is then given by the real part:

$$R_e = \frac{R_1 X_{CO}^2}{R_1^2 + (X + X_{CO})^2} \quad (\text{A1.22})$$

By definition, the crystal is operating at a load point  $C_L$  when it is inductive and resonant with  $C_L$ ; that is when  $X$  resonates with  $C_L + C_0$ . Under these conditions the reactance  $X$  is given by:

$$X = \frac{1}{\omega(C_L + C_O)}$$

so that:

$$R_e = \frac{R_1 X_{CO}^2}{R_1^2 + X_{CO}^2 \left( \frac{C_L}{C_L + C_O} \right)^2} \quad (A1.23)$$

If

$$\left| X_{CO} \left( \frac{C_L}{C_L + C_O} \right) \right| \gg R_1$$

then:

$$R_e = R_1 \left( \frac{C_L + C_O}{C_L} \right)^2 \quad (A1.24)$$

APPENDIX B - EXPERIMENTS WITH A SWITCHED-CAPACITOR  
PROGRAMMABLE CRYSTAL OSCILLATOR

In section 5.4.1 of Chapter 5 attempts were outlined to realise a digitally programmable crystal oscillator using solid-state analogue switches to select various load capacitances. Details of the experiments performed are given here.

A unit was constructed consisting of a conventional oscillator, a 5MHz AT cut crystal requiring a nominal load capacitance of 30pF, and a capacitor selection network using 2 RCA COS/MOS type CD4016 quadruple bilateral switches. The unit is shown in Figure B1. The crystal was first placed in an identical oscillator and a graph of its frequency vs load capacitance was plotted, as shown in Figure B2, curve 1, for capacitance in the range 12pF to 240pF. In anticipation of large values of stray capacitance due to the large track area, the crystal was then placed in the test board with the switch circuits removed from their sockets. It was then found that with  $C_0 = 30\text{pF}$ ,  $f_0 = 4999960\text{Hz}$  corresponding to a load capacitance of 38pF suggesting that the board contributes 8pF to the total load. To verify this,  $C_0$  was reduced to 22pF and  $f_0$  rose to 5000000Hz.

On this basis, capacitors  $C_0$  to  $C_8$  were chosen as the following values:

$$\begin{array}{ll} C_0 = 4\text{pF} & C_5 = 18\text{pF} \\ C_1 = 2.2\text{pF} & C_6 = 33\text{pF} \\ C_2 = 3.3\text{pF} & C_7 = 68\text{pF} \\ C_3 = 4.7\text{pF} & C_8 = 120\text{pF} \\ C_4 = 8.2\text{pF} & \end{array}$$

so that, taking account of the known 8pF stray capacitance, a total load could be selected from 12pF to about 260pF in steps of about 2 to 3pF. The switch circuits were then plugged into the boards and a

plot of frequency vs selected load capacitance was drawn, as shown in Figure B2, curve 2. It is clear from the discrepancy in the curves that the actual load capacitance was much greater than that intended for selection. This extra capacitance was attributable only to the presence of the switch circuits themselves, and appeared to be in the region of 185pF. To verify this,  $C_5$  only was selected so that the total load was:

$$C_L = C_5 + C_0 + \begin{array}{c} \text{stray capacitance} \\ \text{of board} \end{array} + \text{unknown stray}$$

ie, 
$$C_L = 18 + 4 + 8 + C_x \text{ pF}, \text{ say,}$$

and, in accordance with the curve, the resulting frequency was 4999538Hz. The right-hand switch circuit was now removed from the board and the frequency rose to 4999778Hz which corresponds to  $C_L \approx 110\text{pF}$  and hence to  $C_x \approx 80\text{pF}$ . The removal of the circuit had more than halved the unexplained stray capacitance and would hence seem to account for its presence. The two switch circuits, and others of different manufacture, were interchanged at random and it was found that no frequency could be reproduced with a different circuit, conflicting greatly with one of its prime objectives.

Since this configuration had proved inviable, the alternative of Figure B3 was investigated. This had the apparent advantage that the total capacitance could be varied from 15.4 to 68.3pF in steps of less than 0.1pF whilst using large-valued components. It was further proposed that the stray capacitance of the switches could be included in the three fixed capacitors by reducing their value accordingly. In practice it proved no solution. It was found that the equivalent stray capacitance of each of the switches had a differing effect when those switches flanking it in the pack were on or off. The effective stray capacitance, therefore, varied with the

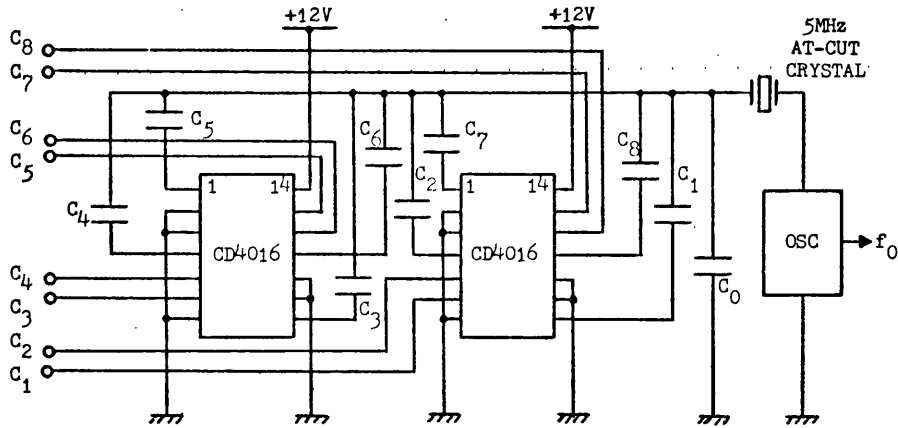


**Figure B1** Switched capacitor digitally programmable crystal oscillator

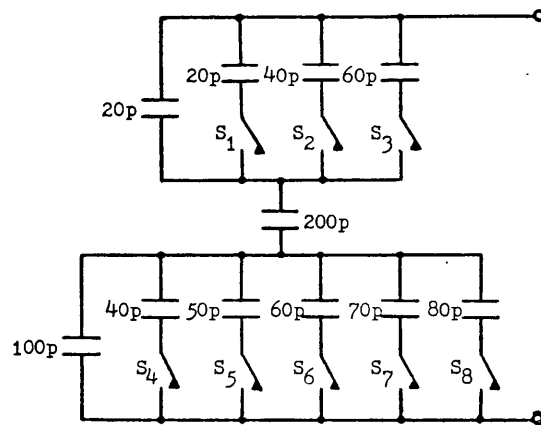


**Figure B3** Alternative configuration of capacitor bank



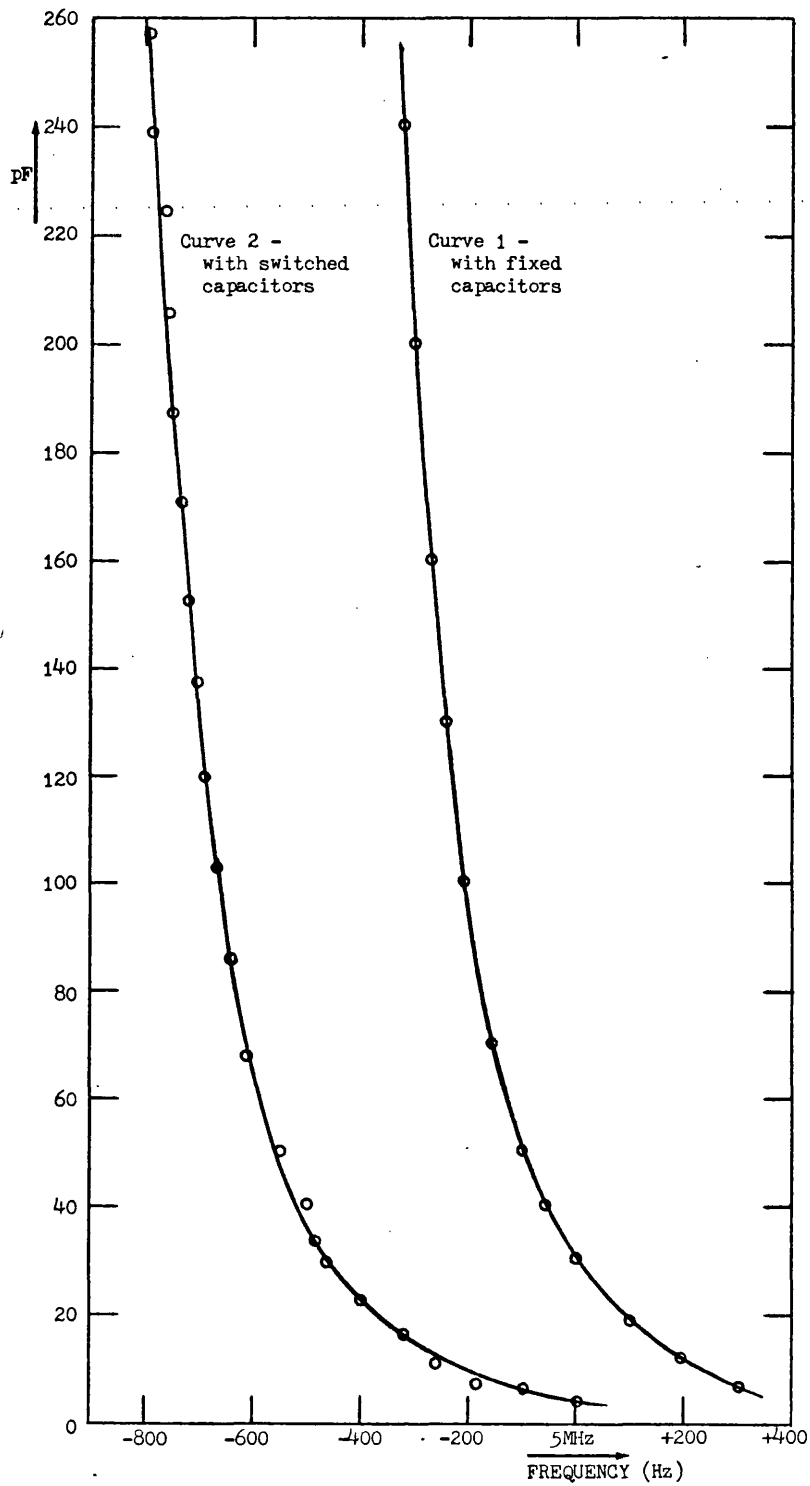


Figure B2 Graphs of selected load capacitance against frequency for the digitally programmable oscillator

digital command to the extent that in some cases a change in command intended to increase the frequency would, in fact, decrease it. The network could be made repeatable, but only by sacrificing capacitance resolution to the extent that the smallest available steps were about 10pF. From the graphs it may be seen that at 5MHz the load characteristic has a slope of about 4Hz/pF so that the frequency resolution would be only 40Hz or about 8 parts per million which was clearly insufficient in this application.

With due consideration to its advantages and disadvantages, this approach to the requirement for a digitally controlled crystal oscillator was abandoned in favour of digital synthesis techniques.

APPENDIX C - "THE FREQUENCY SHIFTING SYNTHESIZER"

The following is a copy of the paper "The frequency shifting synthesizer" published in 'The Radio and Electronic Engineer', Vol.50, No.3, March 1980.

# The frequency shifting synthesizer

G. A. WARWICK, B.Sc.\*

A. J. PRESCOTT, Dip.Tech.(Eng.),  
A.C.T.(Birm.)\*

and

Professor W. GOSLING, B.Sc., A.R.C.S.,  
C.Eng., F.I.E.R.E.\*

## SUMMARY

An unusual class of digital frequency synthesizers is presented capable of very high frequency-resolution. Construction may be made very simple. In typical applications the complexity of the hardware may be reduced by up to 50% compared with earlier approaches. A standard circuit is defined which may be used in a variety of applications, several of which have been outlined as illustrations of the flexibility of the technique.

\* School of Electrical Engineering, University of Bath, Claverton Down, Bath BA2 7AY.

## 1 Theory

Figure 1 shows the functional block diagram of a class of digital frequency synthesizers which has been found useful in applications where high frequency-resolution is required over a limited range. Known as a frequency shifting synthesizer (f.s.s.), it consists of a voltage-controlled oscillator, programmable divider, digital mixer and phase comparator, together with a small number of discrete components.

From Fig. 1, it may be seen that when the loop is phase locked

$$f_2 = f_3$$

and, assuming  $f_1 > f_0$ :

$$f_1 - f_0 = \frac{f_1}{N}$$

from which

$$f_0 = f_1 \left[ \frac{N-1}{N} \right] \quad (1)$$

and

$$f_1 = f_0 \left[ \frac{N}{N-1} \right] \quad (2)$$

Differentiating (1) and (2) with respect to  $N$ , assuming other values constant:

$$\frac{\partial f_0}{\partial N} = f_1 \left[ \frac{1}{N^2} \right] \quad (3)$$

$$\frac{\partial f_1}{\partial N} = -f_0 \left[ \frac{1}{(N-1)^2} \right] \quad (4)$$

(For completeness, the corresponding equations for the case  $f_0 > f_1$  are in the Appendix.)

Equations (1) and (2) indicate the unusual property of this synthesizer that the relationship between input and output frequencies is non-linear with changes in  $N$ . This is illustrated in Fig. 2. For large values of  $N$ , however, the relationship approximates to linear and the ratio  $(N-1)/N$  is close to unity.

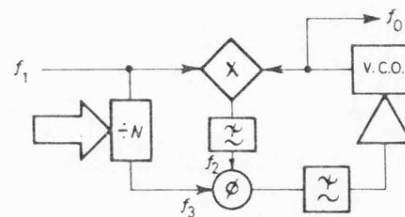


Fig. 1. Basic block diagram of a frequency shifting synthesizer.

The partial derivative equations (3) and (4) represent the frequency resolution of the synthesizer for  $f_1$  constant and  $f_0$  constant respectively. The  $N^2$  or  $(N-1)^2$  terms in the denominators of these expressions yield very small values of frequency resolution for high values of  $N$ .

It is instructive to compare these results with those of conventional synthesizers. Figures 3(a) and 3(b) show

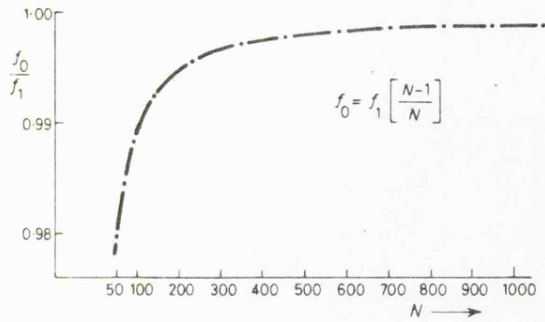


Fig. 2. Relation between input and output frequencies for synthesizer of Fig. 1.

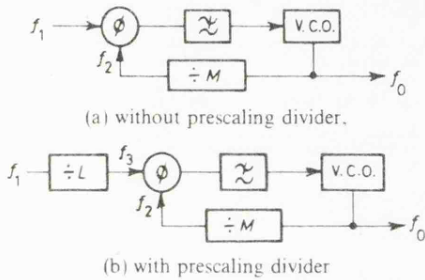


Fig. 3. Conventional feedback synthesizer

feedback synthesizers of a commonly employed type, respectively without and with a prescaling divider ( $L$ ). For these synthesizers, the equations corresponding to (1) and (3) are:

(a) with no prescaling of the reference frequency,

$$f_0 = M f_1 \quad (5)$$

and

$$\frac{\partial f_0}{\partial M} = f_1 \quad (6)$$

(b) with a prescaling divider,

$$f_0 = \frac{M}{L} f_1 \quad (7)$$

$$\frac{\partial f_0}{\partial M} = f_1/L \quad (8)$$

and

$$\frac{\partial f_0}{\partial L} = -\frac{M}{L^2} f_1 \quad (9)$$

Equation (9) describes the frequency resolution for  $M$  constant and  $L$  varied, and suggests that if  $L$  is greater than  $M$  the resolution is improved over that described by equation (8). This can be misleading since the condition  $L > M$  implies (from equation (7)) that  $f_0 < f_1$ , and hence smaller frequency increments are obtainable only in a lower nominal frequency.

Comparison of the three configurations is best achieved by consideration of the fractional resolution,  $F$ , defined by:

$$F = \frac{\partial f_0 / \partial R}{f_0}$$

where  $R$  is the programmable divider modulus. Applying this measure to the three systems:

$$F = \frac{1}{M} \quad \text{for the feedback synthesizer}$$

$$F = \frac{1}{M} \quad \text{for the feedback synthesizer with prescaled reference, varying the feedback divider}$$

$$F = -\frac{1}{L} \quad \text{for the feedback synthesizer with prescaled reference, varying the prescaler modulus}$$

and

$$F = \frac{1}{N(N-1)} \quad \text{for the frequency shifting synthesizer.}$$

These results show the improvement in frequency resolution obtainable using the f.s.s. provided the value of  $N$  is varied about some high value. If that condition is met the synthesizer approximates linearity, the input and output frequencies being nearly equal. The entire synthesizer may be represented by a pair of simple equations permitting rapid system design.

The noise performance of high resolution synthesizers is dependent mainly upon the v.c.o. transfer gain and the loop bandwidth. As will be seen later, in practical applications the v.c.o. of a f.s.s. operates only over a very narrow range. If the v.c.o. is crystal-controlled (v.c.x.o.) the value of its gain may be made small and its free-running frequency stability good. A very narrow bandwidth loop may be employed, therefore, minimizing the resultant phase noise. In addition the output crystal may be driven hard to give good overall signal to noise ratio.

## 2 Design Considerations

### 2.1 Hardware

Construction of each element of the synthesizer of Fig. 1 may be made very simple:

- (a) The mixer may comprise simply a digital D-type flip-flop,<sup>1</sup> obviating the need for a following low-pass filter since this function is performed intrinsically by the action of the device. For reasons described below it is desirable to ensure that the output is a symmetrical squarewave. This may be achieved in most cases by careful choice of input parameters, but otherwise may be ensured by the inclusion of a  $\div 2$  pulse squarer.
- (b) As will be illustrated later, the length of the programmable divider chain is dependent upon the application. In any case the chain may be made up of standard presettable counters or dividers. The output of such a divider is usually a



train of narrow pulses, which is unsuitable as input to an exclusive-OR phase comparator. To overcome this difficulty either a D-type flip-flop phase comparator may be used, or a  $\div 2$  pulse squarer included at the output of the divider. The latter solution is appropriate if a pulse squarer is also included as in (a).

(c) The simple exclusive-OR phase comparator may be employed provided that the duty cycle of both its inputs is close to 50%. If this condition is met, the level of low frequency components at the output will be kept to a minimum, minimizing any residual frequency modulation of the v.c.o. If the input duty cycle is not suitable, then an edge triggered type of digital phase comparator may be employed.<sup>2</sup>

(d) From equations (1) and (8) (see Appendix), the output frequency is given in general by:

$$f_0 = f_1 \frac{N \pm 1}{N}$$

and the offset of  $f_0$  from  $f_1$  by:

$$f_1 - f_0 = \pm \frac{f_1}{N}$$

Care must be taken that the range of the v.c.o. is not sufficient to bring about false locking, so that its range about centre frequency should be rather less than  $\pm f_1/N$ . The range, therefore, becomes narrower as  $N$  increases. This is in accordance with the fact that the resolution increases with  $N$  and hence the required range in practice becomes narrower.

(e) The loop filter and linear amplifier may be of any convenient type.

Figure 4 shows the system configuration using the above simple elements. Provided that a long enough divide chain is employed, this same hardware can perform the required frequency shifting function for a variety of applications.

Some examples of practical designs using this system are perhaps useful as illustrations. To synthesize a frequency offset by nominally 1 kHz from a given

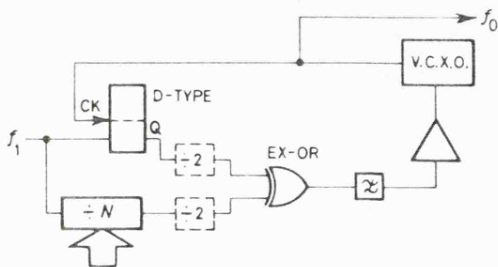


Fig. 4. Synthesizer incorporating digital D-type flip-flop mixer,  $\div 2$  pulse squarer and exclusive-OR phase comparator.

10 MHz frequency source,

i.e.  $f_1 = 10^7$  Hz

and  $f_0 = 9999000$  Hz

then, substituting in equation (1)  $N = 10^4$ .

Substituting into (3), the output frequency resolution obtainable in this case will be

$$\frac{\partial f_0}{\partial N} = 0.1 \text{ Hz.}$$

Similarly, to synthesize an output frequency nominally of 10 MHz variable over a narrow range in steps of 1 Hz, the required parameters are

$$f_1 = 10003162 \text{ Hz}$$

and

$$N = 3163$$

and to generate a frequency with a resolution of 2.5 Hz from a 10 MHz source,

$$N = 2000$$

and

$$f_0 = 9995000 \text{ Hz.}$$

### 2.2 Factors Affecting the Programmable Dividers

The value of  $N$  determined in the basic design of any system defines the minimum number of divider stages required. Whether all of these stages are programmed, however, is a different consideration. As an illustration consider the case of the first example above. A nominal value for  $N$  of 10000 has been arrived at, and this will require at least 14 bits of divider. The total range of a 14-bit divider if all the bits are programmable is:

$$N = 2$$

to

$$N = 16384$$

As discussed previously, the lower end of this range is inappropriate as the non-linearity of the system becomes excessive. The high end of the range presents no problems, provided that the phase comparator frequency does not become excessively low as a consequence. The total frequency range over which the synthesizer operates is, of course, defined by the allowable range of  $N$ .

One factor of importance in certain applications is the number of bits available for programming the synthesizer. Commonly an eight-bit address word only is available, and the effect which this has on the range may be evaluated as follows:

(i) Consider the binary equivalent of the nominal value of  $N$ , in this case:

$$10000_{10} \equiv 10\ 0111\ 0001\ 0000_2$$

(ii) If only the least significant eight bits may be

programmed, then the range of  $N$  obtainable is:

$$10\ 0111\ 0000\ 0000 \equiv 9984$$

to

$$10\ 0111\ 1111\ 1111 \equiv 10239$$

- (iii) Substituting these values into equation (1) the maximum and minimum output frequencies may be determined:

$$|f_{0\min}| = 9998999\ \text{Hz}$$

$$|f_{0\max}| = 9999023\ \text{Hz}$$

- (iv) The worst-case frequency resolution may now be determined from equation (3) by substitution of the minimum value of  $N$

$$\left| \frac{\partial f_0}{\partial N} \right|_{\max} = 0.10003\ \text{Hz}$$

### 2.3 Comparator Frequency

In the second example quoted, it was shown that in order to synthesize a frequency of nominally 10 MHz with a resolution of 1 Hz,  $f_1 = 10003162\ \text{Hz}$ ,  $N = 3163$  and hence the phase comparator frequency is  $f_3 = 3163\ \text{Hz}$ . If this same requirement is applied to the conventional synthesizer of Fig. 3(b) the following values result:

$$L = 10^7$$

$$M = 10^7$$

$$f_1 = 10\ \text{MHz}$$

$$f_3 = 1\ \text{Hz}$$

and

Not only does the f.s.s. show considerable economy of hardware over the conventional approach, but the higher phase comparator frequency involved affords reduced residual f.m., improved acquisition time and less stringent filter requirements.

### 3 Applications

The combination of high frequency resolution and simplicity of construction have rendered the f.s.s. appropriate in applications such as the following.

#### 3.1 A Digitally-temperature-compensated Crystal Oscillator<sup>3,4</sup>

Figure 5 is the block diagram of an all-digital technique for the temperature compensation of crystal oscillators, details of which may be found in reference 3.

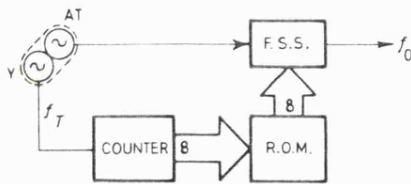


Fig. 5. All-digital technique for temperature compensation of crystal oscillator.

The technique affords considerable improvement in temperature stability and noise performance over conventional corrected oscillators, and could not have been made practical without the very high frequency resolution of a f.s.s.

The heart of the system is a frequency shifting synthesizer which generates a corrected frequency from that of a temperature varying AT-cut quartz crystal oscillator. The synthesizer is addressed according to temperature-law data contained in a read-only memory (r.o.m.), the appropriate data being selected according to temperature information. This is obtained by counting the linearly temperature dependent frequency of a second crystal oscillator controlled by a Y-cut crystal held in close thermal contact with the AT-cut crystal.

The synthesizer employed has as its output a voltage-controlled crystal oscillator which is driven at a high level in order to obtain optimum noise performance. It is capable of correcting the AT-cut crystal oscillator frequency to within 0.5 Hz over the temperature range to 0 to 50°C, representing a frequency stability of 5 parts in 10<sup>8</sup>. An l.s.i. version of the oscillator is currently being developed commercially.

#### 3.2 A Digitally Controlled Clarifier for S.S.B. Radio

When a digital channel synthesizer is employed in a single sideband radio system, the clarifier commonly consists of a fine-tune control on the master oscillator of the synthesizer. When the frequency of the master oscillator is used elsewhere, however, (for example when one high-stability oscillator is used to control several equipments), this fine-tune is not possible. Incorporation of the fine-tune facility into the channel synthesizer would require considerable increase in its complexity.

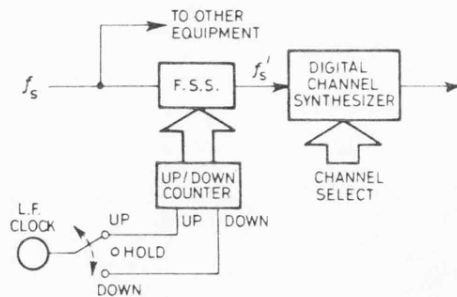


Fig. 6. Digital clarifier for s.s.b. reception using f.s.s.

Figure 6 shows the schematic of a digital clarifier based upon the frequency shifting synthesizer. The f.s.s. is used to vary the clock frequency of the channel synthesizer without disturbing the standard frequency source, leaving the latter available for other uses. The address to the f.s.s. may be obtained from a digital UP/DOWN counter clocked by a low-frequency (say 5 Hz) oscillator. A three-position switch may be employed to gate the clock pulses to either the 'count-up' or 'count-



down' port.

The digital nature of this clarifier makes it suitable for incorporation into an automatic version<sup>5</sup> in which pilot information is encoded onto the transmission. On reception the clarifier is allowed to scan through its range until the pilot information indicates correct tuning, when the output of the counter is latched. Such a system has the advantage over analogue sample/hold arrangements that its memory is indefinite.

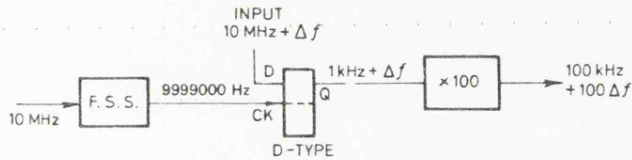
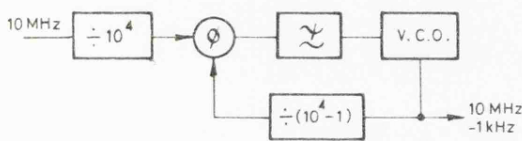
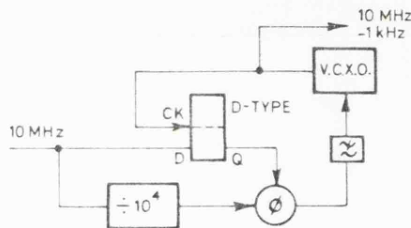


Fig. 7. Simple frequency error multiplier.



(a) Conventional approach.



(b) Using f.s.s. techniques.

Fig. 8. Offset frequency generation

### 3.3 Fixed Offset-frequency Source

The need arises for a synthesizer to generate a 9999000 Hz signal from a 10 MHz frequency standard (similar to the first example of Sect. 2.1), for use in the simple frequency error multiplier of Fig. 7. Figures 8(a) and 8(b) allow comparison of the conventional and f.s.s. approaches to this requirement and show a clear economy in the latter.

### 4 Discussion

The simplicity with which very high frequency resolution may be obtained using a frequency shifting synthesizer makes the technique attractive in many areas. Its relatively low cost allows its effective use in routine as well as exacting applications, for both fixed and programmable frequency generation. The combination of two such synthesizers would broaden the possibilities still further.

### 5 Acknowledgments

The authors acknowledge the receipt of a Science Research Council CASE award (to G. A. Warwick) in collaboration with Racal Instruments Ltd., Windsor, Berkshire. Particular thanks are due to Mr. K. Thrower for helpful discussions throughout the work.

### 6 References

- 1 Nemeč, J., 'A high frequency synthesizer with a digital mixer', *Electronic Design*, 4, pp. 120-2, 15th February 1977.
- 2 Morgan, D. K. and Steudel, G., 'The COS/MOS Phase-locked Loop', RCA application note ICAN-6101.
- 3 Warwick, G. A., Gosling, W. and Prescott, A. J., 'A digital technique for temperature compensation of crystal oscillators', Conference on Radio Receivers and Associated Systems, Southampton, July 1978, IERE Conference Proceedings no. 40, pp. 207-16.
- 4 'Digital compensation technique in crystals yields ultrastability', *Electronics*, September 14th, 1978, pp. 67-8.
- 5 Gosling, W., McGeehan, J. P. and Holland, P. G., 'Receivers for the Wolfson SSB/VHF land mobile radio system', Conference on Radio Receivers and Associated Systems, Southampton, July 1978, IERE Conference Proceedings no. 40, pp. 169-78.

### 7 Appendix

The equations corresponding to (1) to (4) for the case  $f_0 > f_1$  are easily derived as follows:

From Fig. 1, when the loop is phase locked:

$$f_2 = f_3$$

If  $f_0 > f_1$ , then  $f_0 - f_1 = f_1/N$

from which

$$f_0 = f_1 \left[ \frac{N+1}{N} \right] \tag{8}$$

and

$$f_1 = f_0 \left[ \frac{N}{N+1} \right] \tag{9}$$

Differentiating these with respect to  $N$ , assuming other values constant:

$$\frac{\partial f_0}{\partial N} = -f_1 \left[ \frac{1}{N^2} \right] \tag{10}$$

and

$$\frac{\partial f_1}{\partial N} = f_0 \left[ \frac{1}{(N+1)^2} \right] \tag{11}$$

All other aspects of the performance and design of a f.s.s. are identical for  $f_0 < f_1$  and  $f_0 > f_1$ .

*Manuscript first received by the Institution on 19th October 1978 and in revised form on 13th March 1979  
(Paper No. 1922/CC 319)*



APPENDIX D - "A DIGITAL TECHNIQUE FOR TEMPERATURE COMPENSATION OF  
CRYSTAL OSCILLATORS"

The following is a copy of the paper "A Digital Technique for Temperature Compensation of Crystal Oscillators" presented at the Conference on Radio Receivers and Associated Systems, Southampton, July 1978, and published in IERE Conference Proceedings No.40, pp.207-16.

# A DIGITAL TECHNIQUE FOR TEMPERATURE COMPENSATION OF CRYSTAL OSCILLATORS

G A WARWICK,\* W GOSLING,\* A J PRESCOTT \*

## Abstract

A technique is described for the temperature compensation of quartz crystal oscillators which is primarily digital in nature. The system is capable of high stability over a reasonable temperature range, and offers advantages not present in conventional designs. The system may be made conservative in space and power requirements, and competitive in cost. Further reductions in these factors may be made possible by the use of large scale integration.

## 1. SYSTEM CONFIGURATION

The proposed system<sup>(1)</sup> is shown in Figure 1. A high-resolution digital frequency synthesiser is used to derive the stable output frequency,  $f_0$ , from the temperature varying frequency,  $f_1$ , of an oscillator controlled by an AT cut crystal.

A second crystal oscillator controlled by a Y cut crystal is constructed such that the two crystals are in good thermal contact and hence kept at substantially the same temperature. The frequency of this Y cut crystal oscillator,  $f_T$ , is then digitally counted against  $f_0$ . Since the temperature coefficient of frequency of Y cut quartz is large, the output "word" of the counter can be considered to represent the temperature of the crystal pair.

This temperature word is used as the address to a read-only memory (ROM) programmed such that for each individual address the output of the memory is the required synthesiser input word to hold the output at  $f_0$  at the corresponding temperature. In this way for each increment in temperature registered by the Y cut crystal the appropriate correction to  $f_1$  is made to hold  $f_0$  steady.

Typical frequency-temperature curves for AT and Y cut crystals are shown in Figures 2 and 3. From these graphs it is clear that if the counter is capable of resolving a temperature change of  $\Delta\theta^\circ\text{C}$ , and that the point of steepest slope of Figure 2 is  $\Delta f_{\text{AT}} \text{ Hz}/^\circ\text{C}$ , then the maximum excursion,  $e_{\text{max}}$ , of  $f_0$  from the required output frequency is given by:

$$e_{\text{max}} = \Delta f_{\text{AT}} \cdot \Delta\theta \quad (1.1)$$

If the system is required to operate over a total temperature range  $T_{\text{tot}}^\circ\text{C}$ , then assuming linearity of Figure 3, the maximum range of the counter,  $R$ , is given by:

---

\* School of Electrical Engineering, University of Bath

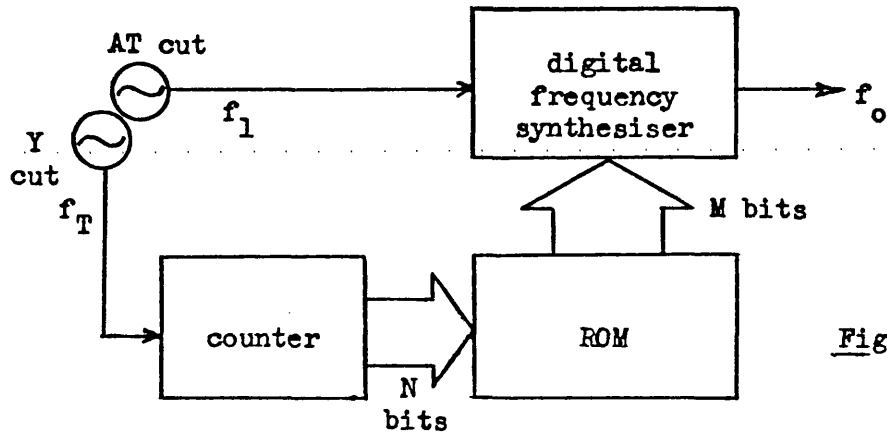


Figure 1.

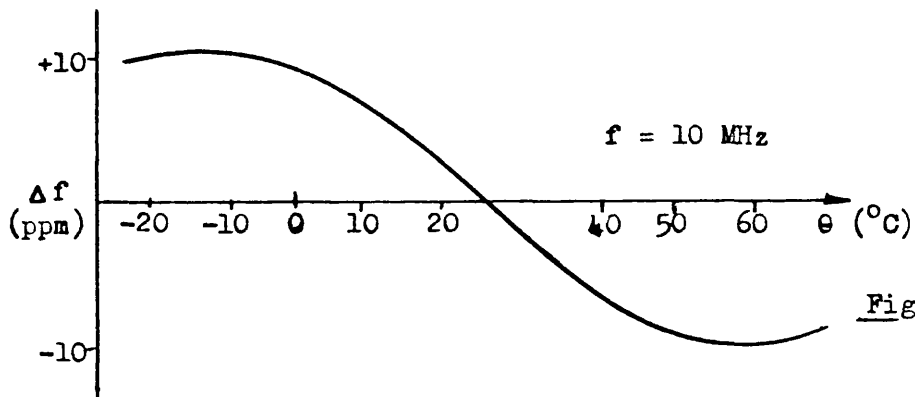


Figure 2.

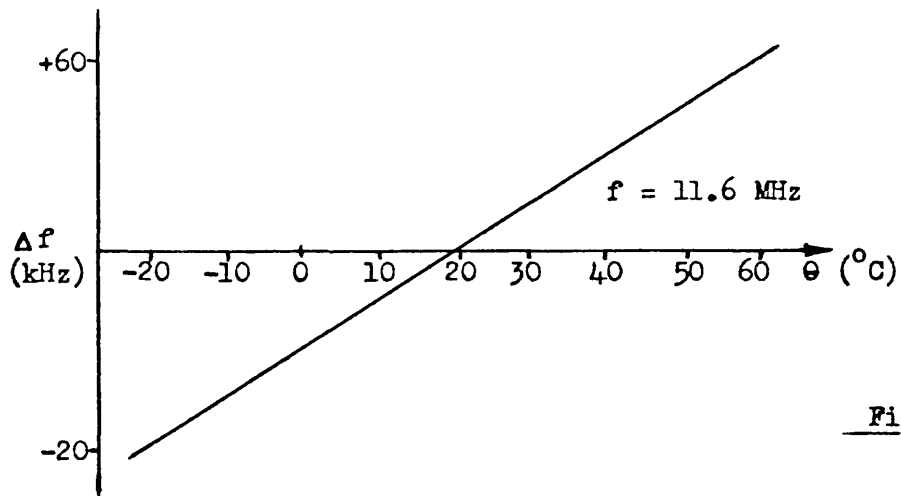


Figure 3.

$$R = \frac{T_{\text{tot}}}{\Delta\theta} \quad (1.2)$$

so that since the number of bits required by the counter, N, is given by:

$$R = 2^N \quad (1.3)$$

then combining (1.2) and (1.3):

$$T_{\text{tot}} = 2^N \cdot \Delta\theta \text{ } ^\circ\text{C} \quad (1.4)$$

In a typical AT cut crystal, similar to that of Figure 2, the value of  $\Delta f_{\text{AT}}$  may be about 0.5 parts in  $10^6/1^\circ\text{C}$ . The value of  $\Delta\theta$  may be controlled by suitable choice of the counter gate time, to, say,  $0.2^\circ\text{C}$ , yielding from (1.1) a maximum frequency error:

$$e_{\text{max}} = (0.5 \times 10^{-6} \times 10^7) \cdot (0.2) = 1.0\text{Hz}$$

assuming an oscillator frequency of 10MHz.

If an overall temperature range of  $50^\circ\text{C}$  is required then, from (1.4) a value for N may be chosen. In this case  $N = 8$ , which is readily available commercially, gives:

$$T_{\text{tot}} = 2^8 \cdot 0.2 = 51.2^\circ\text{C}$$

Provided that each individual element is realisable, therefore, the system is capable of good regulation of frequency over a reasonable temperature range, where the data stored in the ROM corresponds to the temperature characteristics of that particular pair of AT cut and Y cut crystals employed.

As will be shown later, the system is capable of adaptation to a higher level of regulation over a narrower temperature range or to a less stringently controlled frequency over a broader range of temperatures. Furthermore, by extension of the memory capacity both the frequency regulation and the temperature range may be improved as required.

## 2. THE ELEMENTS OF THE PROTOTYPE SYSTEM

On the basis of the values of  $e_{\text{max}}$ , N and  $T_{\text{tot}}$  calculated in Section 1, a prototype system has been constructed. Each of the elements of this system will now be described in some detail.

### 2.1 The Frequency Synthesiser

In order that the system shall be capable of realising the value of  $e_{\text{max}}$  of 1.0Hz, the frequency resolution of the synthesiser must, clearly, be better than this figure. The design of such a high resolution frequency synthesiser calls, under normal circumstances, for a multi-loop system<sup>(2)(3)</sup> incorporating several auxiliary voltage controlled oscillators in addition to the output oscillator. The system considered

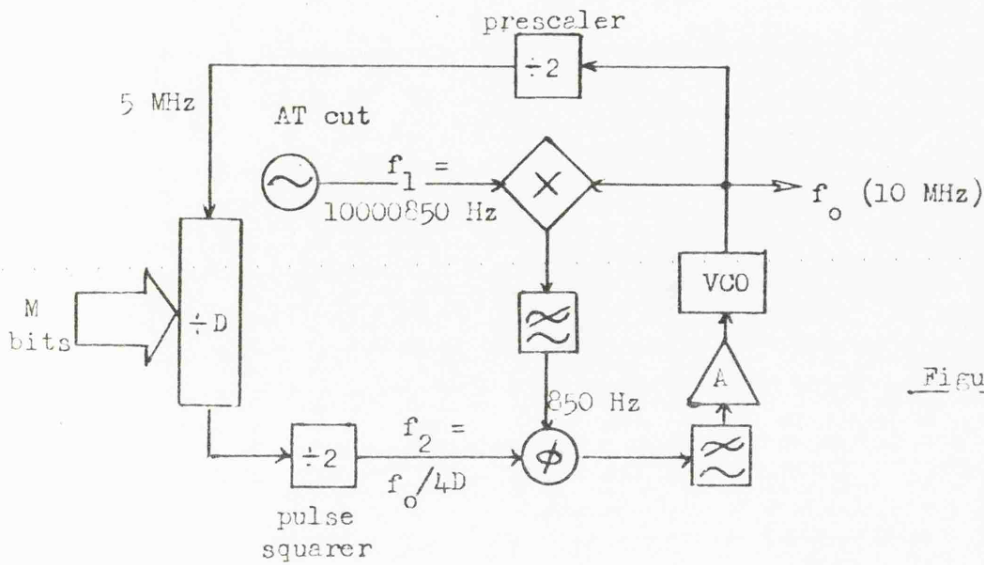


Figure 4.

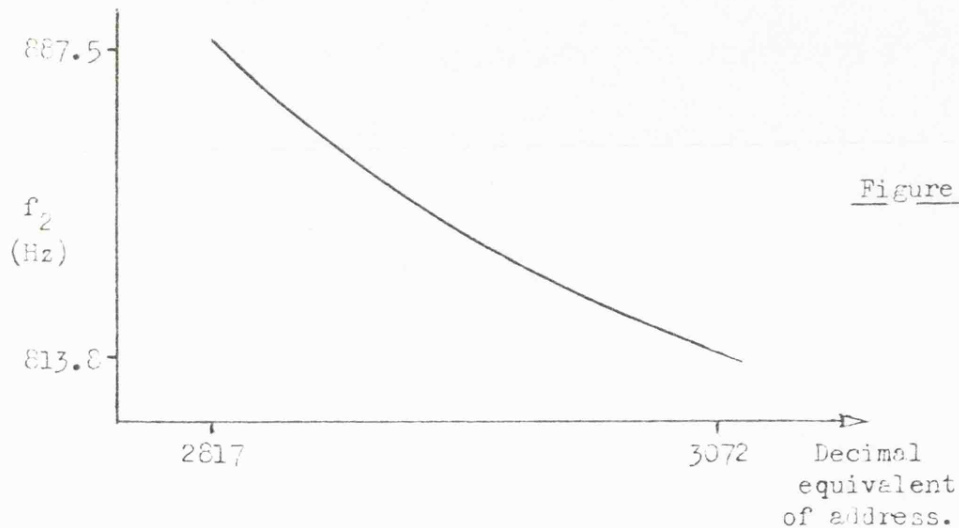


Figure 5.

here, however, only requires high frequency resolution over a very narrow range, and this has led to the development of a single loop synthesiser capable of frequency increments of about 0.3Hz over a range of about 75Hz according to an 8 bit digital command. A block diagram is given in Figure 4.

The voltage controlled oscillator, frequency  $f_0 = 10\text{MHz}$ , is mixed with the output of the AT cut crystal oscillator,  $f_1 = 10\text{MHz} + 850\text{Hz}$  nominally, and the difference frequency compared in a phase sensitive detector (PSD) with a divided version of  $f_0$ . The PSD output is filtered, amplified and fed to the VCO as control voltage. When the loop is phaselocked, therefore:

$$f_1 - f_0 = \frac{f_0}{4D} \quad (2.1)$$

from which:

$$f_0 = \left( \frac{4D}{4D + 1} \right) f_1 \quad (2.2)$$

The programmable divide-by-D counter is 12 bits long, only the least significant 8 bits of which are addressed, the other four having their input code hard-wired. In this way D is variable between 2817 and 3072, so that  $f_2$  is variable between 887.5Hz and 813.8Hz according to the law shown in Figure 5. The non-linearity presents no problem since the address to the synthesiser is stored in the ROM, the content of which may be programmed to make allowance for the law. The frequency increment possible is easily calculated and is shown clearly by Table 1 to be less than 0.32Hz throughout.

<u>D</u>	<u><math>f_2 (= 10^7/4D)</math>Hz</u>	<u><math>\Delta f_2</math> Hz</u>
2817	887.47	
2818	887.15	0.32
2819	886.84	0.31
3070	814.33	
3071	814.07	0.26
3072	813.80	0.27

TABLE 1

The :2 prescaler is included for convenience since it is common with a portion of the counter (see Section 2.2) and serves to aid the design of the programmable divider. The :2 pulse squarer is a D-type flip-flop used to convert the narrow pulse train output from the programmable divider to a square wave suitable for input to the PSD. This is itself a digital exclusive-OR type phase comparator whose characteristics are well known<sup>(5)</sup>, and is chosen for its property that, should one of its inputs fail, its output remains steady at the mid-point of its power supply voltage.

The down-converter is a digital D-type flip-flop used as shown in Figure 6<sup>(6)</sup>. This has the advantage that the low-pass filtering is accomplished automatically by the nature of the device operation, and that the output difference frequency is suitable for direct input to the ex-OR phase comparator.

The amplifier is the only linear part of the whole system, apart from the oscillators themselves, and is a simple SN72741 operational amplifier.

Because the output frequency is held constant, the output VCO may itself be crystal controlled, the voltage tuning being accomplished by varactor diode. This has the advantage that, since the oscillator is



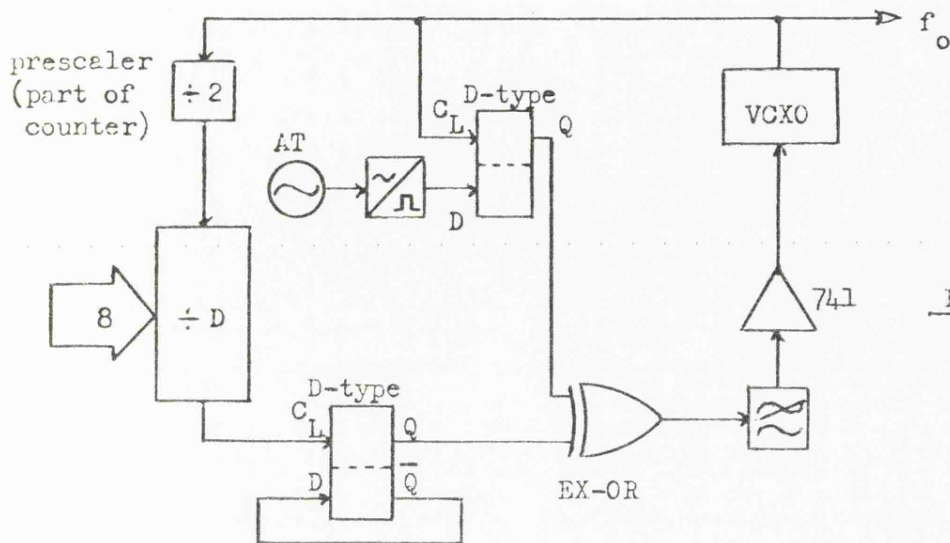


Figure 6.

phase-locked, the ageing rate of the crystal, and hence its drive level, are unimportant. This allows a high level to be employed which greatly improves the output signal-to-noise ratio over both the conventional VCO and free-running crystal oscillators.

As indicated in Figure 6, this form of synthesiser may be made extremely compact, requiring only six integrated circuit packages and a few discrete components. Power consumption has, as yet, not been optimised, but since most of the logic circuitry operates at low speed, low power TTL or CMOS technology may be employed.

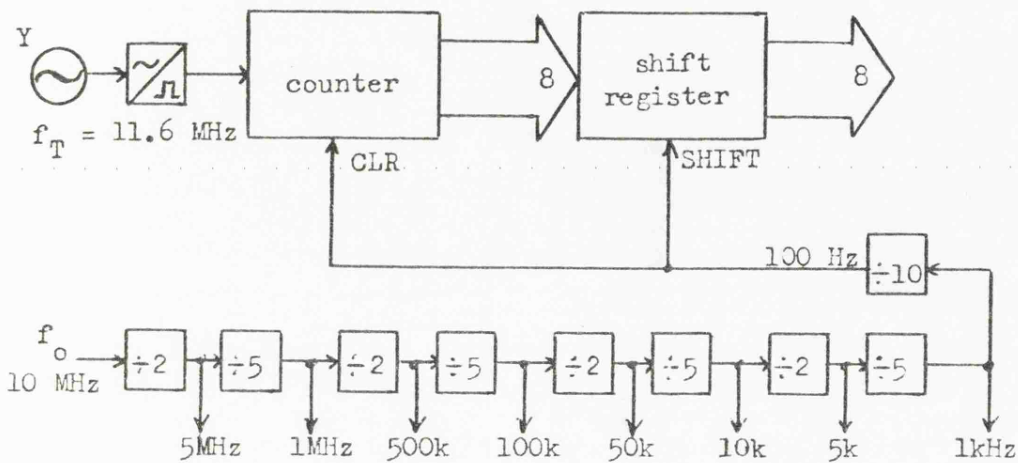
## 2.2 The Counter

The digital counter employed in the prototype is of the simple gated type shown in Figure 7. The output  $f_0$  is divided down to 100Hz by successive decade-counters, arranged so that a divide-by-2 intermediate output is available from each. (In this way nine sub-harmonics of the output frequency are available for use in other parts of the user's equipment, this feature being particularly useful to the designer of a digital channel synthesiser for a radio receiver.) The 100Hz squarewave is then used both to shift the output of the counter through the shift register and to reset the counter. When the CLR input is held high, the count is inhibited so that the total count time is only half of the period of the 100Hz squarewave, namely 5msec. This renders the counter capable of counting the input frequency to the nearest 5msec. As will be shown later (section 2.4), the Y cut crystal oscillator may be designed to have a temperature coefficient of frequency of  $1\text{kHz}/^\circ\text{C}$ , so that when counted as above the temperature resolution of the whole is  $0.2^\circ\text{C}$ , as required.

## 2.3 The Memory

The preceding sections have already defined the size of the input and output words of the ROM as 8 bits each. The memory capacity required is, therefore  $2^8 \times 8 = 2048$  bits - normally referred to as a 256 x 8 bit or 2kbit ROM.

Figure 7.



As was mentioned in Section 1, data stored in the ROM corresponds only to that particular pair of crystals for which it was programmed, and therefore for the purposes of proving the system an easily edited and erasable memory was required. To this end the M1702A ultra-violet erasable programmable ROM (PROM) was chosen for the prototype. This device is TTL compatible throughout and is also compatible with commercially available PROM simulation equipment and programmers. The access time of the device is  $1\mu\text{sec}$ , which is more than adequate for this application.

#### 2.4 The Crystal Oscillators

Both the AT cut and Y cut crystal oscillators are of similar design, with the output a TTL compatible squarewave. The oscillators are positioned together on the circuit board in order that the temperature of the two crystals be approximated. This is done by means of a small aluminium block  $25 \times 20 \times 20$  millimetres into which are milled two slots to accommodate the HC-18/U crystal holders. The crystals are bonded into the block with silver-loaded epoxy resin which affords a low thermal resistance between the crystals and the block. In a closed environment in still air this holds the temperature difference between the crystals to within the required limits. In an adverse environment with draughts and localised heating there is a danger of thermal conduction up the crystal leads predominating, unless care is taken to prevent this. It may be found expedient to mount both crystals in the same holder, but this possibility has yet to be investigated.

The frequency of the Y cut crystals was chosen as  $11.6 \text{ MHz}$  in order that, since the temperature coefficient of Y cut quartz is about  $86 \text{ ppm}/^\circ\text{C}$ , the temperature coefficient of the crystal employed is very close to  $1 \text{ kHz}/^\circ\text{C}$ .

The ageing rate of fundamental AT cut crystals has been the subject of much investigation<sup>(7)(8)(9)</sup> and the constraints which this places on oscillator performance are well known. This system cannot compensate for



this ageing. It has an advantage in this respect over oven-controlled crystal oscillators, however, which operate with their crystals at an elevated temperature for the purposes of control. This inevitably accelerates ageing, an effect which is absent in the system described.

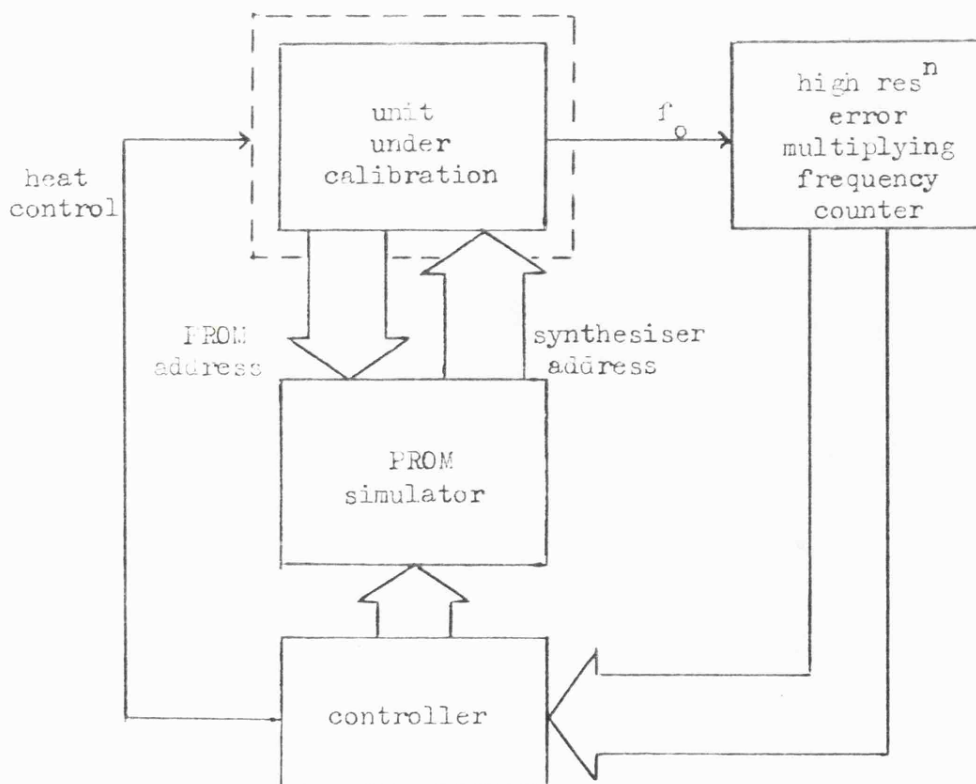
The ageing of the Y cut crystal can be shown to be of little significance in comparison with its frequency change due to change in temperature. The expected magnitude of long-term drift is less than 1 part in  $10^7$ /month (after an initial stabilisation period) and this represents a drift of less than 15Hz in total in the first year, or a temperature-measurement error of about 15 millidegrees Celcius. Since the temperature resolution of the counter is only  $0.2^{\circ}\text{C}$ , ageing is clearly unimportant.

### 3. SYSTEM CALIBRATION

A study of the system reveals its suitability for automatic calibration. One of the most important aspects of this is that, during cycling, no absolute measurement of temperature is required, since it is the temperature increments as registered by the counter which are the governing parameter. One possible technique for automatic calibration is shown in Figure 8.

The unit under calibration is slowly temperature cycled with the memory removed from the circuit and its place taken by a PROM simulator. This consists of a random-access memory of the same configuration but

Figure 8.



controlled by a digital sequencer. For each individual ROM address this sequence controller simply changes the synthesiser address slowly until the digital output from the error-multiplying frequency counter is as close as possible to the required output frequency. (This need not be exactly 10MHz but could, if required, be offset by a small amount.) After the unit has been heated and the relevant data stored in the PROM simulator, this can be verified on cooling. When the cycle is complete the data from the simulator may be programmed into the PROM and the PROM replaced in the circuit.

By using a fast frequency meter and a slow temperature cycle time it may be possible for one controller to programme several units at once.

#### 4. CONCLUSIONS

A system for temperature compensation of crystal oscillators has been presented which is capable of performance comparable with existing designs, but exhibiting several advantages. Firstly, nearly all the control circuitry is digital and is therefore suitable for large scale integration. Secondly, since the output oscillator is a hard driven voltage controlled crystal type, the standard frequency output is of excellent signal-to-noise ratio. Thirdly, stable logic waveforms at sub-harmonics of the output frequency are available, offering considerable advantage to the designer of digital frequency synthesisers. Fourthly, the system is of a form suited to automatic calibration and programming.

#### 5. ACKNOWLEDGEMENTS

The authors acknowledge the receipt of a Science Research Council CASE award (to G A Warwick) in collaboration with Racal Instruments Ltd, Maidenhead, Berkshire, in whose frequency standards laboratory many of the measurements were carried out.

Particular thanks are due to Mr T McKnight of the McKnight Crystal Company, Hythe, Hampshire, for preparation of the Y cut crystals.

#### 6. REFERENCES

- (1) UK Provisional Patent no 39657/77: "Corrected Oscillator"  
(W Gosling, assigned to Racal Instruments Ltd,  
Maidenhead, Berkshire) November 1978.
- (2) MANASSEWITSCH, V., (1976) "Frequency Synthesisers - Theory and Design", New York: John Wiley & Sons.
- (3) STOKES, V. O.: "Techniques of Frequency Synthesis", Proc. IEE,  
Vol 120, No 10R, October 1973.
- (4) EVERS, A. F. and MARTIN, D. J.: "Improved forms of Digital Frequency Synthesisers" in "Digital Frequency Synthesis in Communication Systems", IEE Colloquium Digest 72/11, 1972, pp.9/1 to 9/5.

- (5) MORGAN, D. K., and STEUDEL, G.: "The COS/MOS Phase-Locked-Loop", RCA Application Note ICAN-6101, p.2.
- (6) NEMEC, J. : "A high-frequency synthesiser with a digital mixer", Electronic Design 4, February 15 1977, pp.120-122.
- (7) STEVELS, J. M. and VOLGER, J. M.: "Further experimental investigations on the dielectric losses of quartz crystals in relation to their imperfections", Phillips Research Reports, Vol 17, pp.283-314, June 1962.
- (8) GROIS, O. S.: "One possible mechanism of quartz ageing". Translated in Radio Engineering, Electronic Physics, Vol 7, p.651, April 1963.
- (9) WARNER, A. W., FRASER, D. B., and STOCKBRIDGE, C. D.: "Fundamental Studies of Ageing in Quartz Resonators", IEEE Trans on Sonics and Ultrasonics, Vol SU-12, pp.52-59, June 1965.

APPENDIX E - THE 1702A PROGRAMMABLE READ-ONLY MEMORY

The following is a copy of a data sheet for the Am1702A ultra-violet erasable pROM manufactured by Advanced Micro Devices Inc. The equivalent device available from other manufacturers differs only in some small details and may be considered identical in this application. Factors affecting its application are dealt with more fully in reference 1 of Chapter 6.

# Am1702A

256-Word by 8-Bit Programmable ROMs  
Advanced Micro Devices  
Complex MOS Integrated Circuits



## Distinctive Characteristics

- Field programmable 2048-bit ROMs
- Am1702A can be erased and reprogrammed by UV light
- 100% tested for programmability
- Typical programming time of 2 minutes/device
- Available for operation over full military temperature range
- 100% processing to MIL-STD-883

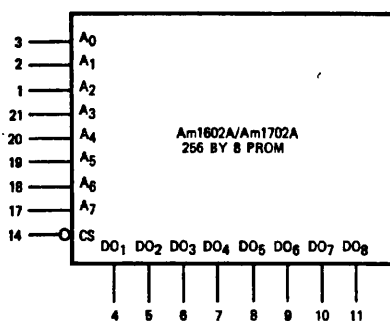
### FUNCTIONAL DESCRIPTION

The Am1702A is a 256-word by 8-bit field programmable MOS read-only memory, differing only in the package. The Am1702A package has a quartz lid through which the PROM can be erased by ultraviolet light.

The device is shipped with all outputs at a logic LOW level. Each bit in the memory can be electrically programmed to a HIGH level. The device has three-state outputs which go to a high-impedance OFF state when the chip select is HIGH. When the chip select is LOW, the outputs can drive one TTL unit load.

The Am1702A can directly replace the Intel 1702A. Except for programming procedure, the Am1702A can replace the 1702. (The Am1702A differs from the Am1702 only in the programming method and in the programmed state. The Am1702 is initially all HIGH, and the LOW's are programmed; the Am1602A/1702A is initially all LOW and the HIGH's are programmed. Once programmed, they are identical).

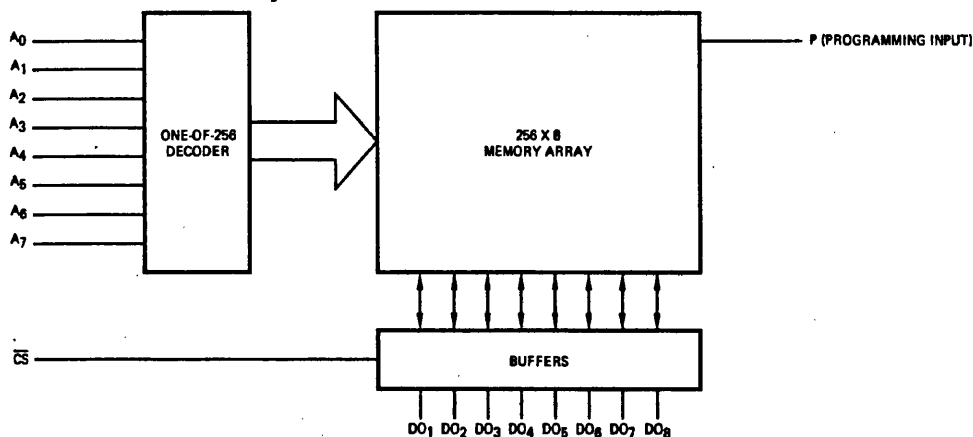
### LOGIC SYMBOL



V<sub>CC</sub> = Pin 12  
V<sub>DD</sub> = Pin 24  
V<sub>GG</sub> = Pin 16  
V<sub>BB</sub> = Pin 15  
P = Pin 13

Pins 22 and 23 must be connected to V<sub>CC</sub>.

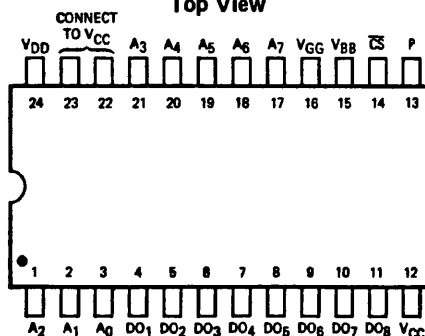
### LOGIC BLOCK DIAGRAM



### ORDERING INFORMATION

Package Type	Temperature Range	Order Number
Hermetic DIP/Quartz Lid	0°C to 70°C	C1702A

### CONNECTION DIAGRAM Top View



Note: Pin 1 is marked for orientation.

**MAXIMUM RATINGS** (Above which the useful life may be impaired)

Storage Temperature	-65°C to +150°C
Temperature (Ambient) Under Bias	-55°C to +125°C
Power Dissipation	1 W
Input and Supply Voltages (Operating)	$V_{CC} - 20\text{ V}$ to $V_{CC} + 0.5\text{ V}$
Input and Supply Voltages (Programming)	-50 V

**OPERATING RANGE**

Part Number	$V_{CC}$	$V_{DD}$	$V_{GG}$	Ambient Temperature
C1702A	+5.0 V $\pm$ 5%	-9.0 V $\pm$ 5%	-9.0 V $\pm$ 5%	0°C to +70°C

- Notes: 1. During operation  $V_{BB} = P = \text{pin } 22 = \text{pin } 23 = V_{CC}$ .  
 2.  $V_{GG}$  may be pulsed to reduce power dissipation.

**D. C. CHARACTERISTICS OVER OPERATING RANGE** (Unless Otherwise Noted)

Parameters	Description	Conditions	Min.	Typ.	Max.	Units
$V_{OH}$	Output HIGH Level	$I_{OH} = -100\ \mu\text{A}$	3.5	4.5		V
$V_{OL}$	Output LOW Level	$I_{OL} = 1.6\ \text{mA}$		-7	0.45	V
$I_{OH}$	Output HIGH Current	$V_{OUT} = 0.0\ \text{V}$	-2.0			mA
$I_{OL}$	Output LOW Current	$V_{OUT} = 0.45\ \text{V}$	1.6	4		mA
$V_{IH}$	Input HIGH Level		$V_{CC} - 2.0$		$V_{CC} + 0.3$	V
$V_{IL}$	Input LOW Level		$V_{CC} - 10.0$		$V_{CC} - 4.2$	V
$I_{LI}$	Input Leakage Current	$V_{IN} = 0.0\ \text{V}$			1.0	$\mu\text{A}$
$I_{LO}$	Output Leakage Current	$\overline{CS} = V_{CC} - 2.0, V_{OUT} = 0.0\ \text{V}$			1.0	$\mu\text{A}$
$I_{CF1}$	Output Clamp Current	$T_A = 0^\circ\text{C}, V_{OUT} = -1.0\ \text{V}$		8	14	mA
$I_{CF2}$	Output Clamp Current	$T_A = 25^\circ\text{C}, V_{OUT} = -1.0\ \text{V}$			13	mA
$I_{GG}$	$V_{GG}$ Current				1.0	$\mu\text{A}$
$I_{DD0}$	$V_{DD}$ Current (Note 1)	$V_{GG} = V_{CC}, I_{OL} = 0$ $\overline{VCS} = V_{CC} - 2.0, T_A = 25^\circ\text{C}$		5	10	mA
$I_{DD1}$		$I_{OL} = 0, \overline{VCS} = V_{CC} - 2.0, T_A = 25^\circ\text{C}$		35	50	mA
$I_{DD2}$		$I_{OL} = 0, \overline{VCS} = 0, T_A = 25^\circ\text{C}$		32	46	mA
$I_{DD3}$		$I_{OL} = 0, \overline{VCS} = V_{CC} - 2.0, T_A = 0^\circ\text{C}$		38.5	60	mA

Note: 1.  $I_{DD}$  may be reduced by pulsing the  $V_{GG}$  supply between  $V_{CC}$  and -9 V.  $V_{DD}$  current will be directly proportional to  $V_{GG}$  duty cycle. The data outputs will be unaffected by address or chip select changes while  $V_{GG}$  is at  $V_{CC}$ .

**CAPACITANCE** ( $T_A = 25^\circ\text{C}$ )

(These parameters are guaranteed by design and are not 100% tested)

Parameters	Description	Conditions	Typ.	Max.	Units
$C_{IN}$	Input Capacitance	All unused pins are at $V_{CC}$	8	15	pF
$C_{OUT}$	Output Capacitance		10	15	pF
$C_{VGG}$	$V_{GG}$ Capacitance			30	pF

## A. C. CHARACTERISTICS OVER OPERATING RANGE

$V_{IL} = 0V$ ,  $V_{IH} = 4.0V$ ,  $t_r = t_f < 50ns$ , Load = 1 TTL Gate.

Parameters	Description	Conditions	Min.	Typ.	Max.	Units
$f_{reg}$	Repetition Rate				1.0	MHz
$t_{OH}$	Previous Read Data Valid				100	ns
$t_{ACC}$	Address to Output Delay			0.7	1.0	$\mu s$
$t_{DVGG}$	Set-up Time, $V_{GG}$		0			$\mu s$
$t_{CS}$	Chip Select Delay				100	ns
$t_{CO}$	Output Delay from $\overline{CS}$				900	ns
$t_{OD}$	Output Deselect	$T_A = 0^\circ C$ to $+70^\circ C$			300	ns
$t_{OHC}$	Data Out Valid from $V_{GG}$ (Note 1)				5.0	$\mu s$

Note: 1. The output will remain valid for  $t_{OHC}$  after the  $V_{GG}$  pin is raised to  $V_{CC}$ , even if address changes occur.

### SWITCHING WAVEFORMS

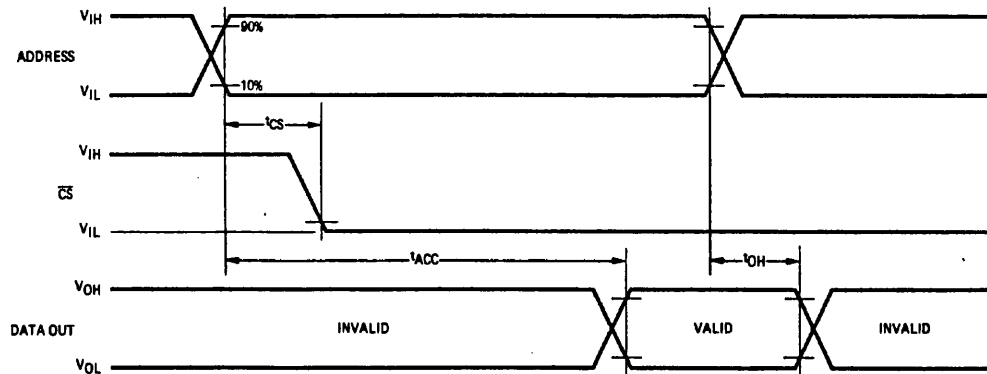


Figure 1. Reading Data

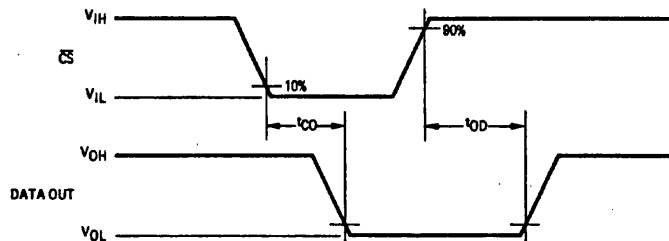


Figure 2. Deselecting Output from Chip Select.

### CLOCKED $V_{GG}$ OPERATION

The  $V_{GG}$  input may be switched between +5 V ( $V_{CC}$ ) and -9 V to save power. To read data, the  $V_{GG}$  level must be lowered to -9 V at least  $t_{DVGG}$  prior to the address selection. Once data has appeared at the output ( $t_{ACC}$ ),  $V_{GG}$  may be raised to +5 V. The data output will remain steady for  $t_{OHC}$ . To deselect the chip,  $\overline{CS}$  must be raised to  $V_{IH}$  prior to raising  $V_{GG}$  to +5 V. If  $\overline{CS}$  goes HIGH while  $V_{GG}$  is at  $V_{CC}$ , deselection of the chip will not occur until  $t_{OD}$  after  $V_{GG}$  goes back to -9 V.

## PROGRAMMING THE Am1702A

Each storage node in the Am1702A consists of an MOS transistor whose gate is not connected to any circuit element. The transistors are all normally off, making all outputs LOW in an unprogrammed device. A bit is programmed to a HIGH by applying a large negative voltage at the MOS transistor; electrons tunnel through the gate insulation onto the gate itself. When the programming voltage is removed, a charge is left on the gate which holds the transistor on. Since the gate is completely isolated, there is no path by which the charge can escape, except for random high energy electrons which might retunnel through the gate insulation. Under ordinary conditions retunneling is not significant. The application of high energy to the chip through X-rays or UV light (via the quartz window) raises energy levels so that the charge can escape the gate region, erasing the program and restoring the device to all LOW.

Programming a bit is accomplished by addressing the desired word using negative 44V logic levels, applying a negative voltage to  $V_{DD}$ ,  $V_{GG}$ , and the outputs to be programmed, and

then applying a -49 volt pulse to the programming pin. The duty cycle on the programming pin should not exceed 20% to avoid over-heating the device. For long-term data retention, at least 32 program pulses should be applied for each address. All eight outputs are programmed simultaneously.

Programming Boards are available for the Data I/O automatic programmer (part number 1010/1011), for the Spectrum Dynamics programmer (part number 434-549), and for the Pro-Log programmer (part number PM9001).

## ERASING THE Am1702A

The Am1702A may be erased (restored to all LOW's) by exposing the die to ultraviolet light from a high intensity source. The recommended dosage is 6 W-sec/cm<sup>2</sup> at a wavelength of 2537 Å. The Ultraviolet Products, Inc., models UVS-54 or S-52 can erase the Am1702A in about 15 minutes, with the devices held one inch from the lamp. (Caution should be used when Am1702A's are inspected under fluorescent lamps after being programmed, as some fluorescent lamps may emit sufficiently in the UV to erase or "soften" the PROM.)

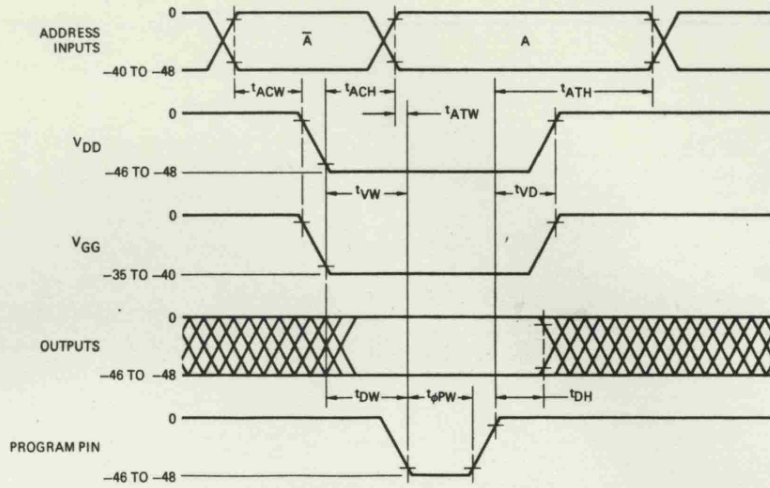
## PROGRAMMING REQUIREMENTS ( $T_A = 25^\circ\text{C}$ , $V_{CC} = 0\text{V}$ , $CS = 0\text{V}$ , $V_{BB} = +12\text{V} \pm 10\%$ )

Parameters	Description	Conditions	Min.	Typ.	Max.	Units
$I_{L1P}$	Input Current, Address and Data	$V_{IN} = -48\text{V}$			10	mA
$I_{L12P}$	Input Current, Program and $V_{GG}$ Inputs	$V_{IN} = -48\text{V}$			10	mA
$I_{BB}$	$V_{BB}$ Current			0.05		mA
$I_{DDP}$	$I_{DD}$ Current During Programming Pulse	$V_{DD} = V_{Prog} = -48\text{V}$ , $V_{GG} = -35\text{V}$		200	Note 1	mA
$V_{IHP}$	Input HIGH Voltage				0.3	Volts
$V_{IL1P}$	Voltage Applied to Output to Program a HIGH		-46		-48	Volts
$V_{IL2P}$	Input LOW Level on Address Inputs		-40		-48	Volts
$V_{IL3P}$	Voltage Applied to $V_{DD}$ and Program Inputs		-46		-48	Volts
$V_{IL4P}$	Voltage Applied to $V_{GG}$ Input		-35		-40	Volts
$t_{pPW}$	Programming Pulse Width	$V_{GG} = -35\text{V}$ , $V_{DD} = V_{Prog} = -48\text{V}$			3	ms
$t_{DW}$	Data Set-up Time		25			$\mu\text{s}$
$t_{DH}$	Data Hold Time		10			$\mu\text{s}$
$t_{VW}$	$V_{GG}$ and $V_{DD}$ Set-up Time		100			$\mu\text{s}$
$t_{VD}$	$V_{GG}$ and $V_{DD}$ Hold Time		10		100	$\mu\text{s}$
$t_{ACW}$	Address Set-up Time (Complement)		25			$\mu\text{s}$
$t_{ACH}$	Address Hold Time (Complement)		25			$\mu\text{s}$
$t_{ATW}$	Address Set-up Time (True)		10			$\mu\text{s}$
$t_{ATH}$	Address Hold Time (True)		10			$\mu\text{s}$
	Duty Cycle				20	%

Note: 1. Do not allow  $I_{DD}$  to exceed 300mA for more than 100 $\mu\text{s}$ .



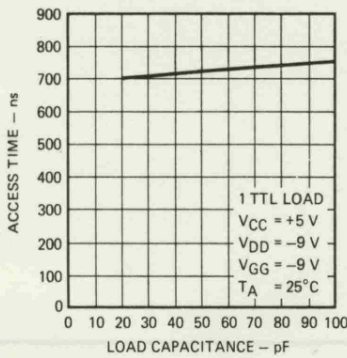
## PROGRAMMING WAVEFORMS



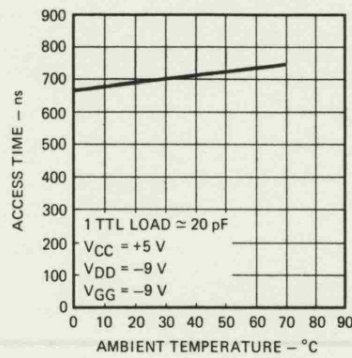
$\bar{A}$  = binary complement of address to be programmed.  
 A = binary address to be programmed.

## TYPICAL PERFORMANCE CURVES

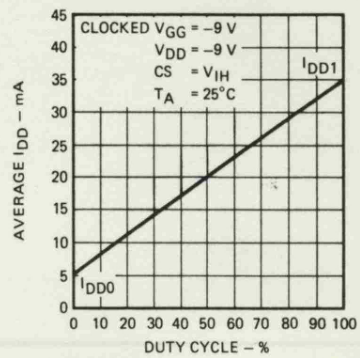
Access Time Versus Load Capacitance



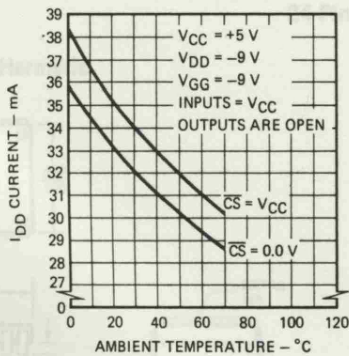
Access Time Versus Temperature



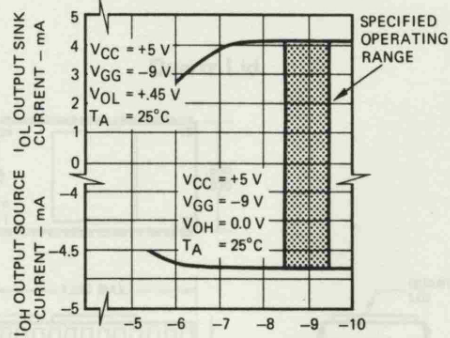
Average Current Versus Duty Cycle for Clocked V<sub>GG</sub>



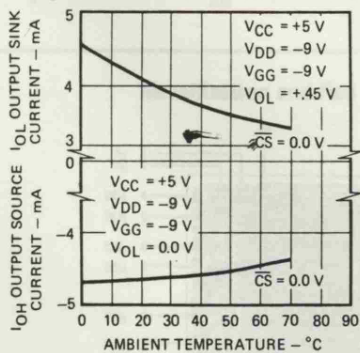
$I_{DD}$  Current Versus Temperature



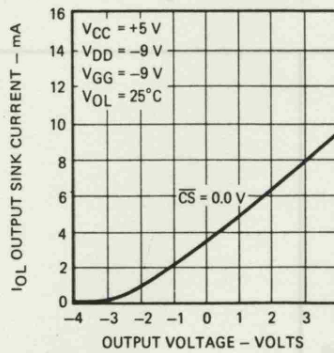
Output Current Versus V<sub>DD</sub> Supply Voltage



Output Current Versus Temperature



Output Sink Current Versus Output Voltage

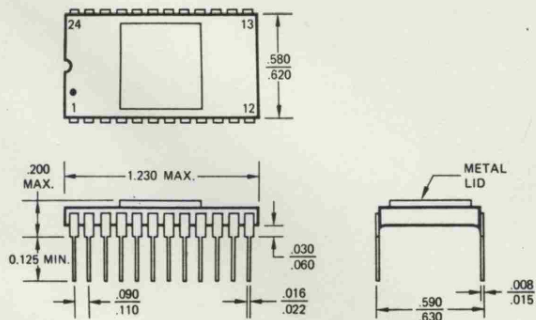


ADVANCED MICRO DEVICES INC.

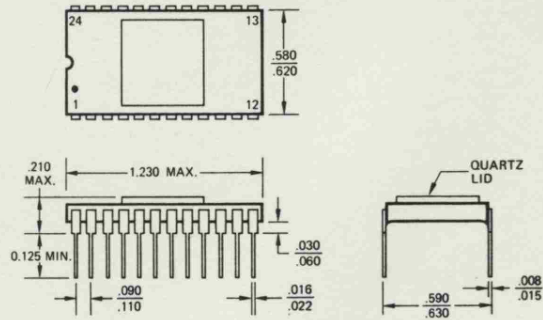
California 94088  
 (415) 753-5000  
 (714) 951-2200  
 TELEX: 34-2000

**PHYSICAL DIMENSIONS**  
Dual-In-Line  
24-Pin Side Brazed

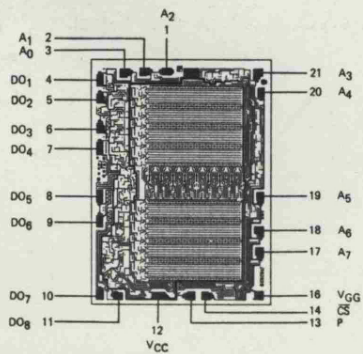
**Hermetic**



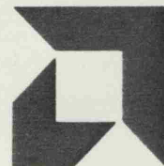
**Quartz Lid**



**Metallization and Pad Layout**



**DIE SIZE**  
0.109" X 0.142"



**ADVANCED  
MICRO  
DEVICES INC.**  
901 Thompson Place  
Sunnyvale  
California 94086  
(408) 732-2400  
TWX: 910-339-9280  
TELEX: 34-6306

APPENDIX F - THE PROM SUPPORT EQUIPMENT

The equipment used in the simulation and programming of the 1702A erasable pROMs was based upon the IIT MICRO MODULE Universal Microprocessor Development System. It consisted of:

- (i) a PSP 1702 Pseudo Prom module,
- (ii) a KL 1 Keyboard Loader,
- (iii) a C-I/A Controller Interface, and
- (iv) a PGM 1702A Programmer module.

Depending upon the particular facilities required at the time, it was possible to employ the equipment in two distinct ways which are now described.

F.1 Memory Simulation Using the Keyboard Loader

The Pseudo Prom module consists of a random-access memory of the same configuration as the pROM to be simulated, in this case 256 x 8 bits. The module interfaces with the user's equipment directly by means of a plug-in header as shown in Figure F1. A built-in battery protects the data when the module is disconnected so that the unit may operate alone in place of a pROM. Data is fed into the Pseudo Prom by means of a Keyboard Loader with which the Pseudo Prom may be mated. The Keyboard Loader operates in two modes. In the KEY mode, any of the available data locations may be accessed by means of the keyboard and its contents set or altered at will. A hexadecimal display indicates the corresponding address and content data continuously. In this way it is possible to programme the Pseudo Prom with data determined by observation of its effect upon the compensated oscillator. In the RUN mode the Pseudo Prom behaves to the oscillator unit exactly as would an actual pROM, whilst it is

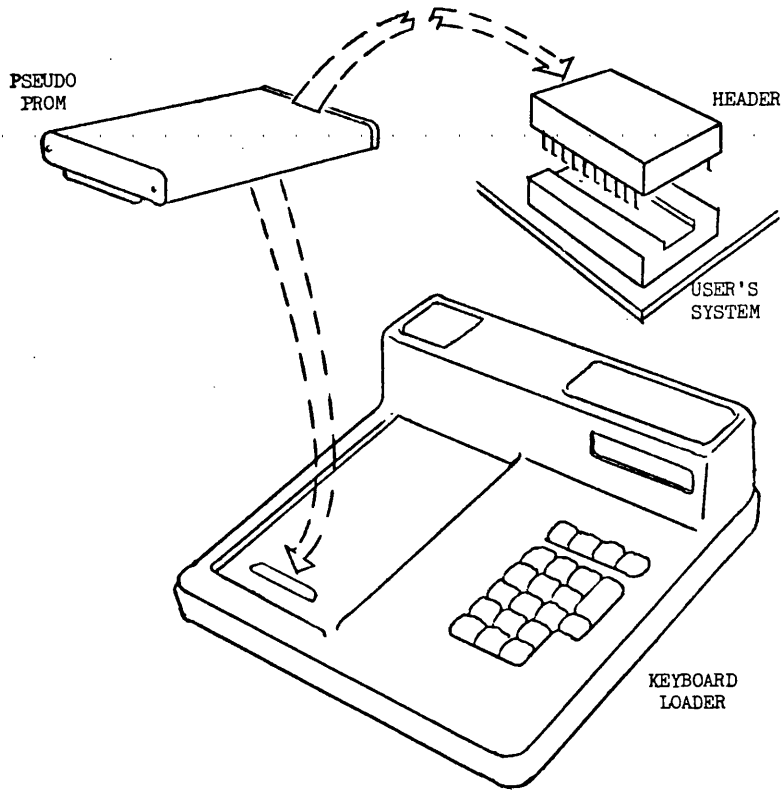


Figure F1

still possible to observe the data acquisition process on the display.

The Keyboard Loader is extremely useful in making small adjustments to the data, observing the pROM action, and in experiments involving an effective opening of the compensation loop. It has the disadvantage, however, that with this method of operation the data arrived at during experimentation or programming may not be recorded or programmed into an actual pROM. In addition, the loading of data into a complete Pseudo Prom by this means is a rather long and tedious process. These disadvantages are overcome by the use of a teletype as now described.

#### F.2 Simulation, Editing, Programming and Copying Using the Controller Interface and Programmer Modules

By combining the Pseudo Prom with the Controller Interface and Programmer modules as shown in Figure F2 it is possible to effect serial data interface with a teletype or VDU. By using one of a set of simple instructions it is then possible to load data into the Pseudo Prom in several ways, to insert data without interrupting the sequence, to move blocks of data within the memory and to copy existing pROMs into the memory. Furthermore it is possible to record the data of the Pseudo Prom in print, as punched paper tape or by programming an actual pROM. The instructions are listed in Table F1.

Each instruction follows the prompt '>' which is generated by the interface module. Those instructions which concern the Programmer module must be preceded by the GO TO command as indicated. Table F2 is an example of a memory map as compiled under instructions LH or LR. The character '[' (shift-K) is used for copying to guard against inadvertent use which could destroy

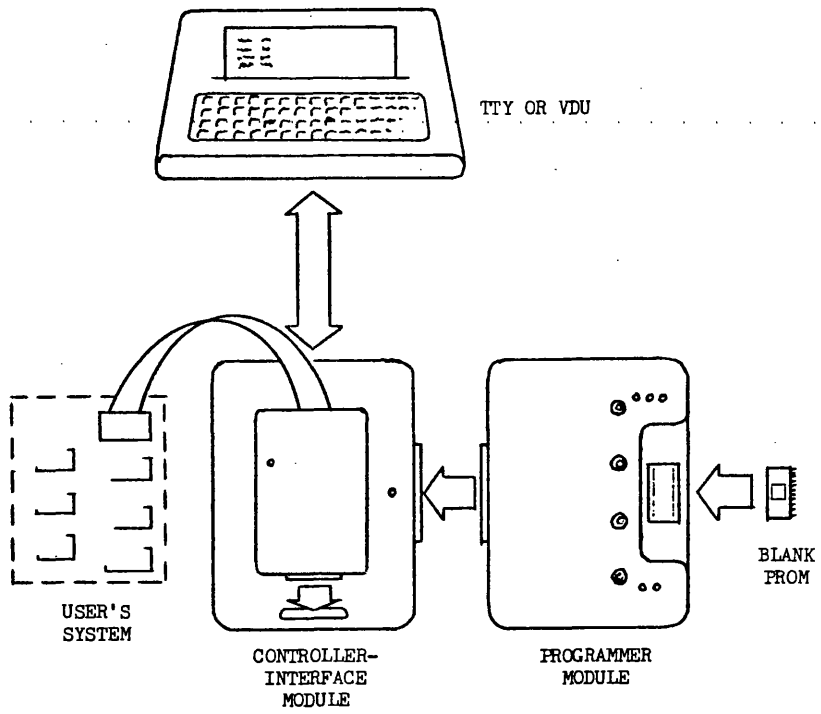


Figure F2

<u>Instruction</u>	<u>Action</u>	<u>Description</u>	<u>Example(s)</u>
WV	WRITE VERTICAL	For Pseudo Prom loading	>WV 0AB
WH	WRITE HORIZONTAL	For Pseudo Prom loading	>WH 09C
LV	LIST VERTICAL	Column print out of data	>LV 016-OFF
LH	LIST HORIZONTAL	Memory map print out	>LH 000-OFF
I	INSERT	Inserts and shifts data to an end stop	>I 020-080
M	MOVE	Relocates a block of data	>M 000-004 = 008-00C
S	SET	Writes the same data into a range of locations	>S 000-OFF 80
P	PUNCH	Punches specified locations onto paper tape	>P 005-OFF
T	TAPE	Reads data from paper tape and loads	>T
G	GO TO	Assigns control to Programmer module	>G >
P	PROGRAM	Programmes a pROM	>G >P 000-OFF
[	COPY	Copies a pROM into the Pseudo Prom	>G >[ 000-080
V	VERIFY	Verifies a programmed pROM	>G >V 000-OFF
LR	LIST ROM	Prints memory map of pROM	>G >LR 000-095

Table F1 - The Software Instruction Set of the pROM Support Equipment

&gt;LH000-OFF

000	1F	20	21	22	23	24	25	26	27	28	29	2A	2B	2C	2D	2E
010	2F	30	30	31	32	33	34	35	36	37	38	39	3A	3B	3C	3D
020	3E	3F	40	40	41	42	43	44	45	46	47	48	49	4A	4B	4C
030	4D	4E	4F	50	51	51	52	53	54	55	56	57	58	59	5A	5B
040	5C	5D	5E	5F	60	61	61	62	63	64	65	66	67	68	69	6A
050	6B	6C	6D	6E	6F	70	71	71	72	73	74	75	76	77	78	79
060	7A	7B	7C	7D	7E	7F	80	81	82	82	83	84	85	86	87	88
070	89	8A	8B	8C	8D	8E	8F	90	91	92	92	93	94	95	96	97
080	98	99	9A	9B	9C	9D	9E	9F	A0	A1	A2	A2	A3	A4	A5	A6
090	A7	A8	A9	AA	AB	AC	AD	AE	AF	B0	B1	B2	B2	B3	B4	B5
0A0	B6	B7	B8	B9	BA	BB	BC	BD	BE	BF	C0	C1	C2	C2	C3	C4
0B0	C5	C6	C7	C8	C9	CA	CB	CC	CD	CE	CF	D0	D1	D2	D2	D3
0C0	D4	D5	D6	D7	D8	D9	DA	DB	DC	DD	DE	DF	E0	E1	E2	E2
0D0	E3	E4	E5	E6	E7	E8	E9	EA	EB	EC	ED	EF	F0	F1	F2	F2
0E0	F3	F4	F5	F6	F7	F8	F9	FA	FB	FC	FD	FE	FF	FF	FF	FF
0F0	00	01	02	03	04	05	06	07	08	09	0A	0B	0C	0D	0E	0F

Table F2 - A Memory Map Compiled by the  
Controller Interface (ROM 2)

unrecorded data. The tape used to load data under the TAPE instruction is coded in standard ASCII format and may be generated elsewhere as discussed in Chapter 7.



APPENDIX G - A STUDY OF SOME THERMAL EFFECTS  
WITHIN THE CRYSTAL ENCLOSURES

In a mounted quartz crystal, it is the temperature of the crystal plate which determines the resonant frequency. The temperature of the holder can, mounting pillars, circuit board conductors, etc are of no direct significance except that it is from and to these portions of the unit that heat may flow to and from the quartz itself. Figures 3.11 and 3.12 of Chapter 3 illustrate that two thermal paths exist between the plate and the external environment. Firstly, as the can changes in temperature heat may flow between it and the plate across the inert gas which fills the sealed enclosure. This occurs predominantly in a direction normal to the faces of the plate, though the edges too must contribute to some extent. Secondly, as the temperature of the conductors of the oscillator circuit board (or in other applications the crystal socket or flying leads) change temperature, heat may flow along the metallic lead-wires and mounting springs. The relative importance of these thermal paths is now investigated by consideration of the thermal resistance of their various elements defined by:

$$R_t = \frac{L}{K.A} \quad (G1.1)$$

where  $R_t$  is the thermal resistance of a conduction path,  $L$  is its length,  $A$  its cross-sectional area and  $K$  is the coefficient of thermal conductivity of the conduction medium.

There exists a clear thermal symmetry due to the geometric symmetry of the mount. It is only necessary, therefore, to consider the conduction path due to one mounting post and due to one face and edge of the plate. The thermal path of the lead-wire and mounting spring may be approximated to that of Figure G1, assuming that the crystal is soldered directly onto a circuit board (as is intended

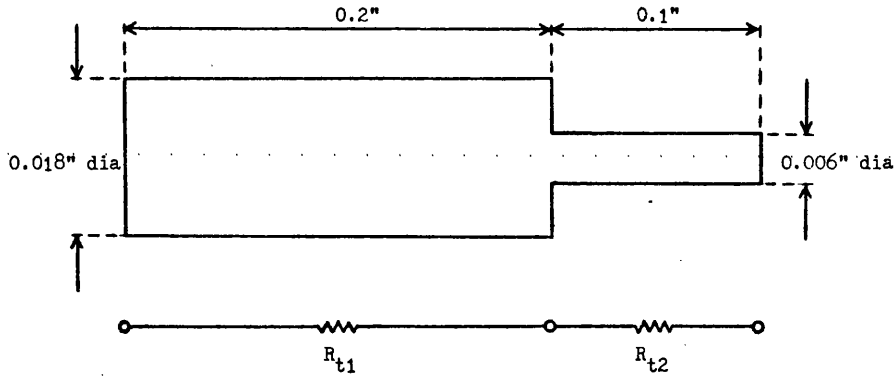


Figure G1

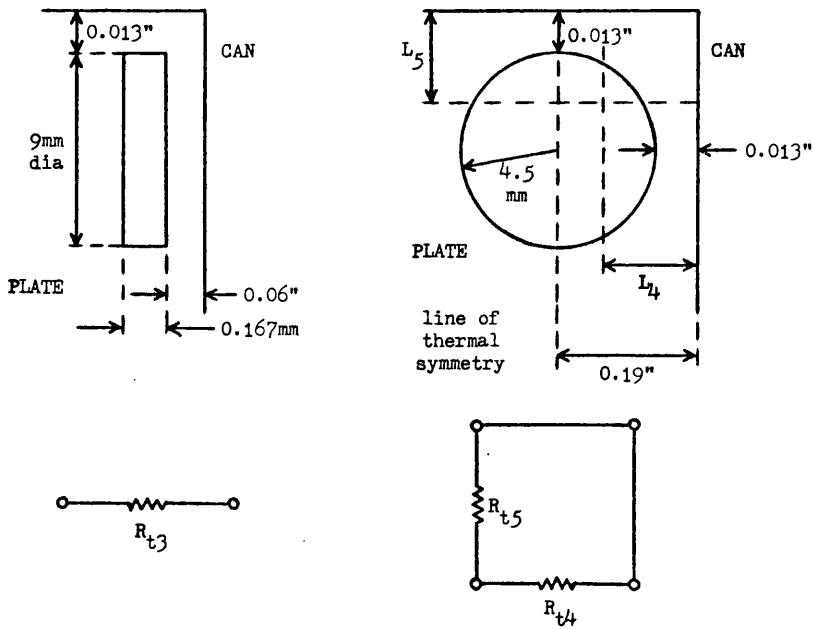


Figure G2

with an HC 18/U holder) with no stand-off, and assuming that the soldered joint at points A and cemented joints at B afford good thermal coupling. Taking the thermal conductivity of steel as  $0.11 \text{ cal. sec}^{-1} \text{ cm}^{-1} \text{ K}^{-1}$  (from Kaye and Laby tables, Chapter 6, reference 3) the equivalent thermal resistance of the path may be evaluated:

$$\begin{aligned} R_{t,M} &= R_{t1} + R_{t2} \\ &= 2813 + 12658 \text{ sec.K.cal}^{-1} \\ &\approx 15500 \text{ sec.K.cal}^{-1} \end{aligned}$$

showing that the thermal resistance of the fine mounting spring dominates that of the lead-wire. Figure G2 shows the approximate equivalent of the thermal path through the flush-gas of the enclosure, assuming a 9mm diameter circular plate of thickness 0.167mm as used in the prototype. The equivalent thermal resistance may then be written:

$$\frac{1}{R_{t,G}} = \frac{1}{R_{t3}} + \frac{1}{R_{t4}} + \frac{1}{R_{t5}} \quad (\text{G1.2})$$

where  $R_{t3}$  is the thermal resistance of the path between the can and the main plate face,  $R_{t4}$  is the thermal resistance from the can to one side edge of the plate and  $R_{t5}$  is the thermal resistance of half of the path from the top of the can to the top edge of the plate. These thermal resistances occur effectively in parallel. Each may be evaluated as follows:

(i)  $R_{t3}$  may be obtained directly from equation (G1.1) as:

$$R_{t3} \approx 4000 \text{ sec.K.cal}^{-1}$$

assuming the thermal conductivity of the medium is about  $0.00006 \text{ cal. sec}^{-1} \text{ cm}^{-1} \text{ K}^{-1}$ , which is the case for diatomic nitrogen at a pressure of  $10^{-4}$  Torr. Hydrogen and helium exhibit a thermal conductivity seven or eight times higher,

and their use would reduce the thermal resistance accordingly.

- (ii)  $R_{t4}$  may be estimated by considering the mean path length from the edge of the can to the plate, so that:

$$L_4 = 0.1 \text{ inches}$$

and:

$$R_{t4} \approx 282000 \text{ sec.K.cal}^{-1}$$

- (iii) Similarly,  $R_{t5}$  may be obtained:

$$R_{t5} \approx 563000 \text{ sec.K.cal}^{-1}$$

It may be seen that, as is to be expected, the effect of the thermal path normal to the main face of the plate predominates. The equivalent thermal resistance is:

$$R_{t,G} \approx 3900 \text{ sec.K.cal}^{-1}$$

These calculations are approximate only, yet serve to illustrate that the two thermal paths have equivalent resistances of the same order of magnitude. Both paths have been considered in their 'worst case' in this respect. If longer lead-wires were to be employed,  $R_{t,M}$  would not change significantly. If the soldered joint at points A in Figure 3.12 of Chapter 3 spreads along the mounting spring, as is quite likely, then the effective thermal length of the spring is reduced having considerable effect upon  $R_{t,M}$ . If hydrogen rather than nitrogen is present in the enclosure,  $R_{t,G}$  could be less than the calculated figure by a factor of seven or eight, unless the residual pressure is much below  $10^{-4}$  Torr in which case the thermal conductivity of gases increases. It is also worthwhile noting that if a true vacuum was achieved in the enclosure during manufacture, then no conduction path could exist from the can to the plate and all heat transfer would take place along the metallic conductors.

APPENDIX H - PARTIAL SPECIFICATION OF THE EFRATOM RUBIDIUM  
ATOMIC FREQUENCY STANDARD, MODEL FRK-H

Output	10MHz sine wave 1V rms, $R_0 = 50$ ohms
Signal to Noise Ratio	>120dB in 1Hz band at more than 200Hz from nominal frequency >150dB in 1Hz band at more than 1000Hz from nominal frequency.
Supply Voltage	28V dc (22V to 32V dc)
Power Consumption	13W at 25°C ambient
Warm-up Characteristic	10 minutes to reach $2 \times 10^{-10}$ (from ambient of 25°C, $I_{\max} = 1.7A$ )
Long-term Stability	$<3 \times 10^{-11}$ /month
Short-term Stability	$<2 \times 10^{-11}$ $\tau = 1\text{sec}$ $<5 \times 10^{-12}$ $\tau = 10\text{sec}$ $<1 \times 10^{-12}$ $\tau = 100\text{sec}$
Environmental Stability	
Voltage	$<1 \times 10^{-11}$ /10%
Temperature	$<4 \times 10^{-10}$ from -25°C to +65°C
Magnetic Field	$<1 \times 10^{-12}$ /Am <sup>-1</sup>
Altitude	$<5 \times 10^{-13}$ /mbar (from 0 to 12000m)
Temperature Range	-25°C to +65°C
Storage Temperature	-40°C to +70°C
Size	100 x 99 x 112mm
Weight	1Kg

APPENDIX I - RESULTS OF THE SHORT-TERM FREQUENCY STABILITY TESTS

Twelve independent tests for short-term frequency stability were performed by the time domain technique. Tests 1, 2 and 3 were performed on an oven controlled crystal oscillator with averaging times 0.1, 1 and 10 seconds respectively. Tests 4, 5 and 6 were performed on the prototype unit with averaging times 0.1, 1 and 10 seconds, each at a low VCXO drive power arranged by setting the VCXO supply voltage at 10 volts. Tests 7, 8 and 9, and 10, 11 and 12 were as 4, 5 and 6 but at medium and high VCXO drive power respectively, corresponding to VCXO supply voltages of 30 volts and 50 volts.

The same conditions applied to all tests. The number of readings employed to evaluate each variance,  $N$ , was two (by definition of the Allan variance). 101 readings were taken in each case. The time between successive readings,  $T$ , was kept at 10 seconds throughout, and the bandwidth of the measuring equipment,  $\Delta B$ , was constant. From equation (6.17), therefore, the Allan variance as measured may be more formally written:

$$\sigma_y^2(2,10,\tau,\Delta B) = \frac{1}{(100f_0)^2} \cdot \frac{1}{100} \sum_{k=1}^{100} \frac{(f_{k+1} - f_k)^2}{2} \quad (\text{II.1})$$

The table overleaf gives a complete list of the results obtained during tests 1, 5, 8 and 12 as an illustration of the technique. For each column of results, the value of  $\sum (f_{k+1} - f_k)^2$  may best be evaluated with the aid of a programmable calculator, the Allan variance following directly from this value as indicated at the foot of the table.

It must be stressed that the values of Allan variance arrived at here are relevant only as a means of comparison. Differences in measurement bandwidth and sample rate prevent comparison of these

results with those examples given in the graph of Figure 2.15 in Chapter 2.

$f_k - f_M$ (Hz)				
k	Test 1	Test 5	Test 8	Test 12
1	-10	01	02	0.0
2	20	-03	04	-0.1
3	00	02	01	0.2
4	10	-01	06	0.1
5	-10	04	00	-0.2
6	00	07	03	-0.3
7	10	01	-02	-0.4
8	00	05	01	0.4
9	-10	02	-04	0.0
10	00	03	00	0.0
11	20	-03	02	0.1
12	-10	-01	04	0.3
13	00	06	-03	0.5
14	10	-03	02	0.0
15	00	02	00	-0.1
16	-10	01	01	-0.4
17	10	03	-04	-0.3
18	00	-02	05	0.1
19	10	05	-02	0.3
20	-10	03	-04	0.0
21	10	00	03	-0.4
22	00	03	-07	-0.1
23	-10	04	-04	0.5
24	00	-02	01	0.4
25	-20	-05	02	0.3
26	00	03	-06	0.1
27	-10	02	-03	-0.4
28	-10	-03	03	-0.2
29	10	-06	02	0.6
30	00	04	-01	0.0
31	00	06	-03	-0.5
32	-10	-05	-06	-0.4
33	20	-02	05	-0.1
34	00	02	-03	0.6
35	-10	00	-01	0.2
36	00	-02	01	0.1
37	10	-04	03	0.4
38	-10	-03	-06	0.0
39	00	04	-04	-0.5
40	10	-05	-05	-0.3
41	-10	06	00	0.0
42	00	04	01	-0.5
43	10	02	03	-0.2
44	00	01	05	0.2
45	20	-03	00	0.4

$f_k - f_M$ (Hz)				
k	Test 1	Test 5	Test 8	Test 12
46	-10	03	-02	0.3
47	00	-01	02	0.1
48	-10	01	-04	0.1
49	10	04	-05	0.4
50	00	-04	03	0.2
51	-20	-06	00	0.6
52	00	-01	-04	-0.2
53	-30	03	-03	0.2
54	10	-01	-05	0.5
55	00	-02	03	0.0
56	-10	04	-03	-0.1
57	-20	-04	-02	0.0
58	10	-02	02	0.6
59	-20	-03	-02	0.1
60	00	01	-03	0.3
61	20	06	-06	-0.3
62	10	-06	01	-0.5
63	-10	02	01	-0.4
64	00	02	-08	0.1
65	-20	-07	05	0.5
66	10	01	02	0.0
67	00	-05	-02	-0.2
68	-10	-01	-06	0.2
69	00	03	00	0.0
70	00	-02	-02	-0.1
71	10	-03	-04	-0.3
72	00	-01	-03	0.1
73	-10	06	01	0.3
74	00	-03	-04	-0.1
75	10	02	05	-0.2
76	00	04	-02	0.0
77	10	01	03	-0.3
78	00	-01	00	0.1
79	10	02	01	-0.2
80	00	-03	-04	-0.2
81	10	01	-01	0.0
82	00	-04	-08	-0.1
83	-10	-01	-02	0.0
84	00	-07	-05	0.2
85	10	00	00	0.1
86	00	01	07	0.3
87	-10	-03	00	0.2
88	00	08	-04	0.6
89	-10	02	01	0.5
90	00	-05	-03	0.0
91	-10	-06	00	0.4
92	00	06	05	0.1
93	10	01	-07	-0.1
94	00	-02	-06	0.0
95	-10	01	00	-0.2
96	10	06	05	0.2



$f_k - f_M$ (Hz)				
k	Test 1	Test 5	Test 8	Test 12
97	00	-05	-02	0.3
98	10	-06	-02	0.1
99	00	-01	-01	-0.3
100	-10	00	03	0.0
101	10	04	-04	-0.1

$\Sigma(f_{k+1} - f_k)^2$	24200	2771	2568	11.67
$\sigma_y^2(\tau)$	$2.42 \times 10^{-16}$	$1.39 \times 10^{-17}$	$1.28 \times 10^{-17}$	$5.84 \times 10^{-20}$

APPENDIX J - STATEMENT LIST OF THE COMPUTER PROGRAMME  
USED FOR THE EVALUATION OF ALGORITHM TWO

```

C
C
C PROGRAM TO PREDICT THE REQUIRED
C MEMORY DATA USING ALGORITHM TWO
C
C PUT L=0 FOR FULL DATA ANALYSIS
C PUT L=3 FOR PREDICTED DATA ONLY
C
C
C DIMENSION X3(260),K(260),JAY(260)
C READ,L
C READ,N
C M=0
C CO=0
C C1=0
C C3=0
C WRITE(6,200)
200 FORMAT(1H1)
300 READ(5,310)IT1,IA1,IT2,IA2,IT3,IA3
310 FORMAT(6(Z2,1X))
C WRITE(6,320)IT1,IA1,IT2,IA2,IT3,IA3
320 FORMAT(1H0,30X,Z2,2X,Z2,/,25X,'DATA',2X,Z2,2X,Z2,/,31X,Z2,2X,Z2)
C T1=FLOAT(IT1)
C A1=FLOAT(1/IA1)
C T2=FLOAT(IT2)
C A2=FLOAT(1/IA2)
C T3=FLOAT(IT3)
C A3=FLOAT(1/IA3)
C M=M+1
C AA=A1
C AB=A2
C AC=A3
350 D2=(T1*T2*((T2**2)-(T1**2)))+(T2*T3*((T3**2)-(T2**2)))+(T1*T3*((T1
/ **2)-(T3**2)))
C EO=(T1*T2*AC*(T2**2-T1**2)+T2*T3*AA*(T3**2-T2**2)+T1*T3*AB*(T1**2-
/ T3**2))/D2
C E1=(AA*(T2**3-T3**3)+AB*(T3**3-T1**3)+AC*(T1**3-T2**3))/D2
C E3=((AA*(T3-T2))+(AB*(T1-T3))+(AC*(T2-T1)))/D2
C CO=(CO+EO)
C C1=(C1+E1)
C C3=(C3+E3)
C IF(M.LT.N)GOTO300
C CONTINUE
C EO=CO/N
C E1=C1/N
C E3=C3/N
370 CONTINUE
C WRITE(6,400)EO,E1,E3
400 FORMAT(1H0,24X,'EO = ',F7.4,/,25X,'E1 = ',F7.4,/,25X,'E3 = ',E10.3
/)
C CONTINUE
450 DO 550 I=1,256,1
C T=FLOAT(I)
C X3(I)=EO+(E1*T)+(E3*(T**3))

```

```

K(I)=IFIX(X3(I))
D=X3(I)-K(I)
IF(D.LT.0.5)GOTO550
K(I)=K(I)+1
550 CONTINUE
570 CONTINUE
IF(L.EQ.0)GOTO800
IF(L.EQ.1)GOTO815
IF(L.EQ.3)GOTO800
DO 600 I=1,256,1
K(I)=JAY(I)-K(I)
IF(K(I).GE.0)GOTO590
K(I)=2816-K(I)
590 CONTINUE
600 CONTINUE
GOTO813
800 CONTINUE
WRITE(6,810)
810 FORMAT(1H0,24X,'PREDICTED DATA',/,25X,'-----')
GOTO817
813 CONTINUE
WRITE(6,814)
814 FORMAT(1H0,24X,'DATA ERROR MAP',4X, ''B'' DENOTES ''MINUS'',/,25X
/, '-----')
GOTO817
815 CONTINUE
WRITE(6,816)
816 FORMAT(1H0,24X,'REQUIRED DATA',/,25X,'-----')
817 CONTINUE
WRITE(6,820)(J,J=1,9,1)
820 FORMAT(1H0,5X,'O',3X,9(I1,3X),'A',3X,'B',3X,'C',3X,'D',3X,'E ',2X,
/'F')
WRITE(6,830)(K(I),I=1,255,1)
830 FORMAT(1H0,1X,'O',2X,'***',1X,15(Z3,1X),/
1      2X,'1',2X,16(Z3,1X),/
2      2X,'2',2X,16(Z3,1X),/
3      2X,'3',2X,16(Z3,1X),/
4      2X,'4',2X,16(Z3,1X),/
5      2X,'5',2X,16(Z3,1X),/
6      2X,'6',2X,16(Z3,1X),/
7      2X,'7',2X,16(Z3,1X),/
8      2X,'8',2X,16(Z3,1X),/
9      2X,'9',2X,16(Z3,1X),/
A      2X,'A',2X,16(Z3,1X),/
B      2X,'B',2X,16(Z3,1X),/
C      2X,'C',2X,16(Z3,1X),/
D      2X,'D',2X,16(Z3,1X),/
E      2X,'E',2X,16(Z3,1X),/
F      2X,'F',2X,16(Z3,1X),/
CONTINUE
IF(L.EQ.1)GOTO910
IF(L.GE.2)GOTO999
DO 900 I=1,256,1
900 JAY(I)=K(I)
910 L=L+1
EO=31.5117
E1=0.9425
E3=-0.160E-07
IF(L.EQ.2)GOTO570

```

```
IF(L.EQ.1)GOTO370  
999 CONTINUE  
STOP  
END
```